HOKKAIDO UNIVERSITY

Title	Intercalation Reactions into Graphite followed by Potenial and their Application to Battery
Author(s)	Norio, Iwashita
Degree Grantor	北海道大学
Degree Name	博士(工学)
Dissertation Number	甲第3055号
Issue Date	1992-03-25
DOI	https://doi.org/10.11501/3060659
Doc URL	https://hdl.handle.net/2115/49793
Type	doctoral thesis
File Information	000000249605.pdf

Hokkaido University Collection of Scholarly and Academic Papers : HUSCAP

Intercalation Reactions into Graphite followed by potential and their Application to Battery

Norio IWASHITA

(1)

Intercalation Reactions into Graphite followed by potential and their Application to Battery

Norio IWASHITA

Content

Abstract in English ---------- I
Abstract in Japanese ---------- IV

Chapter 1: Introduction
1.1. Carbon materials ---------- 1
1.2. Graphite intercalation compounds (GICs) ---------- 4
1.2.1. Short history ---------- 4
1.2.2. Classification ---------- 5
1.2.3. Structure ---------- 6
1.2.4. Synthesis ---------- 9
1.3. Application of GICs ---------- 11
1.3.1. Function ---------- 11
1.3.2. Application of GICs to secondary batteries ---------- 12
1.4. Purpose of the present work ---------- 15
1.5. Construction of the present thesis ---------- 16
References ---------- 17

Chapter 2: Characterization of structure and texture on carbon materials
2.1. Introduction ---------- 19
2.2. Experimental ---------- 20
2.3. Results ---------- 27
2.3.1. Texture seen by microscopy ---------- 27
2.3.2. X-ray crystallographic parameters ---------- 30
2.3.3. Relations among X-ray parameters ---------- 35
2.3.4. Relations between magnetoresistance and X-ray parameters ---- 38
2.4. Discussion ---------- 48
2.4.1. Effect of texture on graphitization of carbon materials ----- 48
2.4.2. Effect of texture on
relations among graphitization parameters ---------- 49
2.5. Summary ---------- 53
References ---------- 53

Chapter 3: Potential change during intercalation of sulfuric acid into graphite by chemical oxidation
3.1. Introduction ---------- 55
3.2. Experimental ---------- 55
3.3. Results ---------- 57
3.3.1. Oxidation by nitric acid ---------- 57
3.3.2. Oxidation by potassium permanganate ---------- 60
3.3.3. Electrolysis with galvanostatic oxidation ---------- 64
3.3.4. Formation of H_2SO_4-GICs in diluted sulfuric acid ---------- 64
3.4. Discussion ---------- 69

3.4.1. Formation process of H_2SO_4-GICs ---------- 69
3.4.2. Overcharging process for the stage-1 H_2SO_4-GICs ---------- 73
3.4.3. Effect of dilution of sulfuric acid on the formation of H_2SO_4-GICs by chemical oxidation ---- 75
3.5. Summary ---------- 77
References ---------- 78

Chapter 4: Effect of host carbon materials on intercalation behavior
4.1. Introduction ---------- 80
4.2. Experimental ---------- 81
4.2.1. Potential measurement ---------- 81
4.2.2. Simulation of potential change ---------- 83
4.3. Results ---------- 86
4.3.1. Potential change during intercalation of sulfuric acid into various carbon materials by chemical oxidation --- 86
4.3.2. Potential change during electrochemical intercalation of sulfuric acid by galvanostatic oxidation --- 101
4.3.3. Simulated potential curves ---------- 105
4.4. Discussion ---------- 106
4.4.1. Effect of host material on intercalation of sulfuric acid --- 106
4.2.2. Effect of reaction rate on intercalation behavior ---------- 114
4.4.3. Criterion for intercalation reaction on host material ------- 115
4.5. Summary ---------- 120
References ---------- 121

Chapter 5: Electrochemical reduction of GIC with sulfuric acid synthesized by chemical oxidation and its application to lead-sulfuric acid battery
5.1. Introduction ---------- 123
5.2. Experimental ---------- 124
5.3. Results ---------- 125
5.3.1. Potential change during electrochemical reduction of H_2SO_4-GICs ---------- 125
5.3.2. Repetition of nitric acid oxidation and electrochemical reduction ---------- 127
5.3.3. Effect of amount of nitric acid on electrochemical reduction 133
5.3.4. Effect of host material on electrochemical reduction -------- 135
5.3.4. Construction of lead-sulfuric acid battery ---------- 138
5.4. Discussion ---------- 140
5.4.1. Potential change during galvanostatic reduction ---------- 140
5.4.2. Repetition process of nitric oxidation and electrochemical reduction ---------- 142
5.4.3. Application to lead-sulfuric acid battery ---------- 144
5.5. Summary ---------- 145

References ---------- 146

Chapter 6: Exchange reaction of metal-chlorides for metal-hydroxides in graphite gallery
6.1 Introduction ---------- 147
6.2 Experimental ---------- 148
6.2.1. Synthesis of chloride-GICs ---------- 148
6.2.2. Electrochemical treatment of chloride-GICs and characterization of treated samples ------- 148
6.3 Results ---------- 151
6.3.1. Structure and composition of chloride-GICs ---------- 151
6.3.2. Electrochemical treatment of chloride-GICs ---------- 153
6.4 Discussion ---------- 166
6.5 Summary ---------- 171
References ---------- 172

Chapter 7: Application of GICs with metal hydroxides to alkaline secondary battery and its performance
7.1. Introduction ---------- 174
7.2. Theory of charge and discharge reactions on nickel hydroxide electrode ---------- 175
7.3. Experimental ---------- 179
7.3.1. Preparation of hydroxide-GIC electrode ---------- 179
7.3.2. Determination of activation energies for charge and discharge reactions on the hydroxide-GIC electrode ------ 179
7.3.3. Discharge performance under a large current density --------- 181
7.4. Results ---------- 181
7.4.1. Activation energy for charge and discharge reactions -------- 181
7.4.2. Discharge performance on hydroxide-GIC electrode ---------- 183
7.5. Discussion ---------- 184
7.6. Summary ---------- 186
References ---------- 186

Chapter 8: Conclusion
8.1. Conclusion for the present work ---------- 188
8.2. Prospect ---------- 190
8.2.1. Potential measurement ---------- 190
8.2.2. Effect of host carbon material on intercalation ---------- 191
8.2.3. Graphite intercalation compounds with metal hydroxide ------- 192
8.2.4. Application to battery ---------- 193
References ---------- 194

List of Publication ---------- 195
Acknowledgment

ABSTRACT

Potential of graphite during intercalation of sulfuric acid by chemical oxidation was found to increase to positive direction in stepwise, which corresponded to the change in stage structure of graphite intercalation compounds with sulfuric acid (H_2SO_4-GICs). It was shown that the intercalation behavior of sulfuric acid into graphite by chemical oxidation could be followed by in-situ measurement of potential.

From the potential change, the intercalation process of sulfuric acid by chemical oxidation was found to be fundamentally the same as that by electrochemical oxidation. The intercalation reaction is divided into two processes; charging of host carbon layers corresponding to potential increase and transformation of stage structure in the gallery of carbon layers showing the plateau on the potential change.

The potential increase of carbon material in sulfuric acid by chemical oxidation is limited by equilibrium potential, which depends strongly on the activities of each chemical species in the solution. The effect of dilution of sulfuric acid on the formation of H_2SO_4-GICs could be explained in term of the balance between upper limit of saturated potential of chemical oxidation and onset potential for each stage structure.

The crystalline structure and texture of various carbon materials were characterized with X-ray powder diffractometry, measurement of electronic properties and high-fidelity scanning microscopy, in order to help understanding of the intercalation behavior. The relations among the structural parameters measured and texture of carbon materials were discussed. It was shown to be important to relax some strain on hexagonal carbon layer planes in order to proceed graphitization. Whether the

strain in carbon layers can be removed during heat-treatment at high temperatures is strongly influenced not only by its starting material, but also its texture.

The intercalation of sulfuric acid into the host with high graphitization degree was found to proceed easily. On the other hand, the host with turbostratic structure could not be intercalated with sulfuric acid. Thus, the host must have certain degree of graphitization in order to from H_2SO_4-GICs. A structural criterion on the host for the intercalation was found to have the crystallite size along the c-axis of more than 20 nm. A electronic criterion on the host seemed to have a positive value of magnetoresistance at room temperature.

For the electrochemical decomposition of H_2SO_4-GICs synthesized by chemical oxidation in sulfuric acid solution with an excess amount of nitric acid, a large amount of electric quantity was needed, much larger than theoretical value. This result was explained by the fact that the chemical oxidation to H_2SO_4-GICs in sulfuric acid solution with nitric acid, which remained in the solution, occurred together with the electrochemical reduction of H_2SO_4-GICs.

The overall rate of intercalation of sulfuric acid by chemical oxidation depended not only on the amount of oxidant added, but also on the structure and texture of host carbon materials. As the result, the electric quantity for de-intercalation from H_2SO_4-GICs synthesized by chemical oxidation depended strongly on the texture of the hosts.

The graphite formed by electrochemical reduction of H_2SO_4-GICs was chemically oxidized by opening the circuit and again sulfuric acid was able to be intercalated into the gallery of graphite, accompanying the increase in potential. Based on the chemical charging and electrochemical discharging, a battery was

constructed by using graphite and lead metal as positive and negative electrodes, respectively. The battery showed high performance with an open circuit voltage of about 1.4 V, well-defined plateau in the discharge and larger capacity than theoretical one.

The graphite intercalation compounds with metal hydroxides (hydroxide-GICs) were synthesized through a galvanostatic oxidation of GICs with corresponding chlorides in an alkaline medium. The amount of nickel hydroxide formed in the graphite gallery could be followed by measuring electric quantity during discharge. Since the exchange reaction of chloride for hydroxide took place at the edge of graphite layers, the nickel efficiency of the original GIC prepared from the host with small flake size was higher than the compound from large size.

The hydroxide-GIC could be applied to positive electrode of alkaline secondary battery. Activation energies for charge and discharge reactions on the hydroxide-GIC electrode were measured from the dependence of potential change after opening the circuit on temperature. The hydroxide-GIC had a surpassing discharge performance with low activation energy for discharge reaction, compared with the conventional electrode of nickel hydroxide mixed with graphite. This high performance is due to structure of hydroxide-GIC, in which a layer of nickel hydroxide is sandwiched in between conductive carbon layers, and electrons are easily transferred from intercalates to host carbon layers.

論　文　要　旨

化学酸化による硫酸の黒鉛へのインターカレーション時のポテンシャルは，生成する黒鉛層間化合物のステージ構造に対応して階段状に上昇することを初めて見出した。これは，硫酸のインターカレーション挙動がポテンシャル変化の測定によって追跡できることを示唆している。

化学酸化による硫酸－黒鉛層間化合物の生成反応が電気化学酸化による生成反応と基本的に同じプロセスであることをポテンシャル変化より明らかにした。そのプロセスは，ポテンシャルの上昇に相当する黒鉛層の充電とポテンシャル変化の平坦部分に相当するステージ構造の移行に大別することができた。

化学酸化による硫酸－黒鉛層間化合物生成には，酸化剤の酸化還元反応に関連する飽和ポテンシャルの上限値が存在した。この飽和ポテンシャルの上限値とステージ構造の移行を示すポテンシャル値の関係から，化学酸化による硫酸－黒鉛層間化合物生成における硫酸濃度の影響を半定量的に説明することができた。

種々の炭素材の構造と組織をＸ線解析，電子物性値測定および走査電子顕微鏡観察によって評価し，その炭素材の構造および組織に関する情報との対応性を検討した。その結果，高温熱処理によって炭素材を黒鉛化するには，炭素六角網平面における歪を緩和することが重要であることが見出された。そして，網平面の歪が除去されるか否かは，炭素材の前駆体だけでなく，組織にも強く依存することを実験的に示した。

化学酸化による硫酸のインターカレーション反応時のポテンシャル変化は，用いた炭素材の構造，組織および粒径に強く依存した。このインターカレーション挙動に対する炭素材の影響は，ポテンシャルの上昇に相当する黒鉛層の充電プロセスとポテンシャル変化の平坦部分に相当するステージ構造の移行プロセスの相対速度の違いによって説明することができた。

硫酸のインターカレーション反応は，黒鉛化度の高い材料ほど容易に進行することがポテンシャル変化より見出された。一方，全く黒鉛的積層構造を持たない（乱層構造を持つ）炭素材へは硫酸がインターカレーションされないことが観察された。この結果は，硫酸のインターカレーション反応に対して，ホスト炭素材においてある基準値が存在すると考えられた。そこで，インターカレーションされた炭素材とされなかった炭素材とを比較，検討した。その結果，ホスト炭素材の構造における基準は，２０ｎｍ以上のｃ軸方向の結晶子サイズを有することで

あった。また，電子物性値における基準は，その炭素材が室温において正の磁気抵抗値を示すことと考えられた。

硝酸を含んだ硫酸溶液中，化学酸化によって合成された硫酸－黒鉛層間化合物を電解還元分解するのに必要な電気量は，理論電気量より大きい結果が得られた。これは，層間化合物への化学酸化が電解還元中においてでさえも作用していると考えられた。

化学酸化によって合成された硫酸－黒鉛層間化合物の分解に必要な電気量は，電解還元反応と化学酸化反応の相対速度によって，変化する結果が得られた。化学酸化による硫酸のインターカレーション反応の速度は，酸化剤の添加量だけでなく，ホスト炭素材の構造および組織に依存するために，化学酸化によって合成された硫酸－黒鉛層間化合物の分解に必要な電気量および電解還元時のポテンシャル変化もまた，炭素材の組織に強く依存することが見出された。

層間化合物の還元によって生成した黒鉛は，開回路状態において硝酸によって酸化され，ポテンシャル上昇をともなって硫酸が再びインターカレートした。この硝酸酸化によるインターカレーション反応が充電に，その逆の電解還元によるデインターカレーション反応が放電に対応することから，正極に黒鉛，負極に金属鉛を使用した電池の応用を検討した。その結果，約１．４Ｖの開回路電圧，平坦性の良い放電曲線および理論量より大きい放電容量が得られた。

金属水酸化物－黒鉛層間化合物は，金属塩化物－黒鉛層間化合物をアルカリ水溶液中，電解酸化を施すことによって合成することができた。これは，塩化物から水酸化物への転換反応が黒鉛層間で起こっていることを示唆する。塩化ニッケルから水酸化ニッケルの転換量は層間化合物電極を電解還元する際の電気量から追跡することができた。この転換反応は，黒鉛構造のエッヂから進行するため，使用したホスト炭素材の粒径に強く依存する結果が得られた。

この金属水酸化物－黒鉛層間化合物は，アルカリ二次電池の正極材として使用することができた。この電極の充放電反応の活性化エネルギーを開回路後のポテンシャル変化の温度依存性から求めた。層間化合物電極の放電反応の活性化エネルギーは，通常の水酸化ニッケル電極の約半分であった。また，層間化合物電極の放電曲線は，放電電流密度が増加してもポテンシャルの低下が小さく，この層間化合物電極は放電性能が良好であることが見出された。これは，電池活物質である水酸化ニッケルが黒鉛の層間に位置し，しかも，黒鉛層との間に電荷移動が存在するためであると考えられた。

CHAPTER 1

Introduction

1.1. Carbon materials

The carbon element, C with atomic number 6, is crystallized into diamond, graphite and carbyne, and in additional to those crystallines a variety of forms with disturbed structures are known. Recently, a new form of pure solid carbon has been synthesized consisting of spherical C_{60} and C_{70} molecules (fullerenes) [1-1]. These fullerenes have attracted the attention of scientists as a quite new carbon material.

The crystal structure of graphite is shown in Fig. 1-1. In the hexagonal net of carbon atom, each carbon atom is bound to three neighboring carbon atoms by strong covalent bond (σ bond) of sp^2 hybrid orbital. One of four valence electrons forms π bond and is equally resonated in the layer plane. The interaction force between layer planes is so weak that it has been said van der Waals force. The ABAB•••• sequence of parallel stacking of layer planes is the most common in natural graphite, of which crystal belongs to the hexagonal system. The unit cell of graphite is shown in Fig. 1-1 by bold line. The lattice constant along the a-axis, a_o is 0.2456 nm and one along the c-axis, c_o, is 0.6708 nm, which is twice of the spacing between two adjacent layer planes (interlayer spacing, $\bar{d}_{002}$, is 0.3354 nm). Another sequence of layer stacking in graphite, ABCABC•••• , (rhombohedral modification) is found in the samples experienced severe shearing stress. The structure, in which graphite-like layer planes stack in parallel but rotate randomly about their normal, is called "turbostratic" one. The interlayer spacing $\bar{d}_{002}$ in this turbostratic structure has been to be 0.344 nm [1-2].

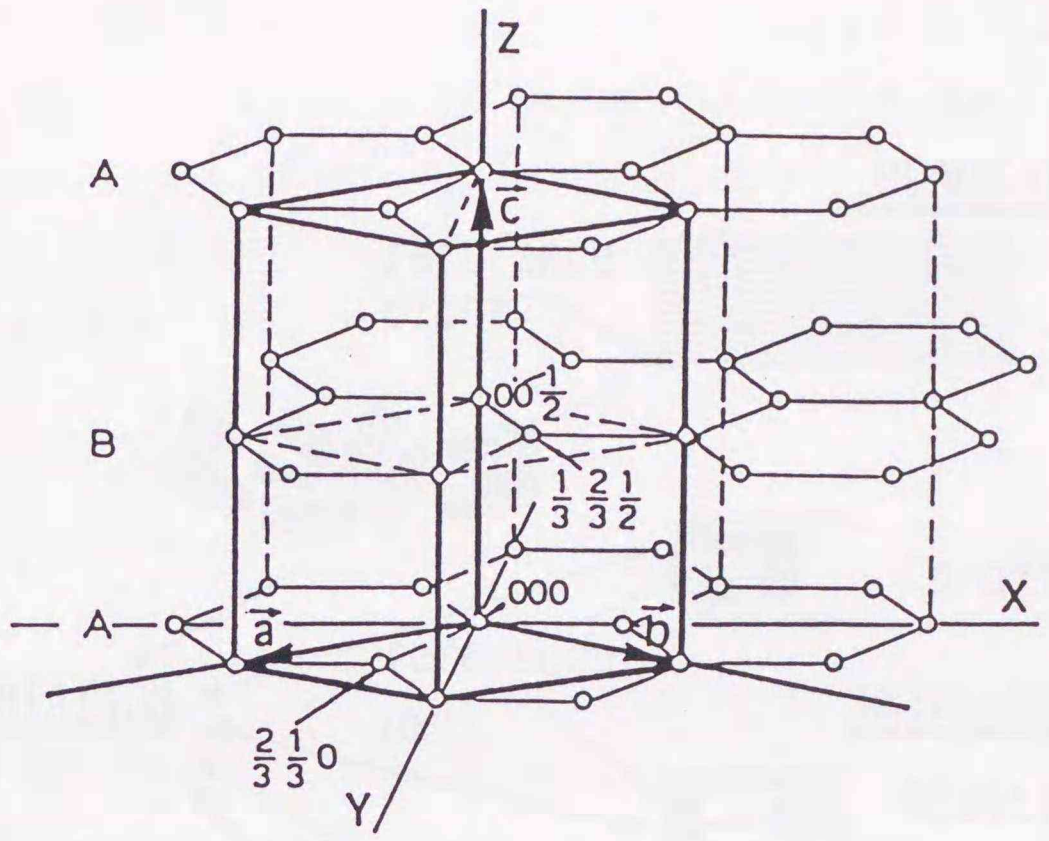


Fig. 1-1 Structure of graphite.

Carbon materials, which are prepared by pyrolysis of various organic substances (carbonization), usually at 1300-1500°C, consist of elemental domains with turbostratic stacking of graphite-like layers with as small diameter as 1-1.5 nm, in which the number of layers stacked is only 2-3 [1-3]. By heat-treatment at above 2000°C, turbostratic structure in carbons gradually changes towards the graphite structure, i. e., three-dimensional ordering of layers and the growth of crystallites occurs (graphitization).

Inagaki [1-4] proposed a classification of "microtexture" of carbon materials on the basis of the scheme of orientation of graphite-like layers, as reproduced in Fig. 1-2. Each carbon material has different microtexture, in other words, different ways of aggregation of the elemental domains. This microtexture of carbon materials is known to govern their graphitization

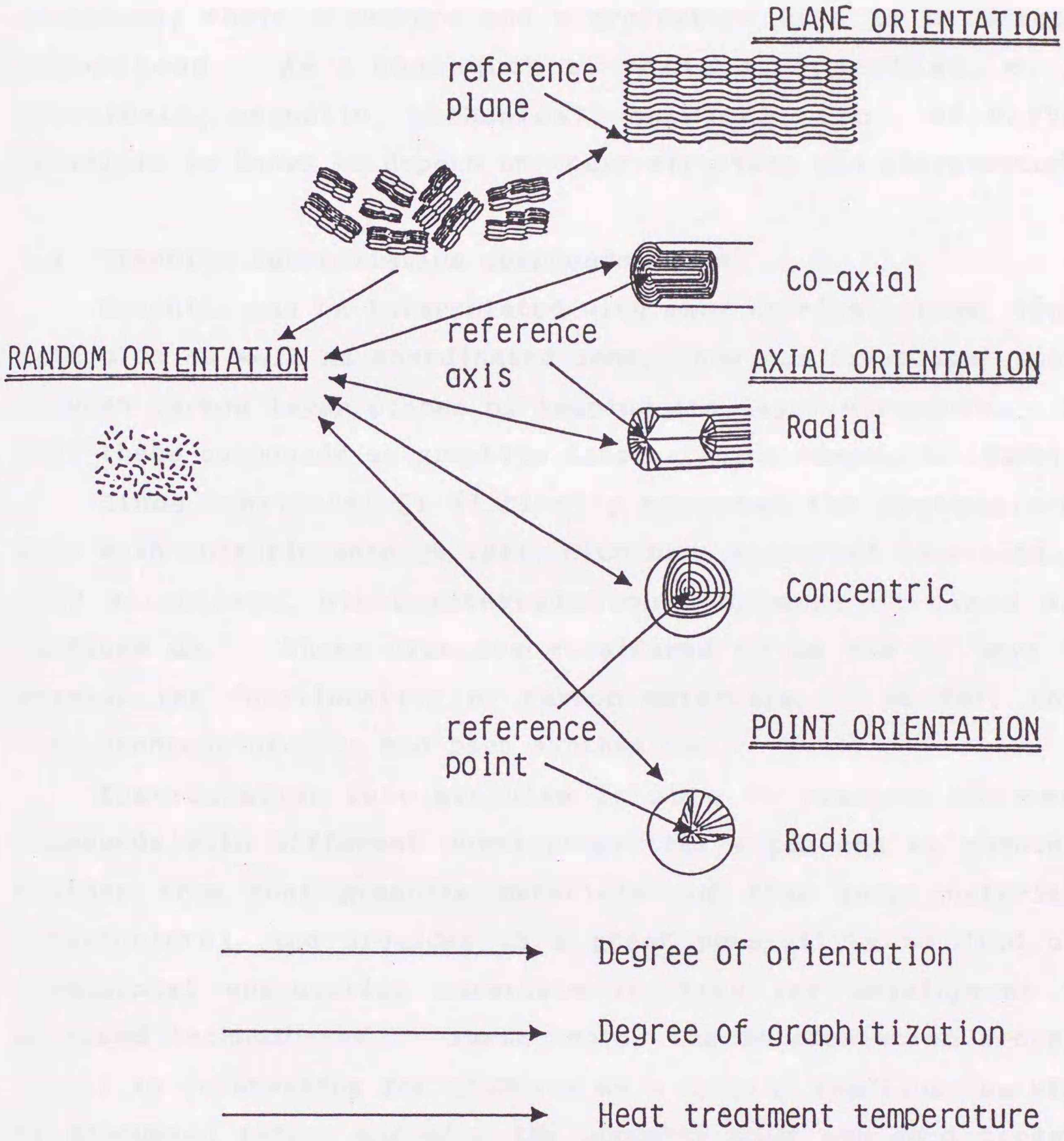


Fig. 1-2 Scheme of classification of microtexture in various carbon materials [1-4].

behavior at high temperatures. To characterize the carbon materials prepared from different precursors and by different processes, their structure and microtexture have to be exactly understood. As a consequence, various properties, e. g. electronic, magnetic, mechanical, chemical, etc., of carbon materials is known to depend on their structure and microtexture.

1.2. Graphite intercalation compounds (GICs)

Graphite can be intercalated with many species, atoms, ions, molecules as well as coordinated ions, into its interlayer space between carbon layer planes by keeping its layer structure. We call these compounds as graphite intercalation compounds (GICs).

Since Schaffautl [1-5] firstly reported the synthesis of GICs with sulfuric acid in 1841, GICs have attracted interests of many scientists, other intercalation compounds of clays and sulfides do. These GICs are considered to be one of ways to develop the functionality of carbon materials. So far, more than hundreds of GICs had been synthesized.

Intercalation into graphite is able to produce numerous compounds with different novel properties which can be obtained neither from host graphite materials nor from guest materials (intercalate), and provides us a great possibility to find out fundamental engineering materials required for development of advanced technologies. Furthermore, the intercalation process itself is interesting for chemists as a special reaction, as will be discussed later, and also the products GICs are good targets for physicists to study on two-dimensional phenomena.

1.2.1. Short history

The history of study on the graphite intercalation compounds seems to be roughly divided into three periods, according to

Inagaki [1-6]; before 1974, from 1974 to 1987 and after 1987. In the first period, attentions were paid mainly on the synthesis of new GICs using various kinds of reagents by different techniques. A lithium primary battery using one of GICs, graphite fluoride, was commercialized in 1974 [1-7]. In 1976, Vogel, et al [1-8, -9] reported that AsF_5-GIC showed electrical conductivity higher than that of metallic copper. It was an epoch in the science and technology of GICs. During the second period, a number of chemists and physicists have done a lot of works on the synthesis, structure, properties and also applications of GICs. In recent few years, people have started to be interested and to work much more, more than anytime before, on the related problem to the applications of GICs, associated with energy and environment problems. Many works are carried out in order to find host carbon materials and intercalates suitable for the application for GICs.

1.2.2. Classification

Graphite intercalation compounds can be divided into two classes, ionic and covalent compounds, according to the nature of bonding between carbon layers and intercalated species.

Graphite fluorides and graphite oxide belong to covalent compounds. The ionic GICs, in which charge transfer occurs between host and guest (intercalate), are further classified into donor-type (electrons are given from guest to host) and acceptor-type (electrons from host to guest) compounds. In Table 1-1, various guest materials which have formed GICs are summarized, according to this classification.

In addition, the residue compounds which are formed from the decomposition of GICs and contain certain amount of guest species with random arrangement in interlayer space between

carbon layers (gallery), may considered as an another kind of GICs in extensive meaning.

Table 1-1 Classification of graphite intercalation compound.

Bond type	State of charge of intercalate	Example of intercalates
ionic	donor-type	Li, Na, K, Rb, Cs, Ca, Sr, Ba, Mn, Fe, Ni, Co, Zn, Mo, Sm, Eu, Yb, K-Hg, Rb-Hg, $K-NH_3$, $Ca-NH_3$, $Eu-NH_3$, $Be-NH_3$, K-THF, $H-NH_3$, K-DMSO, K-DME, Cs-acethylene.
	acceptor-type	Br_2, ICl, IBr, IF_5, $CuCl_2$, $FeCl_2$, $FeCl_3$, $NiCl_2$, $AlCl_3$, $SbCl_5$, AsF_5, SbF_5, NbF_5, XeF_5, CrO_3, MoO_3, $Zn(NO_3)_2$, $Cu(NO_3)_2$, HNO_3, H_2SO_4, $HClO_4$, H_3PO_4, $Ni(OH)_2$, $Fe(OH)_3$, $Cu(OH)_2$, ClO_4^-, PF_6^-, BF_4^-.
covalent		graphite fluoride, graphite oxide.

1.2.3. Structure

a) Along the c-axis (Staging)

GICs are characterized by a stage structure, in which the intercalate layers are distributed periodically in the gallery of

carbon layers. A stage-n structure indicates that two neighboring intercalate layers are separated by (n-1) carbon layers, as shown in Fig. 1-3. Stage structure is characterized by identity period along the c-axis, I_c, which is determined with X-ray powder diffractometry. The spacing of intercalated carbon layer is defined as d_1, and the thickness of intercalate as Δd. These parameters are related with each others, as follows;

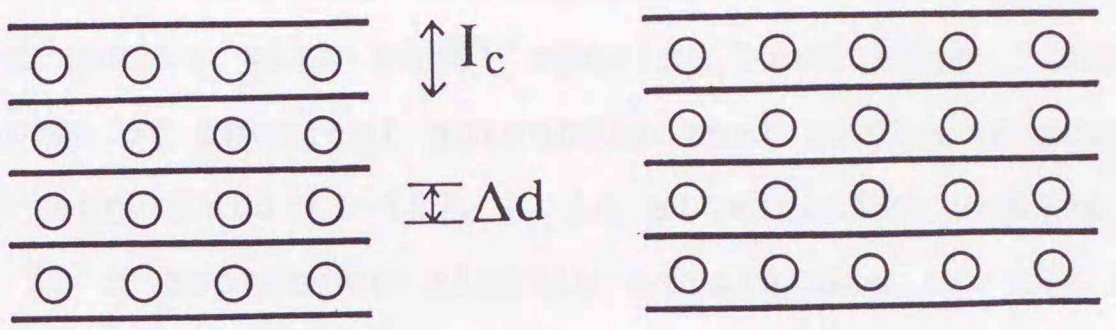
$$d_1 = \Delta d + 0.3354 \ , \qquad (1\text{-}1)$$

$$\begin{aligned} I_c &= d_1 + 0.3354 \cdot (n-1) \ , \\ &= \Delta d + 0.3354 \cdot n \ , \qquad [\text{in nm}] \end{aligned} \qquad (1\text{-}2)$$

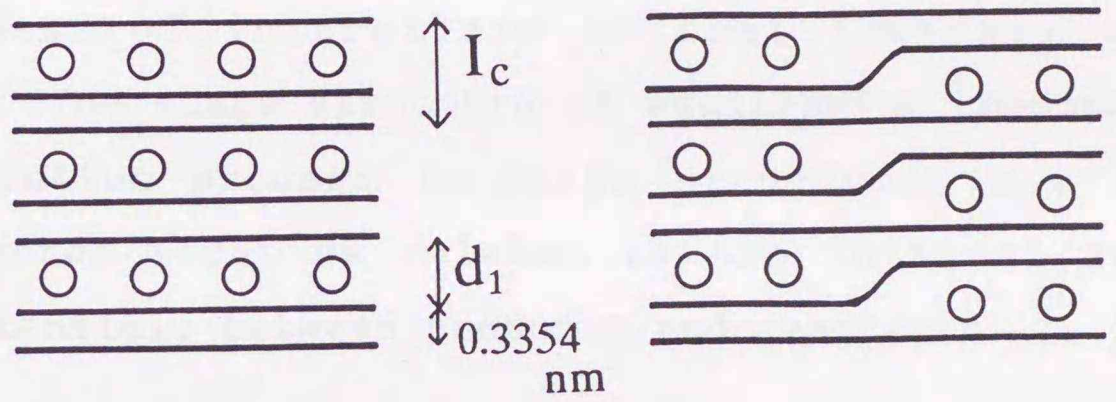
where 0.3354 nm is interlayer spacing in graphite structure and n stage number.

The model for describing the stage structure of GICs, which is widely accepted now, is so-called Doumas-Herold model [1-10], in which each gallery contains certain number of islands of intercalated species and they are arrayed in perpendicular direction (c-axis direction) to form stage structure. In Fig. 1-3, the classical and Doumas-Herold models for different stage structures are compared. In the Doumas-Herold model, the carbon layers are pleated, as shown in Fig. 1-3(b), which is a point for controversy.

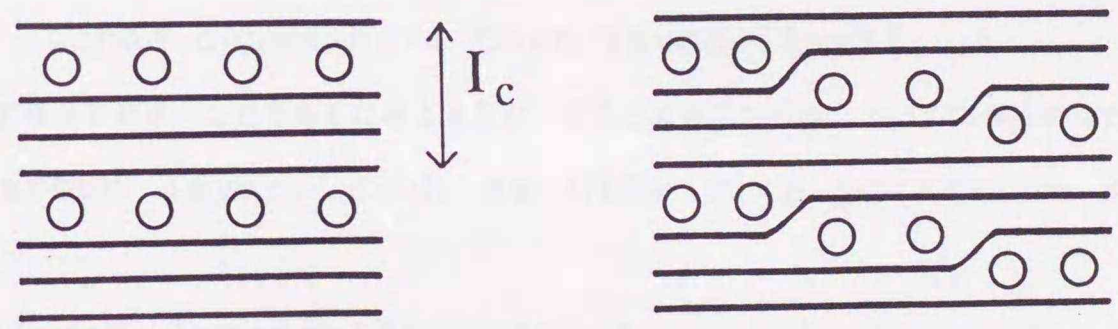
The formation of stage structure (staging phenomenon) has been studied by statistical thermodynamics [1-11, -12] and explained by electrostatic and elastic interactions. Between charged intercalate layers, there exists electrostatic repulsive interaction, which seems to be a main motive force for staging. As a result of the electrostatic energy calculation on a continuum model by Thomas-Fermi equation, it was suggested that at a certain chemical potential, internal energy of intercalates



stage-1



stage-2



stage-3

(a) (b)

Fig. 1-3 Models of stage structure in graphite intercalation compounds.
(a) Classical model, (b) Doumas-Herold model.

is minimized by a certain arrangement of intercalates in the gallery of graphite with equal spacing, and also there is an important range of chemical potential that reflects the stability of the stage structure [1-12]. An alternative motive force for the staging is a repulsive elastic strain due to the separation of gallery of graphite by the intercalation [1-13]. For a stack of intercalate islands in an infinite graphite medium, the elastic interaction is repulsive, which is relaxed by the rearrangement of intercalate so that internal energy is minimized. The stage structure of equilibrium compound as well as the evolution process in stage structure in a specified reaction system might be related to the internal energy and chemical potentials between products and reactants.

b) In-plane

In the in-plane arrangement of intercalates in the gallery of graphite, three cases have been found [1-14];

1) an ordered intercalate structure commensurate with hexagonal carbon layer, such as GICs with potassium metal (KC_8 and KC_{24}).

2) an ordered intercalate structure but incommensurate with carbon layers, e. g. GIC with iron chloride ($FeCl_3$-GIC).

3) a disordered liquid-like intercalate layer, as in the case of GICs with acids.

1.2.4. Synthesis

The methods for synthesis of GIC are divided into reactions of gaseous, liquid and solid phases of guest material with host graphite.

a) Gaseous phase reaction

The classical two-bulb vapor method is the most frequently used for the synthesis of GICs with metal chlorides and alkali metals, by placing host graphite and guest are separately in a reaction ample, as shown schematically in Fig. 1-4. Usually, the graphite site is kept at a temperature (T_g) slightly higher than that of guest site (T_m). In this method, it is easy to get the compounds with well-defined stage structure and composition by controlling precisely the reaction conditions, temperatures of T_g and T_m of two bulbs and reaction time.

The GICs with bromine are formed by contacting with bromine vapor to graphite at room temperature, of which composition depends on partial pressure of the bromine vapor.

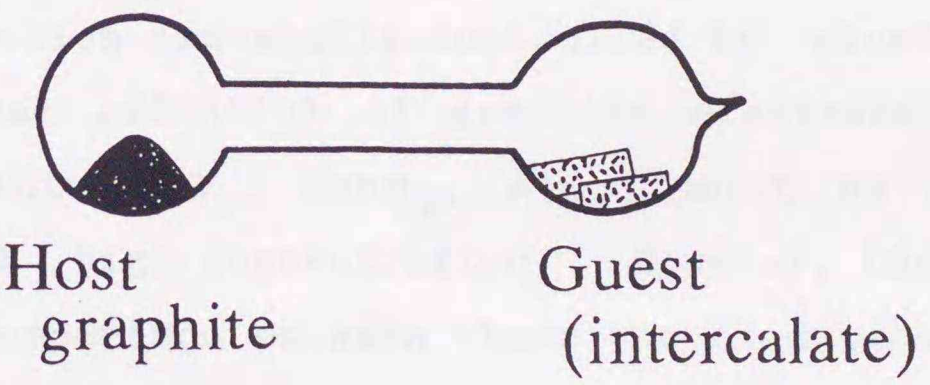


Fig. 1-4 Scheme of reaction ampoule for two-bulb method.

b) Liquid phase reaction

The intercalation into graphite by the reaction with liquid phase of an intercalate is further classified into chemical and electrochemical ones.

A typical example of chemical intercalation is the formation

of GICs with nitric acid (HNO_3-GICs); the stage-2 of HNO_3-GIC is synthesized by immersing a host into fuming nitric acid at room temperature. A group of Inagaki [1-15, -16] established the procedure for the synthesis of GICs with different metal chlorides by using molten salts of corresponding chlorides.

In an organic solvent, e. g. propylene carbonate (PC), nitromethane (NM), dimethylsulfoxide (DMSO), etc., anions (ClO_4^-, PF_6^- and BF_4^-) and cations (alkali and alkaline earth metal ions) are known to intercalate by electrochemical polarization of graphite electrode to cathodic and anodic directions, respectively.

The GIC with sulfuric acid (H_2SO_4-GICs) can be synthesized by either chemical or electrochemical oxidations. The latter has been used by many authors, because stage structure and intercalation reaction are easily controlled by electric current and electrochemical potential of graphite electrode. In the former, an oxidant (HNO_3, $KMnO_4$, etc.) must be added into sulfuric acid with high concentration. However, there has been no quantitative comparison between these two oxidations, which is one of purposes of the present thesis.

c) Solid phase reaction

Guerard, et al. [1-17] synthesized the GICs with lithium by compressing a mixture of graphite with lithium metal and by annealing at 200°C. By this method, GICs with alkaline earth metals (barium, strontium, etc.) were also synthesized [1-18].

1.3. Applications of GICs

1.3.1. Function of GICs

A lot of novel properties may be expected from various kinds of GICs. On the functions of GICs, several excellent reviews

have been published [1-6, -19]. According to these reviews, the possibilities of applications of GICs are summarized into five fields in Table 1-2; highly-conductive materials, electrode materials for batteries, catalysts for organic synthesis, materials for hydrogen-storage and isotope-separation, and others such as exfoliation of graphite, electrochromism, etc.

These applications are based on the following functions of GICs [1-18];

1) creation of a new function by the formation of GICs (highly-conductive materials and electrochromism).

2) efficiency enhancement of functions of guest materials by the formation of GICs (electrode materials for batteries and catalysts for organic synthesis).

3) creation of functional space by the formation of GICs (materials for hydrogen-storage and isotope-separation).

4) function created by intercalation and de-intercalation processes (electrode materials for batteries and exfoliation of graphite).

Of those possibilities, the practical success has been achieved in lithium battery using graphite fluorides as positive electrode material and in the production of exfoliated graphite.

In despite of fascinating possibilities as shown in Table 1-2, the applications of GICs still has not shown much development. One of the reasons is a lack of sufficient properties for the severe requirements from the advanced technologies, particularly the lack of stability and reproducibility of properties of GICs.

1.3.2. Application of GICs to secondary batteries

The applications of GICs for electrode materials of primary and secondary batteries have been reviewed [1-6, -20]. The electrochemical reactions occurring on the electrode are

Table 1-2 Functions of graphite intercalation compounds [1-6].

1. Highly-conductive materials HNO_3, SbF_5, AsF_5, $CuCl_2$, $FeCl_3$, F_2, K-Bi, residual Br_2.	Combinations between host graphite and intercalates
2. Electrode materials in batteries Primary battery $(CF)_n$, $(C_2F)_n$, graphite oxide, F_2, $CoCl_2$, TiF_4, etc.	Efficiency enhancement of function of intercalates
Secondary battery H_2SO_4, $Ni(OH)_2$, $Mn(OH)_2$, HF.	Intercalation and de-intercalation processes
Thermocell Br_2, HNO_3.	
3. Catalysts for organic synthesis Li, K, H-Hg, K-$FeCl_3$, SbF_5, Br_2, H_2SO_4, HNO_3, etc.	Efficiency enhancement of function of intercalates
4. Materials for storage and isotope-separation of hydrogen K, Rb, Cs.	Creation of functional space in intercalation compounds
5. Others Exfoliation of graphite H_2SO_4, HNO_3, $FeCl_3$, K-THF, Na-THF	Intercalation and de-intercalation processes
Thermal energy storage $MnCl_2$-NH_3	
Electrochromism Li-DMSO	

summarized in Table 1-3, by showing both a general scheme and a specific example for each type. In most cases, intercalated ions are often solvated, although the solvating molecules are not shown in the formulae. The secondary batteries used GICs can be divided by the function of GICs into two types; in one type active material for battery is held in the gallery of graphite and in the other intercalation and de-intercalation reactions are regarded as charging and discharging, respectively.

Table 1-3 Electrochemical reactions on the electrodes in battery with graphite intercalation compounds.

General formula	Examples	
$C_nAB \rightleftharpoons C_nA + B^+ + e^-$	$C_nNi(OH)_2 \rightleftharpoons C_nNiOOH + H^+ + e^-$	(1)
$DC_nA \rightleftharpoons C_nA + D^+ + e^-$	$Li_mC_nFeCl_3 \rightleftharpoons C_nFeCl_3 + mLi^+ + e^-$	(2)
$C_nA + B^- \rightleftharpoons C_nAB + e^-$	$C_nFeCl_2 + Cl^- \rightleftharpoons C_nFeCl_3 + e^-$	(3)
$nC + A^- \rightleftharpoons C_nA + e^-$	$nC + ClO_4^- \rightleftharpoons C_nClO_4 + e^-$	(4)
$DC_n \rightleftharpoons nC + D^+ + e^-$	$LiC_n \rightleftharpoons nC + Li^+ + e^-$	(5)

The first three reactions in Table 1-3 belong to the former type, and the GICs used (C_nA and C_nAB in general formulae) must be stable in air, because they have to be synthesized before the construction of batteries. In the reactions (4) and (5) in Table 1-3, on the other hand, the intercalation and de-intercalation reactions of an anion (acceptor-type) and cation

(donor-type) for the graphite electrode are used for battery reaction, in the latter type. The reaction (4) is used as the positive electrode (cathode) and the reaction (5) as the negative one (anode). For the latter type battery, the rates of formation and decomposition processes of GIC is an important factor for battery performance, which depends strongly on the host material employed. On negative electrode of lithium secondary battery having high energy density (reaction (5)), for example, it has been reported that the intercalation and de-intercalation reactions of lithium ions in propylene carbonate (PC) into turbostratic carbon showed better performance than that into graphitic one [1-21].

1.4. Purpose of the present work

In-situ observation during intercalation reaction into graphite is powerful to study the chemistry of intercalation into carbon materials. Transformation of stage structure, diffusion behavior of intercalate into graphite, change of resistivity and expansion along the c-axis accompanied by intercalation has been studied with in-situ measurements of X-ray powder diffractogram [1-22, -23], weight, electrical resistivity [1-24, -25, -26], and size [1-27].

Since graphite itself is a conductive material, reactions of graphite in electrolyte, which are either electrochemical or chemical processes, can be followed by measuring electrochemical potential.

The purpose of the present work is the intercalation reaction of sulfuric acid into various carbon materials and exchange reaction of metal chloride for metal hydroxide in graphite gallery are followed by in-situ measurement of potential. From the measurements of potential, intercalation

process, influence of host material on intercalation behavior and battery performance of GIC electrodes were discussed. The host carbon materials used were characterized with high-fidelity scanning electron microscopy, X-ray powder diffractometry and magnetoresistance measurement, and the relations between these structural parameters were discussed in the relation to the texture in micrometric scale of host carbon materials.

1.5. Construction of the present thesis

The present thesis consists of eight chapters.

In Chapter 1, a general introduction was given on carbon materials and graphite intercalation compounds, and the purpose and construction of the present thesis were described.

The experimental, results and discussion were explained in detail in the following six chapters.

Chapter 2: The crystalline structure and texture of various kinds of carbon materials were characterized with high-fidelity scanning electron microscopy, X-ray powder diffractometry and magnetoresistance measurement, in order to understand their intercalation behaviors. The relations among structural parameters measured were discussed.

Chapter 3: The intercalation of sulfuric acid into graphite by chemical oxidation was followed by measuring potential of graphite electrode. The potential change during the chemical intercalation was compared with the one during electrochemical intercalation.

Chapter 4: Various kinds of carbon materials were used as the host for graphite intercalation compounds with sulfuric acid (H_2SO_4-GICs). The effect of host carbon material on the intercalation behavior was discussed by measuring potential

during the chemical and electrochemical oxidations.

Chapter 5: The electrochemical reduction of H_2SO_4-GICs synthesized by the chemical oxidation was followed by measuring potential, and compared with the compounds synthesized by electrochemical oxidation. The intercalation by chemical oxidation and the de-intercalation by electrochemical reduction were applied to lead-sulfuric acid battery.

Chapter 6: The GICs with metal hydroxides (hydroxide-GICs) were electrochemically synthesized from the GICs with metal chloride (chloride-GICs). The confirmation and mechanism for the exchange reaction of chloride for hydroxide in the gallery of graphite were discussed on the basis of results with measurement of potential, cyclic voltammetry, X-ray powder diffraction and X-ray microprobe analysis.

Chapter 7: The hydroxide-GICs were applied to alkaline secondary battery. The charge and discharge reactions on the hydroxide-GIC electrodes are followed by measuring potential. The performance of charge and discharge reactions on the electrodes was studied by measuring activation energies for both reactions. A possibility of discharge under a large current density was discussed.

Chapter 8: The conclusions of the present work were given.

References

1-1 W. Kratschmer, L. D. Lamb, K. Fostiropoulos and D. R. Huffman, Nature, **347**, 354 (1990).

1-2 J. Biscoe and B. E. Warren, J. Appl. Phys., **13**, 364 (1942).

1-3 A. Oberlin, "Chemistry and Physics of Carbon", Vol. 22, 1989, p. 1

1-4 M. Inagaki, Tanso, **1985[No. 122]**, 144 (1985).

1-5 P. Schaffautl, J. Prakt. Chem., **24**, 155 (1941).

1-6 M. Inagaki, J. Mat. Res., **4**, 1560 (1989).

1-7 N. Watanabe and M. Fukuda, U. S. Patent, 3, 536, 532, (1970) 3, 700, 502.
1-8 F. L. Vogel, Bull. Am. Phys. Soc., 21, 262 (1976).
1-9 G. M. T. Foley, C. Zeller, E. R. Faladeau and F. L. Vogel, Solid Stage Comm., 24, 371 (1977).
1-10 N. Doumas and A. Herold, Bull. Soc. Chim. Fr., 1598 (1971).
1-11 S. A. Safran, Synth. Met., 2, 1 (1980).
1-12 S. A. Safran and D. R. Hamann, Phys. Rev. B, 23, 565 (1981).
1-13 S. A. Safran and D. R. Hamann, Phys. Rev. Lett., 42, 1410 (1979).
1-14 J. E. Fischer, NATO ASI "Chemical Physics of Intercalation", Ed. By A. P. Legrand and S. Flandrois, Plenum, New York, 1988, pp. 57.
1-15 Z. D. Wang and M. Inagaki, Synth. Met., 25, 181 (1988).
1-16 Z. D. Wang, Doctor Thesis, Toyohashi University of Technology (1990).
1-17 D. Guerard and A. Herold, C. R. Acad. Sci. Ser., C, 275, 571 (1972).
1-18 D. Guerard and A. Herold, C. R. Acad. Sci. Ser., C, 279, 455 (1974).
1-19 M. Inagaki, Tanso, 1988(No. 133), 127 (1988).
1-20 S. Flandrois, Synth. Met., 4, 255 (1982).
1-21 T. Kitamura, T. Miyazaki and T. Kawagoe, Synth. Met., 18, 537 (1987).
1-22 R. Fujii, Report of Gov. Ind. Res. Inst., Osaka, No. 353 pp. 5-18 (1978).
1-23 B. Bouayad, H. Fuzellier, M. Lelaurain, A. Metrot and F. Rousseaux, Synth. Met., 7, 325 (1983).
1-24 J. G. Hooley and J. C. Smee, Carbon, 2, 135 (1964).
1-25 M. B. Dowell, D. S. Badorrek, Carbon, 16, 241 (1978).
1-26 N. Akuzawa, Y. Amari, T. Nakajima and Y. Takahashi, J. Mater. Res., 5, 2849 (1990).
1-27 J. G. Hooley, W. G. Garby and J. Valentin, Carbon, 3, 7 (1965).

CHAPTER 2

Characterization of structure and texture of carbon materials

2.1. Introduction

Carbon materials are characteristic to have a strong dependency of properties on their structure and texture, which also depend definitely on staring materials. There is a remarkable effect of the structure and texture of host materials on intercalation reactions and on various properties of graphite intercalation compounds, and it has been reviewed by Inagaki [2-1]. It is important to characterize structure and texture of host carbon materials for the comprehensive understanding of the intercalation chemistry. However, the effect of host materials on intercalation has not been clarified yet.

Average interlayer spacing, magnetoresistance, laser Raman intensity, etc. have been used as parameters of the degree of graphitization for carbon materials [2-2], assuming their definite dependence on the degree of graphitization. Exact relations between these parameters and degree of graphitization have not been clearly understood, but these relations can reasonably be supposed to depend strongly on the texture of carbon materials.

In the present chapter, the crystalline structure and texture of various kinds of carbon materials are characterized with high-fidelity scanning electron microscopy, X-ray powder diffractometry and measurement of magnetoresistance, Hall coefficient and electrical resistivity, in order to help understanding of the intercalation behavior in the following chapters. The relations among the structural parameters measured are discussed.

2.2. Experimental

The samples were selected in a variety of structure and texture, listed in Table 2-1 with their codes used in the present thesis; four kinds of flaky graphite (group code: Flaky, series code: NG, KG, AG, and PI), different cokes with different heat-treatment temperatures (HTT's) (group code: COKE, series code: PV, PC, GL and CB), high-density isotropic carbon blocks with different HTT's (IS), two kinds of pyrolytic carbon blocks commercially available and their heat-treated samples with different temperatures under different pressures (group code: PyC, series code: SSG and PYR), commercial glass-like carbon (GC), mesophase-pitch-based carbon fiber with different texture in their cross-section and with HTT's (group code: MPCF, series code: KOA, I, P, A and B) and vapor-grown carbon fibers with different fiber diameters and different HTT's (group code: VGCF, series code: OVCF, NVCF, LDG). Many of these samples were used as host materials for intercalation in the following chapters.

High-fidelity scanning electron microscopic (SEM) observation was made for selected samples under the acceleration voltage from 2 to 5 kV by using microscope with thermoionic electron gun. The fractured cross-section of the specimen was prepared by cooling it down to liquid nitrogen temperature [2-9]. No metallization of the fractured surface for the SEM observation was made.

X-ray diffraction measurement was performed on the pulverized samples mixed with high purity silicon powder as an inner standard. Average interlayer spacing ($\bar{d}_{002}$) which is a half of the lattice constant along c-axis (c_o) was determined from 002 or 004 diffraction line, and lattice constant along a-axis (a_o) from 110 line, the crystallite sizes $L_c(002)$ and $L_c(004)$ along c-axis from half-maximum width of 002 and 004

Table 2-1 The carbon samples used

Group code	Series code	Sample Code	Description	Supplier and/or Literature
Flaky	NG	NG400	Flaky natural graphite with average size of 400 μm.	Nippon Kokuen Co.
		NG46	〃 46 μm.	〃
		NG5	〃 5 μm.	〃
	KG	KG	Kish graphite grown from molten iron and purified at 2300°C in a flow of freon.	Prof. Hishiyama
	AG	KS15	Artificial graphite powder from LONZA Co. average size of 8 μm.	
	PI	NOVAX30	Graphite film prepared from polyimide "NOVAX" at 3000°C	
COKE	PV	PV-7	The coke prepared from polyvinyl-chloride and heat-treated at 3000°C.	
	PC	PC18	Pitch coke heat-treated at 1800°C.	Ref. [2-12]
		PC20	〃 at 2000°C.	〃
		PC22	〃 at 2280°C.	〃
		PC24	〃 at 2480°C.	〃
		PC27	〃 at 2700°C.	〃
		PC30	〃 at 3000°C.	〃
	GL	GL18	Coke from coal tar (Grate Lakes Co.) heat-treated at 1800°C.	Ref. [2-12]
		GL20	〃 at 2000°C.	〃
		GL22	〃 at 2280°C.	〃
		GL24	〃 at 2480°C.	〃
		GL27	〃 at 2700°C.	〃
		GL30	〃 at 3000°C.	〃
	CB	CB17	Coke B heat-treated at 1700°C for 3hours.	Ref. [2-13]
		CB19	〃 at 1900°C for 3 hours.	〃
		CB21	〃 at 2100°C for 1 hour.	〃
		CB22	〃 at 2200°C for 3 hours.	〃
		CB23	〃 at 2300°C for 1 hour.	〃
		CB25	〃 at 2500°C for 1 hour.	〃

Group code	Series code	Sample Code	Description	Supplier and/or Literature
COKE	CB	CB26	Coke B heat-treated at 2600°C for 3 hours.	Ref. [2-13]
		CB28	〃 at 2800°C for 3 hours.	〃
		CB30	〃 at 3010°C for 3 hours.	〃
IS	IS	IS08	High-density isotropic carbon block heat-treated at 880°C.	Prof. Sakai
		IS10	〃 at 1000°C.	〃
		IS15	〃 at 1500°C.	〃
		IS18	〃 at 1800°C.	〃
		IS23	〃 at 2300°C.	〃
		IS26	〃 at 2600°C.	〃
		IS29	〃 at 2900°C.	〃
PyC	SSG	SSGAS	Pyrolytic carbon block as-deposited.	Toyo Tanso Co.
		SSG25	〃 heat-treated at at 2500°C.	〃
		SSG28	〃 at 2800°C.	〃
		SSG30	〃 at 3000°C.	〃
	PYR	PYRAS	Another rot of pyrolytic carbon block as-deposited.	Toyo Tanso Co.
		PYR25-19	〃 heat-treated by HIP at 2500°C-1900 kgf/cm^2.	〃
		PYR28-10	〃 at 2800°C-1000 kgf/cm^2.	〃
		PYR28-19	〃 at 2800°C-1900 kgf/cm^2.	〃
		PYR32	〃 heat-treated at 3200°C.	〃
GC	GC	GC12	Glass-like carbon powder heat-treated at 1200°C.	
		GC20	〃 block heat-treated at 2000°C.	Tokai Carbon Co.
		GC30	〃 at 3000°C.	〃
MPCF	KOA	KOA-R	Mesophase-pitch-based carbon fiber heat-treated at 3000°C, of which texture is radial with wedge and diameter is 8～10 μm.	Koa Oil Co.
	I	I-1-28	Mesophase-pitch-based carbon fiber heat-treated at 2800°C, of which texture is radial with wedge and diameter is 16 μm.	Ref. [2-19]
		I-1-30	〃 at 3000°C, 〃 19 μm.	〃

Group code	Series code	Sample Code	Description	Supplier and/or Literature
MPCF	I	I-2-28	Mesophase-pitch-based carbon fiber heat-treated at 2800°C, of which texture is radial and diameter is 14 μm.	Ref. [2-19]
		I-2-30	〃 at 3000°C, 〃 14 μm.	〃
		I-3-26	〃 at 2600°C, of which texture is doubly-textured and diameter is 11 μm.	〃
		I-3-30	〃 at 3000°C, 〃 11 μm.	〃
		I-4-26	〃 at 2600°C, of which texture is is concentric (onion-like) and diameter is 11 μm.	〃
		I-4-30	〃 at 3000°C, 〃 11 μm.	〃
	P	P-120	Mesophase-pitch-based carbon fiber (AMOCO Co.)	
	A	A30	Mesophase-pitch-based carbon fiber heat-treated at 3000°C.	
	A	A33	〃 at 3300°C.	
	B	B30	Mesophase-pitch-based carbon fiber heat-treated at 3000°C.	
	B	B33	〃 at 3300°C.	
VGCF	OVCF	OVCF30	Vapor-grown carbon fiber heat-treated at 3000°C, of which texture is concentric (annual-ring) and diameter is 8～13 μm.	Showa Denko K. K.
	NVCF	NVCFAS	Vapor-grown carbon fiber as-grown, of which texture is concentric (annual-ring) and diameter is 0.1～1 μm.	Showa Denko K. K.
		NVCF10	〃 heat-treated at 1000°C, 〃 0.1～1 μm.	〃
		NVCF23	〃 at 2300°C, 〃 0.1～1 μm.	〃
		NVCF28	〃 at 2800°C, 〃 0.1～1 μm.	〃
		NVCF30	〃 at 3000°C, 〃 0.1～1 μm.	〃
	LDG	LDGAS	Vapor-grown carbon fiber as-grown, of which texture is concentric (annual-ring) and diameter is 2 μm.	NKK Corporation

Group code	Series code	Sample Code	Description	Supplier and/or Literature
VGCF	LDG	LDG20	Vapor-grown carbon fiber heat-treated at at 2000°C, of which texture is concentric (annual-ring) and diameter is 2 μm.	NKK Corporation
		LDG20H	〃 at 2000°C, 〃 2 μm.	〃
		LDG22	〃 at 2200°C, 〃 2 μm.	〃
		LDG22H	〃 at 2200°C, 〃 2 μm.	〃
		LDG25	〃 at 2500°C, 〃 2 μm.	〃
		LDG25H	〃 at 2500°C, 〃 2 μm.	〃
		LDG28	〃 at 2800°C, 〃 2 μm.	〃
		LDG28H	〃 at 2800°C, 〃 2 μm.	〃

lines, respectively, and the crystallite size $L_a(110)$ along a-axis from that of 110 line by the conventional method [2-3]. Probability of the nearest neighbor layers having the graphitic relation (P_1), i. e., graphitization degree, [2-4, -5] was determined by Fourier analysis of 10 and 11 diffraction profiles which were measured by a step-scanning technique with 0.02° step and 30 s accumulation (denoted hereafter as $P_1(10)$ and $P_1(11)$, respectively). Probabilities of hexagonal and rhombohedral stackings of the second neighbor layers (P_{ABA} and P_{ABC}, respectively) were calculated from the Fourier coefficients for 10 and 11 diffraction lines.

A magnetoresistance effect means the change in the electrical resistivity of a conductor with magnetic field. Magnetoresistance ($\Delta\rho/\rho$) is defined by

$$\Delta\rho/\rho = [\rho(B) - \rho(0)]/\rho(0), \qquad (2\text{-}1)$$

where $\rho(B)$ and $\rho(0)$ are the resistivities ρ in a magnetic field B and zero, respectively. $(\Delta\rho/\rho)$ was measured at liquid nitrogen temperature in magnetic fields up to 1 T with direct immersion of the specimens into coolant [2-6]. From the dependence of $(\Delta\rho/\rho)$ on magnetic field direction in the plane perpendicular to the current direction of the specimen, the maximum absolute value of magnetoresistance $(\Delta\rho/\rho)_{max}$ and minimum absolute value $(\Delta\rho/\rho)_{Tmin}$ were determined. The other minimum absolute value of magnetoresistance $(\Delta\rho/\rho)_{TLmin}$ was also determined in the plane including the current direction and the one for $(\Delta\rho/\rho)_{max}$. The sum of these three $(\Delta\rho/\rho)$ values was defined as the average crystallite layer plane transverse magnetoresistance, $(\Delta\rho/\rho)_{cr}$, which is positive for graphitic structure but negative for turbostratic one, being a parameter for graphitization [2-6, -7]. The ratios of $(\Delta\rho/\rho)_{Tmin}$ and $(\Delta\rho/\rho)_{TLmin}$ to $(\Delta\rho/\rho)_{max}$ gave the anisotropy ratio r_T and r_{TL}, respectively.

$$(\Delta\rho/\rho)_{cr} = (\Delta\rho/\rho)_{max} + (\Delta\rho/\rho)_{Tmin} + (\Delta\rho/\rho)_{TLmin} \quad (2\text{-}2)$$

$$r_T = (\Delta\rho/\rho)_{Tmin}/(\Delta\rho/\rho)_{max} \quad (2\text{-}3)$$

$$r_{TL} = (\Delta\rho/\rho)_{TLmin}/(\Delta\rho/\rho)_{max} \quad (2\text{-}4)$$

A rectangular of specimen with five-ears was adopted to measure Hall coefficient. When electrical current is flowing along the longitudinal direction of the specimen (x-direction) and magnetic field is applied perpendicular to the surface of the specimen (z-direction), an electric voltage is generated across the width of the specimen, i. e., perpendicular to the plane defined by electrical current and magnetic field direction in y-direction in rectangular coordinate. This phenomenon is known as Hall effect. Hall coefficient, R_H, is defined by the

following equation;

$$R_H = \frac{V_H \cdot t}{B \cdot I} , \qquad (2\text{-}5)$$

where V_H is Hall voltage, t thickness of specimen, B magnetic field and I electric current. The direction of V_H depends carrier species, i. e. electrons or holes. In the present experimental configuration, V_H is measured to be positive for holes and negative for electrons. The R_H was measured at liquid nitrogen temperature in magnetic field up to 1 T [2-8]. For the R_H measurement, a strip-shaped specimen was needed so that only limited number of samples could be used.

For the samples measured R_H, electrical resistivity, ρ, was determined by a direct current four terminal method at liquid nitrogen temperature.

From $(\Delta\rho/\rho)_{cr}$, R_H and ρ-values, the concentration and mobility of carriers in the samples were calculated. It has been known that turbostratic carbon having $(\Delta\rho/\rho)_{cr} < 0$ and graphitic one having $(\Delta\rho/\rho)_{cr} > 0$ is associated with one-carrier and two-carrier conductions, respectively [2-7]. In the case of one-carrier conduction, the R_H-value is positive for hole conduction but negative for electron conduction as described above, and concentration and mobility of carriers can estimated from R_H- and ρ-values by the following equations [2-8];

$$\frac{1}{\rho} = n \cdot e \cdot \mu , \qquad (2\text{-}6)$$

$$R_H = \frac{1}{n \cdot e} , \qquad (2\text{-}7)$$

where n is the carrier concentration, μ the mobility, and e the elementary electric charge ($e = 1.6 \times 10^{-19}$ C).

In graphitic carbon, two-carrier conduction must be assumed because of positive value of $(\Delta\rho/\rho)_{cr}$. If carrier concentrations of electron and hole (n_e and n_h, respectively) were assumed to be equal with each other, i. e., $n = n_e = n_h$, mobilities of electron and hole (μ_e and μ_h, respectively) could be determined by the following equations [2-8];

$$\frac{1}{\rho} = n \cdot e \cdot (\mu_e + \mu_h) , \qquad (2\text{-}8)$$

$$R_H = \frac{1}{n \cdot e} \cdot \frac{(\mu_e - \mu_h)}{(\mu_e + \mu_h)} , \qquad (2\text{-}9)$$

$$(\Delta\rho/\rho)_{cr} = \mu_e \cdot \mu_h \cdot B^2 , \qquad (2\text{-}10)$$

where B is magnetic field.

2.3. Results

2.3.1. Texture seen by microscopy

SEM micrographs of the sample SSG30 are shown in Fig. 2-1. In the basal plane of the pyrolytic carbons prepared by cleaving, pebble structure is observed and remained even after the heat-treatment at 3000°C (Fig. 2-1(a) and (b)). Consequently, some strains on carbon layer planes corresponding to the pebble structure are clearly seen on the edge plane in the fractured surface of the sample SSG30 (Fig. 2-1(c) and (d)).

SEM micrographs of the texture in the cross-section of the sample group of mesophase-pitch-based carbon fibers (MPCF) are shown in Fig. 2-2. Radial texture in the fibers KOA-R, I-1 and I-2, and concentric texture (onion-like texture) in the fibers I-4 are clearly seen. The fibers KOA-R and I-1 have an open wedge. The opening angle of wedge in the fiber KOA-R (Fig. 2-2(a)) is larger than the one in the fiber I-1-30 (Fig. 2-2(b)), though the HTT is the same as 3000°C. In the fibers I-3, radial

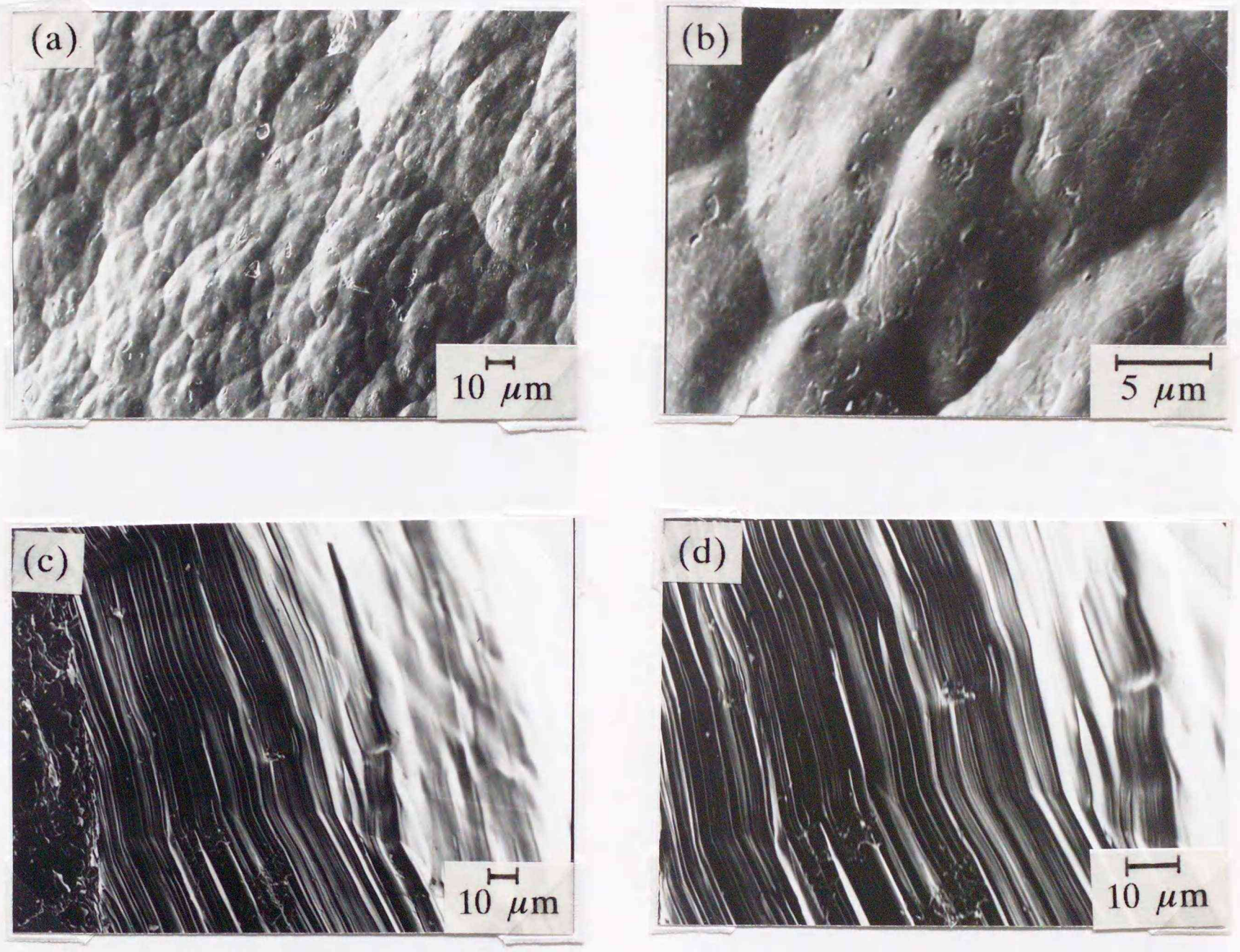
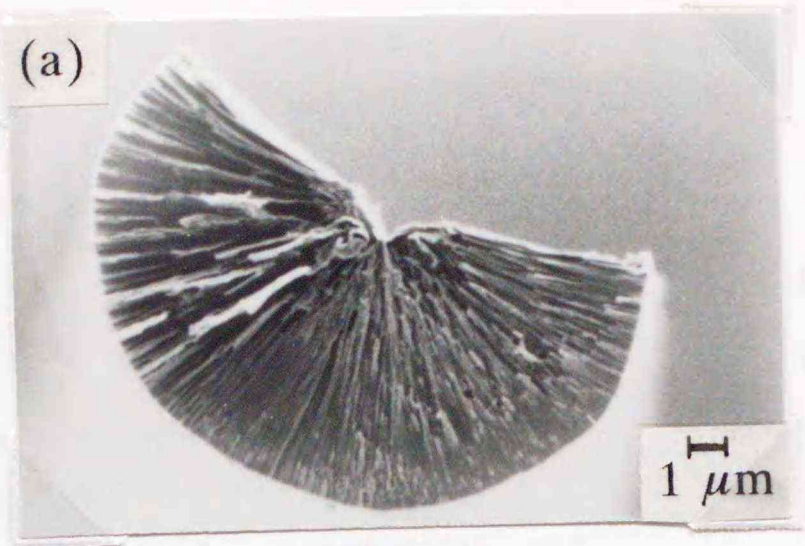
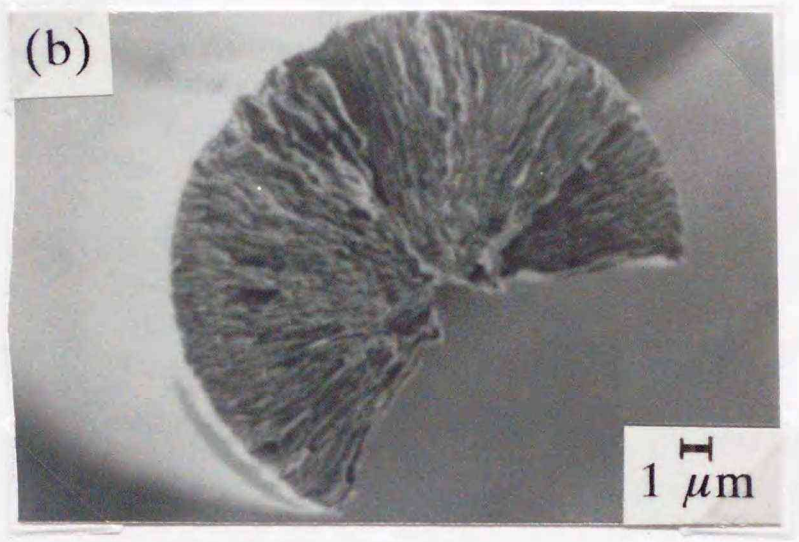


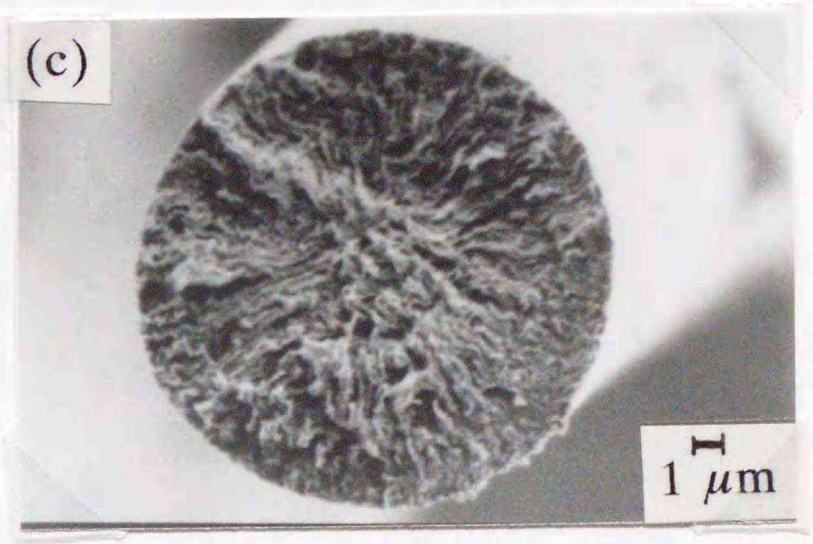
Fig. 2-1 SEM micrographs of the sample SSG30.



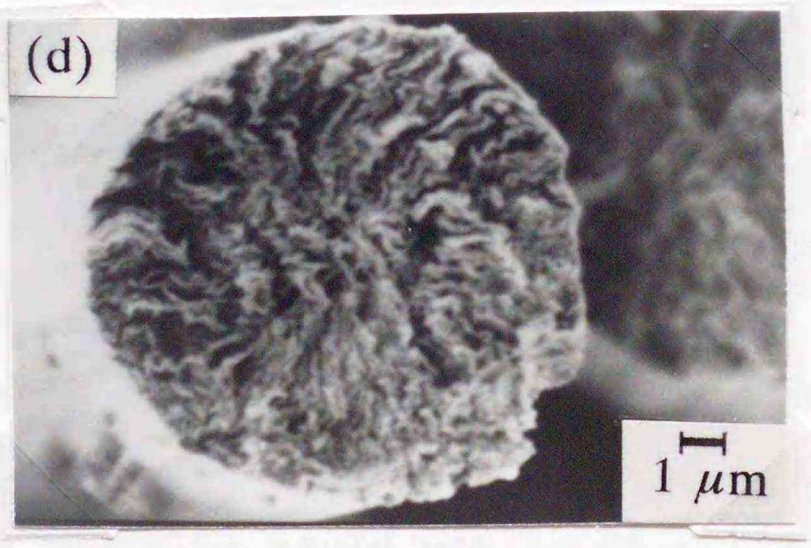
KOA-R



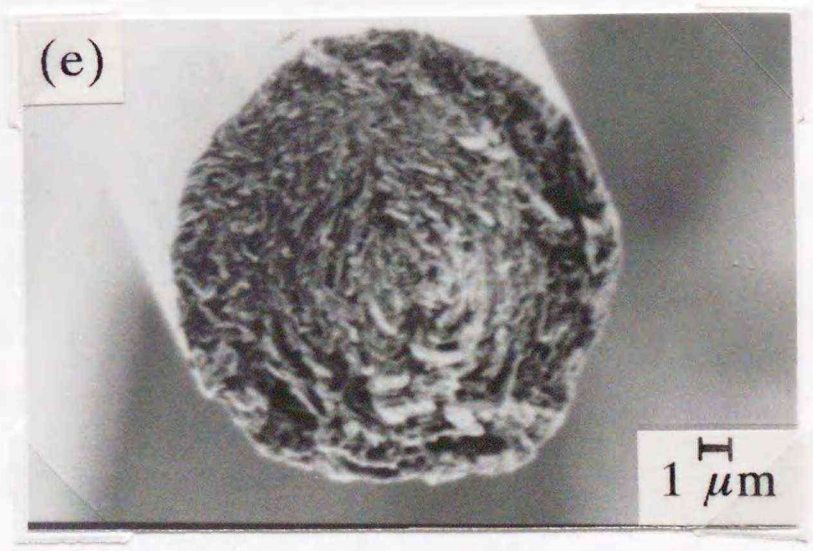
I-1-30



I-2-30



I-3-30



I-4-30

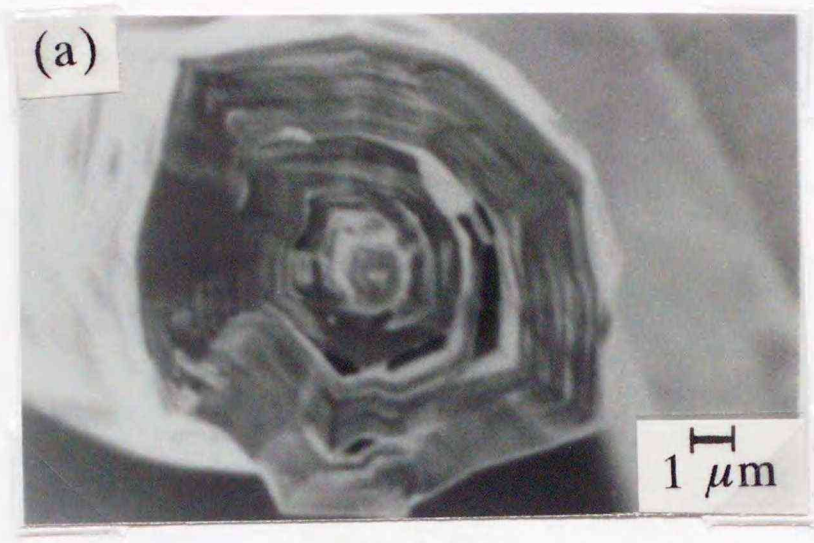
Fig. 2-2 SEM micrographs of the cross-sections of mesophase-pitch-based carbon fibers.

texture can be recognized, particularly at the center of the fiber. A different radial texture from that in the center can be observed even in the edge part (Fig. 2-2(d)). Therefore, the texture in micrometric scale of this fiber was classified as doubly-textured in Table 2-1. The I-series are mesophase-pitch-based carbon fibers are prepared from the same precursor pitch, but have different textures in their cross-sections.

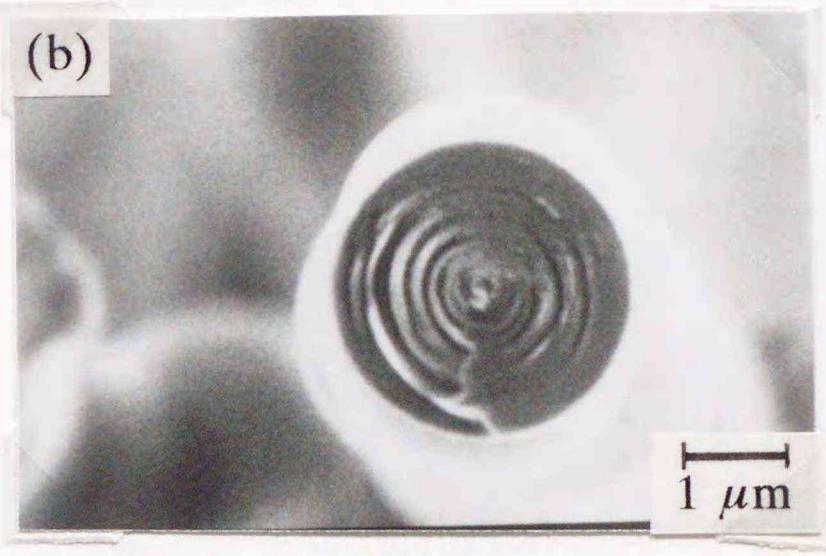
SEM micrographs of the sample group of vapor-grown carbon fibers (VGCF) are shown in Fig. 2-3. Concentric texture (annual-ring texture) are clearly seen on the cross-sections of the fibers. Although the fibers NVCF were too thin to observe their cross-sections, these series seemed to have the same concentric texture as other fibers in the VGCF-group. It is characteristic for these fibers to be observed polygonization of the fibers after high temperature heat-treatments (Fig. 2-3(a), (b), (e), (f) and (g)).

2.3.2. X-ray crystallographic parameters

Numerical data of crystallographic parameters by X-ray powder diffraction on the samples used are listed in Table 2-2. For flaky natural graphite powders with large size (NG400 and NG46) and kish graphite (KG), hk0 diffraction profiles (i. e., 100 and 110) could not be observed by a conventional alignment of goniometer. However, they are reasonably assumed to have the graphitization degree of 1.0 (P_1 = 1.0). On the other hand, the flaky natural graphite powder with small size of 5 μm (NG5) shows the P_1-value of about 0.95, a little lower than 1.0. This P_1-value seems to be due to the introduction of stacking disorder during severe pulverizing process, which also reflects on the appearance of rhombohedral stacking [2-2]. This difference in P_1-value among the NG-series can be considered to be smaller in



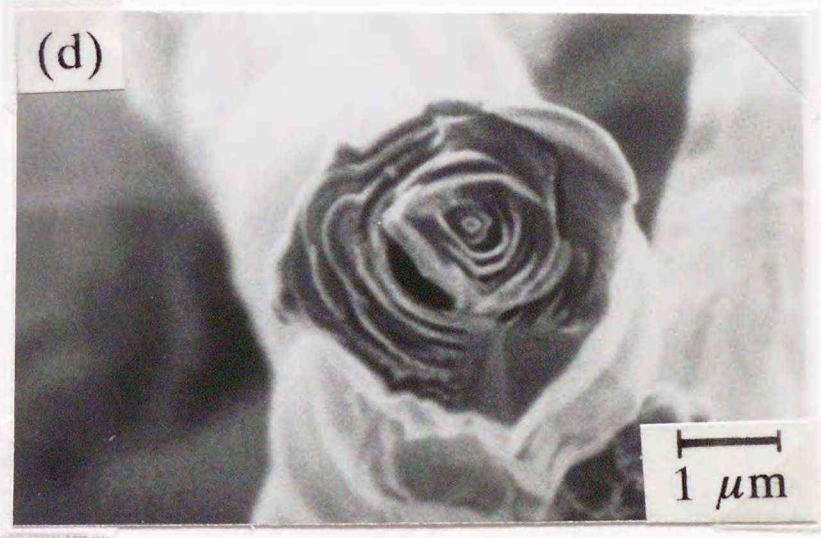
OVCF30



LDGAS

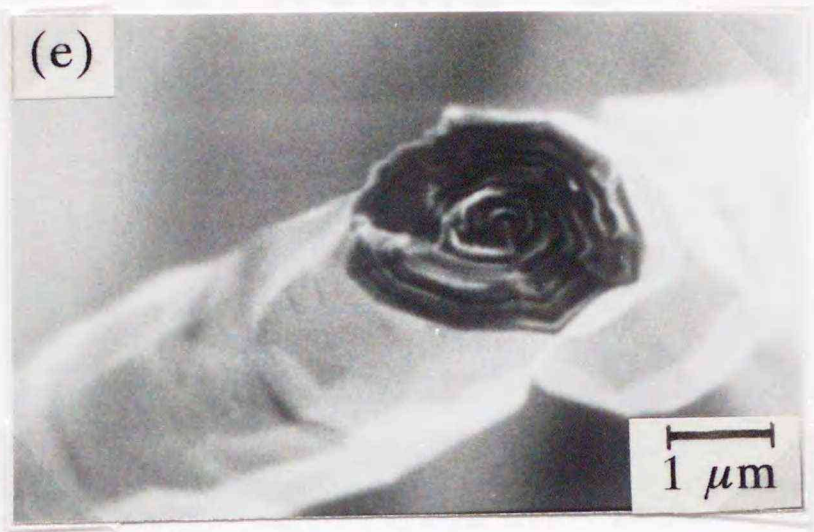


LDG20

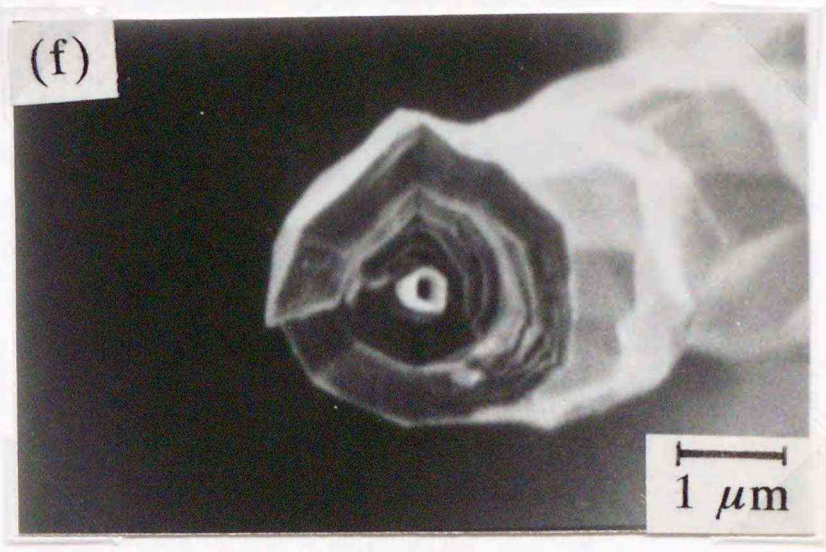


LDG22

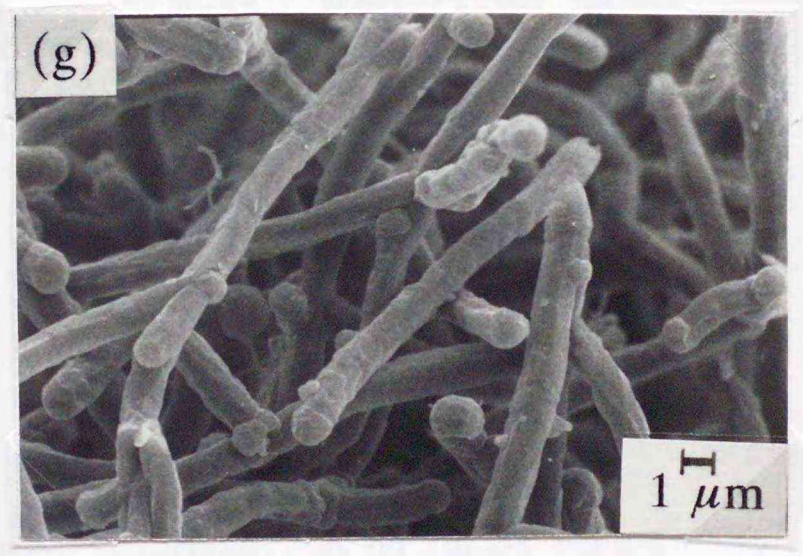
Fig. 2-3-1 SEM micrographs of vapor-grown carbon fibers.



LDG25



LDG28



NVCF30

Fig. 2-3-2 SEM micrographs of vapor-grown carbon fibers.

Table 2-2 Crystallographic parameters of the carbon materials used

Sample code	$P_1(10)$	$P_1(11)$	P_{ABA}	P_{ABC}	$\overline{d}_{002}$ [nm]	$L_c(002)$ [nm]	$L_c(004)$ [nm]	a_o [nm]	$L_a(110)$ [nm]
NG400	--	--	--	--	0.3355	--	360	--	--
NG46	--	--	--	--	0.3355	--	200	--	--
NG5	0.97	0.93	0.69	0.17	0.3355	--	270	0.2460	240
KG	--	--	--	--	0.3354	--	--	--	--
KS15	0.85	0.86	0.53	0.21	0.3359	140	107	0.2463	170
NOVAX30	--	0.75	--	--	0.3355	300	130	--	--
PV-7	0.86	0.81	0.67	0.16	0.3360	--	120	0.2460	140
PC18	--	0.11	--	--	0.3436	10	5	--	--
PC20	--	0.14	--	--	0.3425	18	11	0.2452	14
PC22	--	0.19	--	--	0.3415	36	14	--	--
PC24	0.51	0.45	0.13	0.08	0.3381	51	26	0.2460	48
PC27	0.57	0.57	0.18	0.10	0.3377	55	38	0.2459	51
PC30	0.69	0.65	0.27	0.14	0.3369	66	42	0.2462	59
GL18	--	0.07	--	--	0.3431	11	7	--	--
GL20	0.20	0.17	0.05	0.04	0.3429	18	10	0.2457	8
GL22	0.23	0.20	0.06	0.04	0.3416	30	17	0.2456	21
GL24	0.45	0.44	0.11	0.06	0.3390	23	13	0.2460	41
GL27	0.58	0.58	0.19	0.12	0.3375	50	26	0.2460	49
GL30	0.68	0.67	0.29	0.12	0.3371	69	35	0.2460	63
CB18	0.10	0.12	0.00	0.00	0.3430	14	8	0.2450	12
CB20	0.15	0.15	0.07	0.01	0.3425	27	15	0.2452	15
CB21	0.44	0.42	0.14	0.08	0.3384	47	29	0.2459	41
CB22	0.39	0.27	0.07	0.03	0.3405	40	22	0.2460	29
CB23	0.52	0.52	0.28	0.09	0.3369	74	40	0.2461	60
CB25	0.60	0.58	0.27	0.02	0.3363	96	68	0.2465	61
CB26	0.58	0.56	0.25	0.04	0.3367	78	63	0.2461	80
CB28	0.64	0.66	0.42	0.04	0.3362	101	87	0.2462	82
CB30	0.77	0.73	0.48	0.11	0.3361	120	112	0.2460	111
IS08	--	--	--	--	0.3497	3	--	--	--
IS10	--	--	--	--	0.3493	3	--	--	--
IS15	--	--	--	--	0.3446	7	--	--	--
IS18	0.12	0.10	0.00	0.00	0.3431	18	5	--	--
IS23	0.50	0.45	0.16	0.07	0.3376	42	27	0.2459	55
IS26	0.60	0.53	0.21	0.08	0.3371	50	30	0.2461	67
IS29	0.71	0.66	0.28	0.10	0.3364	70	36	0.2460	104
SSGAS	0.24	0.23	0.14	0.07	0.3421	23	10	0.2457	11
SSG25	0.54	0.51	0.14	0.08	0.3374	50	27	0.2465	63
SSG28	0.58	0.62	0.46	0.14	0.3362	180	84	--	--
SSG30	0.73	0.71	0.48	0.22	0.3359	200	120	--	--

Sample code	$P_1(10)$	$P_1(11)$	P_{ABA}	P_{ABC}	$\bar{d}_{002}$ [nm]	$L_c(002)$ [nm]	$L_c(004)$ [nm]	a_o [nm]	$L_a(110)$ [nm]
PYRAS	0.17	0.11	0.10	0.06	0.3421	22	14	0.2457	15
PYR25-19	0.57	0.53	0.12	0.06	0.3379	50	19	0.2464	58
PYR28-10	0.70	0.68	0.41	0.16	0.3357	170	120	--	--
PYR28-19	0.71	0.70	0.47	0.12	0.3357	170	140	--	--
PYR32	0.72	0.76	0.49	0.15	0.3355	240	200	--	--
GC12	--	--	--	--	0.3682	1	--	--	--
GC20	--	0.06	--	--	0.3528	2	--	--	--
GC30	--	0.09	--	--	0.3480	3	--	--	--
KOA-R	0.53	0.52	0.28	0.04	0.3368	46	29	0.2463	86
I-1-28	0.35	0.37	0.19	0.00	0.3371	35	18	0.2457	64
I-1-30	0.40	0.41	0.25	0.04	0.3368	49	32	0.2462	82
I-2-28	0.26	0.25	0.09	0.01	0.3401	17	9	0.2455	20
I-2-30	0.34	0.30	0.10	0.03	0.3385	24	12	0.2460	40
I-3-26	0.29	0.28	0.10	0.01	0.3395	18	10	0.2457	23
I-3-30	0.39	0.32	0.12	0.01	0.3380	27	13	0.2460	45
I-4-26	0.25	0.26	0.10	0.01	0.3392	18	10	0.2459	29
I-4-30	0.36	0.35	0.13	0.04	0.3379	27	14	0.2459	56
P-120	0.41	0.43	0.19	0.05	0.3374	37	20	--	--
A30	0.32	0.34	0.13	0.03	0.3382	25	15	--	--
A33	0.40	0.39	0.18	0.00	0.3376	30	16	--	--
B30	0.35	0.38	0.16	0.02	0.3376	30	--	--	--
B33	0.44	0.42	0.17	0.04	0.3371	33	--	--	--
OVCF30	0.70	0.80	0.55	0.25	0.3360	200	115	0.2461	160
NVCFAS	0.07	0.05	0.00	0.00	0.3458	5	--	--	--
NVCF10	0.07	0.04	0.00	0.00	0.3461	4	--	--	--
NVCF23	0.20	0.18	0.04	0.03	0.3416	22	14	0.2455	18
NVCF28	0.33	0.34	0.16	0.03	0.3372	30	20	0.2461	42
NVCF30	0.38	0.37	0.15	0.10	0.3368	45	23	0.2458	60
LDGAS	0.05	0.06	0.00	0.00	0.3457	5	--	--	--
LDG20	0.25	0.25	0.06	0.04	0.3397	32	16	0.2459	29
LDG20H	0.23	0.18	0.03	0.02	0.3421	26	13	0.2455	24
LDG22	0.57	0.58	0.24	0.15	0.3369	62	39	0.2462	50
LDG22H	0.35	0.26	0.07	0.02	0.3396	36	20	0.2458	32
LDG25	0.70	0.69	0.38	0.19	0.3362	134	91	0.2466	104
LDG25H	0.56	0.57	0.29	0.12	0.3376	74	61	0.2463	67
LDG28	0.70	0.70	0.35	0.20	0.3362	175	99	0.2462	123
LDG28H	0.69	0.66	0.34	0.15	0.3366	82	66	0.2462	70

comparison with large change in P_1-value in other groups of the samples. Therefore, only the difference in the NG-series is their average particle size.

By heat-treatment at high temperatures, usually above 2800°C, the groups of cokes (COKE), isotropic carbons (IS) and pyrolytic carbons (PyC) showed relatively high P_1-values. These groups are defined as graphitizable carbon or "soft carbon". On the other hand, the graphitization degree in the group of glass-like carbons (GC) is very low, even after the heat-treatment at 3000°C. Thus, the GC-group have been classified into non-graphitizable carbon or "hard carbon".

In the group of MPCF, the sample KOA-R which has radial texture with open wedge gives the highest P_1-value. The fiber I-1-30, radial texture with open wedge, also has rather high degree of graphitization among the fibers in I-series, which is also shown by other X-ray parameters. However, the fiber I-2-30, which has the radial texture without open wedge, shows rather low graphitization degree. The fibers I-3-30 (doubly-textured) and I-4-30 (concentric texture) are graphitized better than the fiber I-2-30.

The P_1-value of the fiber NVCF28 which is as thin as less than 1 μm is 0.34, much smaller than that of the fibers LDG28 and LDG28H with diameter of 2 μm. The P_1-value in the fiber OVCF30 with average diameter of 10 μm is the highest among the VGCF-group.

2.3.3. Relations among X-ray parameters

The relations between graphitization degree, P_1, and average interlayer spacing, $\bar{d}_{002}$, on the carbon samples used are shown in Fig. 2-4. The $\bar{d}_{002}$-value decreases with increase in the P_1-value and then approaches to the one for natural graphite ($\bar{d}_{002}$ =

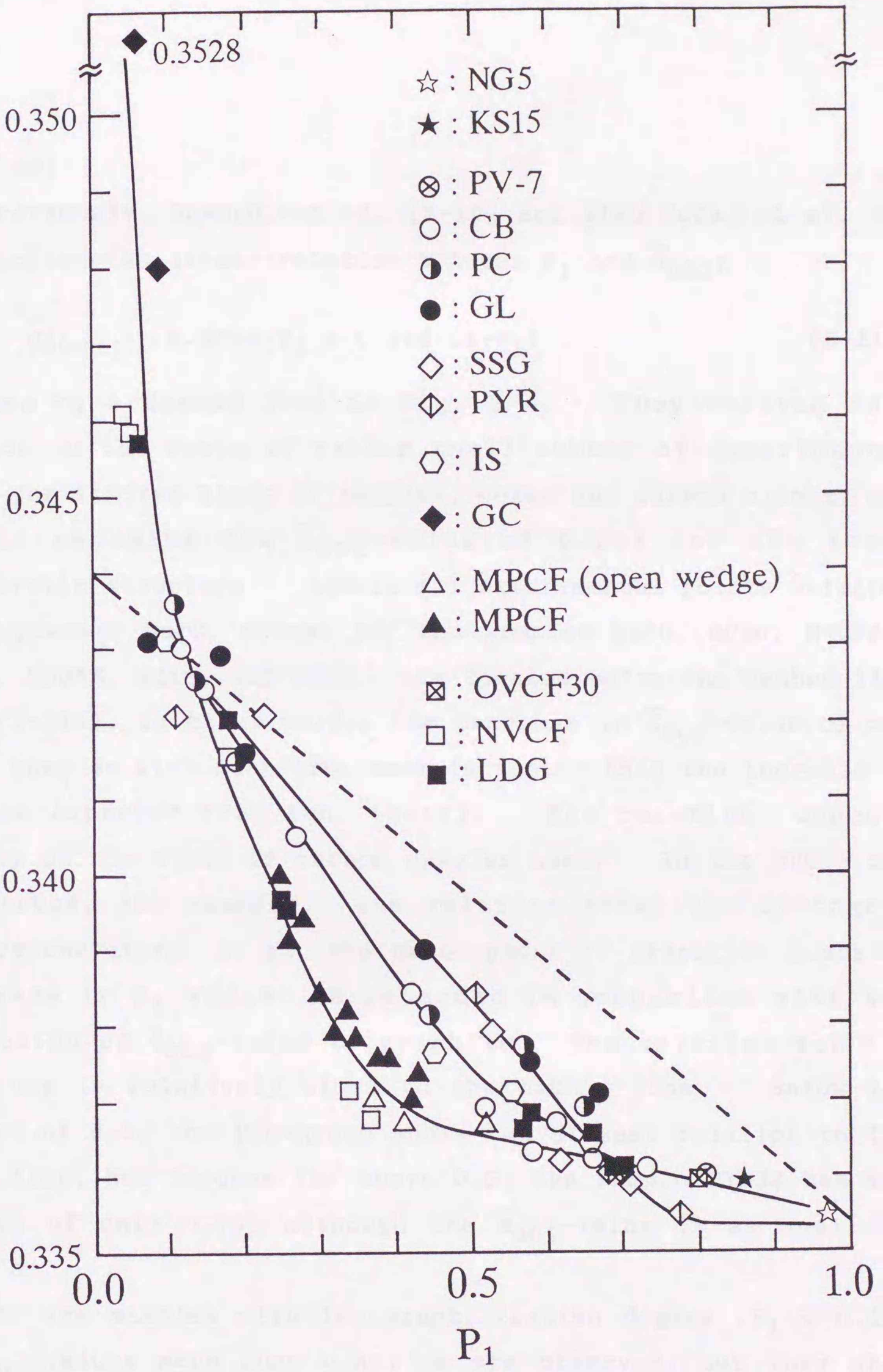


Fig. 2-4 The relation between graphitization degree P_1 and average interlayer spacing $\bar{d}_{002}$ in the carbon samples used.

0.3354 nm).

Previously, Bowman, et al. [2-10] and also Noda, et al. [2-11] reported the linear relation between P_1 and $\bar{d}_{002}$;

$$\bar{d}_{002} = 0.3354 \cdot P_1 + 0.344 \cdot (1-P_1) , \qquad (2-11)$$

as shown by a dashed line in Fig. 2-4. They derived this relation on the basis of rather small number of experimental points for limited kinds of samples, cokes and carbon blacks, and also by assuming the $\bar{d}_{002}$-value of 0.344 for the ideal turbostratic structure. Almost all experimental points obtained in the present work, except for the samples GC20, GC30, NVCFAS, NVCF10, LDGAS, PC18, and GL20 , are located below the dashed line (Eqn. (2-11)), in other words, the decrease in $\bar{d}_{002}$-value of all carbon samples with heat-treatment is faster than the increase in P_1-value expected from Eqn. (2-11). The relation depends strongly on the kinds of carbon samples used. In the MPCF- and VGCF-groups, for example, the relation shows the strongest downward curvature, i. e., the development of graphitic stacking (increase in P_1-value) is retarded in comparison with the approaching of $\bar{d}_{002}$-value to graphite. The relation for the COKE-group is relatively close to the dashed line. Below the P_1-value of 0.5, the PyC-group shows the closest relation to the dashed line, but becomes far above 0.5; the sample PYR32 has the P_1-value of only 0.76, although the $\bar{d}_{002}$-value is as small as 0.3355 nm.

For the samples with low graphitization degree ($P_1 < 0.1$), the $\bar{d}_{002}$-values more than 0.344 nm are observed, but they show certain relation to P_1-value. This result show that the carbons of which P_1-values are as small as zero can have interlayer spacing larger than 0.344 nm, even more than 0.353 nm. The crystallite size of carbon, of which the P_1-value is close to

zero, is too small to be determined, as shown by broadening of diffraction lines. This result seems to suggest that a quite non-graphitized carbon (P_1 = 0) has rather non-periodic stacking of carbon hexagonal layer planes.

In Fig. 2-5, the crystallite sizes $L_a(110)$, $L_c(002)$ and $L_c(004)$ are plotted against the P_1-value. The crystallite size along the a-axis, $L_a(110)$, grows gradually with development of graphitic structure. For the samples in MPCF-group and NVCF-series, rapid increase in $L_a(110)$ was observed in a range of graphitization degree between 0.3 and 0.5 (Fig. 2-5(a)). The LDG-series shows the similar relation to the COKE-, IS- and PyC-groups. On the other hand, a unique relation seems to be obtained between P_1 and either crystallite size along c-axis $L_c(002)$ or $L_c(004)$ independent of carbon samples (Fig. 2-5(b) and (c)).

The relations between $\bar{d}_{002}$ and crystallite sizes are shown in Fig. 2-6, on the abscissa $\bar{d}_{002}$-value decreasing from left to right, in order to have a correspondence to Fig. 2-5. In the relations of $L_c(004)$ vs. $\bar{d}_{002}$, characteristic plateaux are observed, which are different on the sample COKE-, PyC- and MPCF-groups (Fig. 2-6(c)). Below the $\bar{d}_{002}$-value of around 0.338 nm, $L_c(004)$-value rapidly increases, no differentiation of the sample groups being possible. The similar relations of $L_c(002)$ vs. $\bar{d}_{002}$ were obtained, plateaux depending on the groups and a rapid increase in $L_c(002)$ below $\bar{d}_{002}$-value of 0.338 nm (Fig. 2-6(b)). The relation of $L_a(110)$ vs. $\bar{d}_{002}$ seems to be unique, regardless of the kind of carbon materials (Fig. 2-6(a)).

2.3.4. Relations between magnetoresistance and X-ray parameters

The plots of magnetoresistance $(\Delta\rho/\rho)_{cr}$ against X-ray parameters, P_1, $\bar{d}_{002}$ and $L_a(110)$, on the samples in COKE-, PyC-

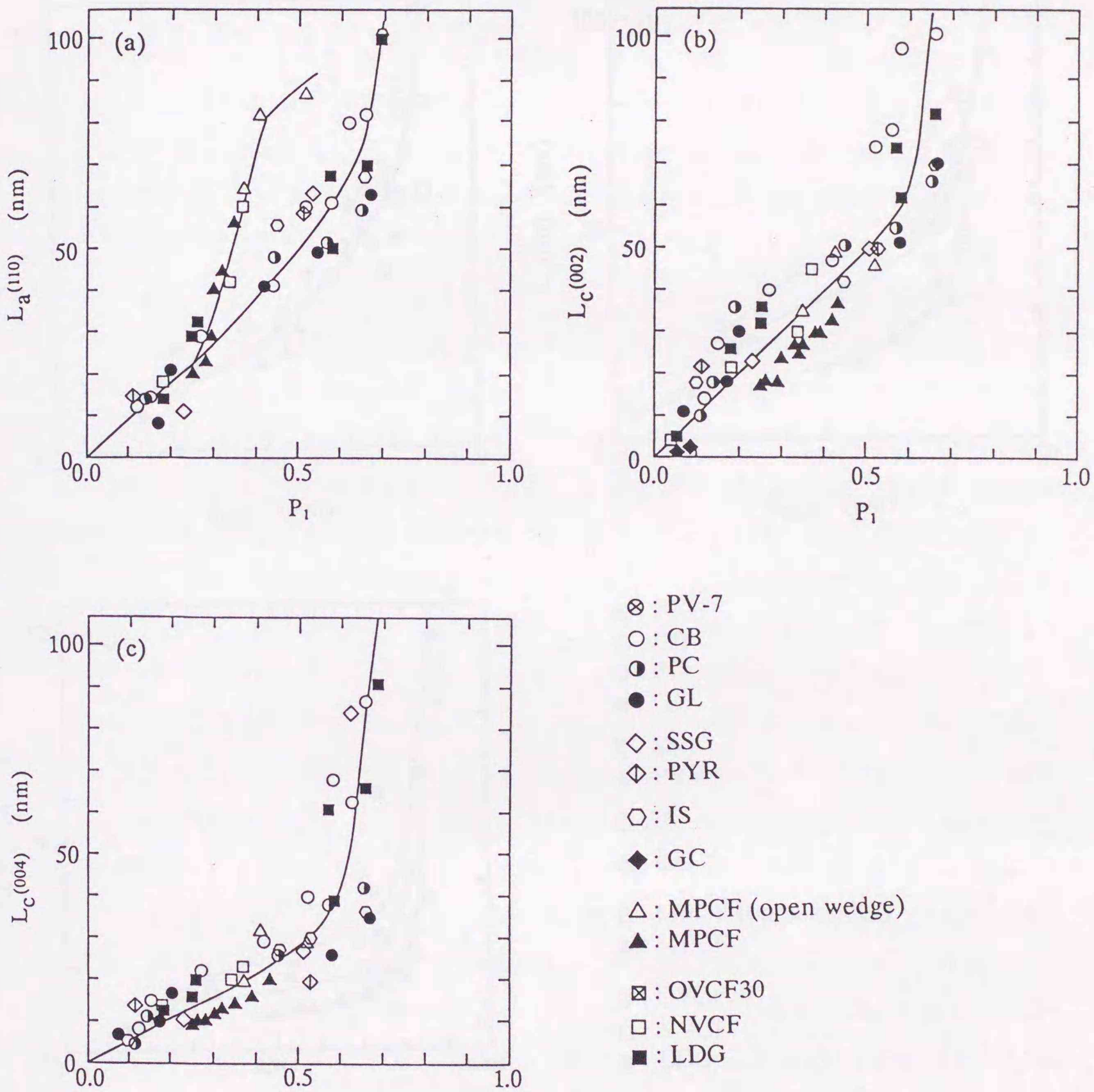


Fig. 2-5 The plots of crystallite sizes against graphitization degree P_1 in the carbon samples used.
(a) P_1-$L_a(110)$, (b) P_1-$L_c(002)$,
(c) P_1-$L_c(004)$.

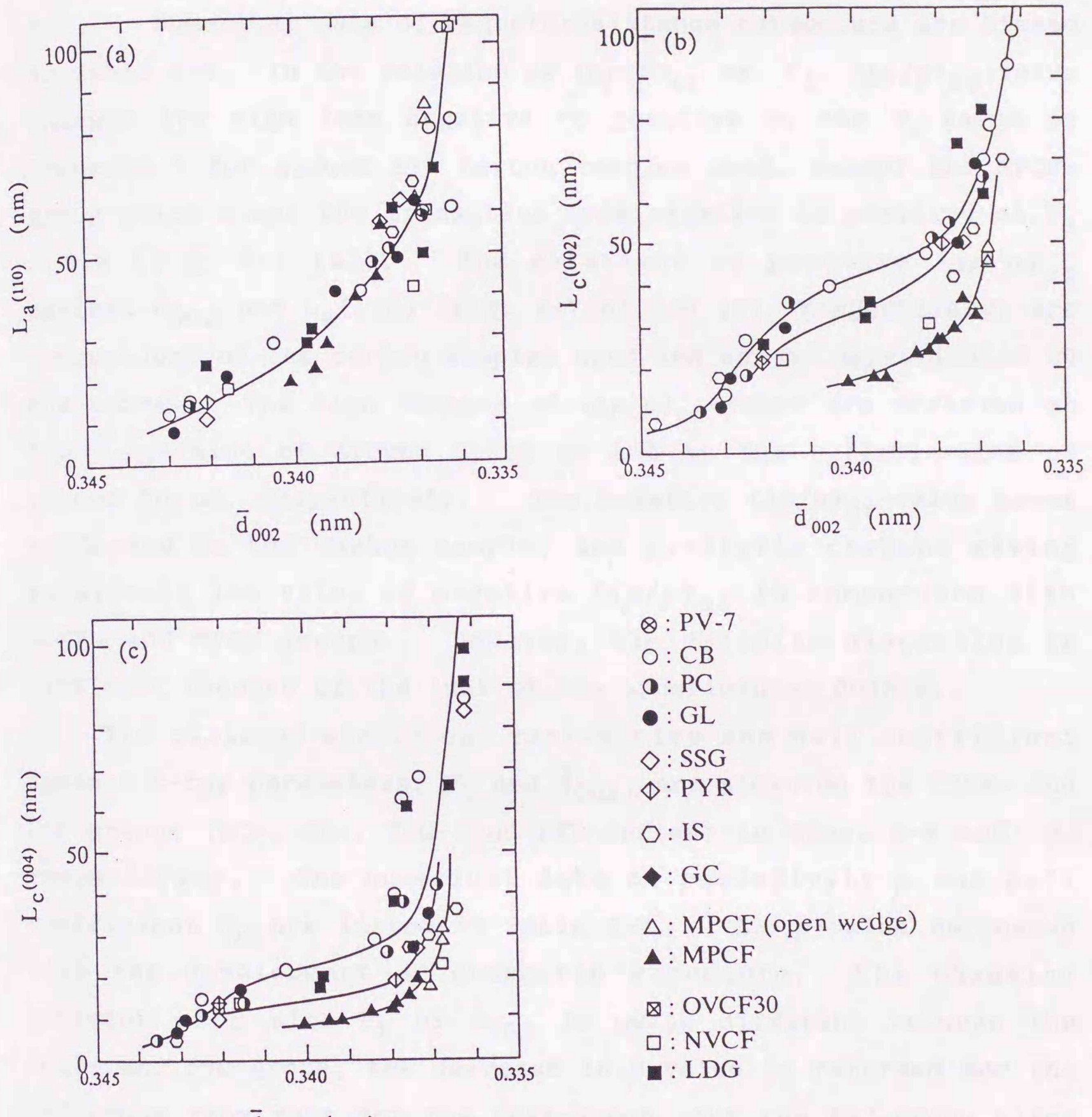
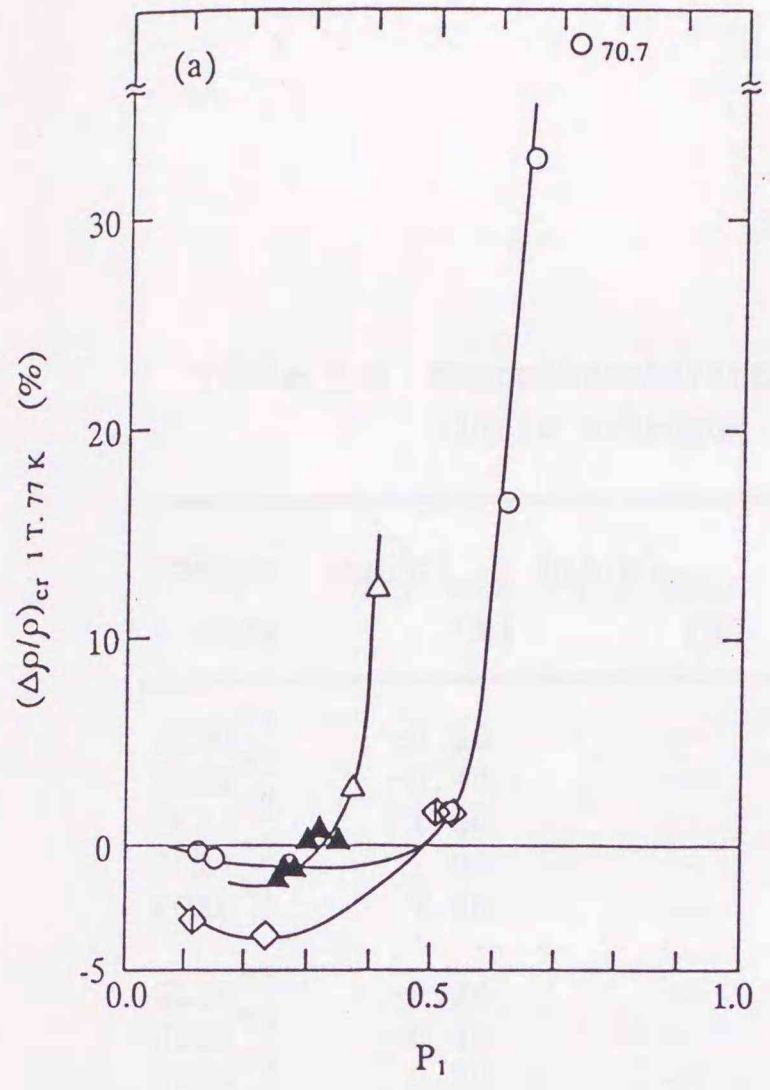
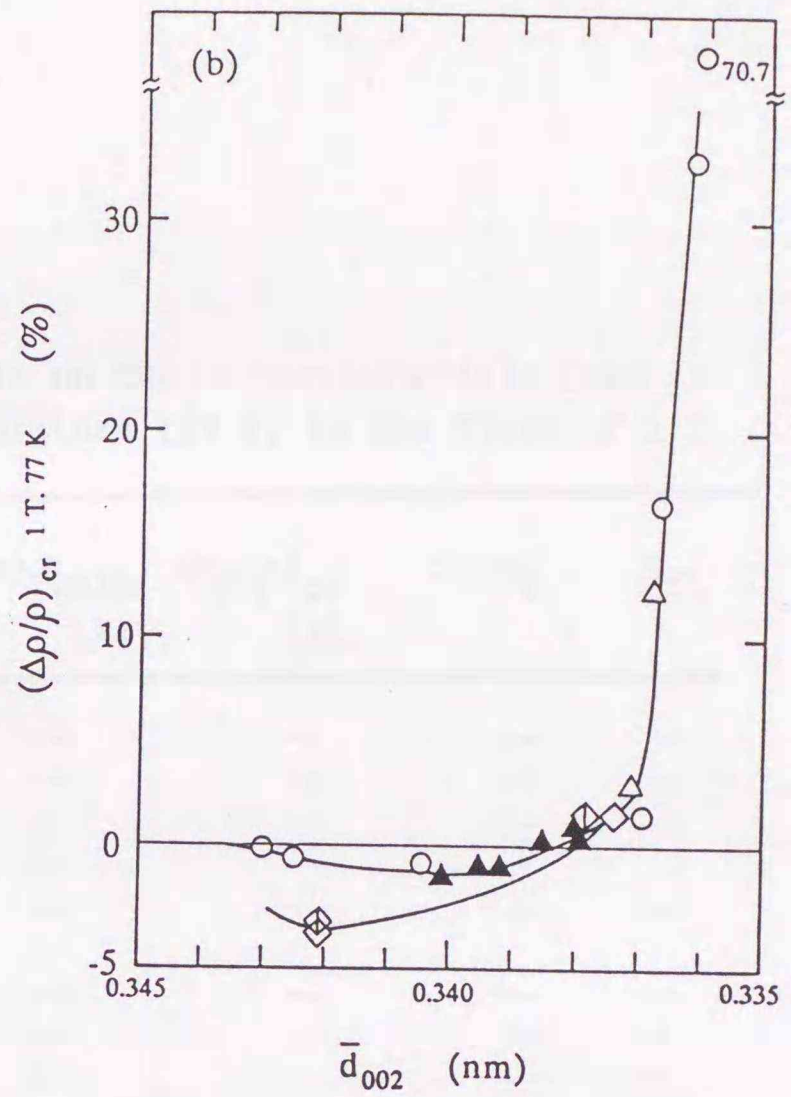


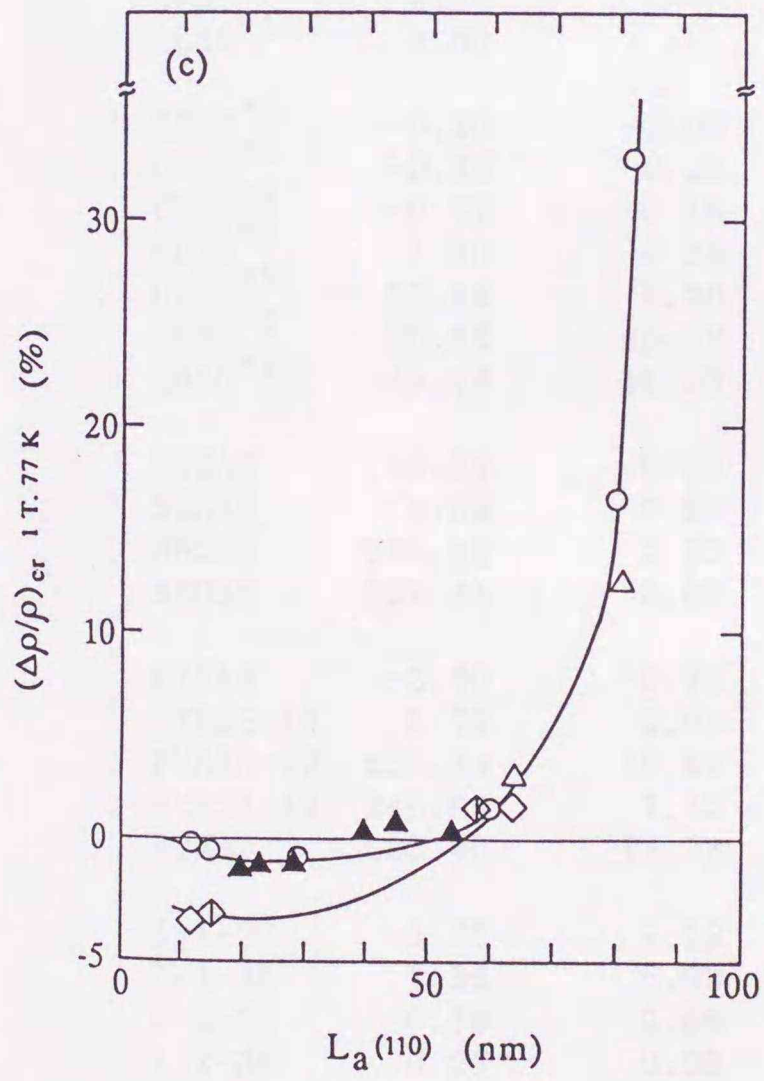
Fig. 2-6 The plots of crystallite sizes against average interlayer spacing $\bar{d}_{002}$ in the carbon samples used.
(a) $\bar{d}_{002}$-$L_a(110)$, (b) $\bar{d}_{002}$-$L_c(002)$,
(c) $\bar{d}_{002}$-$L_c(004)$.

and MPCF-groups (CB-, SSG-, PYR- and I-series) are shown in Fig. 2-7. Numerical data of magnetoresistance parameters are listed in Table 2-3. In the relation of $(\Delta\rho/\rho)_{cr}$ vs. P_1, $(\Delta\rho/\rho)_{cr}$-value changes its sign from negative to positive at the P_1-value of around 0.5 for almost all carbon samples used, except the MPCF-group which shows the transition from negative to positive at P_1 = 0.3 (Fig. 2-7 (a)). The relations of positive $(\Delta\rho/\rho)_{cr}$ against $\bar{d}_{002}$ and $L_a(110)$ (Fig. 2-7(b) and (c), respectively) are independent of the carbon samples used and can be approximated by one curve. The sign changes of $(\Delta\rho/\rho)_{cr}$-value are observed at the $\bar{d}_{002}$-value of around 0.338 nm and at the $L_a(110)$-value of around 50 nm, respectively. The negative $(\Delta\rho/\rho)_{cr}$-value seems to depend on the carbon sample; the pyrolytic carbons giving relatively low value of negative $(\Delta\rho/\rho)_{cr}$ in comparison with COKE- and MPCF-groups. However, the definite discussion is difficult because of the lack of the experimental points.

The plots of electrical resistivity and Hall coefficient against X-ray parameters, P_1 and $\bar{d}_{002}$, are shown on the COKE- and PyC-groups (PC-, GL-, SSG- and PYR-series) in Figs. 2-8 and -9, respectively. The numerical data of resistivity ρ and Hall coefficient R_H are listed in Table 2-4. The ρ-value decreases with the development of graphitic structure. The changing behavior of ρ with P_1 or $\bar{d}_{002}$ is quite different between the COKE- and PyC-group; the decrease in ρ-value is retarded for the PyC-group from that for the COKE-group, but the PyC-group gives much lower ρ-value at high P_1-value than the COKE-group does. The largest positive R_H-value was observed at P_1-value of around 0.2 and at $\bar{d}_{002}$-value of around 0.342 nm. The change of sign in Hall coefficient R_H from positive to negative is observed at P_1 = 0.5 and at $\bar{d}_{002}$ = 0.338 nm, which correspond to the respective point for the sign change of $(\Delta\rho/\rho)_{cr}$, regardless of the kind of







○ : CB
◇ : SSG
◈ : PYR
△ : MPCF (open wedge)
▲ : MPCF

Fig. 2-7 The plots of crystallite magnetoresistance $(\Delta\rho/\rho)_{cr}$ against X-ray parameters in the carbon samples used.
(a) P_1-$(\Delta\rho/\rho)_{cr}$, (b) $\bar{d}_{002}$-$(\Delta\rho/\rho)_{cr}$,
(c) $L_a(110)$-$(\Delta\rho/\rho)_{cr}$.

Table 2-3 Magnetoresistance data on the carbon materials used at liquid nitrogen temperature (77 K) in the field of 1 T.

Sample code	$(\Delta\rho/\rho)_{max}$ [%]	$(\Delta\rho/\rho)_{Tmin}$ [%]	$(\Delta\rho/\rho)_{TLmin}$ [%]	$(\Delta\rho/\rho)_{cr}$ [%]	r_T	r_{TL}
PC20*1	-0.20	--	--	--	--	--
PC22*1	-0.40	--	--	--	--	--
PC24*1	1.00	--	--	--	--	--
PC27*1	1.90	--	--	--	--	--
PC30*1	7.50	--	--	--	--	--
GL20*1	-0.20	--	--	--	--	--
GL22*1	-0.40	--	--	--	--	--
GL24*1	0.30	--	--	--	--	--
GL27*1	2.10	--	--	--	--	--
GL30*1	4.00	--	--	--	--	--
CB17*2	-0.10	-0.06	-0.18	-0.18	0.57	0.15
CB19*2	-0.35	-0.22	-0.05	-0.62	0.62	0.15
CB22*2	-0.67	-0.18	-0.07	-0.92	0.27	0.11
CB24*2	1.20	0.34	0.05	1.59	0.28	0.04
CB26*2	10.93	4.26	1.31	16.50	0.39	0.12
CB28*2	20.62	10.52	1.86	33.00	0.51	0.09
CB30*2	49.44	15.33	5.93	70.70	0.31	0.12
SSGAS	-3.24	-0.69	-0.38	-4.32	0.21	0.12
SSG25	4.59	0.23	0.23	5.06	0.05	0.05
SSG28	155.88	2.99	3.30	162.17	0.02	0.02
SSG30	354.44	6.08	6.08	366.59	0.02	0.02
PYRAS	-2.80	-0.71	-0.41	-3.92	0.25	0.15
PYR25-19	1.73	0.02	0.04	1.80	0.01	0.03
PYR28-10	616.44	10.52	12.33	639.59	0.02	0.02
PYR28-19	346.99	7.40	6.32	360.71	0.02	0.02
PYR32	823.46	14.03	11.61	849.09	0.02	0.01
I-1-28	1.77	1.19	0.03	2.99	0.67	0.02
I-1-30	7.38	5.02	0.05	12.45	0.68	0.01
I-2-28	-0.78	-0.66	-0.02	-1.46	0.85	0.03
I-2-30	0.29	0.09	-0.01	0.37	0.30	--
I-3-26	-0.58	-0.53	-0.04	-1.15	0.92	0.06
I-3-30	0.54	0.32	-0.01	0.85	0.60	--
I-4-26	-0.56	-0.50	-0.02	-1.08	0.89	0.04
I-4-30	0.24	0.12	-0.01	0.35	0.48	--

Sample code	$(\Delta\rho/\rho)_{max}$ [%]	$(\Delta\rho/\rho)_{Tmin}$ [%]	$(\Delta\rho/\rho)_{TLmin}$ [%]	$(\Delta\rho/\rho)_{cr}$ [%]	r_T	r_{TL}
LDG20	-0.33	--	--	--	--	--
LDG22	0.39	--	--	--	--	--
LDG25	23.40	--	--	--	--	--
LDG28	25.80	--	--	--	--	--
SSGAS*3	4.67	0.13	0.25	5.05	0.03	0.05

*1: From Ref. [18].
*2: From Ref. [19].
*3: Data at room temperature, will be discussed in Chapter 4.

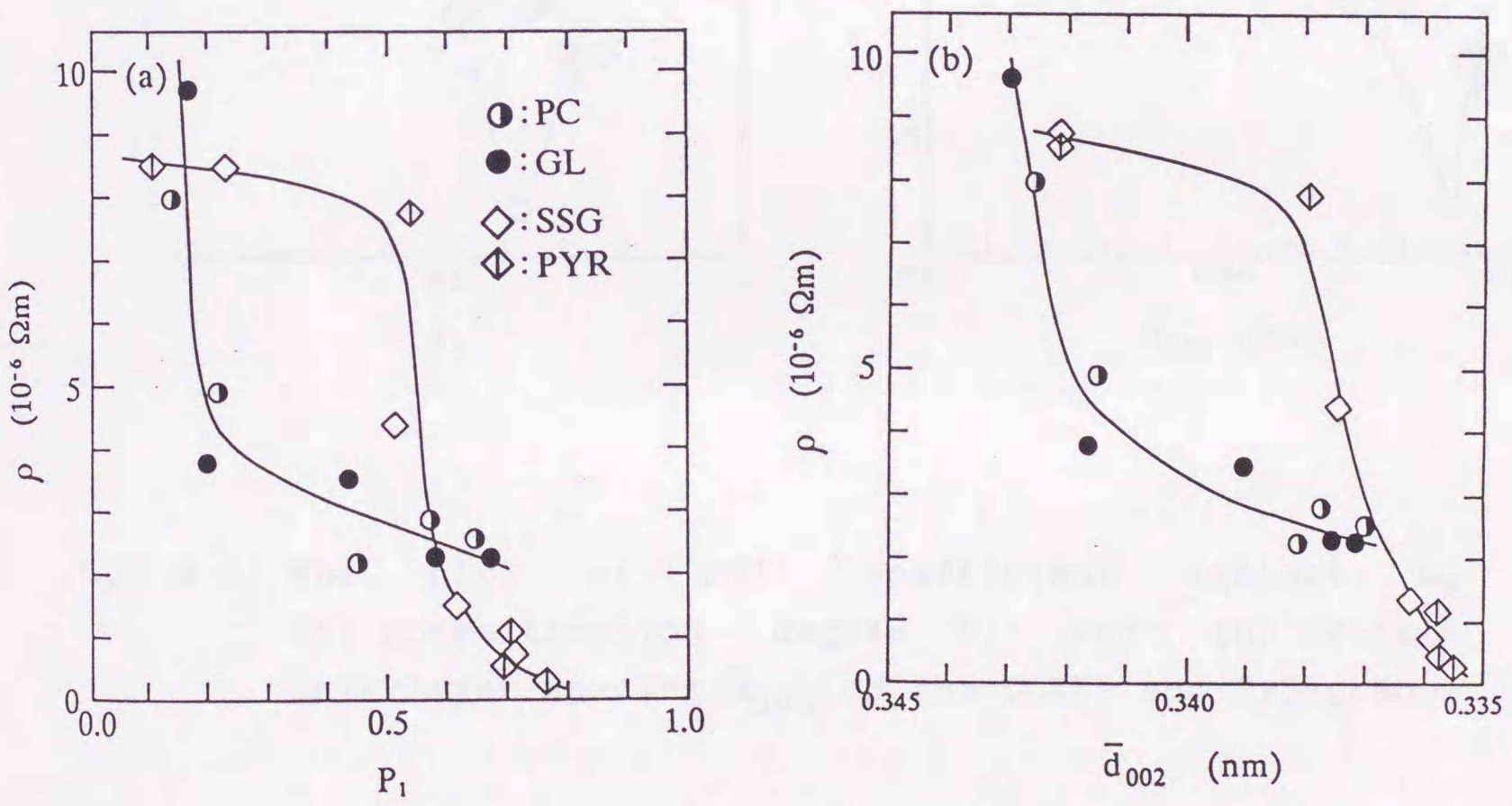


Fig. 2-8 The plots of resistivity ρ against (a) graphitization degree P_1 and (b) average interlayer spacing $\bar{d}_{002}$ on the COKE- and PyC-groups.

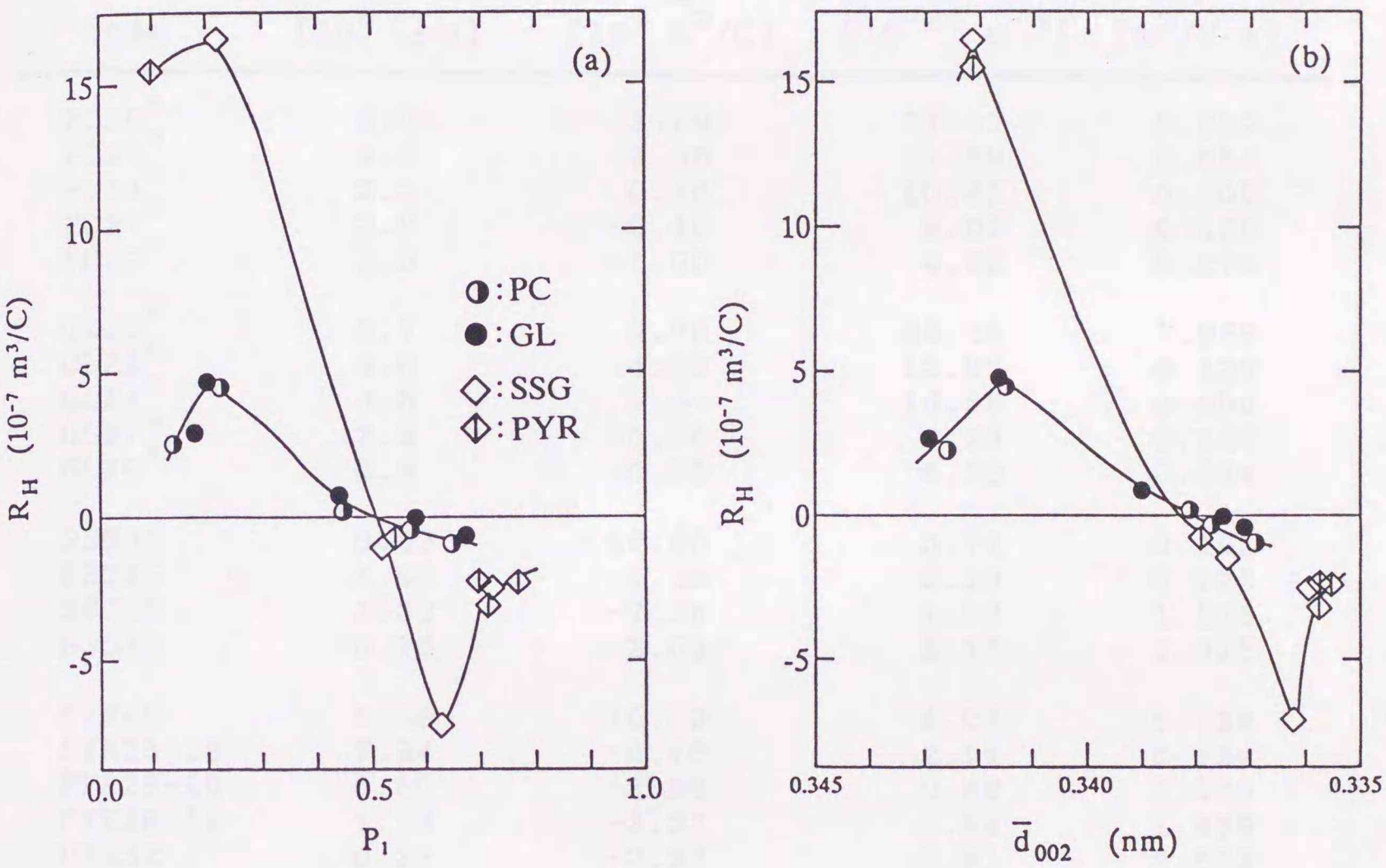


Fig. 2-9 The plot of Hall coefficient against R_H (a) graphitization degree P_1 and (b) average interlayer spacing $\bar{d}_{002}$ on the COKE- and PyC-groups.

Table 2-4 Resistivity ρ, Hall coefficient R_H, carrier concentration n and mobility $\bar{\mu}$ of the carbon materials used at liquid nitrogen temperature (77 K).

Sample code	ρ [10^6 Ω·m]	R_H [10^7 m^3/C]	n [10^{-24} m^{-3}]	$\bar{\mu}$ [m^2/V·s]
PC20*	8.0	2.30	27.17	0.029
PC22*	4.9	4.60	13.59	0.094
PC24*	2.2	0.20	10.42	0.100
PC27*	2.8	-0.40	8.09	0.138
PC30*	2.5	-1.00	4.55	0.274
GL20*	9.7	2.70	23.15	0.028
GL22*	3.8	4.82	12.97	0.128
GL24*	3.5	0.97	10.58	0.055
GL27*	2.3	-0.05	9.38	0.145
GL30*	2.3	-0.65	6.78	0.234
SSGAS	8.63	16.60	3.77	0.192
SSG25	4.43	-1.15	3.13	0.225
SSG28	1.32	-7.16	1.82	1.273
SSG30	0.75	-2.53	2.17	1.915
PYRAS	8.49	15.50	4.03	0.139
PYR25-19	7.84	-0.76	2.97	0.134
PYR28-10	0.50	-2.38	2.46	2.529
PYR28-19	1.14	-3.22	1.44	1.899
PYR32	0.38	-2.37	2.81	2.652

*: From Ref. [18].

carbon materials. The change of R_H with P_1 or $\bar{d}_{002}$ is very similar between the COKE- and PyC-group, but the absolute values of R_H for the COKE-group are always smaller than those for the PyC-group.

The numerical data of carrier concentration n and mean square root of mobility $\bar{\mu}$, defined as $\bar{\mu} = \sqrt{\mu_h \cdot \mu_e}$, are also listed in Table 2-4. Since the samples PC20, PC22, GL20, GL22, SSGAS and PYRAS had the negative $(\Delta\rho/\rho)_{cr}$-value and the positive R_H-

value, n and $\bar{\mu}$ were calculated by assuming the one-carrier (hole) conduction. The other samples were regarded to have the two carriers, holes and electrons.

The plots of concentration n and mobility $\bar{\mu}$ of carriers against P_1-value are shown on the four sample series in Fig. 2-10. These sample show general trends of n and $\bar{\mu}$ with P_1-value; for P_1-value below 0.2 and above 0.5, the concentration n

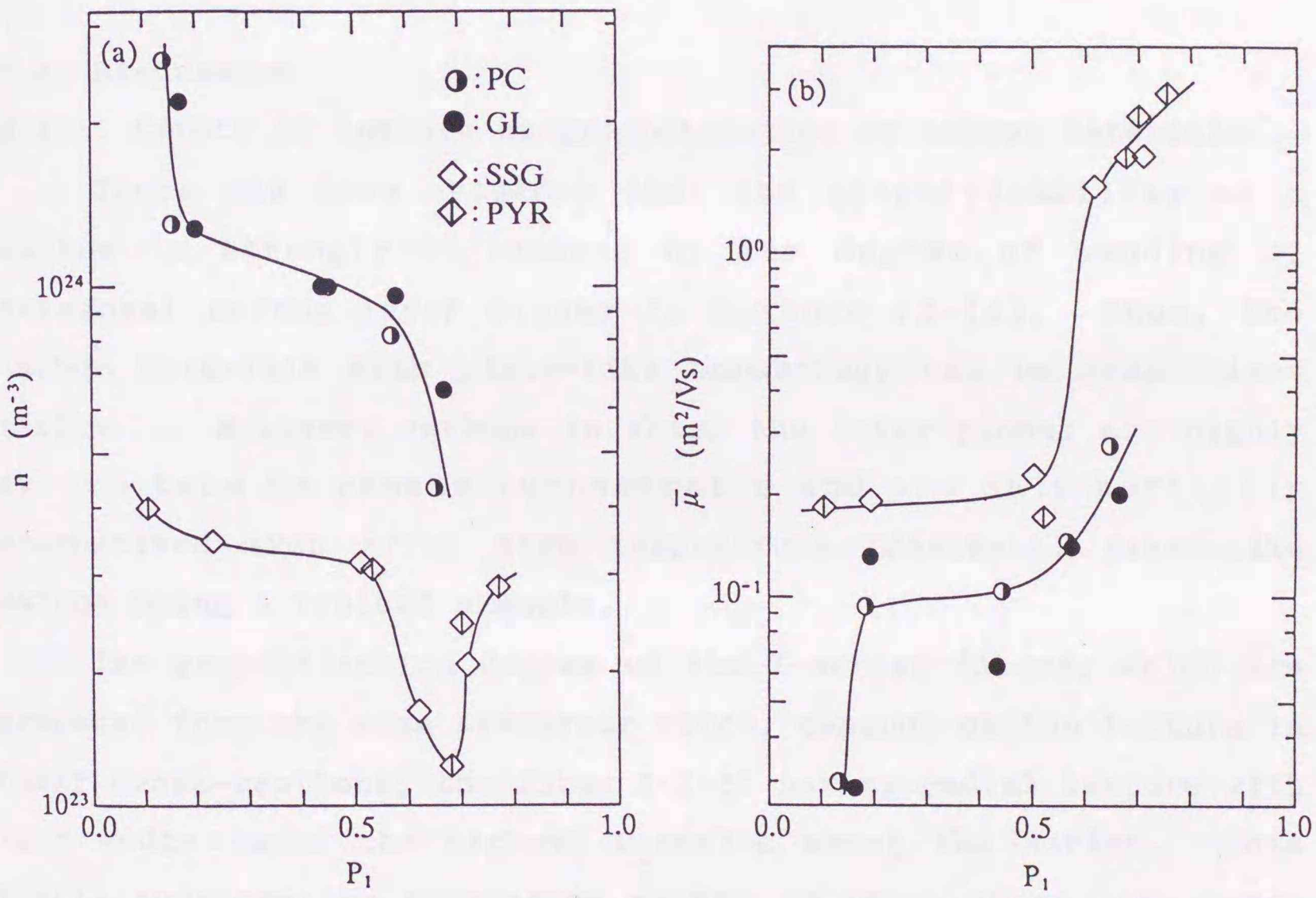


Fig. 2-10 The plots of (a) carrier concentration n and (b) mobility $\bar{\mu}$ against graphitization degree P_1 on the COKE- and PyC-groups.

decreases and the mobility $\bar{\mu}$ increases with the increase in P_1-value. Between the P_1-value of 0.2 and 0.5, where the conduction type changes from one-carrier to two-carrier systems, concentration and mobility look like not to change in great extent. At the P_1-value of about 0.7, the carrier concentration shows a minimum on the PyC-group (1.82×10^{24} m^{-3}). For the COKE-group, the minimum could not show clearly, because of their low graphitization degrees. The PyC-group shows a larger mobility and a smaller carrier concentration than the COKE-group.

2.4. Discussion

2.4.1. Effect of texture on graphitization of carbon materials

There has been evidence that the graphitizability of a carbon is strongly influenced by the degree of bending of hexagonal carbon layer planes in texture [2-14]. Thus, the carbon materials with plate-like morphology can be graphitized easily. However, carbons in which the layer planes are highly curved tend to remain turbostratic and are only partially graphitized even after high temperature treatment, glass-like carbon being a typical example.

The graphitization degree of the I-series fibers, which are prepared from the same precursor pitch, depends on the texture in their cross-sections; the fiber I-1-30 having radial texture with open wedge shows the highest P_1-value among the series. This result suggests the importance of the presence of an open wedge for graphitization, which may relax the strain due to crystallite growth in the cross-section of fibers during high temperature treatment. The opening of the wedge was observed to increase after the heat-treatment at high temperatures and also large smooth flakes were observed under SEM, as shown in Fig. 2-2(b). From this discussion, it is reasonable that the fiber

KOA-R having the largest opening of wedge shows the highest degree of graphitization among the group of MPCF (Fig. 2-2(a)).

The group of VGCF with concentric texture in their cross-section shows the dependence of graphitization on their diameters. Speck, et al. [2-15] calculated the change of free energy with graphitization from the cylindrical geometry of the vapor-grown carbon fiber. In other words, the release of strain energy in the transformation from a curved carbon layers to a flat ones could be estimated from the radius of curvature of layer planes in the fiber. As the result of the theoretical calculation, the larger diameter of carbon fiber showed the lower energy needed for graphitization. This result can be supported by the present experiment that the higher P_1-value is obtained in the fiber with the larger diameter.

2.4.2. Effect of texture on relations among graphitization parameters

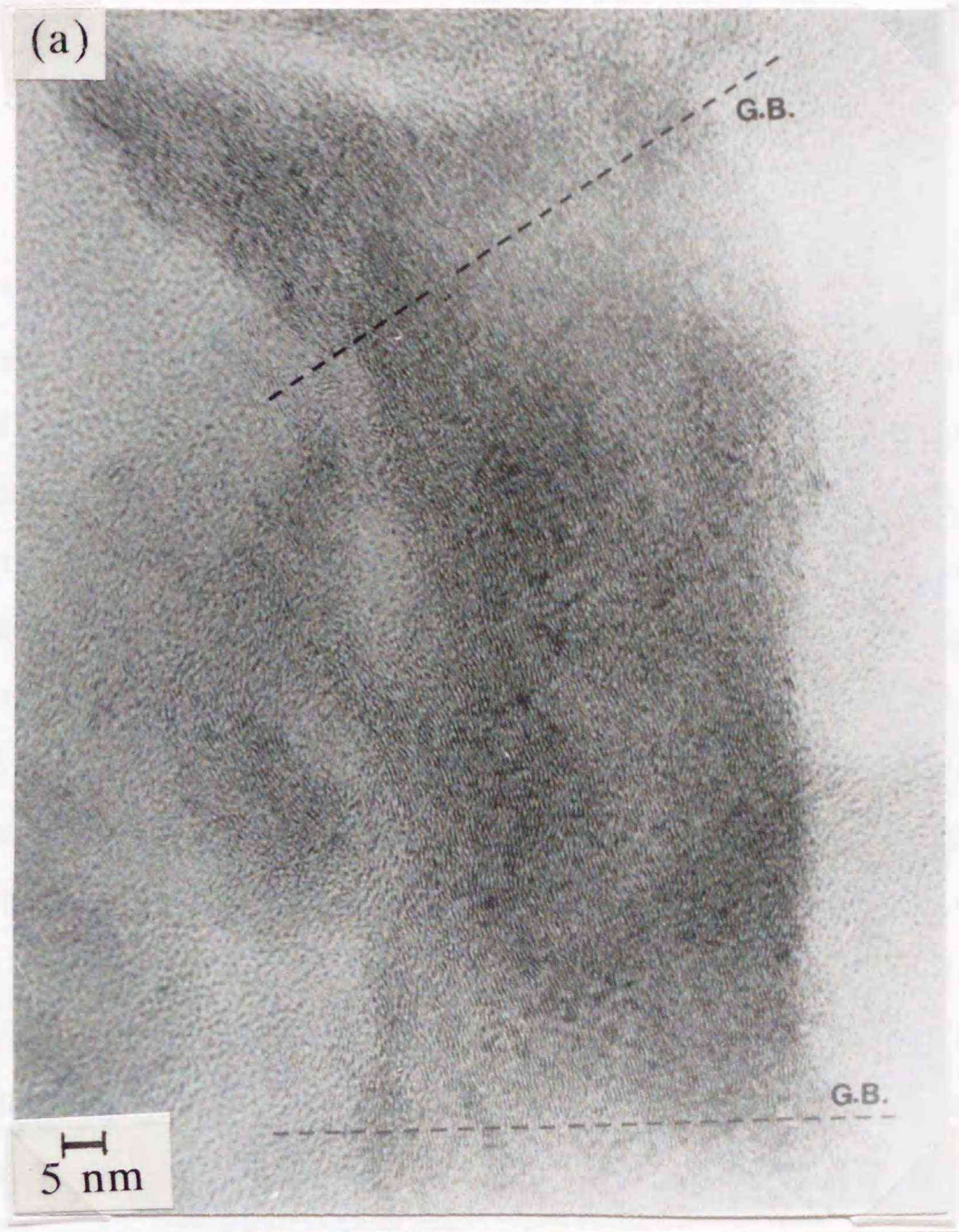
The graphitization degree, P_1, in fact, is estimated as a deviation from the structure from ideal graphitic one which has three-dimensional stacking of the hexagonal carbon layer planes. Thus, the P_1-value is a volume fraction of graphitic structure in a carbon material. On the other hand, average interlayer spacing, $\bar{d}_{002}$, is an average distance of between carbon layers, which is calculated from the Bragg angle of either 002 or 004 diffraction lines. Since 00ℓ diffraction lines are observed as higher and sharper line profile for graphitized carbon than for turbostratic carbon. Therefore, a well-graphitized region strongly reflects on the $\bar{d}_{002}$-value determined from the observed profiles. Even though turbostratic structure partially remains in a carbon material of which the major part is graphitic structure, it is reasonably supposed that turbostratic structure

can not reflect on the $\bar{d}_{002}$-value, but can reflect on the P_1-value. This is the reason for the downward deflection of the observed relation of $\bar{d}_{002}$ vs. P_1 from the hypothetical linear relation.

Empirical calculations for the relation between P_1 and $\bar{d}_{002}$ had been studied by many authors [2-16, -17, -18]. They did not take into account of the fact that there is inhomogeneity even interlayer spacing in most of carbon materials. As the graphitization process, e. g. above the P_1-value of 0.5, the possibility that the graphitic staking extends to whole crystallite, giving strong reflection on 00ℓ diffraction lines, increases and results in low $\bar{d}_{002}$-value. Consequently, a remarkable downward deflection from the linear relation. Such inhomogeneity is reasonably supposed to depend strongly on the texture of carbon material.

The PyC-group, which has a strong orientation of carbon layers, showed the $\bar{d}_{002}$-value close to graphite after high temperature heat-treatment. Under SEM observation, it was obviously observed that certain strain remained on carbon layers in these samples corresponding to the pebble structure, even after graphitization, as shown in Fig. 2-1. Because of the strain, graphitic structure of the sample heat-treated at high temperature seems to be incomplete, i. e., the P_1-value does not reach 1.0. This prediction agrees with the positions of the PyC-group in the relation of $\bar{d}_{002}$ vs. P_1.

The micrographs of the cross-section of the carbonized fiber I-1-12 and the graphitized fiber I-1-28 (radial texture with wedge) with high-resolution transmission electron microscopy (TEM) is shown in Fig. 2-11 [2-19]. Some strain on the oriented layer planes of the cross-section in the fibers is observed as "zig-zag" layers separated by boundaries. Each



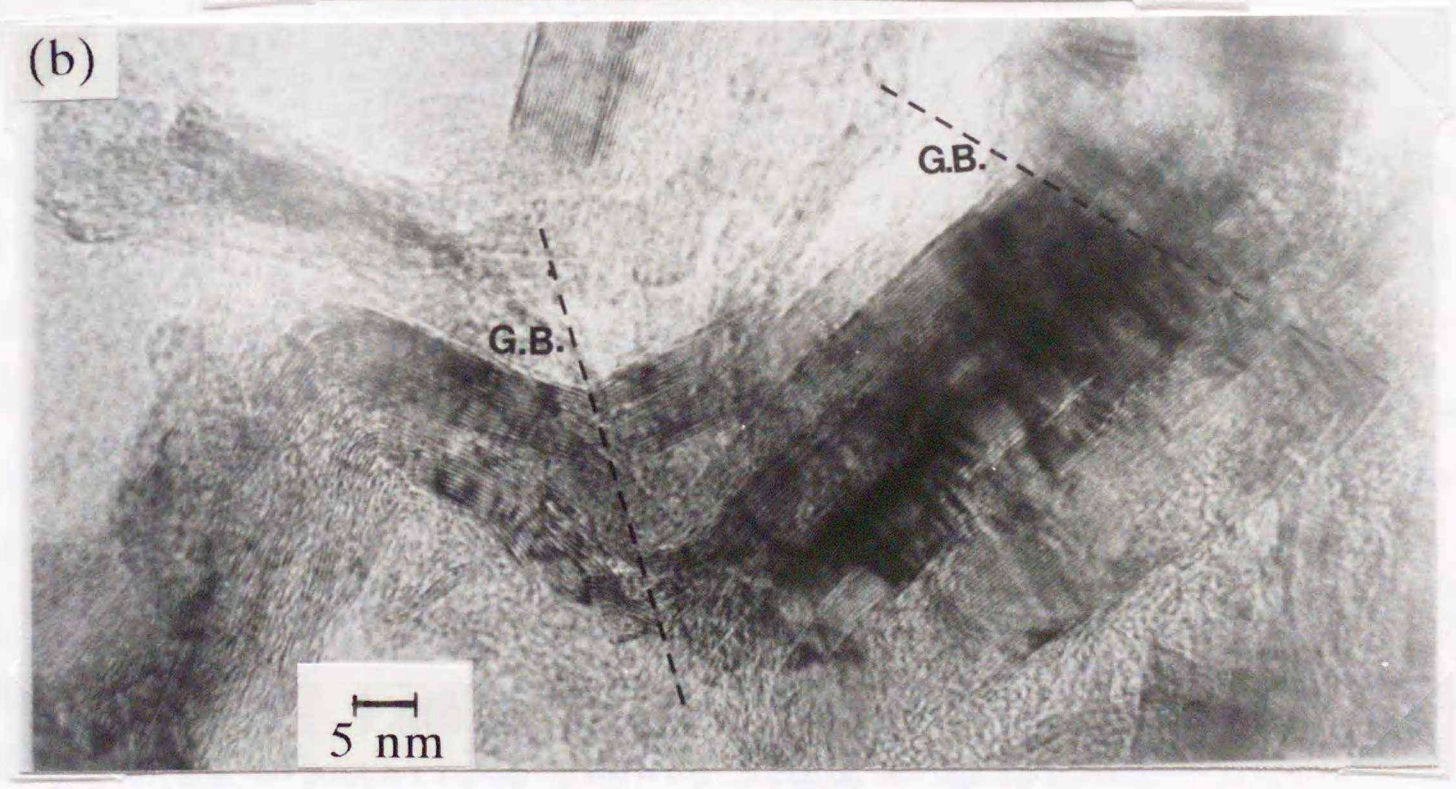


Fig. 2-11 TEM micrographs of the oriented region in the cross-section of (a) the carbonized fiber I-1-12 and (b) the graphitized fiber I-1-28 [2-19].

oriented region forms a grain. The transversal size of oriented region did not change after high temperature treatment (Fig. 2-11(b)). Therefore, the strain of carbon layers in the cross-section could not be released even after high temperature treatment, so that the volume fraction of graphitic structure in the fiber dose not increase remarkably. However, the oriented region is graphitized, which reflect on $\overline{d}_{002}$-value, as discussed before. Consequently, the MPCF-group shows the strongest downward deflection in the relation of $\overline{d}_{002}$ vs. P_1 (Fig. 2-4).

On the other hand, it was observed that the longitudinal size of the oriented region which was a major part of the fiber was graphitized and its size grew along fiber axis [2-19]. This anisotropy for the crystallite size along a-axis between transversal and longitudinal in the oriented region is interpreted by axial orientation in the carbon fiber. The MPCF-group shows rapid crystallite growth along a-axis, as observed on the relation of $L_a(110)$ vs. P_1 (Fig. 2-5(a)), in comparison with other samples. It seems to be explained by the fact that the crystallite can grow easier along the fiber axis than in the cross-section. Because the present technique for X-ray powder diffraction can not be distinguished between crystallite size along the fiber axis and the one in the cross-section, the overall crystallite size is measured to be larger.

The relations of $L_c(004)$ and $L_c(002)$ vs. P_1 are independent of carbon samples used, probably due to no appreciable effect of sample texture on crystallite growth along c-axis.

Magnetoresistance, $(\Delta\rho/\rho)_{cr}$, value is mostly defined by the electrical carrier motion in the hexagonal carbon layers and hence is sensitive to the size of carbon layers and also to the presence of imperfections in the layers [2-7]. Therefore, it is reasonable that the $(\Delta\rho/\rho)_{cr}$-value shows a unique relation with

$L_a(110)$, as shown in Fig. 2-7(c). The relation of $(\Delta\rho/\rho)_{cr}$ vs. $\bar{d}_{002}$ seems to be a unique, but is not definite because the region of $\bar{d}_{002}$-value corresponding to positive $(\Delta\rho/\rho)_{cr}$-value is limited in small range ($0.3380 < \bar{d}_{002} < 0.3354$ nm). The relation of $(\Delta\rho/\rho)_{cr}$ vs. P_1 for the MPCF-group is different from that for the COKE- and PyC-group, which can be understood by the same interpretation as the case of the relation of $L_a(110)$ vs. P_1.

2.5. Summary

The experimental results suggest the importance of the relaxation of some strain on hexagonal carbon layer planes for graphitization. Thus, whether strain in a carbon material can be removed during heat-treatment at high temperatures is strongly influenced not only by its starting material, but also by its texture.

The graphitization degree P_1 was a volume fraction of the graphitic structure in a carbon material, but the average interlayer spacing $\bar{d}_{002}$ was affected by a well-graphitized region. Between these two parameters, P_1 and $\bar{d}_{002}$, therefore, an exponential relation was observed on the basis of a number of experimental points on various carbon samples. The magnetoresistance was found to have certain relation with the crystallite size of carbon layers L_a, regardless of the kind of carbon. The relation between degree of graphitization and other graphitization parameters depended strongly on the kind of carbon materials.

An effect of the structural characteristics of host carbon material on intercalation reaction of sulfuric acid shall be discussed in Chapter 4.

References

2-1 M. Inagaki, J. Mater. Res., 4, 1560 (1989).
2-2 M. Inagaki, M. Shiraishi, M. Nakamizo and Y. Hishiyama, Tanso, 1984[No. 118], 165 (1984).
2-3 M. Inagaki, Tanso, 1963[No. 36], 28 (1963).
2-4 B. E. Warren, Phys. Rev., 59, 693 (1941).
2-5 C. R. Houska and B. E. Warren, J. Appl. Phys., 25, 1503 (1954).
2-6 Y. Hishiyama, A. Ono and M. Hashimoto, Jap. J. Appl. Phys., 10, 416 (1971).
2-7 Y. Hishiyama, Y. Kaburagi and M. Inagaki, "Chemistry and Physics of Carbon" Vol. 23 (1991) p. 1.
2-8 Y. Hishiyama, "Introduction to Carbon Material" pp.41-54. Kakaku Gizyutsu Sya, (1984).
2-9 A. Yoshida and Y. Hishiyama, Tanso, 1987[No. 130], 110 (1987).
2-10 J. C. Bowman, "Proc. 1st and 2nd Cof. on Carbon", Buffalo Univ., (1956) 59.
2-11 T. Noda, M. Iwatsuki and M. Inagaki, Tanso, 1966[No. 47], 14 (1966).
2-12 A. Ono, Doctor Thesis, Nihon Uviversity.
2-13 Y. Hishiyama and Y. Kaburagi, Tanso, 1979[No. 98], 89 (1979).
2-14 A. Oberlin. Carbon, 22, 521 (1984).
2-15 J. P. Speck, M. Endo and M. S. Dresselhaus, J. Cryst. Growth, 94, 834 (1989).
2-16 R. E. Franlkin, Acta Cryst., 4, 253 (1951).
2-17 G. E. Bacon, Acta Cryst, 4, 558 (1951).
2-18 J. Maire and J. Méring, "les carbones" Vol. 1, Masson et Cie, (1965) pp.129.
2-19 M. Inagaki, N. Iwashita, Y. Hishiyama, Y. Kaburagi, A. Yoshida, A. Oberlin, K. Lafdi, S. Bonnamy and Y. Yamada, Tanso, 1991[No. 147], 57 (1991).

CHAPTER 3

Potential change during intercalation of sulfuric acid into graphite by chemical oxidation

3.1. Introduction

There are two methods for synthesis of graphite intercalation compounds with sulfuric acid(H_2SO_4-GICs); chemical and electrochemical oxidations. In the case of the latter, it has been known that potential curve against electric quantity during intercalation of sulfuric acid into graphite by galvanostatic oxidation is shown to increase in stepwise. The potential curve has been quantitatively studied by many authors. Metrot [3-1,2] discussed the potential curve observed on the electrode of a highly oriented pyrolytic graphite (HOPG) by using a two-capacitor model. On the other hand, the former method has been used as the simplest one for synthesis of H_2SO_4-GICs and industrially employed for the production of exfoliated graphite. The oxidants used for the synthesis of H_2SO_4-GICs are HNO_3, CrO_3, $KMnO_4$, PbO_2, etc. [3-3]. However, there has been no quantitative comparison between these two methods.

In the present chapter, the intercalation of sulfuric acid by chemical oxidation with nitric acid and potassium permanganate is followed by measuring the potential of graphite electrode. The potential change during the chemical intercalation is compared with the one during electrochemical intercalation. The formation process of H_2SO_4-GICs and effect of dilution of sulfuric acid are discussed by using the potential changes obtained.

3.2. Experimental

Flaky natural graphite powders with average size of 400 μm

(sample code: NG400) were used as host material. The graphite electrode and test cell used are schematically shown in Fig. 3-1. In order to measure potential, the graphite powders of 50 mg were held between plastic plates (30 X 30 mm^2) with platinum wire as a supporting electrode (Fig. 3-1(b)). The electrode of $Hg/HgSO_4$ with Luggin capillary was adopted as a reference. 50 cm^3 of sulfuric acids with different concentrations (10, 14 and 18 mol/dm^3) and that with 18 mol/dm^3 plus dissolved sodium nitrite ($NaNO_2$) were used. Nitric acid (13.8 mol/dm^3) and potassium permanganate (powders), $KMnO_4$, were used as chemical oxidants to synthesize the GICs.

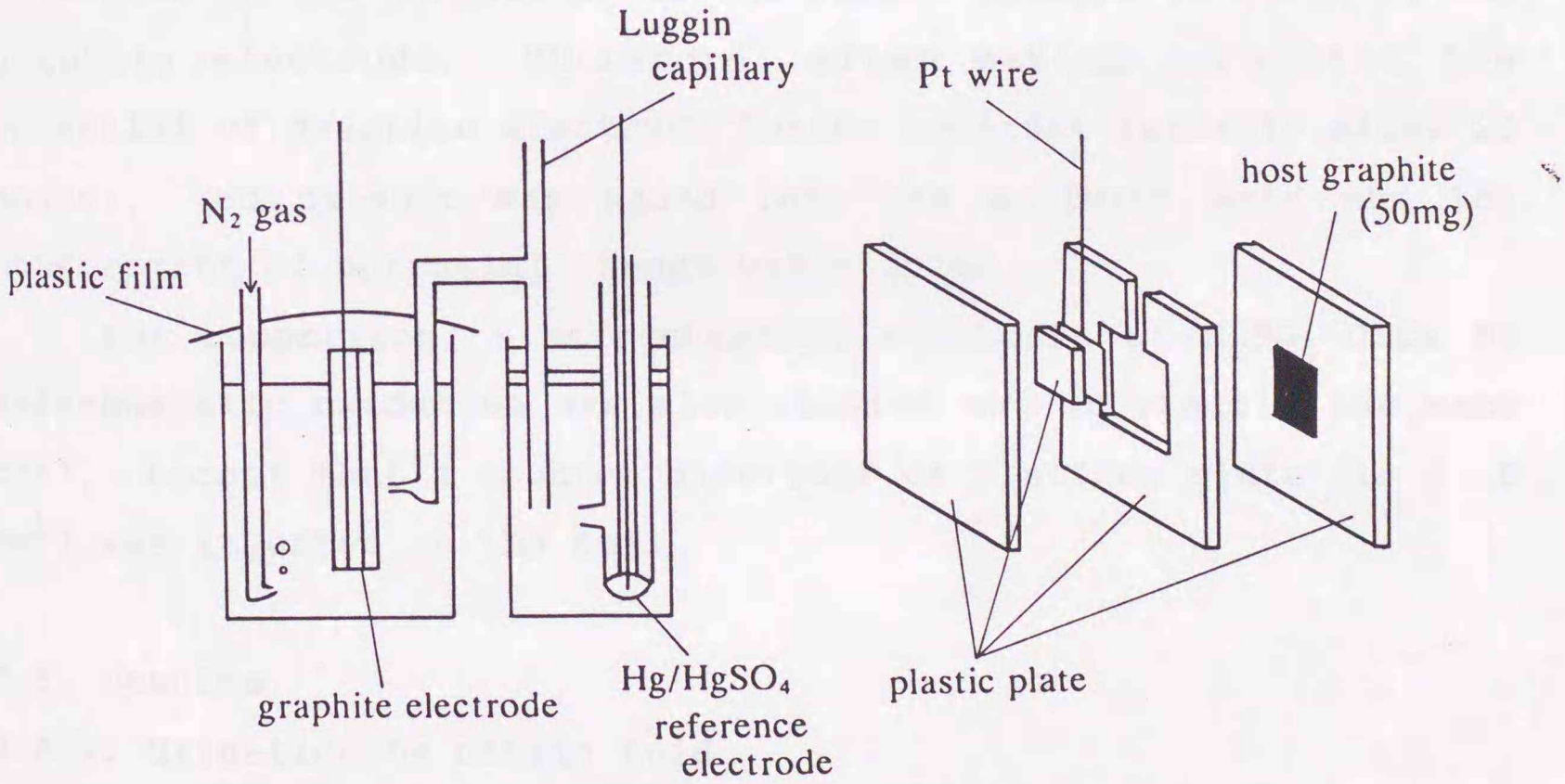


Fig. 3-1 Scheme of cell assembly.
(a) Electrochemical cell, (b) Graphite electrode.

The test cell was covered with a plastic film to prevent absorption of moisture in air by sulfuric acid and also kept at constant temperature of 0°C by using a bath with ice-water mixture. The sulfuric acid solutions were bubbled by nitrogen gas and also magnetically stirred.

The potential of the working electrode with time after the addition of certain amount of an oxidant was continuously recorded. Characterization of the synthesized H_2SO_4-GICs was carried out with X-ray powder diffractometry by preventing the decomposition in a polyethylene bag.

By immersing a graphite electrode into sulfuric acid, the potential gradually increased and saturated at a certain value after 20 hours, probably due either to the adsorption of H_2SO_4 molecules on the surface or to the change in work function of the graphite electrode. Therefore, after making sure that the potential of graphite electrode became constant (usually after 20 hours), an oxidant was added into the sulfuric acid and the measurement of potential change was started.

For comparison, electrochemical synthesis of H_2SO_4-GICs by galvanostatic oxidation was also carried out in exactly the same cell, except that a counter electrode of platinum plate (10 X 10 mm^2) was inserted in the cell.

3.3. Results

3.3.1. Oxidation by nitric acid

The curves of potential against reaction time in H_2SO_4 of 18 mol/dm^3 are shown in Fig. 3-2, when nitric acid is used as a chemical oxidant. The molar ratios of HNO_3 to carbon are 16.6, 3.3, 0.33 and 0.17, respectively. X-ray powder patterns of the sample electrodes oxidized up to the points a to e in Fig. 3-2 are shown in Fig. 3-3.

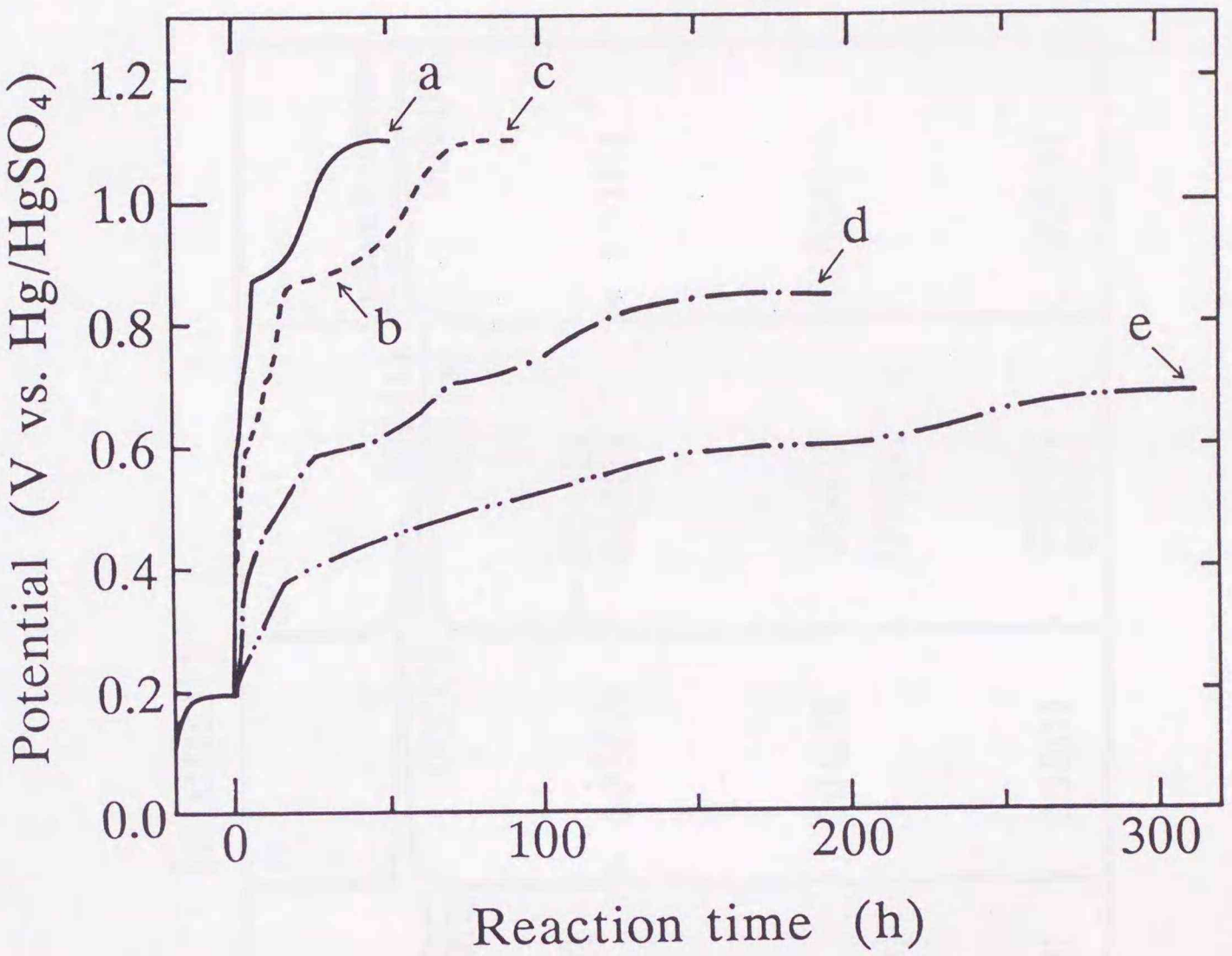


Fig. 3-2 Potential changes of graphite electrode with reaction time in H_2SO_4 of 18 mol/dm^3 by chemical oxidation with nitric acid.
——— : HNO_3/carbon (in mole) = 16.6,
- - - - - - : 3.3, ——·—— : 0.33, ——··—— : 0.17.

The potential increases to positive direction in stepwise. A plateau at a potential around 0.9 V is characteristic. Additionally, faint plateaux can be recognized around 0.7 and 0.6 V. The rate of potential changes and the potential reached after

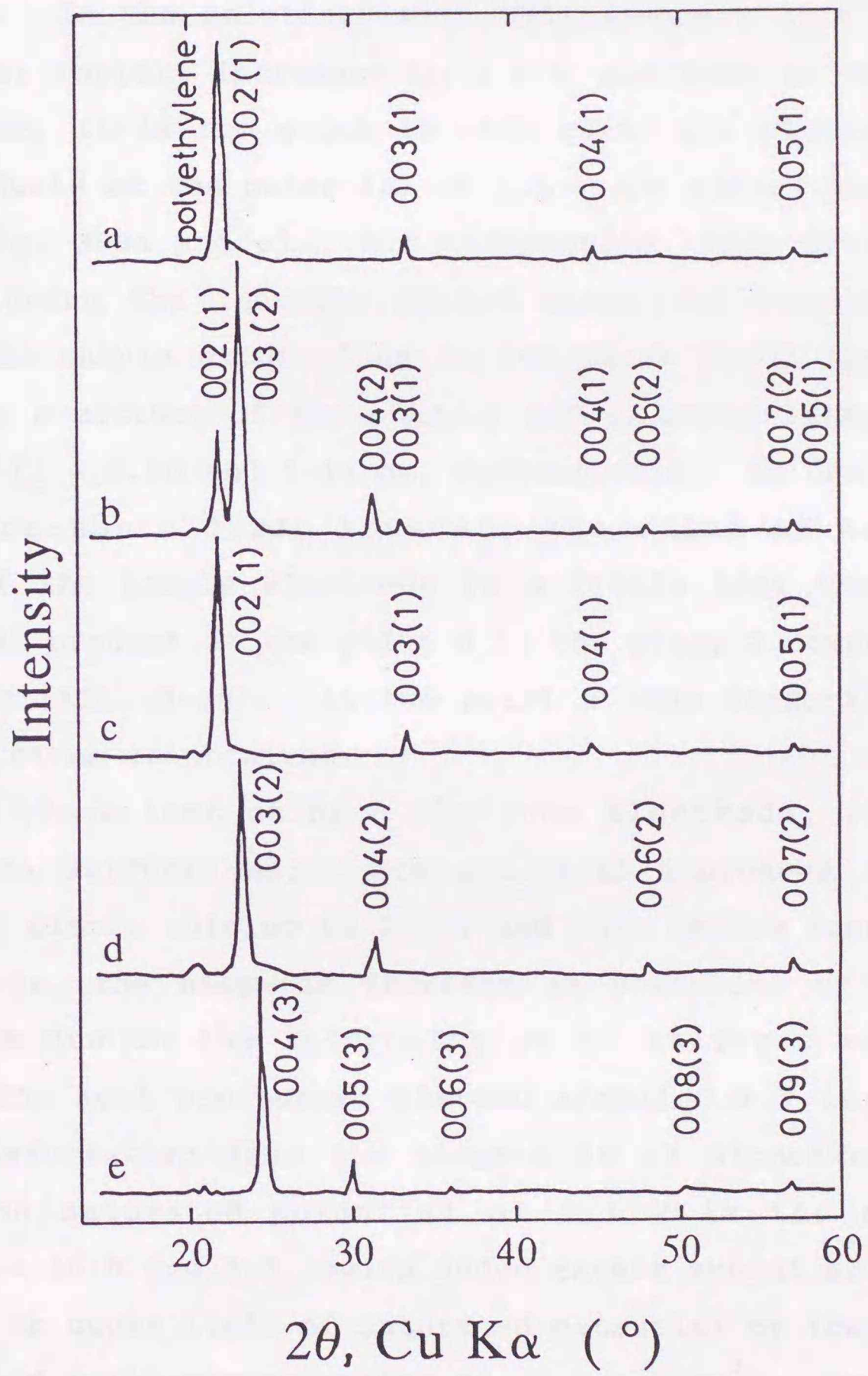


Fig. 3-3 X-ray powder patterns for H_2SO_4-GICs formed by chemical oxidation with nitric acid. Each pattern corresponds to the respective point on the potential curves in Fig. 3-2.

long reaction time (saturated potential) depend on the amount of nitric acid. In the solutions with HNO_3/carbon = 16.6 and 3.3, the potential rapidly increases to 1.1 V and then is saturated. In the former, it is too quick to make clear the plateau at 0.9 V. The products at the potential of 1.1 V are always the stage-1 compound (Fig. 3-3a and c). All diffraction lines observed are indexed by using the identity period along the c-axis, I_c, of 0.80 nm. The sample oxidized up to the point b (on the plateau at 0.9 V) is a mixture of the stage-1 and -2 structures (Fig. 3-3b), giving I_c = 0.80 and 1.14 nm, respectively. In the solution with HNO_3/carbon = 0.33, however, the value of saturated potential of the sample electrode is a little less than 0.9 V, and the final product at the point d is the stage-2 compound with I_c = 1.14 nm (Fig. 3-3d). At the point e, the stage-3 compound with I_c = 1.47 nm is obtained.

In the blank test using a platinum electrode, which was unreactive to sulfuric acid, its potential increased instantly after adding nitric acid up to 1.1 V and then became constant.

Therefore, the stepwise increase in potential of graphite electrode is due to the intercalation of sulfuric acid into graphite. The most pronounced plateau around 0.9 V is produced by the transformation from the stage-2 to -1 structures. The value of the saturated potential of 1.1 V in the cases of HNO_3/carbon = 16.6 and 3.3, being added excess amount of oxidant, seems to be an upper limit of saturated potential by the addition of nitric acid (with concentration of 13.8 mol/dm^3) into H_2SO_4 of 18 mol/dm^3.

3.3.2. Oxidation by potassium permanganate

The potential changes by the addition of potassium permanganate in H_2SO_4 of 18 mol/dm^3 are shown in Fig. 3-4. The

relative amounts of added potassium permanganate to carbon are 3.3 and 1.5 and 0.33 in molar ratios. X-ray powder patterns at the points f to h in Fig. 3-4 are shown in Fig. 3-5. Characteristic plateaux in the potential changes around 0.9, 0.7 and 0.6 V are also observed. The compound on the plateau at 0.9 V (at the point g) is a mixture of the stage-1 and -2 structures (Fig. 3-5g), exactly the same as the case of nitric acid. The plateau at 0.6 V appears more distinctly than that in the case of nitric acid. The value of saturated potential by adding small amounts of oxidant ($KMnO_4$/carbon = 0.33) is below 0.5 V, so that the final product at the point h is a mixture of unreacted graphite and the compounds with undefined high stage numbers (Fig. 3-5h). On the plateau at 0.6 V, the stage-3 structure was detected. Therefore, the plateau at 0.6 V seems to correspond to the stage transformation from high stage (seemingly stage-4) to stage-3 structures.

Even if the oxidant having more than $KMnO_4$/carbon = 1.5 is added, some amount of the oxidant undissolves and the rate of potential increase does not change, suggesting that the potential increase depends mostly on the solubility of potassium permanganate into H_2SO_4 of 18 mol/dm^3. The saturated potential of 1.3 V in the case of $KMnO_4$/carbon = 1.5 and 3.3 seems to be the upper limit of saturated potential by the addition of potassium permanganate powders into H_2SO_4 of 18 mol/dm^3, and this value is higher than that by nitric acid. I_c of the stage-1 compound finally obtained after attaining the upper limit of saturated potential (at the point f) was 0.79 nm, slightly smaller than the same stage compound obtained by nitric acid (the point a and c in Fig. 3-2).

Precipitates with red-brown color were produced in the solution after formation of the stage-1 compound. The as-

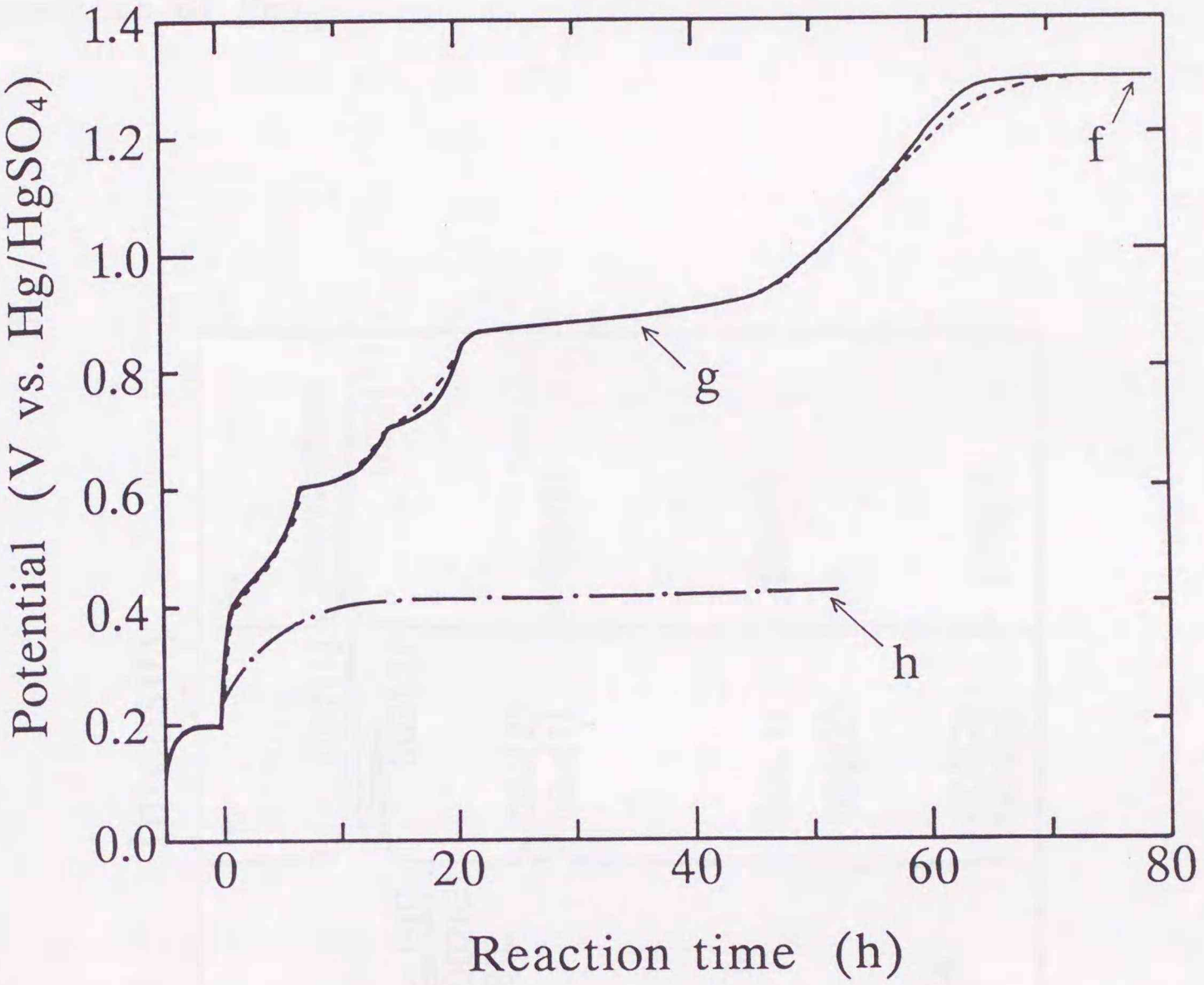


Fig. 3-4 Potential changes of graphite electrode with reaction time in H_2SO_4 of 18 mol/dm^3 by chemical oxidation with potassium permanganate.
——— : $KMnO_4$/carbon (in mole) = 3.3,
- - - - - - : 1.5, —·— : 0.33.

precipitates was amorphous, but the ones heat-treated up to 1000^{o}C in nitrogen atmosphere were identified as Mn_3O_4 from its X-ray powder pattern. From the weight change during heat-treatment with thermogravimetry and from the differential thermal

analysis curve, the as-precipitates were supposed to have the composition of MnO_3.

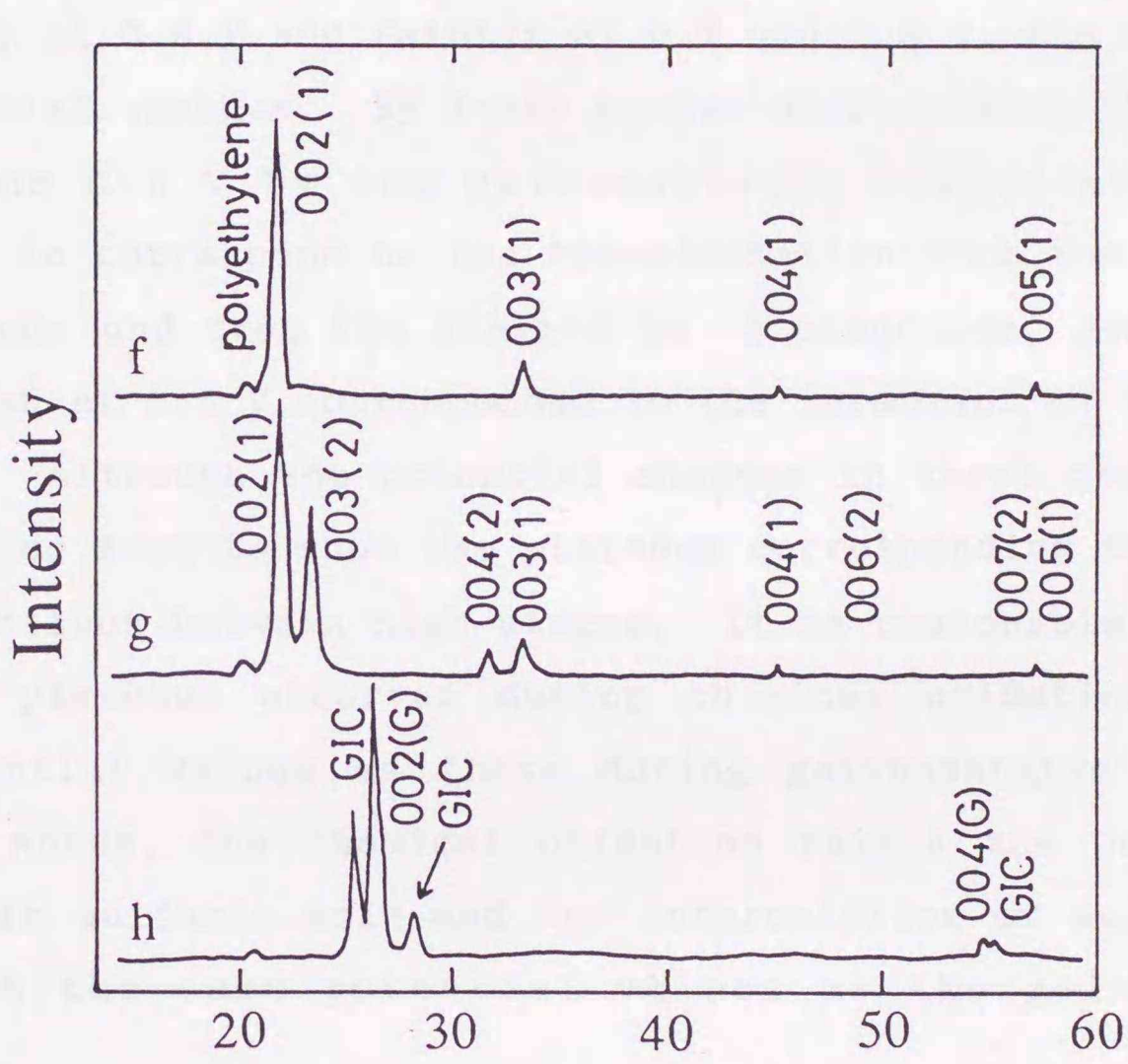


Fig. 3-5 X-ray powder patterns for H_2SO_4-GICs formed by chemical oxidation with potassium permanganate. Each pattern corresponds to the respective point on the potential curves in Fig. 3-4.

3.3.3. Electrolysis with galvanostatic oxidation

The curve of potential against electric quantity during galvanostatic oxidation in sulfuric acid of 18 mol/dm^3 with 200 μA (4 mA/g-carbon) is shown in Fig. 3-6. For comparison, the observed curves during chemical oxidation in H_2SO_4 of 18 mol/dm^3 are shown in the same figure. Characteristic plateaux, distinctly at 0.9 V and faintly at 0.7 and 0.6 V, are observed on all potential changes. By X-ray powder diffraction, the plateaux at 0.7 and 0.9 V by the galvanostatic oxidation was also confirmed to correspond to the transformation from the stage-2 to -1 compounds and from the stage-3 to -2 compounds, respectively. The plateau at 0.6 V corresponded to the formation of the stage-3 compound. Although the potential changes in three cases in Fig. 3-7 were too fast to show the plateaux corresponding to all stage transformations between high stages, it is reasonable to suppose that the plateaux observed during chemical oxidation have the same potential values as those during galvanostatic oxidation. In other words, the chemical oxidation raises the potential of graphite in sulfuric acid and the intercalation of sulfuric acid occurs at the same potential values as the galvanostatic oxidation.

3.3.4. Formation of H_2SO_4-GICs in diluted sulfuric acid

The potential changes during chemical and galvanostatic oxidations, and X-ray powder patterns for the compounds obtained after reaching the upper limit of saturated potential in H_2SO_4 of 14 and 10 mol/dm^3 are shown in Figs. 3-7 and 3-8, respectively. In the chemical oxidation process, enough amounts of oxidant was added to reach the upper limit of potential in each concentration of sulfuric acid.

The final product obtained by galvanostatic oxidation at the

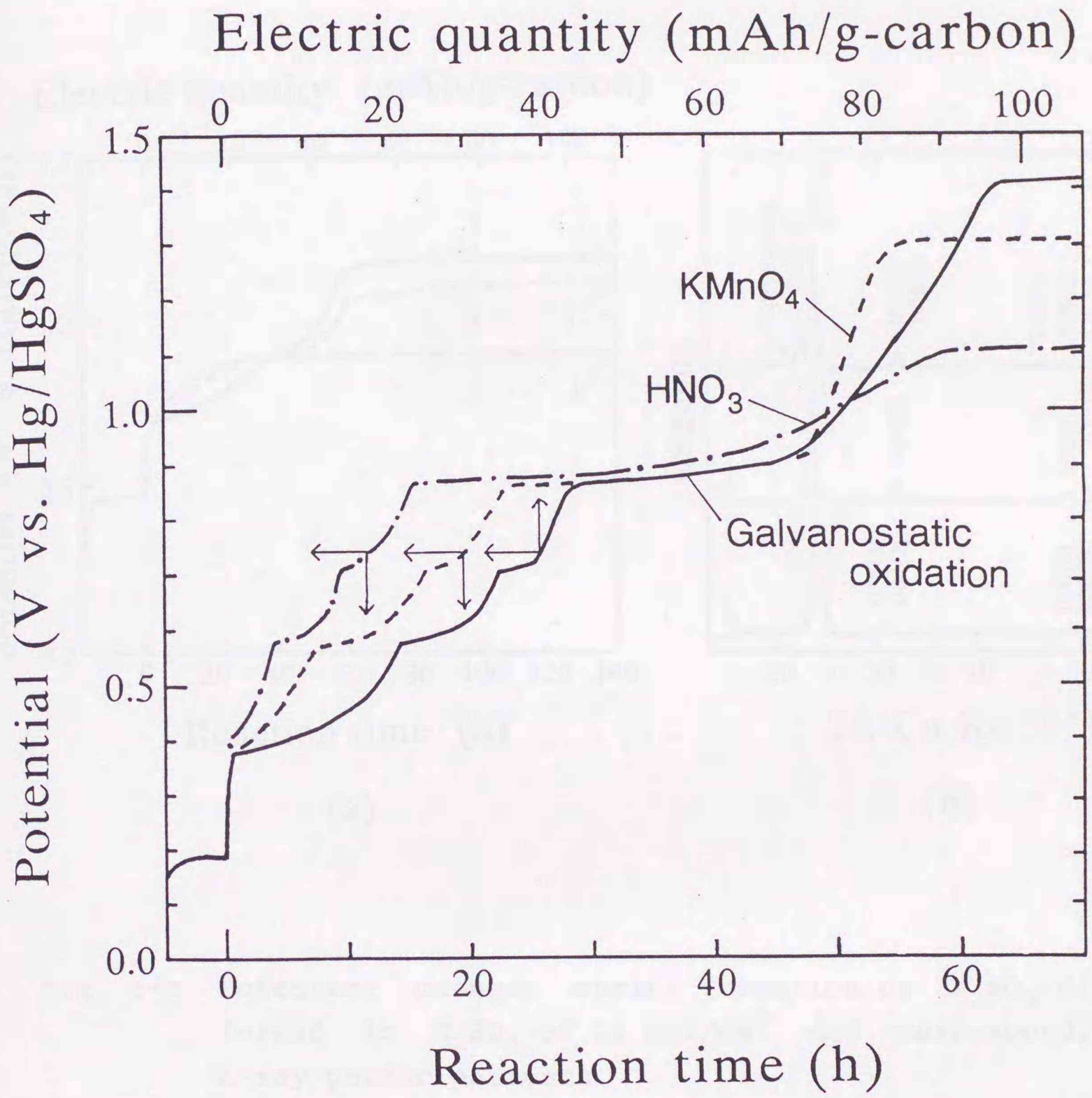


Fig. 3-6 Potential changes during formation of H_2SO_4-GICs in H_2SO_4 of 18 mol/dm^3.

———— : by galvanostatic oxidation (200 μA),

------ : by chemical oxidation with potassium permanganate ($KMnO_4$/carbon = 1.5),

——·—— : by chemical oxidation with nitric acid (HNO_3/carbon = 3.3).

(1 mAh = 3.6 C)

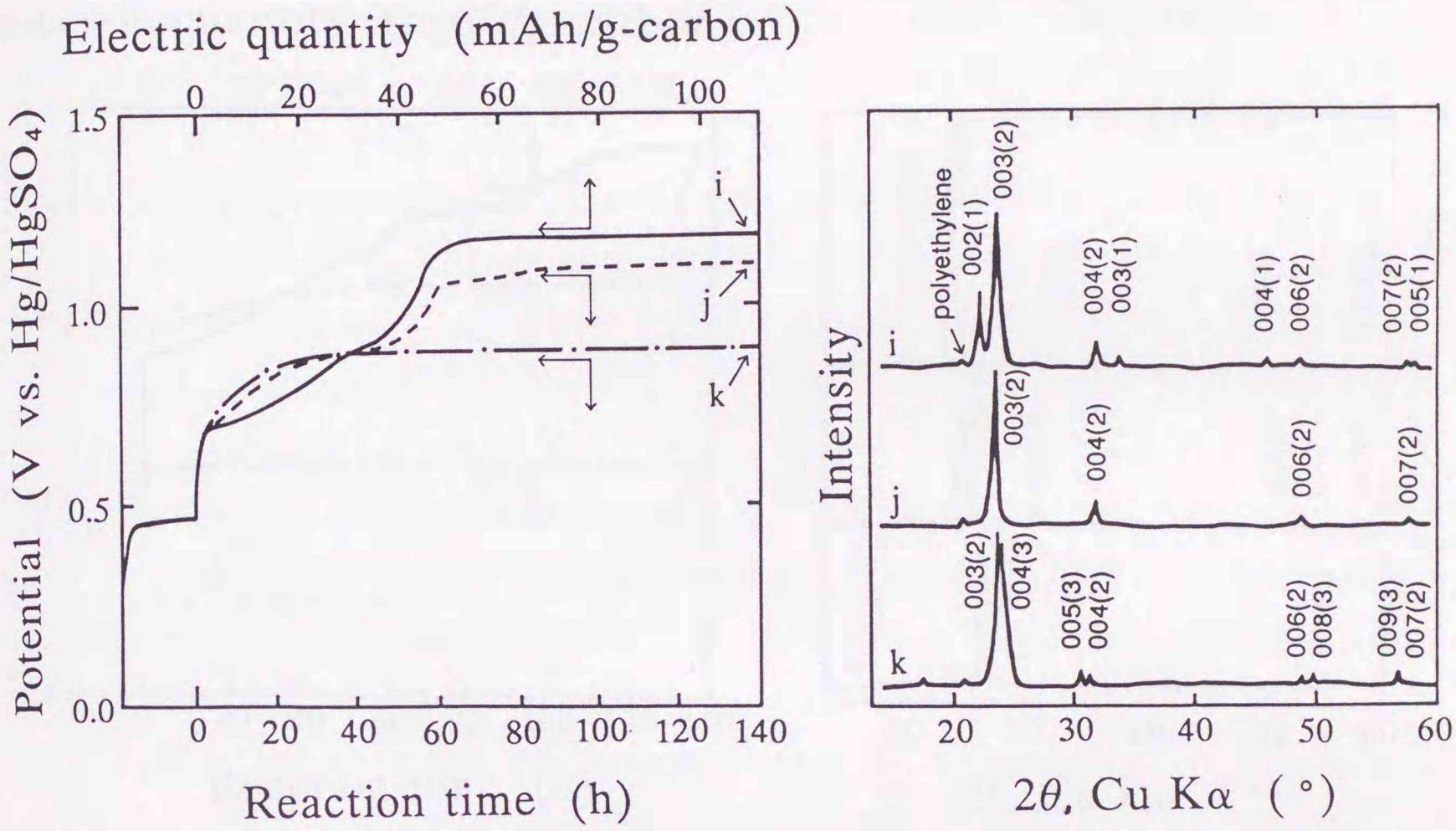


Fig. 3-7 Potential changes during formation of H_2SO_4-GICs formed in H_2SO_4 of 14 mol/dm^3 and corresponding X-ray powder patterns.

(a) potential changes ———— : galvanostatic, ------ : potassium permanganate ($KMnO_4$/carbon = 1.5), ——·—— : nitric acid (HNO_3/carbon = 3.3) oxidations.

(b) X-ray powder patterns for the respective point on potential curves.

(1 mAh = 3.6 C)

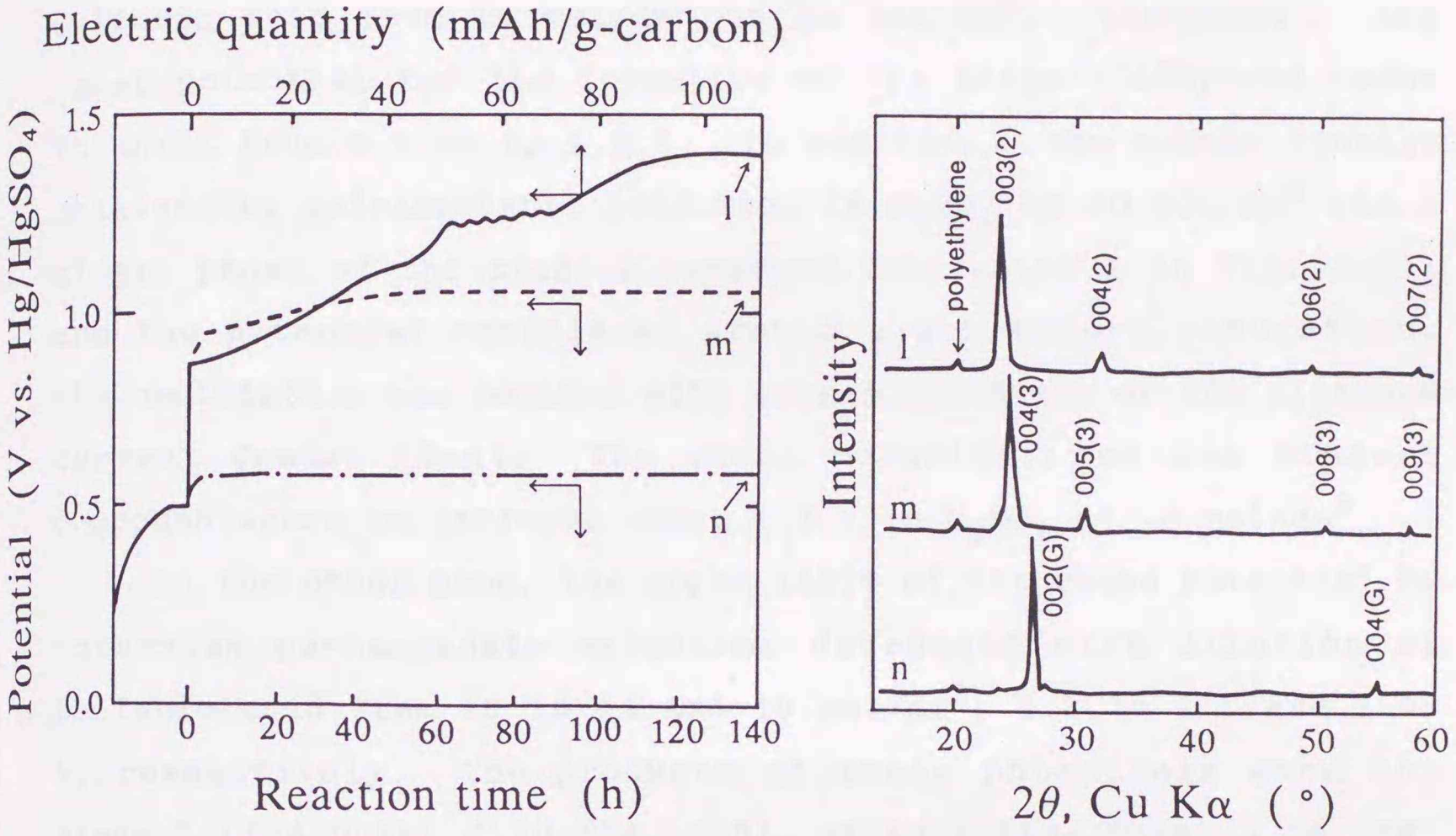


Fig. 3-8 Potential changes during formation of H_2SO_4-GICs formed in H_2SO_4 of 10 mol/dm^3 and corresponding X-ray powder patterns.

(a) potential changes ——— : galvanostatic, ------ : potassium permanganate ($KMnO_4$/carbon = 1.5), ——·—— : nitric acid (HNO_3/carbon = 3.3) oxidations.

(b) X-ray powder patterns for the respective point on potential curves.

(1 mAh = 3.6 C)

potential of 1.2 V in H_2SO_4 of 14 mol/dm^3 is a mixture of the stage-1 and -2 structures (the point i in Fig. 3-7). By diluting sulfuric acid from 18 mol/dm^3 to 14 mol/dm^3, therefore, the onset potential for the formation of the stage-1 compound seems to shift from 0.9 up to 1.2 V. In addition, the sample finally obtained by galvanostatic oxidation in H_2SO_4 of 10 mol/dm^3 was a single phase of the stage-2 compound (the point l in Fig. 3-8), and the potential oscillates around 1.2 V before saturation. The oscillation was related with oxygen evolution on the platinum current feeder [3-4]. The onset potential for the stage-1 compound seems to increase above 1.4 V in H_2SO_4 of 10 mol/dm^3.

On the other hand, the upper limit of saturated potential by potassium permanganate oxidation decreased with dilution of sulfuric acid from 18 to 14 and 10 mol/dm^3; 1.3 to 1.1 and 1.05 V, respectively. The products at these potentials were the stage-1 (the point f in Fig. 3-5), stage-2 (the point j in Fig. 3-8), and stage-3 (the point m in Fig. 3-8), respectively. This result is consistent with the increase of onset potential for stage transformation in H_2SO_4-GICs with dilution of sulfuric acid. The upper limit of saturated potential by nitric acid oxidation also decreased with dilution of sulfuric acid and stage structure of final product became a higher stage number. The product at upper limit of saturated potential of 0.9 V by nitric acid oxidation in H_2SO_4 of 14 mol/dm^3 was a mixture of the stage-2 and -3 structures (the point k in Fig. 3-7). In H_2SO_4 of 10 mol/dm^3, the potential slightly increased during chemical oxidation with nitric acid and, even at the upper limit of the potential of 0.6 V, no intercalation of sulfuric acid was detected (the point n in Fig. 3-8).

The present results agree with the experimental fact that the formation of H_2SO_4-GICs by chemical oxidation gets the more

difficult in the more dilute sulfuric acid [3-5]. In the following section 3.4.3, effect of dilution of sulfuric acid on the formation of H_2SO_4-GICs will be discussed more quantitatively.

The potential change during chemical oxidation with nitric acid in H_2SO_4 of 18 mol/dm^3 plus dissolved sodium nitrite of 0.29 g ($NaNO_2/HNO_3$ = 1.0, in molar ratio), was almost the same as that in the sulfuric acid solution with nitric acid. The upper limit of saturated potential was at 1.05 V, which was slightly lower than that in the sulfuric acid solution without the addition of $NaNO_2$, and the final product at the saturated potential was the stage-1 compound.

3.4. Discussion

3.4.1. Formation process of H_2SO_4-GICs

For the formation of GICs, both donor and acceptor-type compounds, electron transfer between carbon layers and guest materials (intercalates) has to be accomplished. In the case of acceptor-type compounds, for example H_2SO_4-GICs, electrons have to be extracted from the layers of host graphite either by electrochemical or by chemical oxidations. According to Metrot [3-1, -2], as a consequence of extraction of electrons, an electrical double layer on interface between graphite electrode and electrolyte (interfacial capacitance) is formed, and the potential of host graphite is raised as proved experimentally in the present work. The extraction of electrons from carbon layers is defined as charging process.

When the potential of the host graphite reached at a specific value, which is expressed by threshold potential, the intercalation of bisulfate ions takes place, accompanying neutral sulfuric acid molecules. Consequently, the Fermi level of energy

bands of host graphite is depressed [3-1, -2]. The potential is kept constant during intercalation until the completion of each stage structure, which is observed as the plateau in the curves of potential against the electric quantity or reaction time, as shown in the previous figures. During the potential plateau, stage structure is transformed by intercalation of additional sulfuric acid and by its rearrangement to lower stage one, which is defined as stage transformation process. Therefore, a mixture of stage-n and stage-(n-1) structures is observed on the plateau. A mixture of the stage-1 and -2 structures, for instance, is observed on the distinct potential plateau at 0.9 V in H_2SO_4 of 18 mol/dm^3 The potential value of transformation to each stage structure, showing the potential plateau, is expressed by onset potential for each stage. In Fig 3-9, the terms of these processes during the intercalation reaction of sulfuric acid into graphite are shown on a representative curve of potential change with reaction time by nitric acid oxidation.

During galvanostatic oxidation, electrons extracted from the host graphite flow to the counter electrode and are consumed by hydrogen evolution. During chemical oxidation, however, nitrate or permanganate ions pull out electrons from host graphite and reduce themselves. Permanganate ions, MnO_4^-, seemed to be reduced and then to precipitate as amorphous MnO_3. On nitrate ions, the reduction to HNO_2 seemed to be highly probable, which was soluble in sulfuric acid. So the following equations for each oxidants may be written;

$$NO_3^- + 3H^+ + 2e^- \longrightarrow HNO_2 + H_2O \ , \qquad (3\text{-}1)$$

$$MnO_4^- + 2H^+ + e^- \longrightarrow MnO_3\downarrow + H_2O \ , \qquad (3\text{-}2)$$

where e^- has to come from the host graphite, in other words, the

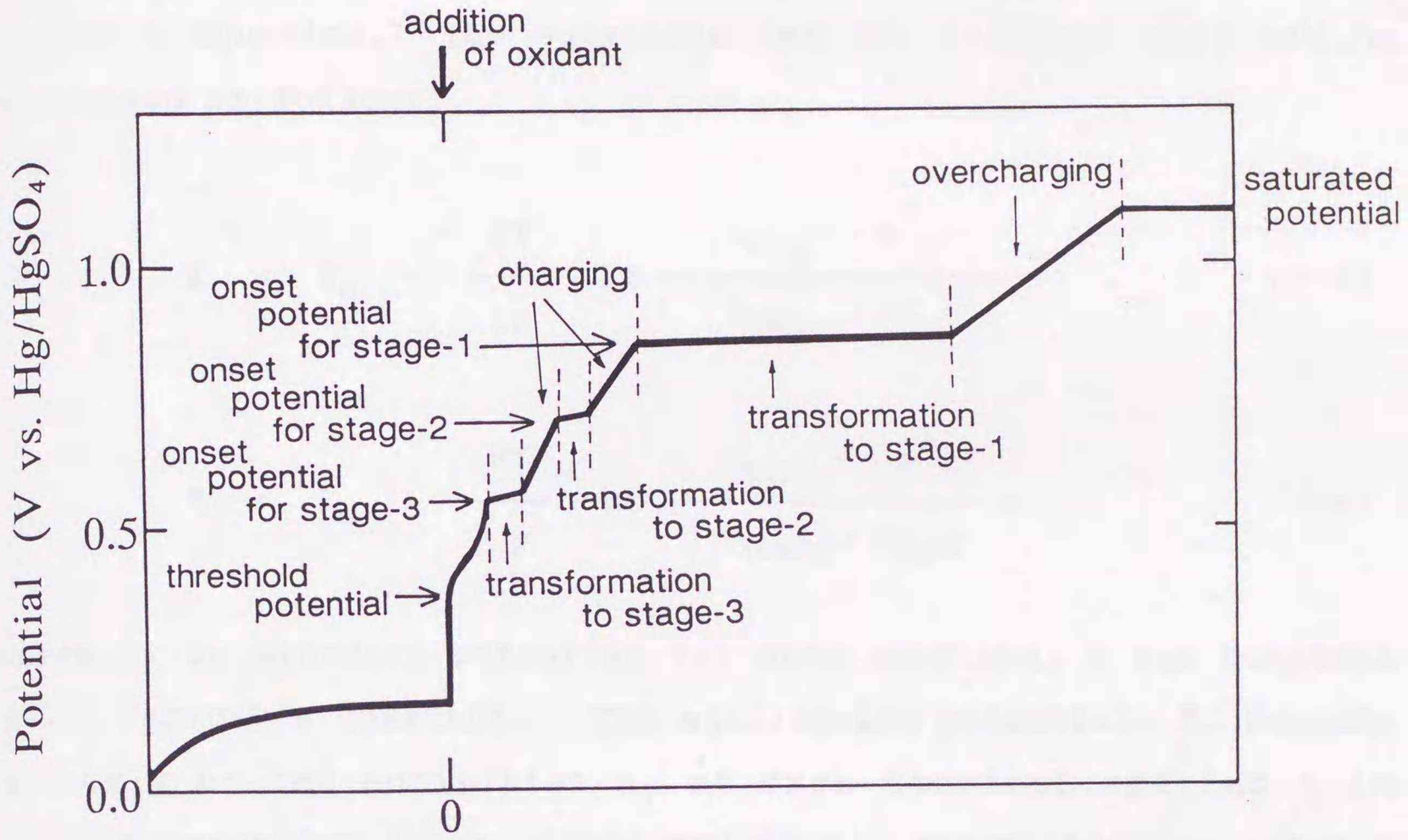


Fig. 3-9 Representative potential change during intercalation of sulfuric acid into flaky natural graphite by chemical oxidation with nitric acid in H_2SO_4 of 18 mol/dm^3.

extraction of electron from the host graphite. In the synthesis of H_2SO_4-GICs by chemical and electrochemical oxidations, therefore, only the difference is how to consume the electrons extracted from host graphite.

In the present results, the saturated potential reached by chemical oxidation depends on a relative amount of oxidant to carbon. It is reasonable to assume that the value of saturated

potential is related to the equilibrium potential given by Nernst's equation. The equations for two oxidants used can be expressed as follows;

$$E = E_o + \frac{RT}{2F} \cdot \ln \frac{a_{NO_3^-} \cdot a^3_{H^+}}{a_{HNO_2} \cdot a_{H_2O}}, \qquad (3\text{-}3)$$

$$E = E_o + \frac{RT}{F} \cdot \ln \frac{a_{MnO_4^-} \cdot a^2_{H^+}}{a_{MnO_3} \cdot a_{H_2O}}, \qquad (3\text{-}4)$$

where E_o is standard potential for each reaction, R gas constant and F Faraday's constant. The equilibrium potential, E, depends strongly on the activities a_i of each chemical species i in reducing reaction (Eqns. (3-1) and (3-2), respectively). When a small amount of oxidant is used for chemical oxidation of host graphite in sulfuric acid, activity of reduced product, a_{HNO_2} for example, is high in comparison with that of the remained oxidant, $a_{NO_3^-}$, and so equilibrium potentials determined by Eqn. (3-3) must be low. The value of saturated potential by a small amount of oxidant was actually low, and high stage compounds were obtained, as experimentally shown in Figs. 3-2, -3, -4 and -5. When excess amount of oxidant is used, activity $a_{NO_3^-}$ is still high in comparison with a_{HNO_2}, so that the equilibrium potential must be high. Actually the saturated potential reached to the value of upper limit for each oxidant and consequently low stage compounds were obtained. At the saturated potential reached by chemical oxidation, the intercalation reaction of sulfuric acid into graphite is equilibrated.

The present experiment suggests that there is an upper limit of saturated potential, even if an excess amount of the oxidant

is used. In other words, there is a limit of oxidation depending on the oxidant. This upper limit of saturated potential also depends on the concentration of sulfuric acid on. It is probably explained also by Eqns. (3-3) and (3-4). In diluted sulfuric acid, the activity of water, a_{H_2O}, is so high that a value of upper limit of saturated potential lowered.

In Fig. 3-10, the upper limit of saturated potential for nitric acid oxidation and the onset potential for stage-1 structure are plotted against the relative amount of $NaNO_2$ to HNO_3 added into the sulfuric acid solution with 18 mol/dm_3. The upper limit of potential decreases with addition of $NaNO_2$, but only slight even with the addition of equal equivalent of nitrite to nitric acid ($NaNO_2/HNO_3$/carbon = 3.3/3.3/1.0). Onset potentials for the stage-1 structure of H_2SO_4-GICs seem to have no relation with the addition of $NaNO_2$. These experimental results might suggest that the co-existence of $NaNO_2$ in sulfuric acid dose not have any effect on the activity of nitrous acid, a_{HNO_2}, in Eqn. (3-3). However, it is necessary to take into account the presence of a counter ions, Na^+, in the system in the present case.

3.4.2. Overcharging in the stage-1 H_2SO_4-GICs

The upper limit of saturated potential observed in H_2SO_4 of 18 mol/dm^3 by either nitric acid or potassium permanganate are higher than the onset potential for stage-1 of H_2SO_4-GIC, as shown in Figs. 3-2 and -4. Therefore, the charging of carbon layers is continued even after the completion of the formation of stage-1 structure and consequently the potential increases up to the upper limit of saturated potential for each oxidant. This fact corresponds to so-called "overcharging process" which has been pointed out in electrochemical oxidation [3-6] and it is reported to cause a slight decrease in identity period along the

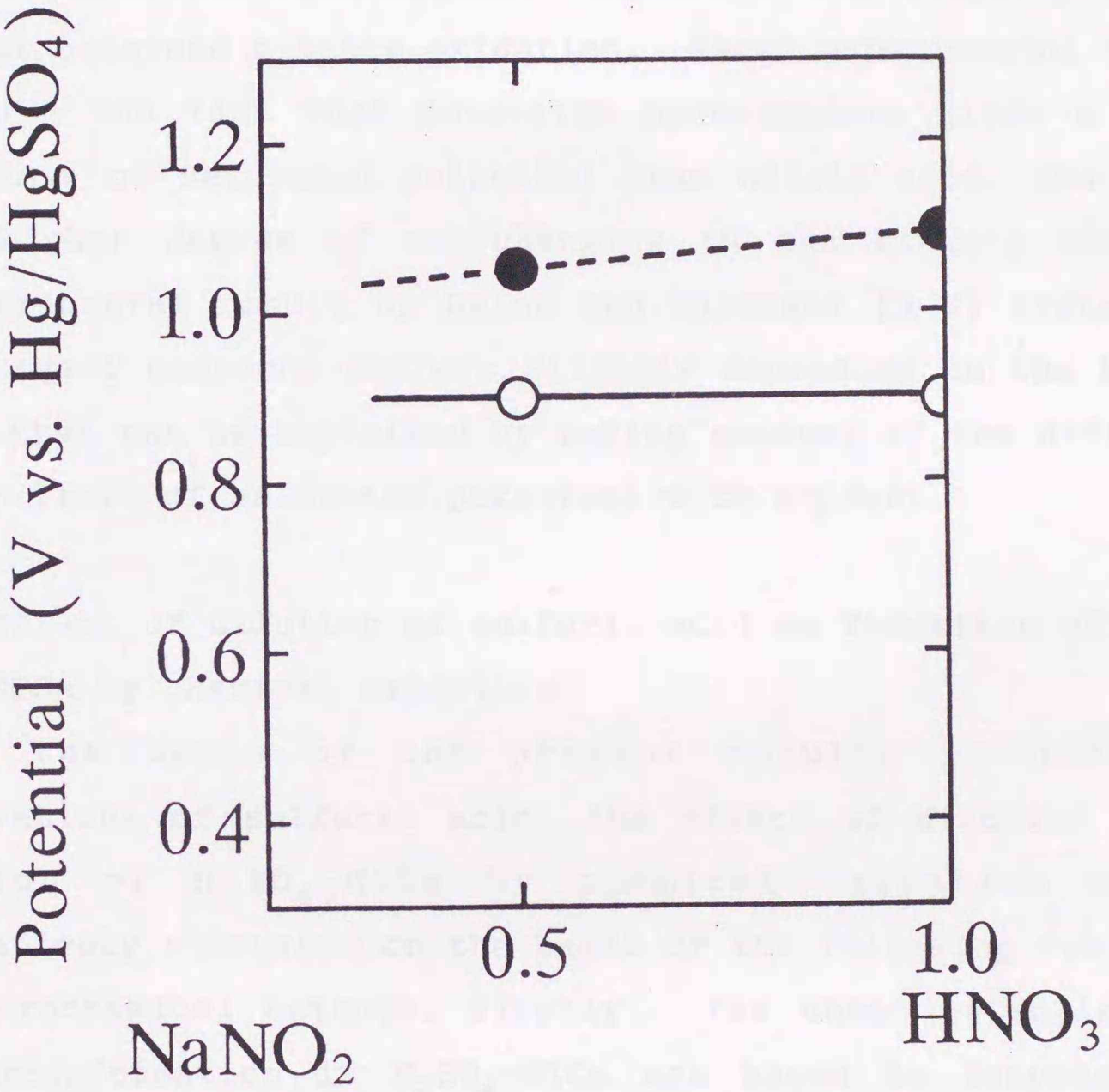


Fig. 3-10 Onset potential for the stage-1 and upper limit of saturated potential by chemical oxidation with nitric acid as a function of relative amount of $NaNO_2$ to HNO_3.
Onset potentials of stage-1 of H_2SO_4-GICs (○).
Upper limit of saturated potential with nitric acid oxidation (●).

c-axis, I_c, of the stage-1 compound with increasing potential [3-7].

In the present work, the value of I_c for the stage-1 compound obtained by permanganate oxidation was slightly smaller than that obtained nitrate oxidation. These experimental results agree with the fact that potassium permanganate gives a higher upper limit of saturated potential than nitric acid, the former giving higher degree of overcharging to the stage-1 compound. The experimental result by Daioh and Mizutani [3-8] states that I_c of stage-1 compound differs slightly depending on the kind of oxidant that can be explained by taking account of the difference in upper limit of saturated potential with oxidant.

3.4.3. Effect of dilution of sulfuric acid on formation of H_2SO_4-GICs by chemical oxidation

On the basis of the present results in different concentrations of sulfuric acid, the effect of dilution on the formation of H_2SO_4-GICs by chemical oxidation can be quantitatively discussed on the basis of the following two facts. By electrochemical methods, firstly, the onset potentials for stage transformation in H_2SO_4-GICs are known to increase with dilution of sulfuric acid, being pointed out by different authors [3-9, -10, -11], and also shown in the present work. Secondary, the potential of graphite by chemical oxidation increases up to an upper limit of saturated potential, which is found to depend on the oxidant used, even if an excess amount of oxidant is added. The upper limit of potential is also shown experimentally to decrease with dilution of sulfuric acid.

In Fig. 3-11, the onset potentials for each stage structure, determined by galvanostatic oxidation, are plotted against the molarity of sulfuric acid by open marks, which are shown to be

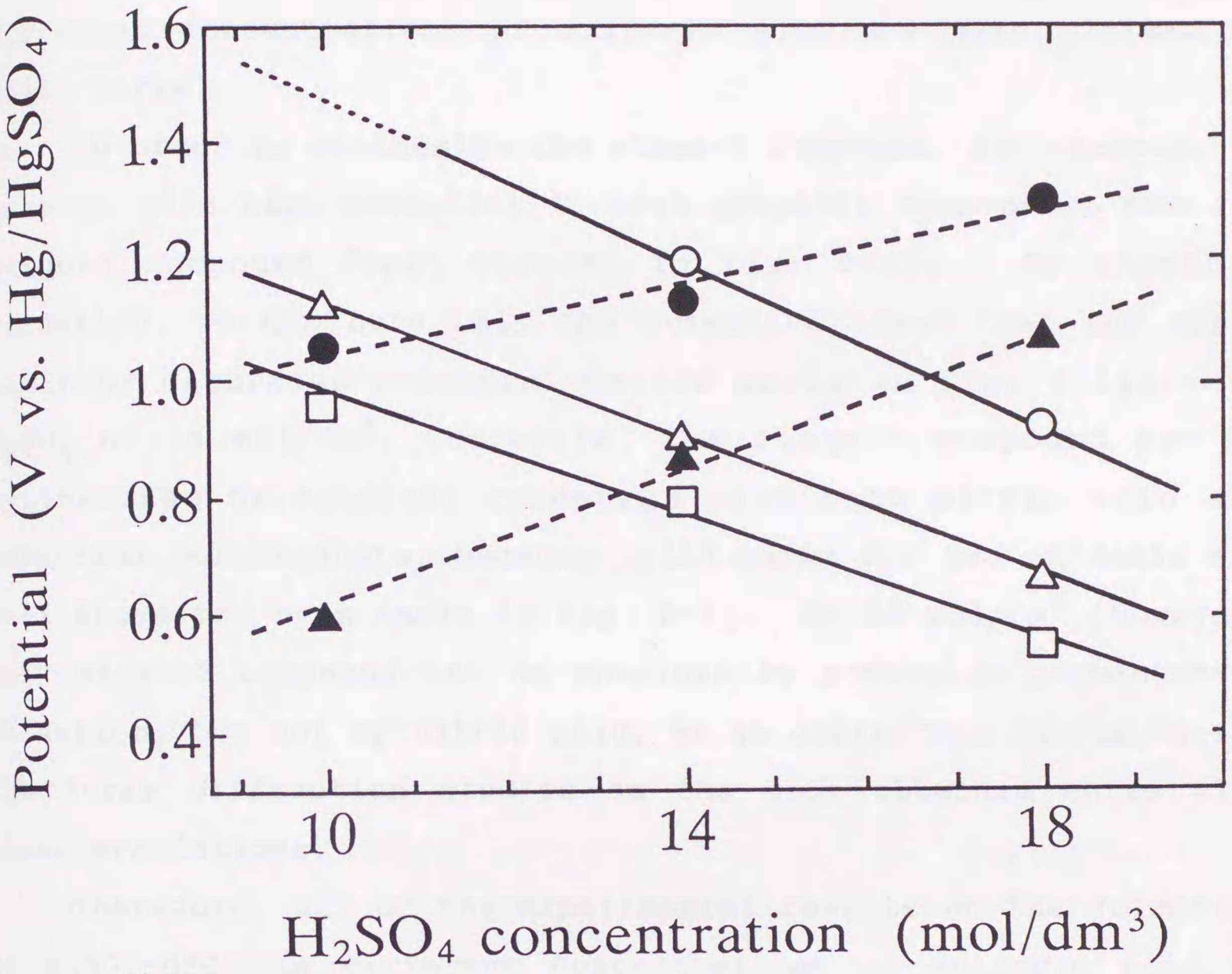


Fig. 3-11 Onset potentials for the stage-1, -2 and -3 of H_2SO_4-GICs, and upper limits of saturated potential by chemical oxidation as a function of molarity of H_2SO_4.
Onset potentials of stage-1 (○), stage-2 (△) and stage-3 (□) of H_2SO_4-GICs.
Upper limit of saturated potential by potassium permanganate (●) and nitric acid (▲) oxidations.

linear [3-11]. In the same figure, the upper limit of saturated potential for nitric acid and potassium permanganate in three different concentrations of sulfuric acid are also plotted by solid marks.

In order to synthesize the stage-1 compound, for example, we have to give high potential to host graphite than onset one for stage-1 compound (open circles in Fig. 3-11). By chemical oxidation, we can have only the potential lower than the upper limit of saturated potential (solid marks in Fig. 3-11). In H_2SO_4 of 18 mol/dm^3, therefore, the stage-1 compound can be synthesized by chemical oxidation with both nitric acid and potassium permanganate, because solid marks for two oxidants are well above the open marks in Fig. 3-11. In 10 mol/dm^3, however, only stage-3 compound can be obtained by potassium permanganate oxidation, but not by nitric acid, as is clear from in Fig. 3-11. The X-ray diffraction studies on the GICs obtained agree with these predictions.

Therefore, all of the experimental results on the formation of H_2SO_4-GICs in different concentrations of sulfuric acid by using different chemical oxidants can be understood from the relation between onset potentials for each stage structures and upper limits of saturated potential for each oxidants.

3.5. Summary

The present results lead to the conclusion that the intercalation process of sulfuric acid into graphite by chemical oxidation is fundamentally the same as that by electrochemical oxidation. The potential of graphite electrode increases by the charging of carbon layers. When it reaches an onset potential for each stage structure, which depends strongly on the concentration of sulfuric acid, the intercalation of sulfuric

acid proceeds. From the potential change, the intercalation reaction is divided into two processes; 1) charging of carbon layers corresponding to potential increase and 2) transformation of stage structure in the gallery of graphite showing the plateau on potential change. Therefore, the intercalation behavior into host graphite by chemical oxidation can be followed in situ by measuring the potential.

The oxidation of graphite by chemical oxidation, in other words, the potential increase of graphite, is limited by equilibrium potential, which is given by Nernst's equation of oxidant used and also depends strongly on the activities of each chemical species in the solution. The relation between upper limit of saturated potential of the oxidant used and onset potential for each stage structure governs the intercalation of sulfuric acid into graphite in sulfuric acid solution by chemical oxidation.

Various experimental results published on the intercalation of sulfuric acid into graphite by chemical oxidation can be explained by monitoring of the potential change. The present concept, potential increase with the charging of carbon layers and consequent stage transformation by the intercalation, can be applied for understanding the intercalation reactions into various host carbon materials.

References

3-1. A. Metrot, Synth. Met., 7, 177 (1983).

3-2. A. Metrot and M. Tihli, Synth. Met., 12, 517 (1985).

3-3. H. Thiele, Z. anorg. allg. Chem., 206, 407 (1932).

3-4. J. O. Besenhard, M. Bindi, and H. Möhwald, Proc. of Carbon '88 Baden-Baden, pp. 414-416, (1986).

3-5. W. Rüdorff and U. Hofmann, Z. anorg. allg. Chem., 238, 1 (1938).

3-6. A. Metrot and J. E. Fischer, Synth. Met., 3, 201 (1981).
3-7. H. Shioyama and R. Fujii, Carbon, 25, 771 (1987).
3-8. H. Daioh and Y. Mizutani, Tanso 1985[No. 123], 177 (1985).
3-9. F. Beck, W. Kaiser and H. Krohn, Angew. Chem. Suppl., 57 (1978).
3-10. R. Fujii, Report of Gov. Ind. Res. Inst., Osaka, No. 353, pp. 19-24, (1978).
3-11. A. Pruss and F. Beck, J. Electroanal. Chem., 172, 281 (1984).

CHAPTER 4

Effect of host graphite materials on intercalation behavior

4.1. Introduction

On intercalation reaction into graphite, sample shape and degree of graphitization of host material have been shown to give strong influences. In the intercalation of bromine, for instance, the threshold pressure [2-1, -2] and the reaction rate, which was interpreted by diffusion of guest material (intercalate) [2-3, -4], were studied on the effect of host materials. The host materials used in these studies, however, were natural graphites produced at various places and pyrolytic carbons with different heat-treatments. In the electrochemical intercalation of sulfuric acid, a remarkable effect of host graphite was shown by using different hosts, for example, cokes and carbon fibers [4-5, -6]. However, the effects of crystalline structure, texture and also sample morphology of host carbon materials on intercalation were not understood well.

In Chapter 3, the intercalation of sulfuric acid into graphite by chemical oxidation was found to be fundamentally the same process as that by electrochemical oxidation, on the basis of the measurement of potential change during the reaction. The effect of dilution of sulfuric acid on the formation of graphite intercalation compounds with sulfuric acid (H_2SO_4-GICs) could be explained in term of the balance between saturated potential of chemical oxidation and onset potential for stage structure. The measurement of potential has an advantage to follow in situ the intercalation behavior of sulfuric acid into various kinds of host materials by chemical and electrochemical oxidation.

Metrot, et al. [4-7, -8] quantitatively discussed the curve of potential versus electric quantity during

electrochemical intercalation by galvanostatic oxidation of sulfuric acid into highly oriented pyrolytic graphite (HOPG), and proposed a model involving two series of capacitors.

In the present chapter, various kinds of carbon materials, which are characterized in Chapter 2, are used as the host for H_2SO_4-GICs. The effects of crystalline structure, texture and particle size of host materials on the intercalation behavior of sulfuric acid are discussed by measuring potential during the chemical and galvanostatic oxidations. The simulation of the potential change is also carried out on the basis of the two-capacitor model and is compared with the curves obtained experimentally.

4.2. Experimental

4.2.1. Potential measurement

The group code and sample code of carbon materials used are listed in Table 4-1. The graphitization parameters and texture of these samples were listed already in Table 2-2. The samples were selected in wide ranges of structure, texture and particle size; flaky graphites with different sizes (Flaky-group: NG-series, KG, PI), different cokes with different heat-treatment temperatures (HTT's) (COKE-group: PV-, PC- and GL-series), two kinds of pyrolytic carbons with different graphitization degrees (PyC-group: SSG- and PYR-series), glass-like carbons (GC-series), mesophase-pitch-based carbon fibers with different textures in their cross-section and with different HTT's (MPCF-group: KOA- and I-series) and vapor-grown carbon fibers with different fiber diameters (VGCF-group: OVCF and NVCF-series).

Either a carbon powder or a bundle of carbon fiber (length of 10 mm) of 50 mg was held between plastic plates with platinum wire as a supporting electrode, as already shown in Chapter 3

(Fig. 3-1(b)). The electrochemical cell used was the same one as the previous (Fig. 3-1(a)).

Table 4-1 Carbon samples used in the present chapter

Flaky-group	**COKE-group**
NG400, NG5,	PV-7, PV-7A*,
KG,	PC18, PC20, PC22, PC24, PC27, PC30,
NOVAX30,	GL18, GL20, GL22, GL24, GL27, GL30.
PyC-group	**GC-group**
SSGAS, SSG25, SSG28, SSG30,	GC12, GC30.
PYRAS, PYR25-19, PYR28-10, PYR28-19, PYR32.	
MPCF-group	**VGCF-group**
KOA-R,	OVCF30, NVCF30.
I-1-28, I-1-30, I-2-28, I-2-30,	
I-3-26, I-3-30, I-4-26, I-4-30.	

* : prepared by pulverizing PV-7 in a mortar.

In all experiments, sulfuric acid of 18 mol/dm^3 (50 cm^3) was used as electrolyte. Nitric acid of 13.8 mol/dm^3 (1 cm^3) was used as chemical oxidant to synthesized the GICs. The molar ratio of nitric acid to carbon was 3.3. For comparison, electrolysis with galvanostatic oxidation was carried out with different current values in the same cell. The detailed conditions and procedure for experiment were exactly the same as those described in the previous chapter.

Characterization of the H_2SO_4-GICs synthesized was carried out with X-ray powder diffractometry by preventing the decomposition in a polyethylene bag and with high-fidelity

scanning electron microscopy (SEM) after the sample was washed by water repeatedly and dried at room temperature.

4.2.2. Simulation of potential change

The intercalation of sulfuric acid into HOPG by galvanostatic oxidation with a very small current value gives rise to a characteristic quasi-equilibrium curve of potential against electric quantity, E = f(Q), where E is the potential of graphite electrode and Q the accumulated electric quantity per unit mole of graphite. The idealized potential change is shown in Fig. 4-1 [4-8]. The steep rise of potential corresponds to the charging of host carbon layers by oxidation, while the plateau to the transformation from stage-n to stage-(n-1) structures of GIC by additional intercalation of sulfuric acid, as already discussed in Chapter 3. The close succession of steep potential increases and plateaux for high stages results in the seemingly straight segment AB on the potential curve in Fig. 4-1. On the potential curve, there are the following features;

1) the starting points B, C and D for charging of graphite layers in each pure stage compounds appear to be aligned with the threshold point A for the start of intercalation (threshold potential).

2) the electric quantity corresponding to the points B, C and D is nearly inversely proportional to the corresponding stage number.

3) the slopes BE, CF and DG for charging processes seem to converge on the same point Ω on the ordinate.

4) since two successive stage structures are in equilibrium during the stage transformation process, it is reasonably assumed that potential is kept constant, i. e., $dE/dQ = 0$.

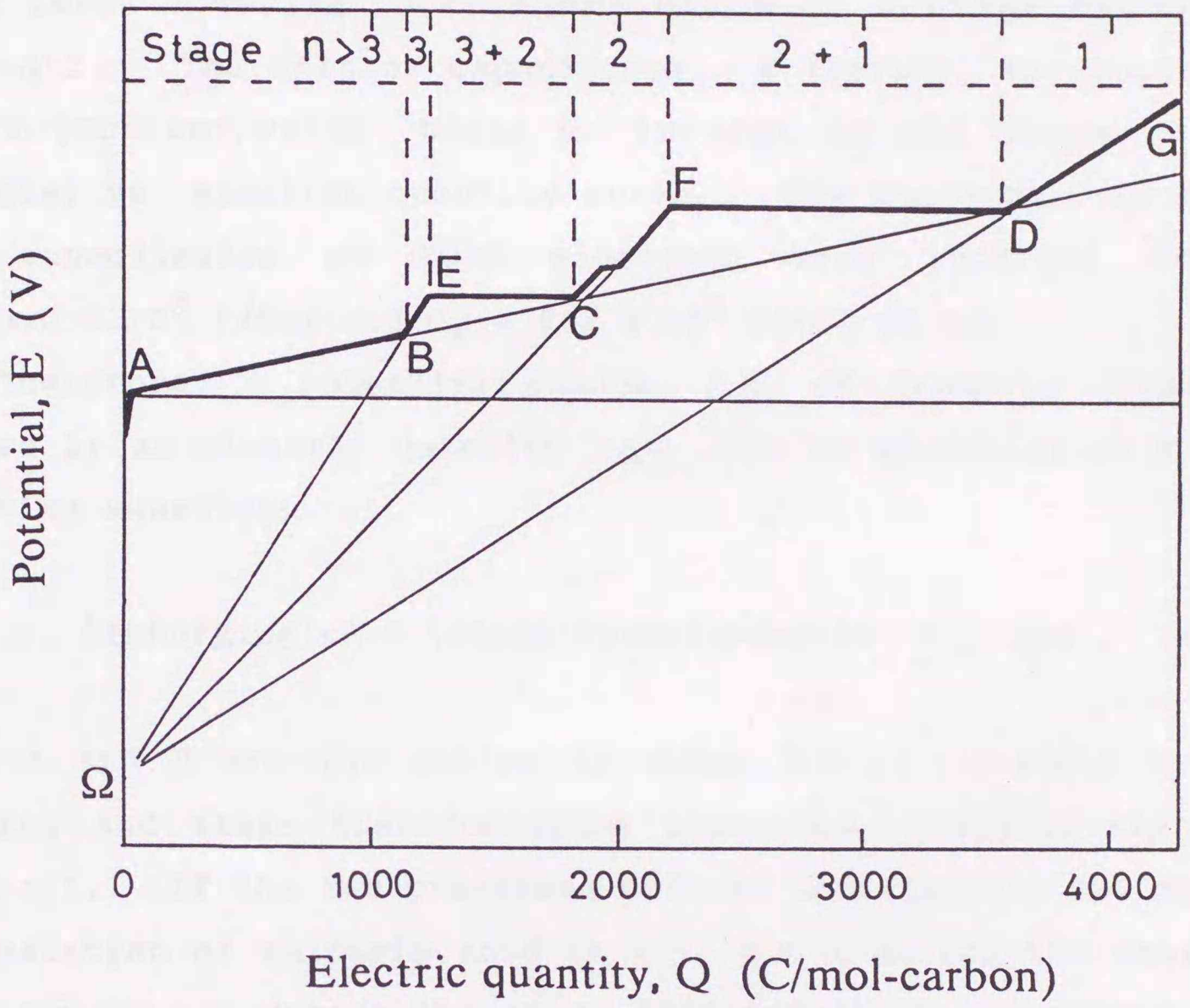


Fig. 4-1 Curve of potential against electric quantity observed during galvanostatic intercalation of sulfuric acid of 18 mol/dm^3 into HOPG [4-8].

Metrot, et al. [4-7, -8] explained the slopes of steep increases on the curve of potential vs. electric quantity, dE/dQ, from these features, as follows;

$$\frac{dE}{dQ} = \frac{n}{C_A} + \frac{1}{C_F} \quad , \qquad (4\text{-}1)$$

where C_A is defined as internal interfacial capacitance, C_F as Fermi level lowering capacitance and n is a stage number of H_2SO_4-GIC. The unit of capacitance, F (Farad), is equivalent to C/V (Coulomb/Volt), being an inverse of the slope in the potential vs. electric quantity curve. The numerical values of these capacitances on HOPG electrode were reported to be $C_A = 3.0 \times 10^3$ F/mol and $C_F = 6.2 \times 10^3$ F/mol [4-8].

Therefore, a potential change, ΔE, of graphite electrode charged by an electric quantity, ΔQ, can be approximated by the following equation;

$$\Delta E = \{(\text{charging}) \cdot A + (\text{stage transformation}) \cdot B\} \cdot \Delta Q \ , \quad (4\text{-}2)$$

where A and B are the ratios in which ΔQ is consumed to the charging and stage transformation processes, respectively, and A + B = 1. If the two processes proceed individually during the intercalation of sulfuric acid (A = 1, B = 0 during the charging and A = 0, B = 1 during the stage transformation processes), the stepwise increases in potential are obtained, as shown in Fig. 4-1.

As mentioned in Chapter 3, when the potential of a host reaches at onset potential for a certain stage structure, additional intercalation of sulfuric acid begins and the stage structure starts to be transformed to lower stage one. In other words, the transformation from a stage to the next can occur only when the electrode reaches to certain potential (onset potential). On the other hand, the charging process is independent of potential value. In the intercalation of sulfuric acid, it seems to happen that a certain part of charging process is overlapped to the stage transformation process. The potential change with electric quantity during the

galvanostatic intercalation of sulfuric acid is simulated by varying the relative ratio of both processes, i. e., by changing the consumption ratio of electric quantity to the charging process, the ratio A in Eqn. (4-2), during the stage transformation process.

The simulation was carried out as follows;

1) A certain electric quantity, at first, was consumed for the charging of graphite layers until the potential of host electrode reaches a threshold value for intercalation of sulfuric acid.

2) During the stage transformation process to the stage-n compound, a certain amount of electric quantity was consumed for the charging of the stage-n compound.

3) After the stage-n compound was completely formed, the potential increased up to the onset value for the further intercalation to the stage-(n-1) compound (by the charging process).

4) The processes 2) and 3) was repeated until the formation of the stage-1 compound.

5) After the formation of the stage-1 compound, potential increased up to the saturated potential by the charging process.

The threshold and saturated potential values obtained in Chapter 3 were employed for the simulation. The onset potential values for each stage structures and the electric quantity needed for the formation of the stage-1 compounds were referred from the previous reports [2-9, -10].

4.3. Results

4.3.1. Potential change during intercalation of sulfuric acid into various carbon materials by chemical oxidation

a) Flaky samples

The curves of potential against reaction time during chemical intercalation of sulfuric acid into the samples NG400, NG5, PV-7, PV-7A, KG and NOVAX30 are shown in Fig. 4-2. On the potential change in the samples NG400 of which average particle size is 400 μm, well-defined plateaux corresponding to the transformation to the stage-3, stage-2 and stage-1 structures from respective higher stages are observed around 0.6, 0.7 and 0.9 V, respectively. Any appreciable plateau except around 0.9 V was not observed on the potential change of the sample NG5 which has small particle size as 5 μm (Fig. 4-2(a)), although the overall rate of potential increase is almost the same as the case of the sample NG400.

In the case of the sample PV-7, the potential is found to increase in stepwise (Fig. 4-2(b)). The sample PV-7A, which was prepared by pulverizing the sample PV-7 in a mortar, does not show a potential plateau at 0.6 V. In other words, the potential plateau at 0.6 V in the sample PV-7 disappears by pulverization.

BET surface area for nitrogen gas of the samples NG400, NG5, PV-7 and PV-7A is 1.06, 18.75, 0.16 and 1.99 m^2/g, respectively. The disappearance of potential plateau by pulverizing the sample seems to be resulted from the decrease in particle size, as detected by the extension of surface area.

The samples KG and NOVAX30, which are the largest flake in the flaky samples used and the graphitized carbon film (10 X 10 mm^2), respectively, show stepwise increase in potential, being similar to the case of the sample NG400 (Fig. 4-2(c)). The sample NOVAX30 was so thin (about 11 μm) and light (2 mg) that molar ratio of oxidant to carbon could not be reduced less than 33.3, being 10 times larger than other experiments. Although overall rate of increase in potential observed on the sample

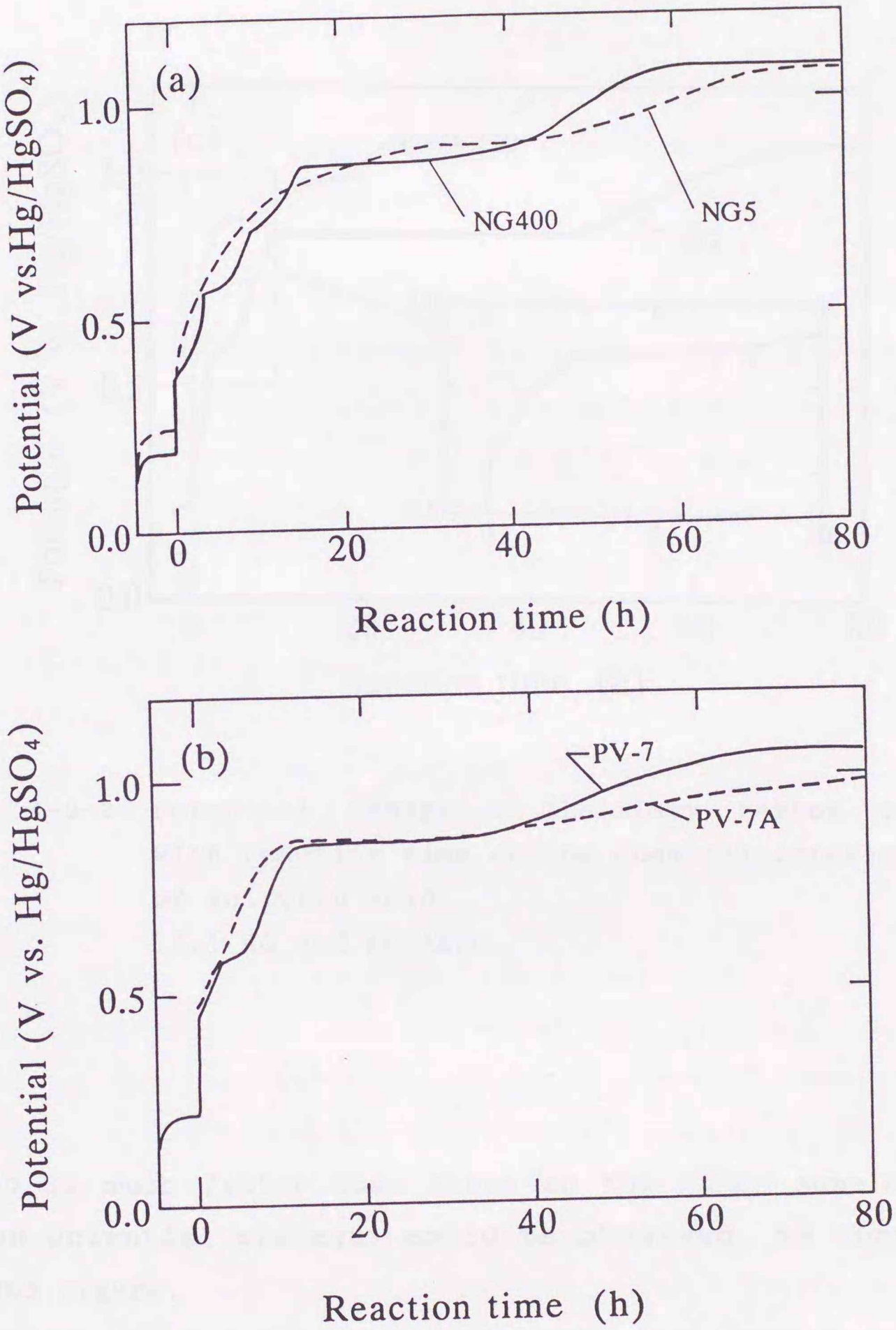


Fig. 4-2-1 Potential changes of the flaky carbon samples with reaction time during chemical intercalation of sulfuric acid.
(a) NG400 and NG5, (b) PV-7 and PV-7A.

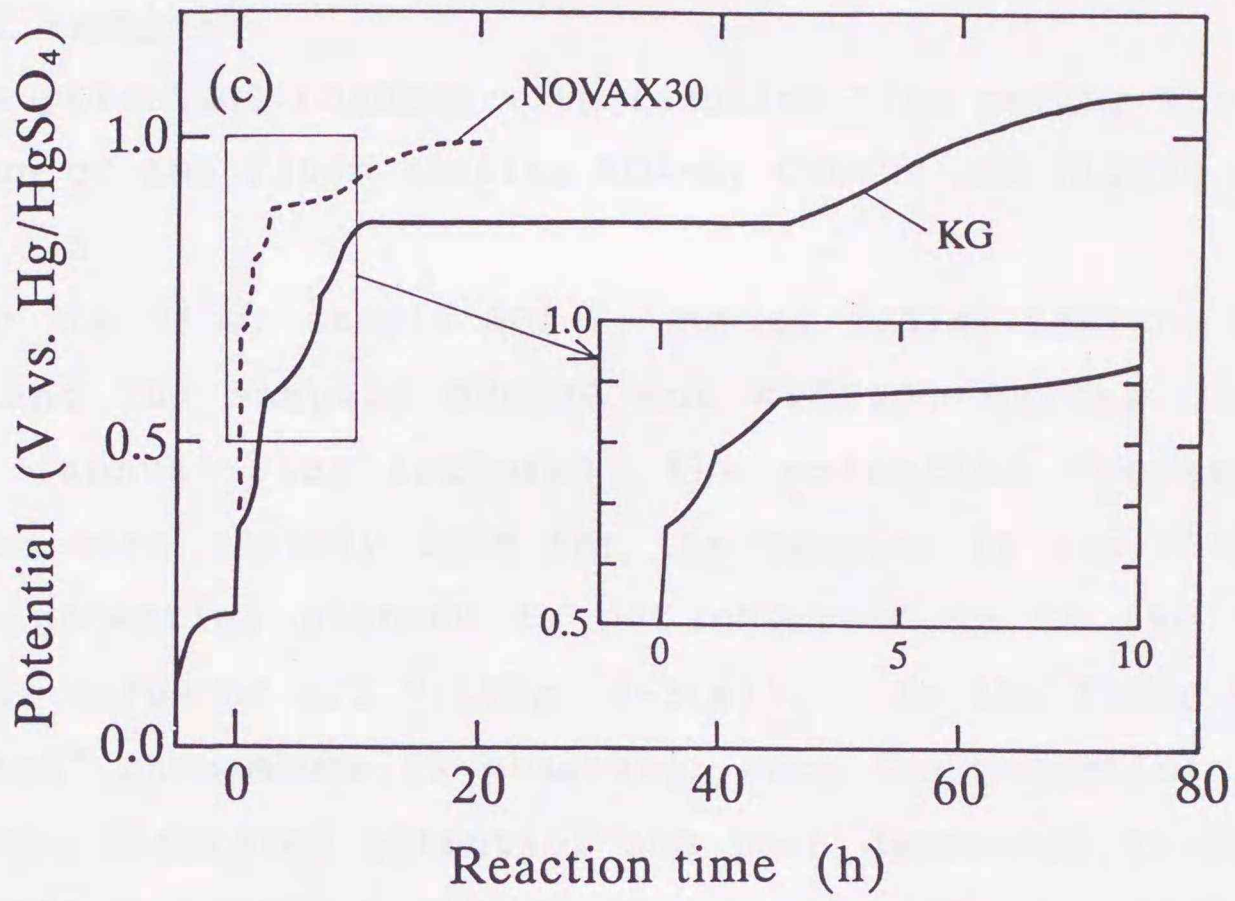


Fig. 4-2-2 Potential changes of the flaky carbon samples with reaction time during chemical intercalation of sulfuric acid.
(c) KG and NOVAX30.

NOVAX30 is much faster than those on the other samples, well-defined potential plateaux could be observed, as shown by an enlarged figure.

All of the samples in Flaky-group were transformed to the stage-1 compounds at the saturated potential, which had identity period along the c-axis, I_c, of 0.80 nm. After the intercalation, color of these samples changed from black to blue, but any visible crack was not generated on the surface of these samples.

b) Fiber samples

The potential changes with reaction time during the chemical oxidation of the fiber samples KOA-R, OVCF30 and NVCF30 are shown in Fig. 4-3.

For the fiber sample KOA-R, having radial texture with open wedge, and the samples OVCF30 and NVCF30, having concentric texture (annual-ring texture), the potential increases with oxidation more rapidly than for the samples in the Flaky-group, and any potential plateau is not observed up to the saturated potential value of 1.1 V (Fig. 4-3(a)). In the fiber NVCF30, a "over-shot" phenomenon is observed; once the potential increases beyond the saturated potential and then decreases to around 1.0 V. After oxidized for 80 hours, the all samples could be transformed to the stage-1 compounds, which had I_c = 0.80 nm.

After the stage-1 compounds synthesized from the samples KOA-R, OVCF30 and NG400 were electrochemically reduced, as will be discussed in the next chapter, sulfuric acid was intercalated again into the samples. The potential changes during the intercalation into the samples NG400 and KOA-R in second time were almost the same as those in the first time. In the case of the sample OVCF30, however, the potential plateau corresponding to the transformation from stage-2 to -1 structures became clear during the second intercalation, as shown in Fig. 4-3(b).

The SEM micrographs of the fibers KOA-R, OVCF30 and NVCF30 after the chemical intercalation of sulfuric acid are shown in Fig. 4-4. In the fiber KOA-R, a crack in its cross-section and fiber fractured along the fiber axis are observed after intercalation (Fig. 4-4(a) and (b), respectively), but its radial texture is reserved. In the fibers OVCF30 and NVCF30, on the other hand, fractures along the fiber axis appear clearly on the

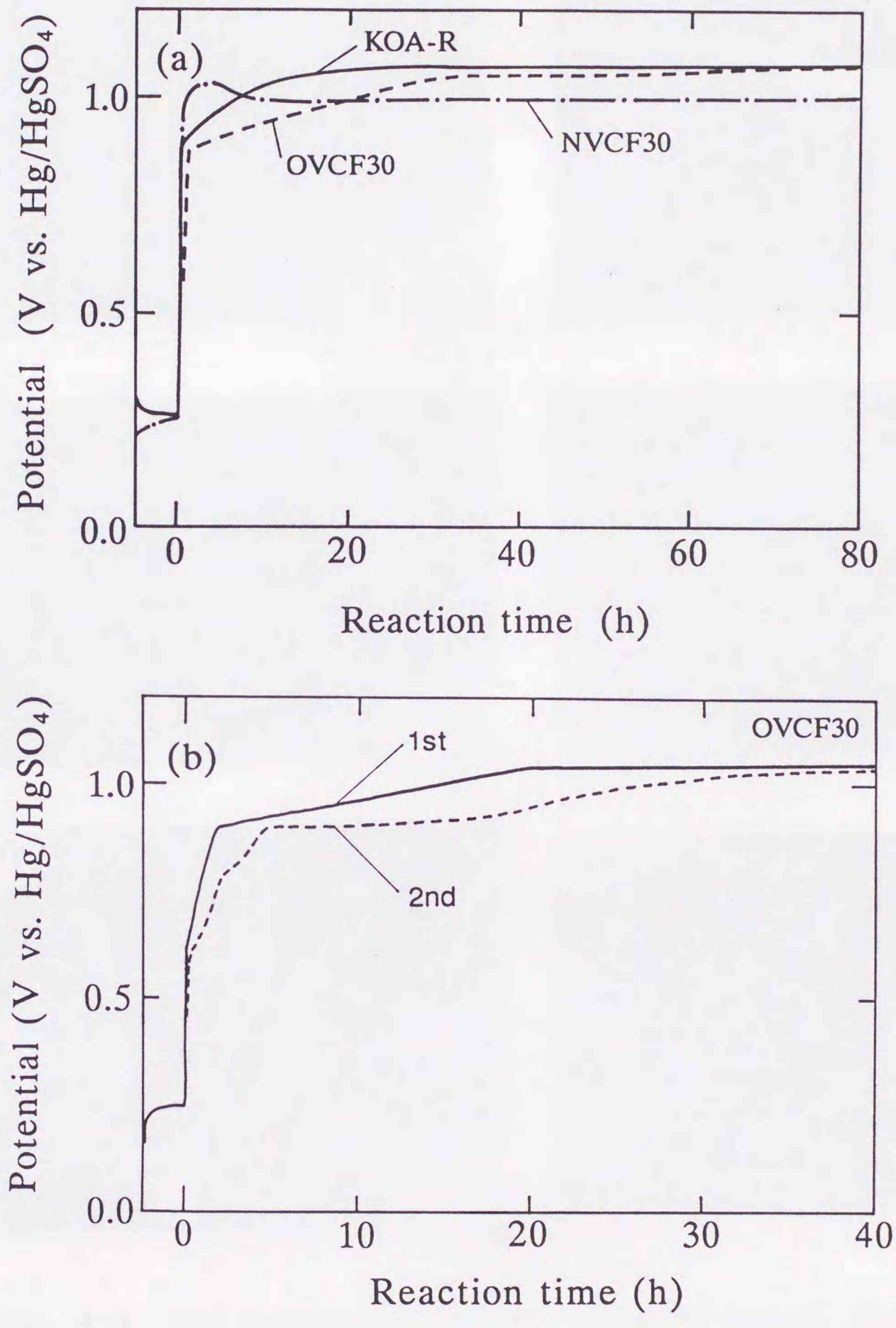


Fig. 4-3 Potential changes of the carbon fiber samples with reaction time during chemical intercalation of sulfuric acid.
(a) KOA-R, OVCF30 and NVCF30,
(b) repetition of chemical intercalation on OVCF30.

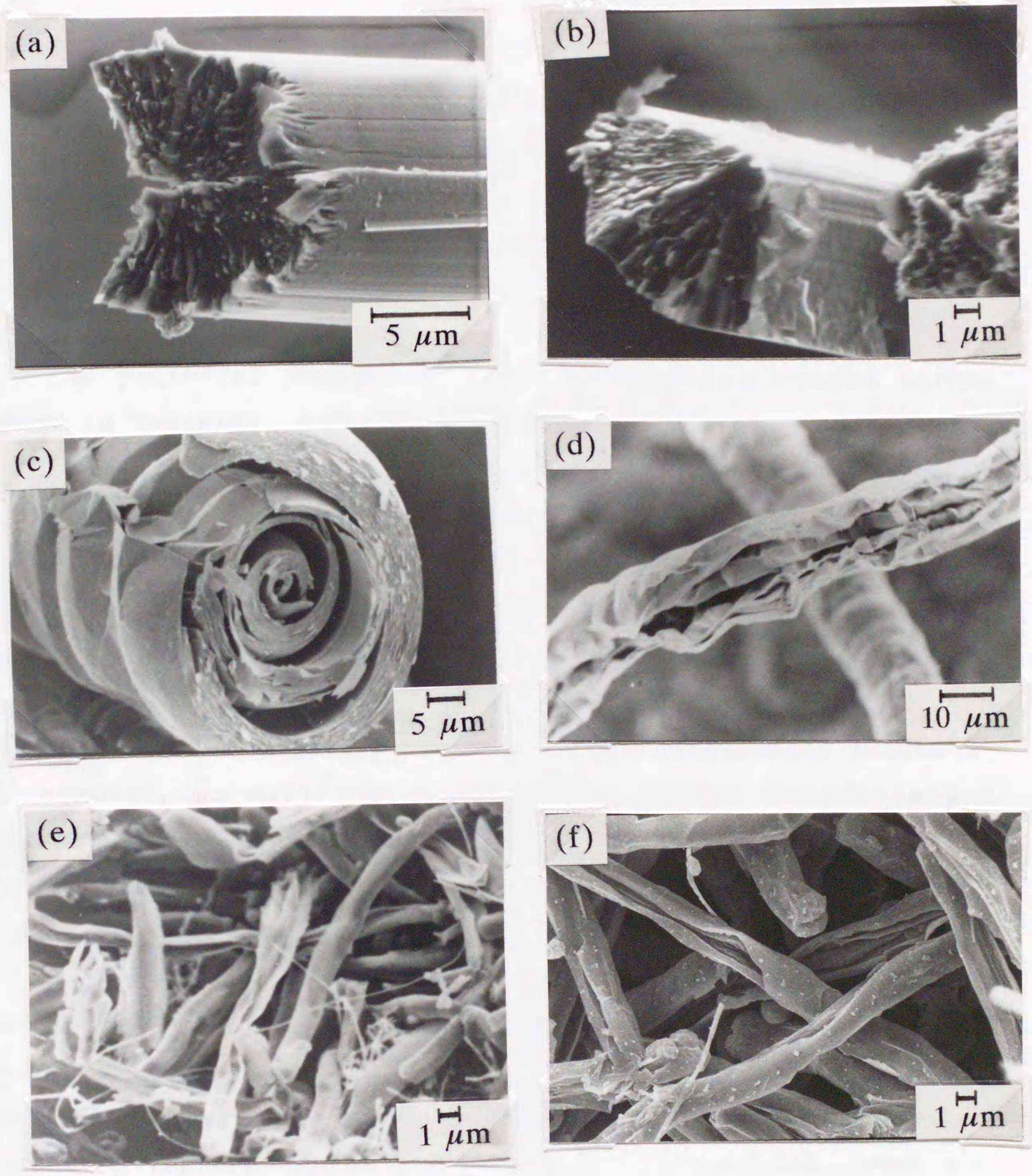


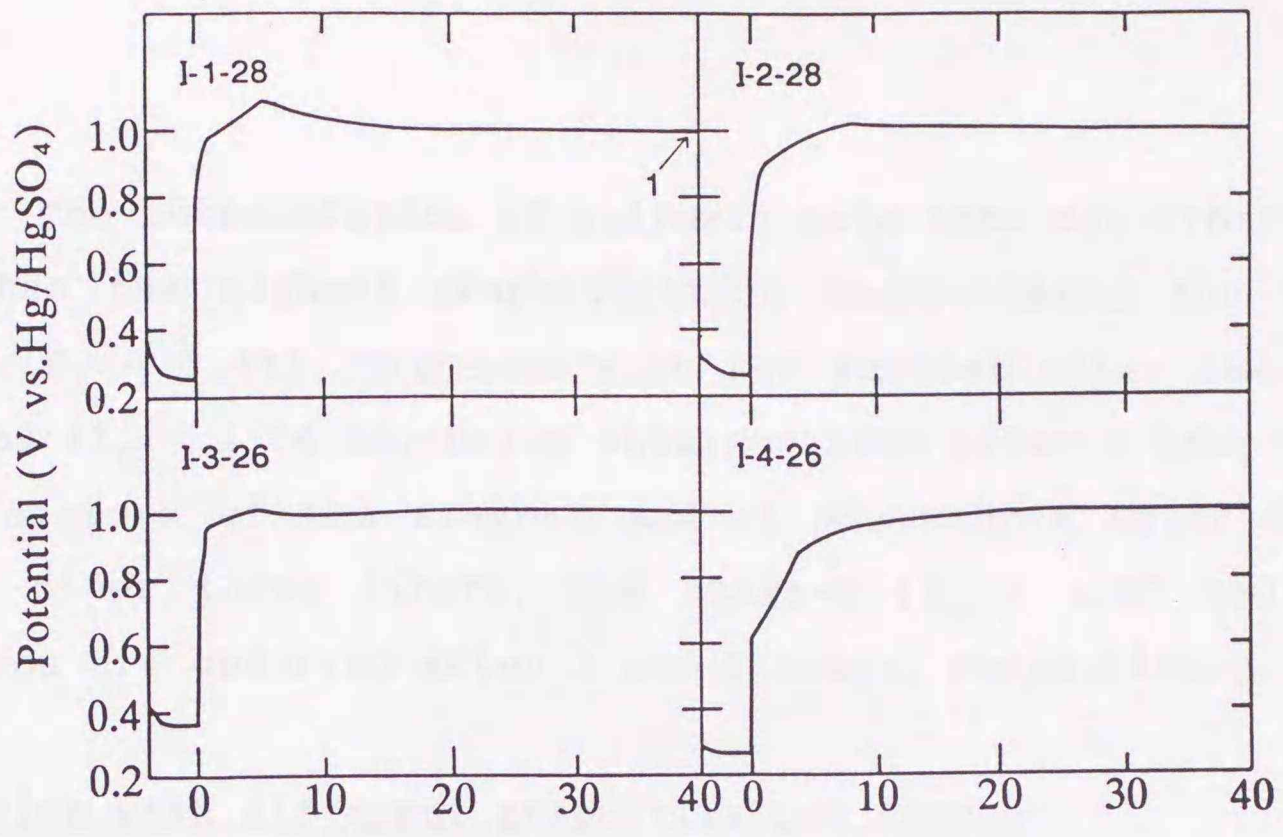
Fig. 4-4 SEM micrographs of the samples KOA-R, OVCF30 and NVCF30 after intercalation of sulfuric acid.
(a) and (b) KOA-R, (c) and (d) OVCF30,
(e) and (f) NVCF30.

fiber surface after intercalation (Fig. 4-4 (c), (d), (e) and (f)), and their concentric texture looks to be destroyed. The fracture of concentric texture and characteristic exfoliation of a graphitized vapor-grown carbon fiber were observed in graphite ternary intercalation compound with potassium and tetrahydrofurane [4-11].

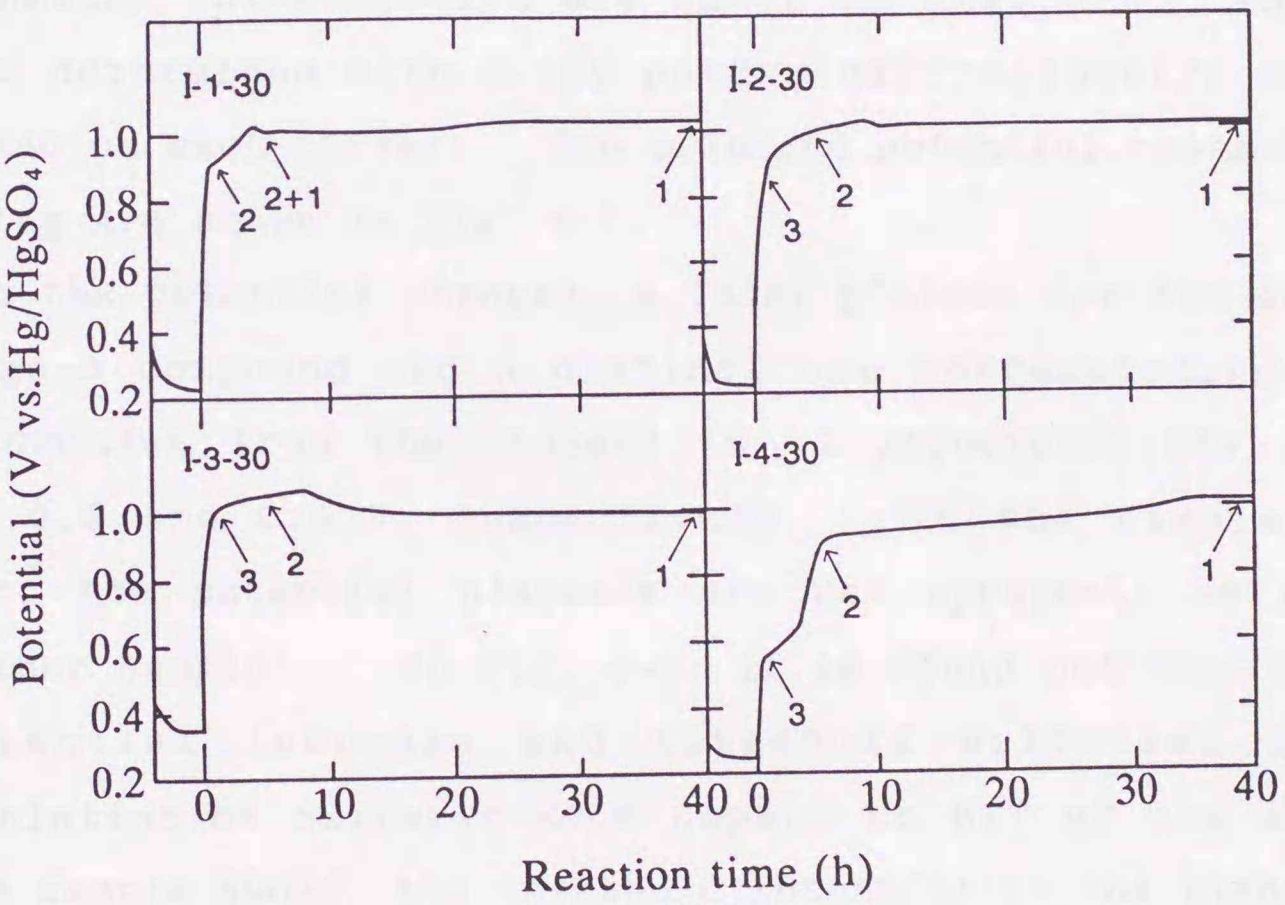
The potential changes of the mesophase-pitch-based carbon fibers in I-series with reaction time during the intercalation are shown in Fig. 4-5. In the figures, the stage numbers determined from X-ray powder patterns of each sample oxidized for 1, 5 and 40 hours are indicated. All fibers heat-treated at 3000^{o}C are transformed to the stage-1 compounds (I_c = 0.80 nm). The fiber I-1-28, which has a radial texture with open wedge, is transformed to the stage-1. For the fibers I-2-28, I-3-26 and I-4-26 which have negative values of magnetoresistance (Table 2-3), however, no diffraction lines due to the intercalation compounds are detected on their powder patterns, suggesting no intercalation of sulfuric acid into these fibers even after the oxidation for 40 hours.

Regardless of HTT, the potential of the fibers I-1, I-2 and I-3 increases rapidly up to around 0.9 V and then increases gradually. On the fibers I-1-28, I-1-30, I-2-30, and I-3-30, a over-shot phenomenon is observed. The fiber I-4-30 having concentric texture (onion-like texture), in contrast, does not show any over-shot phenomenon and gives a stepwise potential change, with two distinct plateaux at 0.6 and 0.9 V. The same series of the fiber heat-treated at a low temperature (I-4-26) dose not show any distinct plateau, but no over-shot phenomenon on its potential change.

The stage numbers of 3000^{o}C-treated fibers oxidized for 1 and 5 hours are also indicated on the potential curves in Fig. 4-



(a)



(b)

Fig. 4-5 Potential changes of the mesophase-pitch-based carbon fibers in I-series with reaction time during chemical intercalation of sulfuric acid. The numbers in the figures stand for the stage numbers of the intercalation compounds formed.
(a) fibers heat-treated at 2600～2800°C,
(b) fibers heat-treated at 3000°C.

5(b). The intercalation of sulfuric acid into the fiber I-1-30, which has the highest graphitization degree among the I-series fibers (P_1 = 0.41), proceeds with the fastest rate; the stage-2 compound (I_c = 1.14 nm) being obtained even after 1 hour reaction and a mixture of the stage-2 and -1 structures after 5 hours. In the other three fibers, the stage-3 (I_c = 1.47 nm) and -2 compounds are observed after 1 and 5 hours, respectively.

c) Samples with different graphitization degree

The potential changes of the pyrolytic carbons heat-treated at different temperatures (SSG-series) with reaction time during the chemical intercalation are shown in Fig. 4-6. The stage numbers determined with X-ray powder diffractometry are also indicated on each curves. The enlarged potential changes in the beginning are shown in Fig. 4-7.

On the potential changes, a faint plateau for the formation of stage-3 compound and a distinct one corresponding to the transformation from the stage-2 to -1 structures are observed around 0.6 and 0.9 V, respectively. In the sample SSG25, however, the potential plateaux are not apparent, as compared with other samples. In Fig. 4-7, it is found out that the rate of potential increase and threshold potential for the intercalation of sulfuric acid depend on HTT of the samples. For the sample SSGAS, the threshold potential is the highest, but the potential increase is not the fastest among the series of samples. Consequently, the potential plateau in the sample SSGAS is observed around 0.9 V, which is lower than potential value for the sample SSG25. The sample SSG30 with the highest graphitization degree among the SSG-series shows the lowest threshold potential for the intercalation on the potential change.

In the PYR-series, the situation of potential change was similar. The stage-1 compounds (I_c = 0.80 nm) were formed from all samples in PyC-group after 50 hours, even from the samples SSGAS and PYRAS which have the lowest graphitization degree among the SSG- and PYR-series, respectively.

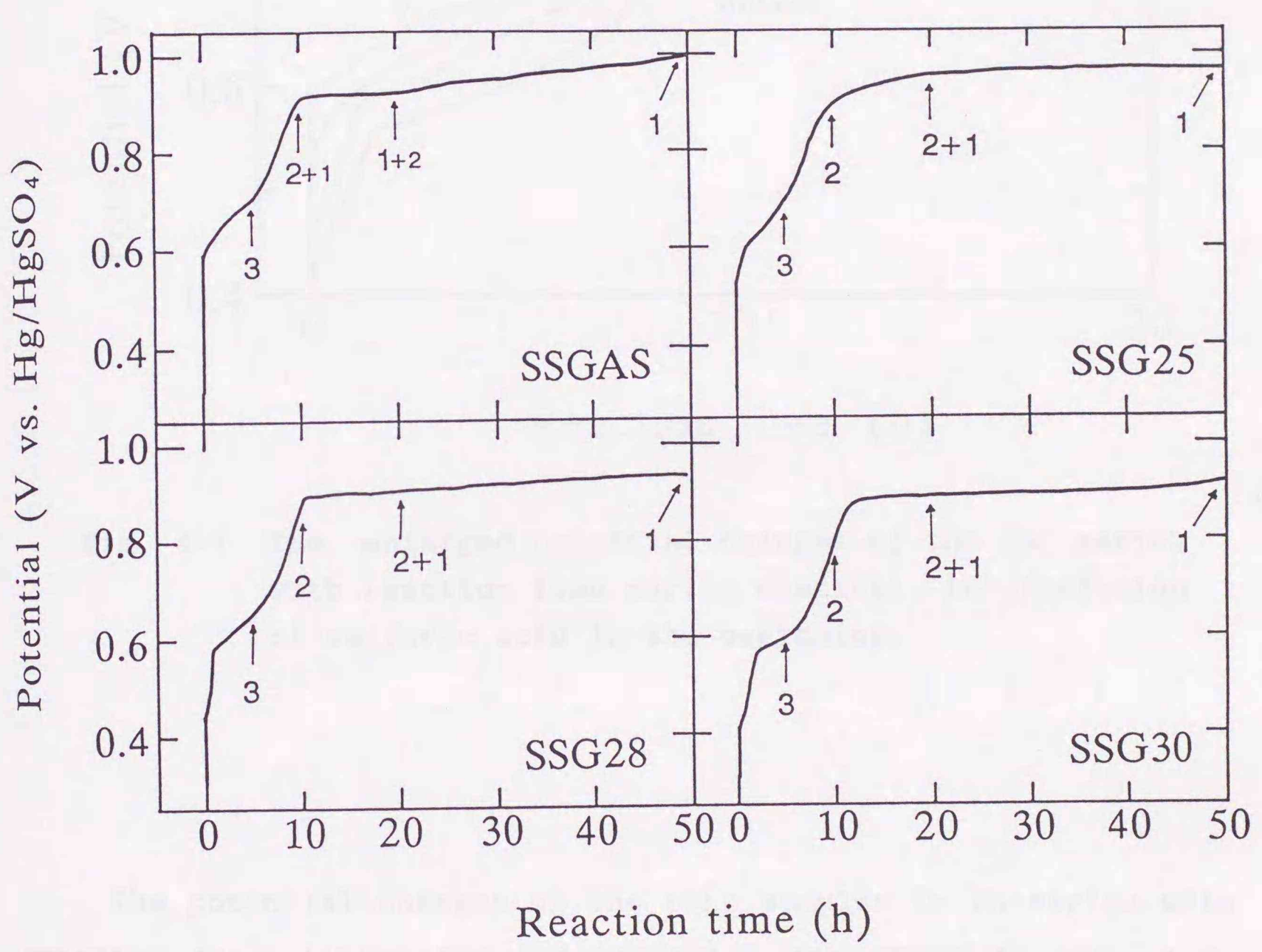


Fig. 4-6 Potential changes of the pyrolytic carbon samples in SSG-series, heat-treated at different temperatures, with reaction time during chemical intercalation of sulfuric acid.

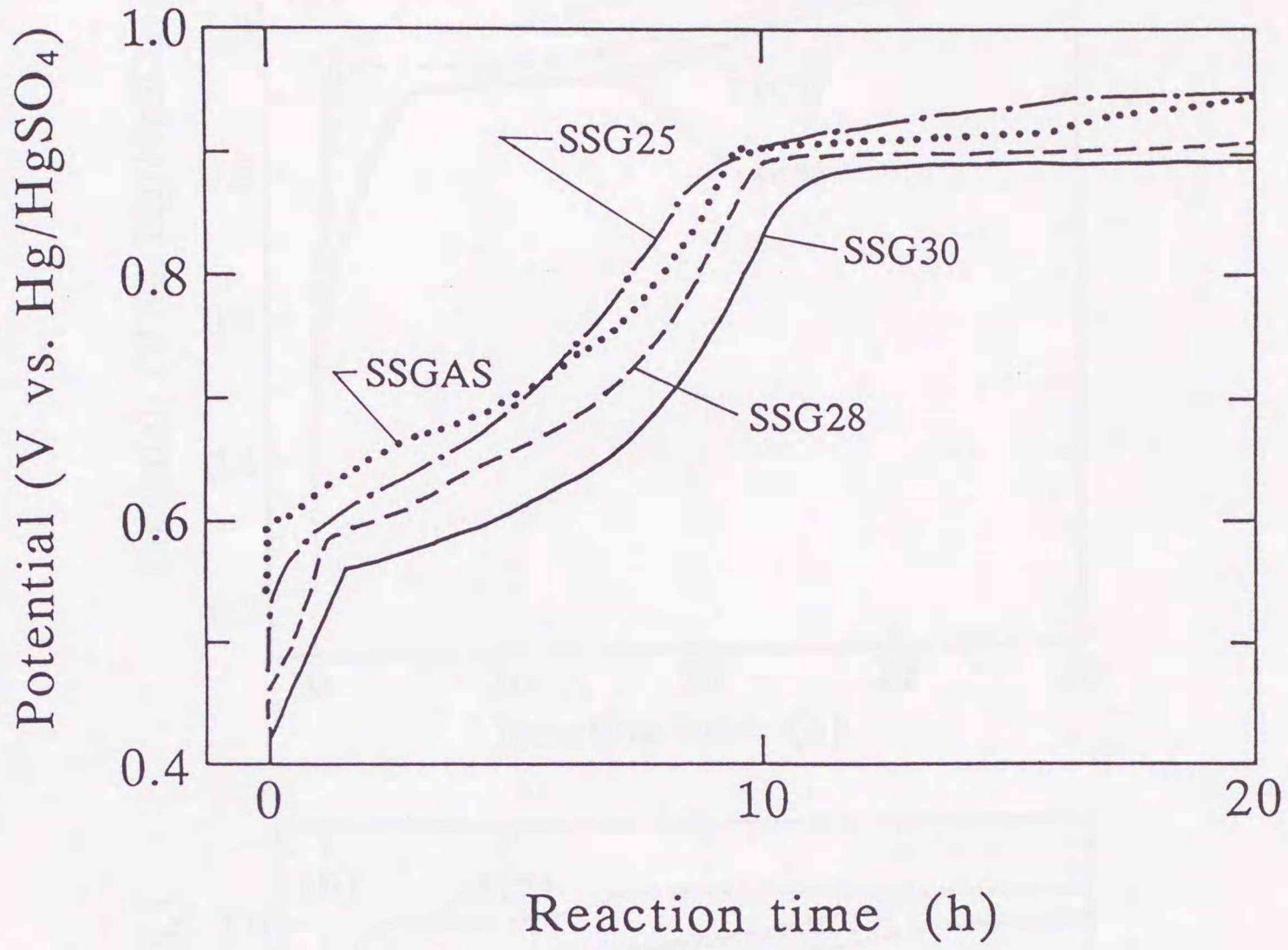


Fig. 4-7 The enlarged potential changes of the SSG-series with reaction time during chemical intercalation of sulfuric acid in the beginning.

The potential changes of the coke samples in PC-series with reaction time during the intercalation are shown in Fig. 4-8. X-ray powder patterns of the samples in PC-series oxidized for 40 hours are shown in Fig. 4-9. The potential curves may be divided into two families with respect to HTT, above and below 2400^{o}C.

For the samples heat-treated at high temperatures (PC24, PC27 and PC30) the potential is found to increase in stepwise

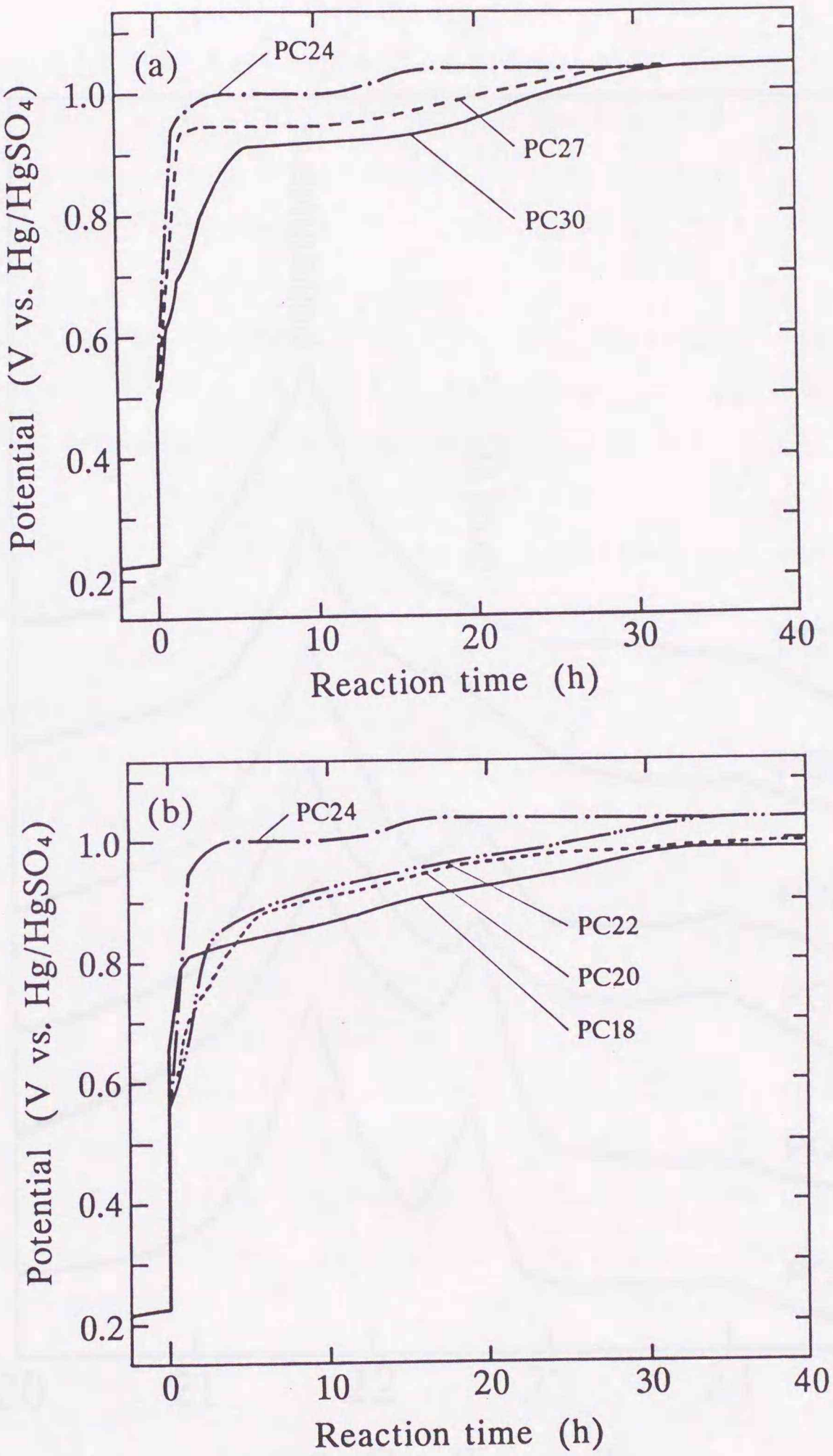


Fig. 4-8 Potential changes of the coke samples in PC-series, heat-treated at different temperatures, with reaction time during chemical intercalation of sulfuric acid.
(a) cokes with high HTT's, (b) cokes with low HTT's.

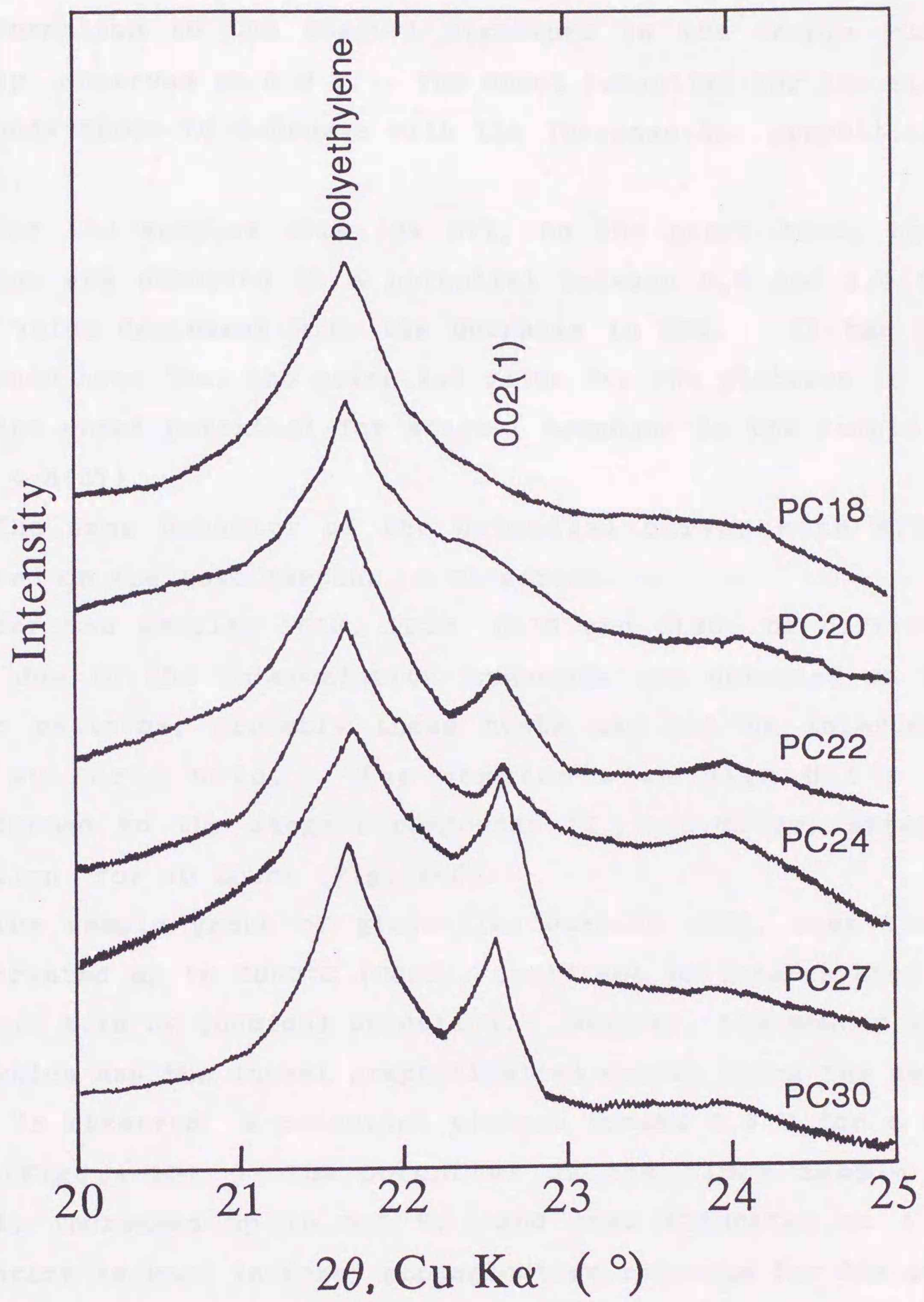


Fig. 4-9 X-ray powder patterns of the sample in PC-series oxidized in sulfuric acid for 40 hours.

(Fig. 4-8(a)). The potential plateau corresponding to transformation to the stage-1 structure in the sample PC30 is clearly observed at 0.9 V. The onset potential for the stage-1 compounds tends to decrease with the increase in graphitization degree.

For the samples with low HTT, on the other hand, obscure plateaux are observed at a potential between 0.8 and 1.0 V, of which value decreases with the decrease in HTT. It has to be mentioned here that the potential value for the plateaux is lower than the onset potential for stage-1 compound in the sample PC24 (Fig. 4-8(b)).

The same behavior of the potential curves with HTT was observed on the coke samples in GL-series.

For the samples PC18, PC20, GL18 and GL20, no diffraction lines due to the intercalation compounds are detected on their powder patterns, probably these hosts can not be intercalated with sulfuric acid. The samples with high HTT's are transformed to the stage-1 compounds (I_c = 0.80 nm) after the oxidation for 40 hours (Fig. 4-9).

The sample group of glass-like carbons (GC), even the one heat-treated up to 3000^{o}C (GC30), could not be intercalated with sulfuric acid by chemical oxidation. However, the powder sample GC12 which has the lowest graphitization degree among the samples used is observed a potential plateau around 0.6 V for a short time (Fig. 4-10). The potential of the block sample GC30 quickly increased up to 0.9 V, and then saturated at 1.0 V. The carbon 1s band in X-ray photoelectron spectrum for the sample GC30 after chemical oxidation showed a tailing toward high binding energy. The intensity ratio of oxygen 1s to carbon 1s bands changed from 0.127 to 0.625 with the oxidation.

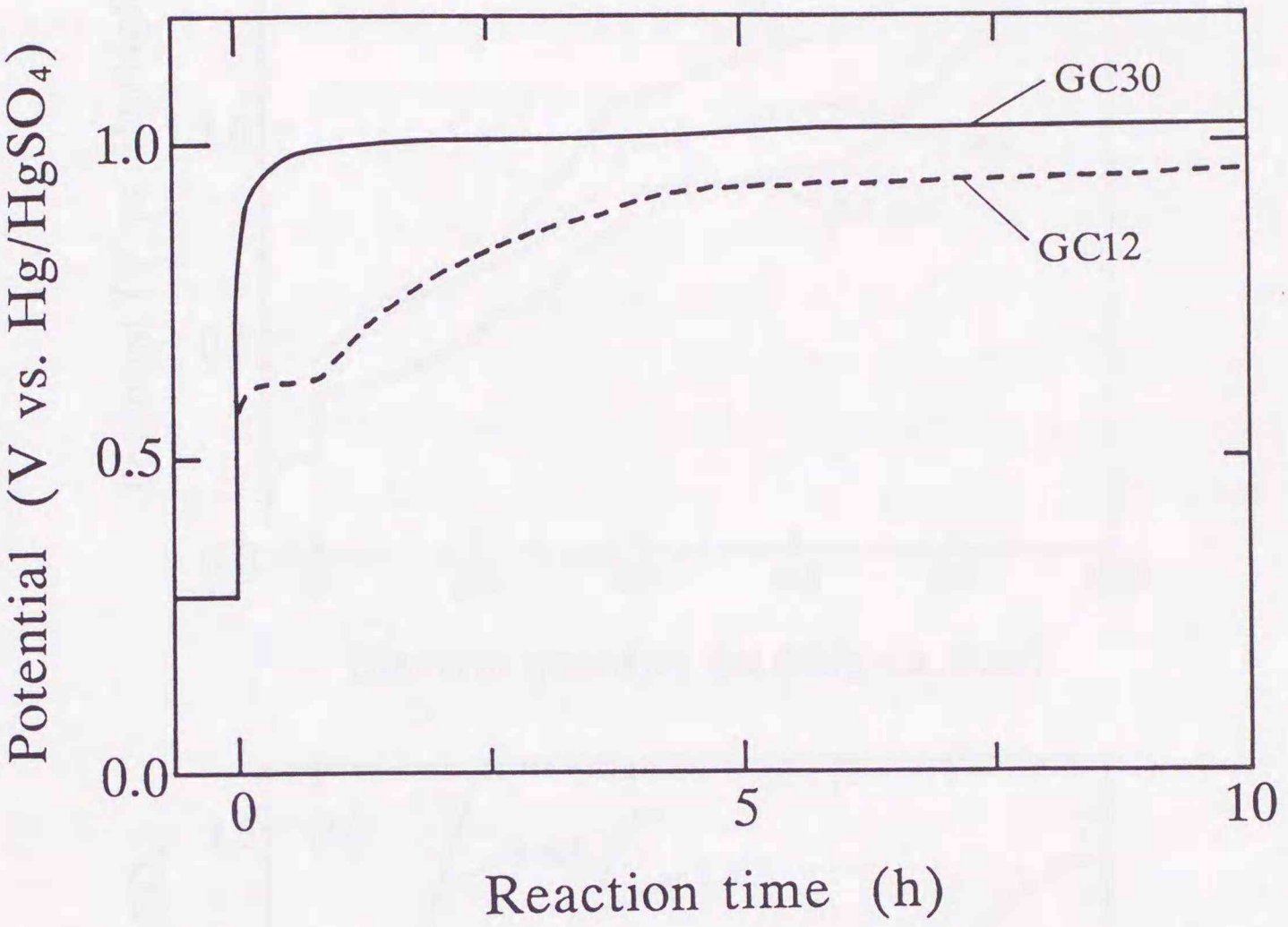


Fig. 4-10 Potential changes of the glass-like carbon samples with reaction time during chemical intercalation of sulfuric acid.

4.3.2. Potential change during electrochemical intercalation of sulfuric acid by galvanostatic oxidation

The potential changes during intercalation of sulfuric acid into the sample NG400 by galvanostatic oxidation with 0.4, 1.0 and 2.0 mA are shown in Fig. 4-11. On the curves of potential against electric quantity (Fig. 4-11(a)), the potential increase in the charging process becomes steep and the slope on the stage

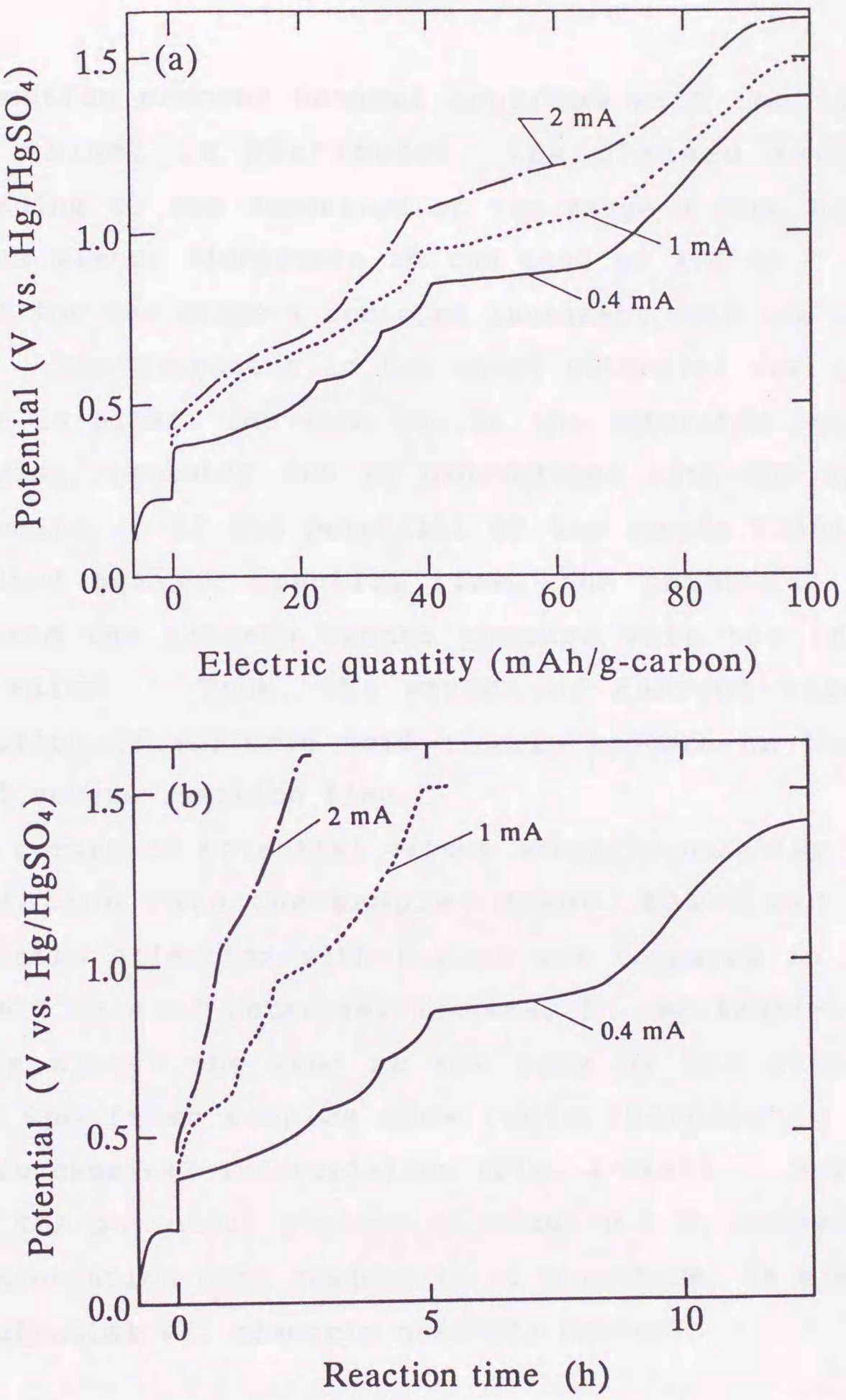


Fig. 4-11 Potential changes of the sample NG400 during galvanostatic intercalation of sulfuric acid with different current values.
(a) potential versus electric quantity,
(b) potential versus reaction time.
(1 mAh = 3.6 C)

transformation process becomes apparent with the increase in current value; in particular, the plateau around 0.6 V corresponding to the formation of the stage-3 from higher stage structures almost disappears in the case of 2.0 mA. The onset potential for the stage-1 compound increases with the increase in current. The increment in the onset potential for the stage-1 structure is almost the same one in the saturated potential for overcharging, probably due to overvoltage with the increase in current value. If the potential of the sample NG400 electrode was plotted against reaction time, the potential increased rapidly and the plateau became obscure with the increase in current value. Thus, the effect of current value on the intercalation of sulfuric acid clearly appears on the curve of potential versus reaction time.

The curves of potential versus electric quantity during the intercalation into the samples NG400, KOA-R and OVCF30 by galvanostatic oxidation with 0.4 mA are compared in Fig. 4-12. The overall rate of potential increase in the samples KOA-R and OVCF30 is almost the same as the case of the sample NG400, although the fiber samples show rapid increase in potential during the chemical intercalation (Fig. 4-3(a)). For the fiber samples, the potential plateau at about 0.9 V, corresponding to the transformation from stage-2 to -1 structure, is also detected on the potential vs. electric quantity curves.

4.3.3. Simulated potential curves

The changes of potential with electric quantity obtained by the simulation are summarized in Fig. 4-13. The curve simulated by assuming completely independent charging and stage transformation processes (Fig. 4-13(a)) is exactly the same as the idealized curves reported in the previous paper [4-8] shown

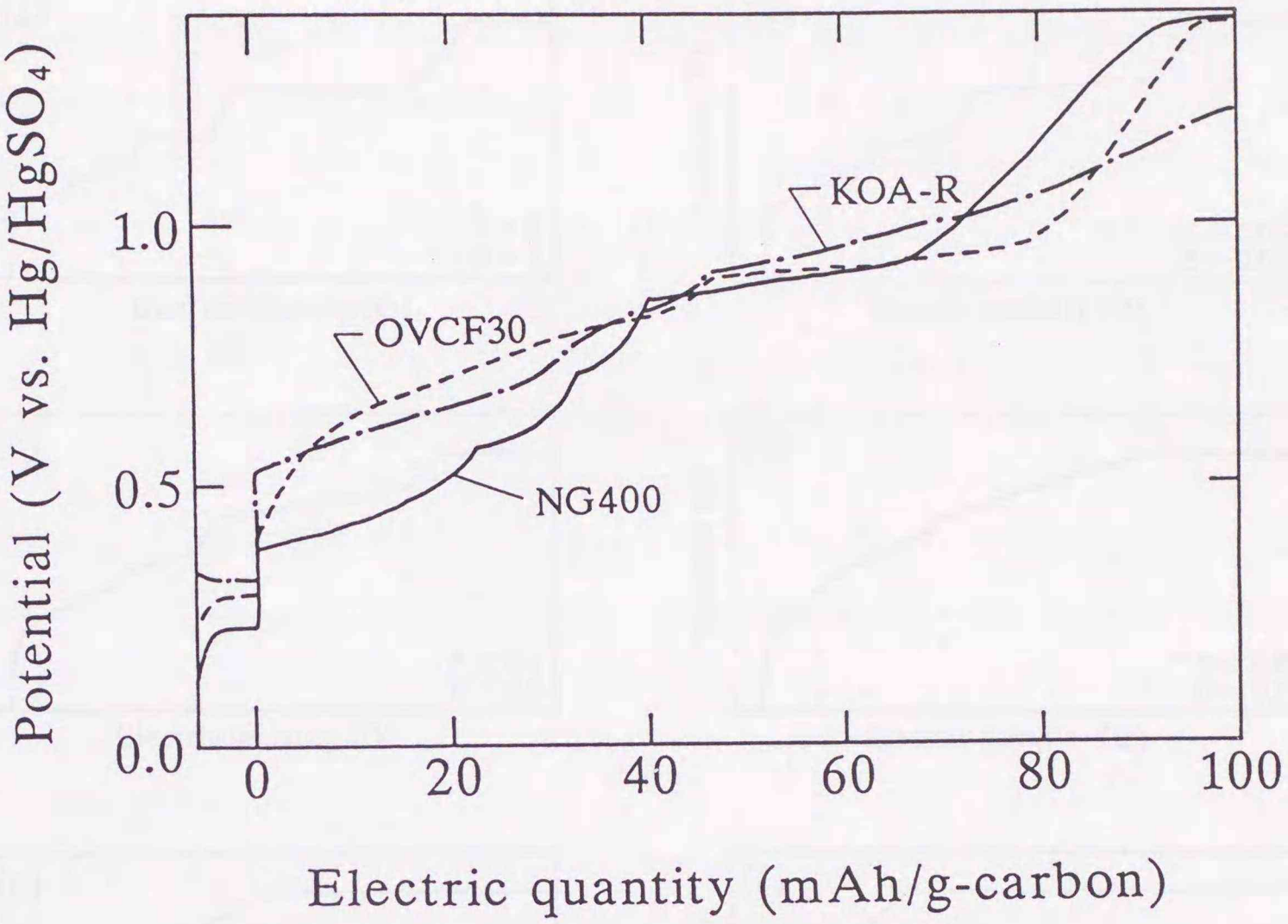


Fig. 4-12 Potential changes of the samples NG400, KOA-R and OVCF30 during galvanostatic intercalation of sulfuric acid with 0.4 mA. (1 mAh = 3.6 C)

in Fig. 4-1. With the increase in consumption ratio A of electric quantity to the charging process, (see Eqn. (4-2)), the potential plateau corresponding to the stage transformation process becomes obscure (Fig. 4-13(b) and (c)). For the ratio A above 0.8, plateau is difficult to be recognized, and the potential increases quickly until the saturated potential (Fig. 4-13(d), (e) and (f)).

During transformation from stage-n to -(n-1) structures,

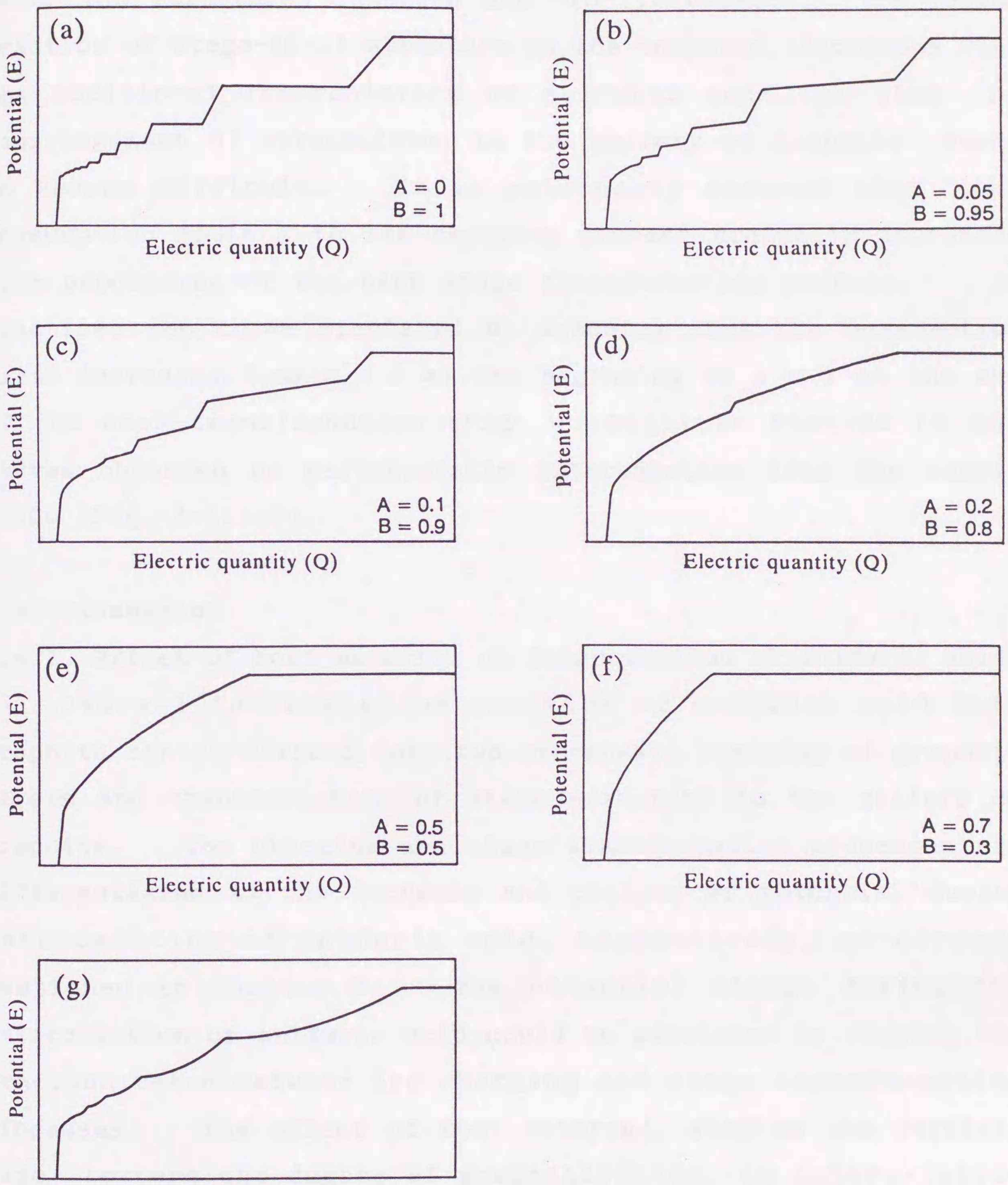


Fig. 4-13 Simulated curves of potential against electric quantity during galvanostatic intercalation of sulfuric acid.

where two structures (stage-n and -(n-1)) coexist, the volume fraction of stage-(n-1) structure in the compound increases with the additional intercalation of sulfuric acid, so that the rearrangement of intercalates in the gallery of graphite seems to become difficult. It is reasonably assumed that the consumption ratio A to the charging process gradually increases with proceeding of the each stage transformation process. In practice, the curve simulated by assuming that the consumption ratio increases from A = 0 at the beginning to A = 1 at the end of the each transformation (Fig. 4-13(g)) is similar to the curves observed by galvanostatic intercalation into the sample NG400 (Fig. 4-11(a)).

4.4. Discussion

4.4.1. Effect of host material on intercalation of sulfuric acid

Overall intercalation reaction of sulfuric acid into graphite can be divided into two processes; charging of graphite layers and transformation of stage structure in the gallery of graphite. The charging and stage transformation processes are differentiated as the increase and plateau of potential during intercalation of sulfuric acid, respectively, as already mentioned in Chapter 3. The potential change during the intercalation of sulfuric acid could be simulated by varying the reaction rates between the charging and stage transformation processes. The effect of host material, such as its particle size, texture and degree of graphitization, on intercalation behavior is discussed by taking into account of these two processes.

a) Effect of particle size

The charging of graphite layers reasonably supposed to

proceed preferentially at the edge of graphitic layers, particularly in the case of chemical oxidation. Thus, the charging process is reasonably supposed to depend on the edge surface area. On the other hand, the transformation from high to low stage structures in the gallery of graphite is associated with the intercalation of additional sulfuric acid and also with rearrangement of guests. Therefore, it is reasonably expected that the stage transformation process depends on particle size or crystallite size of graphitic structure.

The potential changes during intercalation into the Flaky-group samples (NG400, KG, and NOVAX30) and powder sample PV-7, which relatively large particle size, showed well-defined plateaux corresponding to the stage transformations. Since these flaky samples have high degree of graphitization and large flake or particle size (i. e., small edge surface area), it is reasonable that charging process is slow, and so well-defined stepwise potential increases are observed. For the samples NG5 and PV-7A with a large surface area, on the other hand, the charging and stage transformation processes would not be distinguished on the potential changes, probably because of both processes proceed quickly. The disappearance of the potential plateau was shown by simulation when the electric quantity of only 20 % was consumed to the charging process during stage transformation process (Fig. 4-13(c)). Therefore, relative rate of the charging process seems to be sensitive for the potential change during intercalation of sulfuric acid.

b) Effect of texture

The samples PV-7 and OVCF30 have equal values of graphitization degree, P_1, which are 0.81 and 0.80, respectively. The comparison between the potential changes of these samples

shows the effect of texture of host materials on intercalation behavior clearly, because the fiber OVCF30 has characteristic concentric texture, but the sample PV-7 is powder.

The mesophase-pitch-based carbon fibers KOA-R, I-1, I-2 have radial textures in their cross-section. The texture of the fibers I-3 is classified as doubly-textured, because of a little difference between the edge and center regions, as already shown in Chapter 2, but the fundamental arrangement of layers in the cross-section is radial in micrometric scale. In the fibers having radial texture, therefore, the edge surface of graphite layers, where charging process easily proceeds, are reasonably supposed to be exposed to the sulfuric acid solution with oxidant in high possibility, being higher than in the fibers I-4 and also VGCF-group with concentric texture. This is the reason why the potential increases so rapidly, and probably as a consequence, no plateaux corresponding to stage transformations are observed in these fibers with radial texture (Figs. 4-3 and -5). The charging process in the fiber I-4-30 was relatively slow probably because of its concentric texture, so that potential plateaux corresponding to the transformation to the stage-3 and stage-1 compounds were observed around 0.6 and 0.9 V, respectively (Fig. 4-5(b)).

On the simulation curve in which the consumption ratio to the charging process is larger than that to stage transformation process ($A > 0.5$), the potential plateau also disappeared (Fig. 4-13(e) and (f)). The disappearance of potential plateau by rapid charging process can be supported from the simulation. Even though no potential plateaux were observed, the transformation of stage structure was proved by X-ray powder patterns on the I-series fibers, as shown in Fig. 4-5(b).

During intercalation, host material must be expanded along

the c-axis; in the case of sulfuric acid, from 0.3354 nm for graphite to 0.80 nm (about 2.4 times). If the stage-1 compound is formed from the fiber sample OVCF30 having concentric texture (annual-ring texture) and average diameter of 10 μm, the most outer carbon layer plane of the fiber have to be about 75 μm (= 2.4 X 10 X π).

Average values of Young's modulus and tensile strength of the fiber OVCF30 are 220 and 2 GPa, respectively [4-12]. Thus, the fiber OVCF30 has so high modulus that its concentric carbon layers may not be stretched by expansion along the c-axis accompanied with intercalation. Therefore, the rapid potential increase in the fiber sample OVCF30 seems to be interpreted by the fact that the intercalation of sulfuric acid is very much limited because of the constraint by its annual-ring texture.

Fujii [4-9] was found out that intercalation reaction of sulfuric acid by galvanostatic oxidation could not proceed under the compression from 1 to 10 GPa. The strength of the carbon layers has almost the same order as pressure that the intercalation reaction is prevented, although stress directions on the both cases are different. In order to proceed the intercalation, this annual-ring texture must be fractured. Actually, such a fracture was observed on the fibers OVCF30 and NVCF30 along the fiber axis after intercalation, as shown in Fig. 4-4(c) (d) (e) and (f). As a consequence of the fracture, the constraint for intercalation into the sample OVCF30 could be partially removed, and the potential plateau corresponding to stage transformation appeared on potential change during the intercalation in second time (Fig. 4-3(b)).

In the case of the fiber NVCF30, the effect of fracture of concentric texture was not observed apparently on potential change during the chemical intercalation, probably because it was

so thin. However, a remarkable effect of the repetition of intercalation and de-intercalation was observed with cyclic voltammetry with a very slow scanning rate (5 mV/min); current peak due to the intercalation of sulfuric acid increased with the increase in the cycle number and onset potential of the peak shifted toward low value by repetition of cycle (Fig. 4-14).

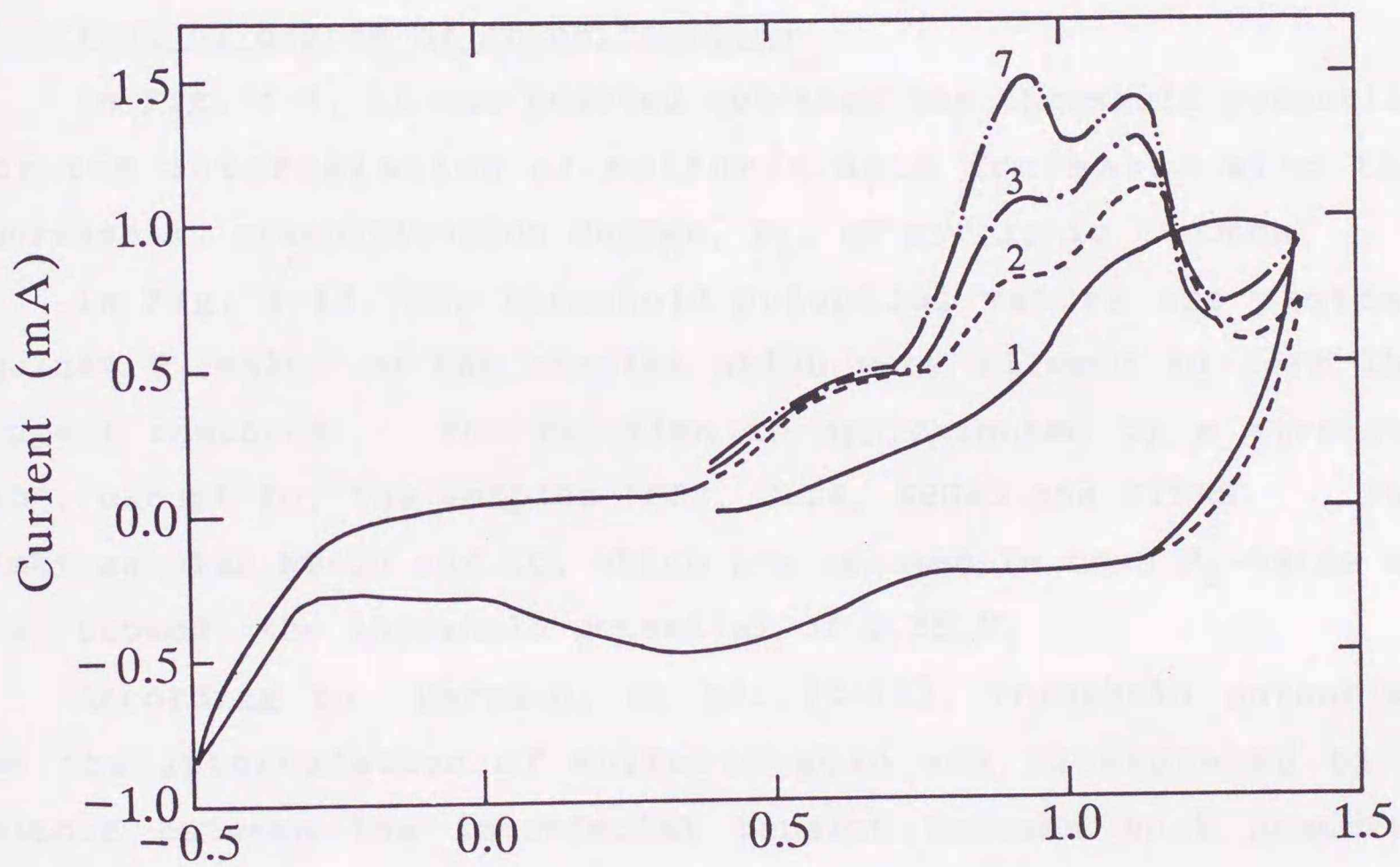


Fig. 4-14 Cyclic voltamograms of the sample NVCF30 in H_2SO_4 of 18 mol/dm^3. Scanning rate of 5 mV/min.

For the fiber KOA-R having radial texture with open wedge, although fracture along the fiber axis was observed after intercalation (Fig. 4-4 (a) and (b)), radial texture was fundamentally reserved. As the result, the potential behavior during the intercalation dose not change by repetition of reaction. On the other hand, the samples in Flaky-group seems to be easy for the expansion along the c-axis accompanied by intercalation, because any visible crack was not observed after intercalation.

c) Effect of degree of graphitization

In Fig. 4-7, it was pointed out that the threshold potential for the intercalation of sulfuric acid decreased with the increase in graphitization degree, P_1, of pyrolytic carbons.

In Fig. 4-15, the threshold potential values are plotted against P_1-value on the samples which were allowed to form the stage-1 compound. The relation is approximated by a straight line, except for the samples PC22, GL22, SSGAS and PYRAS. The flaky samples NG400 and KG, which are assumed to have P_1-value of 1.0, showed the threshold potential of 0.35 V.

According to Harrach, et al. [4-13], threshold potential for the intercalation of sulfuric acid was interpreted by a balance between the interfacial tension between host graphite electrode and sulfuric acid, which is as a function of potential, and the work per unit surface area of the host, which is needed for separating carbon layer planes by intercalation of sulfuric acid [4-14]. In other words, when potential of host reaches the threshold value, the interfacial tension corresponds to the work for the separation of carbon layer planes. It is reasonably supposed that the interfacial tension and the work separation of carbon layer planes in host carbon material depends strongly on

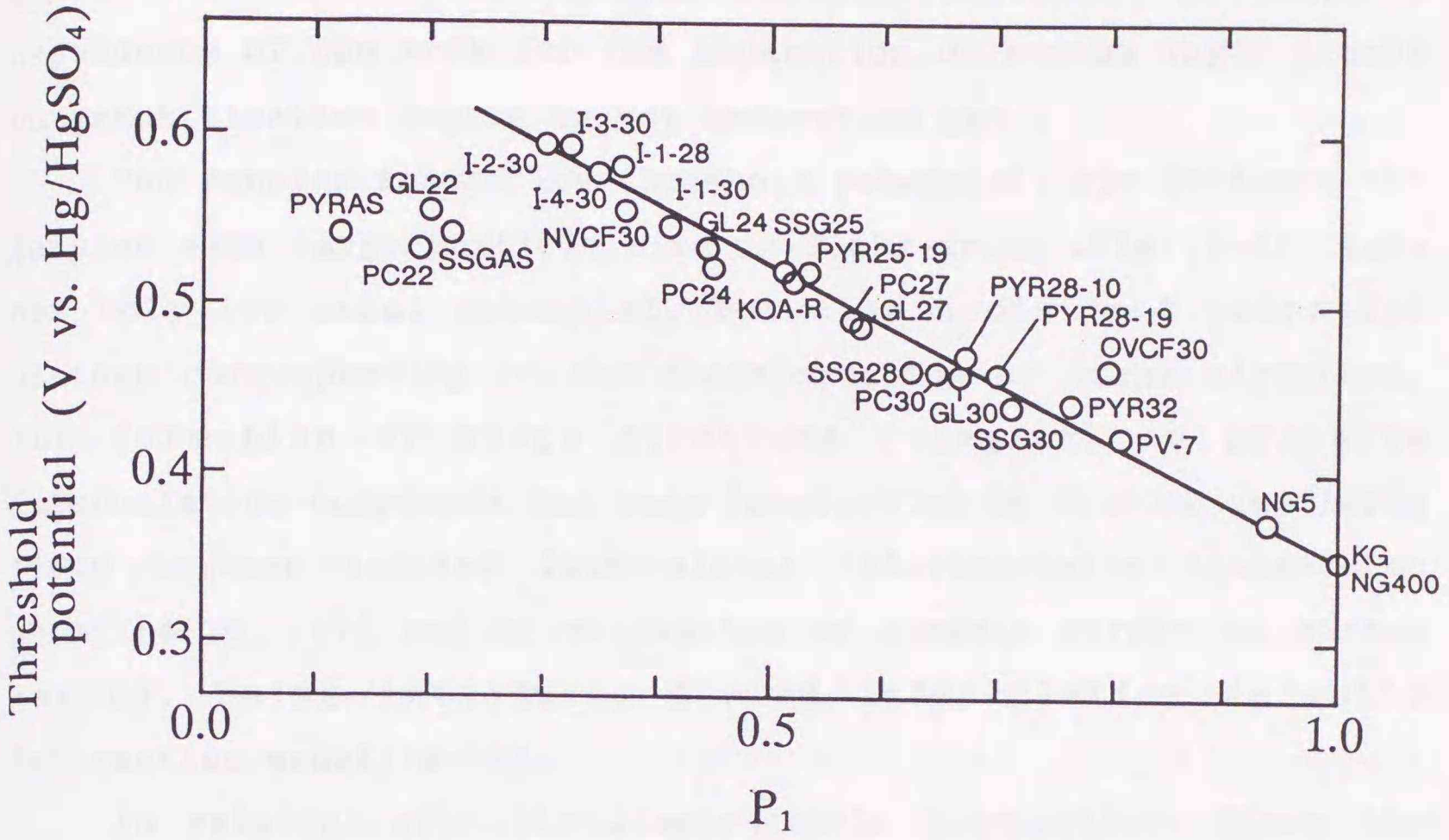


Fig. 4-15 Relation between threshold potential for intercalation of sulfuric acid and graphitization degree, P_1, on the host samples.

the graphitization degree. The electrical double layer capacitance in between carbon electrode and sulfuric acid tends to increase with the increase in graphitization degree [4-15]. The interfacial tension, which is estimated by twice integral of the double layer capacitance against potential, also seems to increase with the increase in graphitization degree, even at the same potential value. Therefore, the present result that the threshold potential for the intercalation of sulfuric acid decreases with the increase in graphitization degree, as shown in Fig. 4-15, is qualitatively interpreted by the dependence of

interfacial tension on graphitization degree, although a dependence of the work for the separation of carbon layer planes on graphitization degree is not understood yet.

The samples showed low threshold potential, for instance the samples with large particle size in Flaky-group (Fig. 4-2), gave not only low onset potential, but also a distinct potential plateau corresponding to the transformation of stage structure. The formation of stage structure (staging) in graphite intercalation compounds has been interpreted by coulomb repulsion force between ionized intercalates (electrostatic interaction model)[4-16, -17] and by relaxation of elastic strain on carbon layers, being introduced during intercalation (elastic interaction model)[4-18].

In relation with the electrostatic interaction, since the charge created on the carbon layers by intercalation has to move on the layers during the stage transformation, it is reasonable that the stage transformation depends on the motion of electric carrier on the carbon layers, i. e., mobility of carrier in host carbon. The mobility increases with the increase in graphitization degree, as already shown in Chapter 2 (Fig. 2-10).

Sakai, et al. [4-19] was found out that the graphitized carbons showed remarkable quasi-plastic deformation, but the non-graphitized carbons an elastic behavior during indentation test. Relating with elastic interaction, this result suggests that it is easy for host carbons with high graphitization degree to relax elastic strain on the carbon layers associated with the intercalation by plastic deformation, i. e., gliding process of carbon layers.

Due to high mobility of carrier on the carbon layers and also to easy relaxation of strain, therefore, the host with high graphitization degree is easily intercalated with sulfuric acid

and the intercalates are easily rearranged in the gallery of graphite. As a results of easy intercalation, low onset potentials and apparent plateaux corresponding to stage transformations are observed on the potential change.

During the chemical oxidation of the samples PC18, PC20 and GC12 (Figs. 4-9 and -11), the obscure potential plateau was observed, in despite of these samples could not be intercalated with sulfuric acid. Since such samples with a low graphitization degree show a large electrical resistivity (Chapter 2), it is reasonably supposed that the oxidation with nitric acid is localized at the surface of samples.

By electrochemical oxidation of a carbon material in sulfuric acid solution, it has been known that oxides is formed on its surface [2-20, -21]. In the present result, it was shown for the sample GC30, which was not intercalated with sulfuric acid, that the relative intensity of oxygen 1s peak to carbon 1s one with XPS increased after the chemical oxidation with nitric acid, probably due to the formation of oxide on the surface.

The obscure potential plateau observed at around 0.9 V in the samples PC18, PC20 and GC12 seems to be based on the formation of the oxides on the these surfaces. The intercalation into the samples SSGAS and PC22 seems to occur together with the oxidation of their surface during the chemical oxidation, because these samples showed rather low threshold potentials than the value expected from the linear relation in Fig. 4-15.

4.4.2. Effect of reaction rate on intercalation behavior

In the case of intercalation of sulfuric acid by galvanostatic oxidation, the reaction rate is controlled by the current value, which is one of the merits for the study on

formation of H_2SO_4-GICs by electrochemical method. However, the effect of reaction rate (current value) on the potential change is remarkably observed on the curve of potential versus reaction time rather than that of potential versus. electric quantity, as shown in Fig. 4-11(b).

In the chemical intercalation by nitric acid oxidation, on the other hand, the reaction rate is not constant for the oxidation and its absolute value can not be known. However, it was shown in Figs. 3-2 and also in 4-2(c) that the reaction rate in the chemical intercalation depends on the amount of oxidant; the overall rate of the potential changes and the time reached the saturated potential increase with the increase in amount of oxidant added. As discussed in the previous section, the fiber samples KOA-R and OVCF30 showed quick increase in potential (Fig. 4-3), due to their radial and concentric textures, respectively. In the case of the galvanostatic intercalation into these fibers and the sample NG400 (Fig. 4-12), obvious difference in overall rate of their potential changes was not observed. Therefore, not only the amount of oxidant, but also structure and texture of the host material give certain influence on the reaction rate in the case of the chemical intercalation.

4.4.3. Criterion for intercalation reaction on host material

For acceptor-type intercalates, for instance sulfuric acid, bromine and metal halides, rather limited host materials such as natural graphite and pyrolytic carbons heat-treated at high temperatures have been used. Only a few works on the electrochemical intercalation of sulfuric acid [4-5, -6] were performed by using the host with a wide range of structure, but there was no discussion on the criterion of host structures. In the present work, a number of carbon materials were employed as

host for intercalation of sulfuric acid. Fig. 4-15 shows that intercalation of sulfuric acid into host with lower graphitization degree became difficult, and sulfuric acid can not intercalate into carbons with the P_1-value lower than 0.1. There must be a criterion for intercalation reaction of sulfuric acid on graphitization degree of host carbon material. Here, therefore, the structural and electronic criteria for intercalation of sulfuric acid are discussed on the basis of structural characteristic described in Chapter 2 and intercalation behavior studied in this chapter.

In Fig. 4-16, the plot of crystallite size along the c-axis, $L_c(002)$, against the degree of graphitization, P_1, is reproduced from Fig. 2-5(b) for the part of $P_1 < 0.6$. In this figure, the samples which are intercalated with sulfuric acid are indicated as open marks and those not intercalated as solid ones with the sample codes. It is clearly shown that the samples with $L_c(002)$-value less than 20 nm are not intercalated with sulfuric acid. This result points out that an enough thickness of carbon layers (above 20 nm) needs for intercalation of sulfuric acid.

The simple models of band structure for turbostratic and graphitic carbons (simple two band model [4-22]) are schematically shown in Fig. 4-17. The conduction and valence bands are separated in turbostratic carbons (Fig. 4-17(a)), but overlapped in graphitic carbons (Fig. 4-17(b)). Since Fermi level in the turbostratic carbon places at the upper part of the valence band, its conduction is governed by holes. On the other hand, in the graphitic carbons, Fermi level places at the middle of the overlapped regions of the two bands, and the carriers are electrons and holes. In most graphite intercalation compounds, except graphite fluoride with covalent bonding, certain amount of charge transfer occurs between intercalate (guest) and host

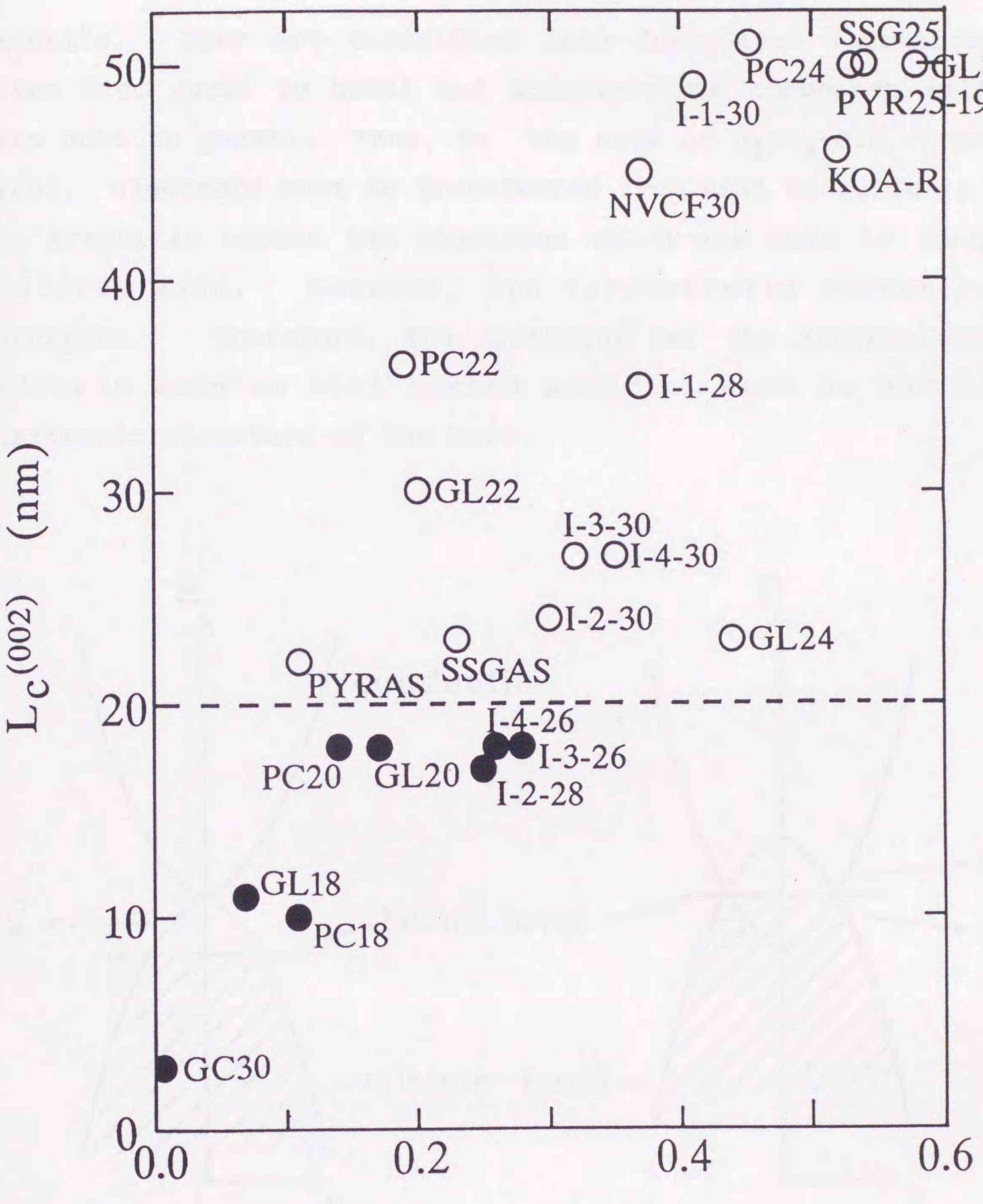
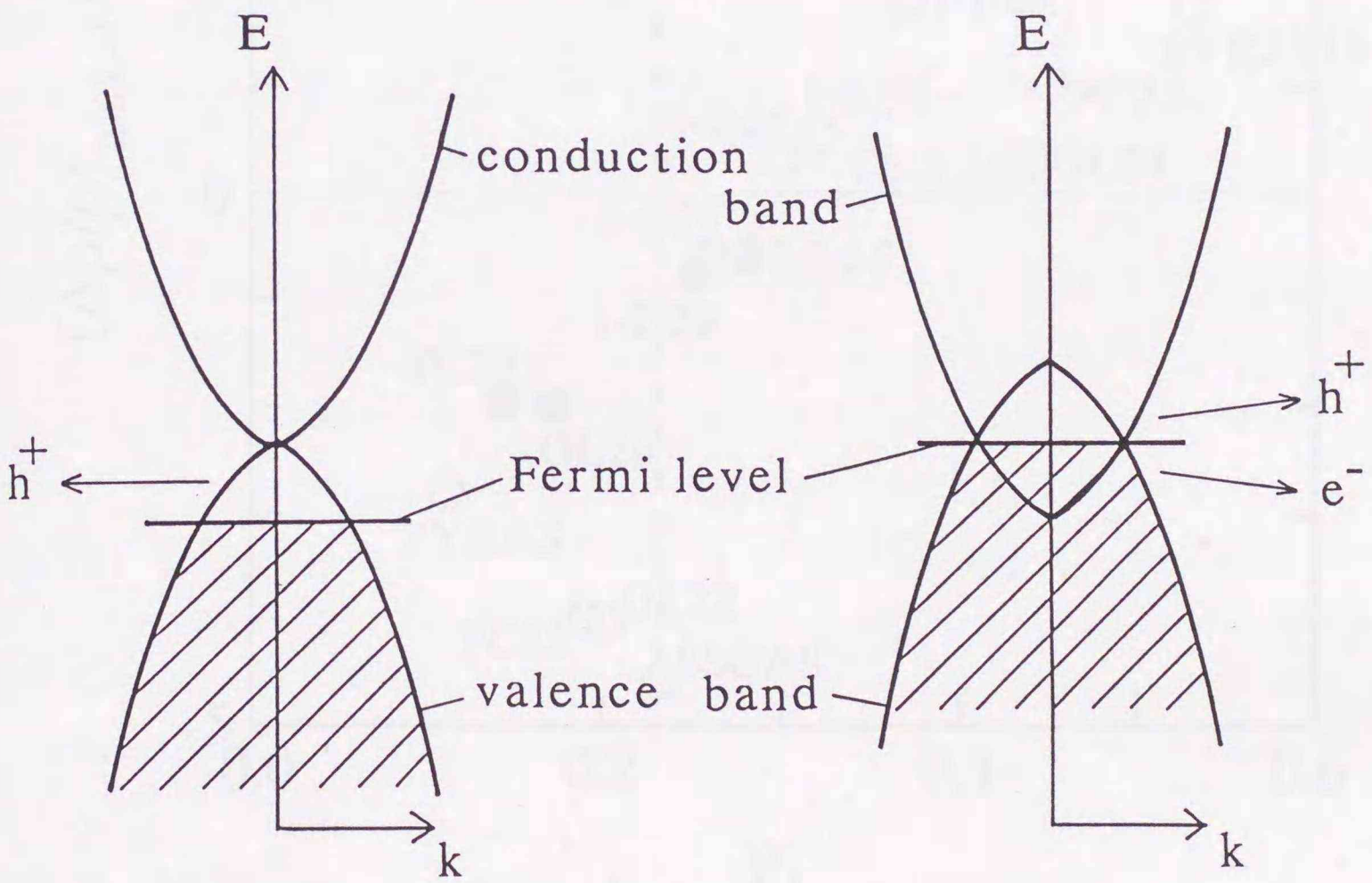


Fig. 4-16 Relation between crystallite size along the c-axis, $L_c(002)$, and graphitization degree, P_1.
The open mark stand for the sample intercalated with sulfuric acid, and the solid mark for those not intercalated.

graphite. They are classified into donor-type (electrons are given from guest to host) and acceptor-type compounds (electron from host to guest). Thus, in the case of H_2SO_4-GIC (acceptor-type), electrons must be transferred from host to sulfuric acid. The graphitic carbon has electrons which are able to donate to sulfuric acid. However, the turbostratic carbon has no electrons. Therefore, the criterion for the intercalation of sulfuric acid on host carbon material must be defined by electronic structure of the host.



(a) (b)

Fig. 4-17 Band structures for carbon materials (simple two band model [4-22]).
(a) turbostratic carbon, (b) graphitic carbon.
(h^+: hole, e^-: electron)

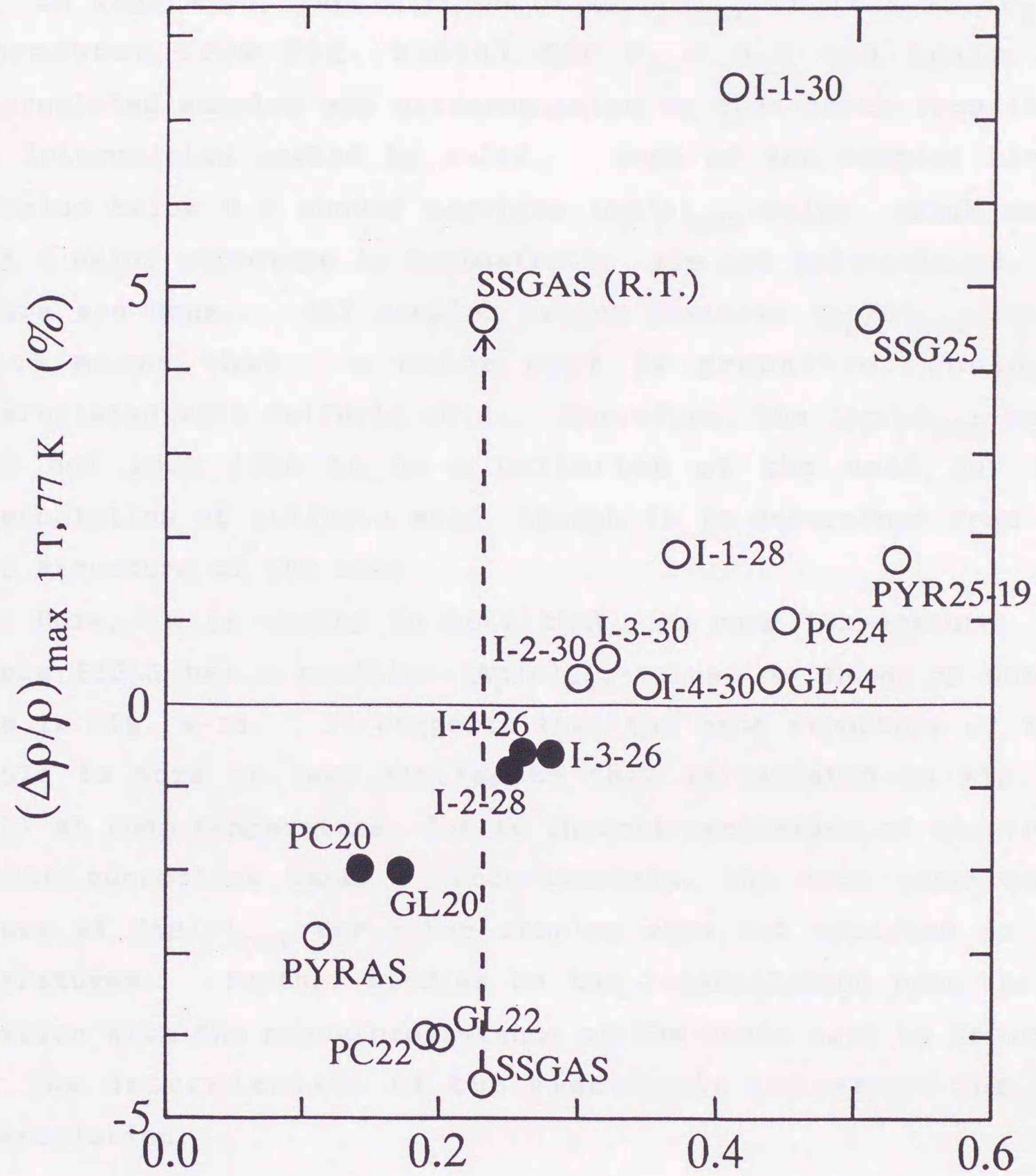


Fig. 4-18 Relation between magnetoresistance, $(\Delta\rho/\rho)_{max}$ at 77 K, and graphitization degree, P_1.
The open mark stand for the sample intercalated with sulfuric acid, and the solid mark for those not intercalated.

In Fig. 4-18, the relation of $(\Delta\rho/\rho)_{max}$ at 77 K vs. P_1 is reproduced from Fig. 2-6(a) for $P_1 < 0.6$ and again the intercalated samples are differentiated by open marks from those not intercalated marked by solid. Some of the samples having P_1-value below 0.3 showed negative $(\Delta\rho/\rho)_{max}$-value, which means that a major structure is turbostratic, are not intercalated, but others are done. All samples having positive $(\Delta\rho/\rho)_{max}$-value, which means that a major part is graphitic, could be intercalated with sulfuric acid. Therefore, the $(\Delta\rho/\rho)_{max}$-value does not look like to be a criterion of the host for the intercalation of sulfuric acid, though it is determined from the band structure of the host.

Here, it is worthy to note that, at room temperature, the sample SSGAS has a positive $(\Delta\rho/\rho)_{max}$-value, as shown by dashed line in Fig. 4-18. It suggests that the band structure of this sample is more or less similar to that illustrated in Fig. 4-17(b) at room temperature, due to thermal excitation of electrons to the conduction band. Unfortunately, the room temperature values of $(\Delta\rho/\rho)_{max}$ for other samples were not reported in the literatures. Further studies on the intercalation behavior in relation with the magnetoresistance of the hosts will be fruitful for the determination of the electronic criterion for the intercalation.

4.5. Summary

The present results lead to the following three important points.

1) The intercalation behavior of sulfuric acid by chemical oxidation depends strongly on structure, texture and particle size of host carbon materials. The effect of hosts on potential change during the chemical intercalation could be explained on

the basis of the competition of reaction rates between the charging of carbon layer planes in the host and the transformation of stage structure in the gallery of graphite. The charging process corresponding to the increase in potential is strongly influenced by the area of edge surface of graphitic structure. The stage transformation process showing plateau on the potential change easily proceeds in the host with high graphitization degree.

2) The overall rate of intercalation of sulfuric acid by chemical oxidation depends not only on the amount of oxidant added, but also on the structure and texture of host carbon material. Although absolute value of reaction rate for the chemical intercalation was not known, relative rate could be estimated from overall rate of the potential change with reaction time.

3) The host must have certain degree of graphitization in order to form graphite intercalation compounds with sulfuric acid. A criterion on host structure for the intercalation is to have the crystallite thickness along the c-axis, $L_c(002)$, of more than 20 nm. Because the intercalation reaction involves charge transfer between host and intercalate (guest), there must be a criterion on electronic structure of host for the intercalation. From the present results, the positive magnetoresistance $(\Delta\rho/\rho)_{max}$ at room temperature is expected to be a criterion.

References

4-1 G. A. Sunders, A. R. Ubbelode and D. A. Young, Proc. Roy. Soc., A273, 499 (1963).

4-2 J. G. Hooley, W. G. Garby and J. Valentin, Carbon, 3, 7 (1965).

4-3 J. G. Hooley and J. C. Smee, Carbon, 2, 135 (1964).

4-4 M. B. Dowell, D. S. Badorrek, Carbon, 16, 241 (1978).

4-5 D. Horn and H. P. Boehm, Z. anorg. allg. Chem., 456, 117 (1979).
4-6 Y. Maeda, Y. Okemoto and M. Inagaki, J. Electrochem. Soc., 132, 2369 (1985).
4-7 A. Metrot, Synth. Met., 7, 177 (1983).
4-8 A. Metrot and M. Tihli, Synth. Met., 12, 517 (1985).
4-9 R. Fujii, Report of Gov. Ind. Res. Inst., Osaka, No. 353 pp. 13-44 (1978).
4-10 B. Bouayad, H. Fuzellier, M. Lelaurain, A. Metrot and F. Rousseaux, Synth. Met., 7, 325 (1983).
4-11 A. Yoshida, Y. Hishiyama and M. Inagaki, Carbon, 28, 539 (1990).
4-12 A. Sudoh, H. Daioh and S. Morimoto, Ext. Abs. "Int. Sump. on Carbon", Tukuba (1990) pp. 518-521.
4-13 A. Harrach and A. Metrot, Electrochim. Acta, 34, 1877 (1989).
4-14 A. Herold, NATO ASI "Chemical Physics of Intercalation", Ed. By A. P. Legrand and S. Flandrois, Plenum, New York, 1988, pp.3.
4-15 K. Kinoshita, " Characteristics and Properties of Carbon Electrodes", John Wily & Sons, pp. 293-380.
4-16 F. J. Salzano and S. Aronson, J. Chem. Phys., 45, 2221 (1966).
4-17 S. A. Safran, Synth. Met., 2, 1 (1980).
4-18 S. A. Safran and D. R. Hamann, Phys. Rev. Lett., 42, 1410 (1979).
4-19 M. Sakai, H. Hanyu and H. Ichikawa, to be published.
4-20 H. P. Boehm, High Temp.-High Press., 22, 275 (1990).
4-21 N. L. Weinberg and T. B. Reddy, J. Appl. Electrochem., 3, 73 (1973).
4-22 C. A. Klein, Rev. Mod. Phys., 34, 656 (1962).

CHAPTER 5

Electrochemical reduction of GIC with sulfuric acid synthesized by chemical oxidation and its application to lead-sulfuric acid battery

5.1 Introduction

Graphite intercalation compounds with sulfuric acid (H_2SO_4-GICs) were applied to the production of exfoliated graphite [5-1], to the reagent of organic reaction [5-2], and to the precursor of graphite oxide, which have been used as positive electrode of lithium primary battery [5-3]. The formation of H_2SO_4-GICs by electrochemical oxidation and decomposition of the GICs by electrochemical reduction, in other words, intercalation and de-intercalation for graphite, can be considered to be charge and discharge reactions for a secondary battery, respectively. Fujii [5-4] attempted to apply H_2SO_4-GIC to a secondary battery, in which a pyrolytic carbon heat-treated at 3000 ^oC was used as positive electrode, a copper metal as negative electrode and a sulfuric acid of 12 mol/dm^3 as electrolyte. It showed high performance with an open circuit voltage of about 1.5 V, high efficiency of electric quantities between charge and discharge close to 100 % and long life cycle for repetition of charge-discharge more than 6500 times.

In Chapter 3, the intercalation of sulfuric acid into graphite by chemical oxidation was quantitatively discussed by measuring potential. From the potential changes, the intercalation by chemical oxidation was found to be fundamentally the same process as the electrochemical one.

In the present chapter, electrochemical reduction of H_2SO_4-GICs synthesized by chemical oxidation is followed by measuring potential, and compared with the one for the compounds

synthesized by electrochemical oxidation. The effects of amount of oxidant added and host graphite material on the electrochemical reduction is also discussed on the basis of the potential change. The electrochemical reduction of H_2SO_4-GICs is applied to lead-sulfuric acid battery.

5.2 Experimental

Flaky natural graphite powder with average flake size of 400 μm (sample code: NG400) was mostly used as the host material. In order to study the effect of host carbon material on the electrochemical reduction, different carbon materials were selected mesophase-pitch-based carbon fiber having radial texture with open wedge (KOA-R), vapor-grown carbon fiber having concentric texture (OVCF30), both of which were heat-treated at 3000^{o}C and pyrolytic carbons heat-treated at different temperatures (SSGAS, SSG25, SSG28 and SSG30).

The host material of 50 mg was held between plastic plates, as already shown in Fig. 3-1(b), and the test cell was used the same one as Fig. 3-1(a). A platinum plate (10 X 10 mm^2) and lead metal sheet (5 X 30 mm^2) were used as counter electrode in the cases of measurement of potential on host electrode and of testing of battery performance, respectively.

In all experiments, sulfuric acid of 18 mol/dm^3 (50 cm^3) was used as electrolyte. Nitric acid (13.8 mol/dm^3) and potassium permanganate (powder) were used as oxidant. After reaching the saturated potential by chemical oxidation either with nitric acid or potassium permanganate, the galvanostatic reduction of H_2SO_4-GICs synthesized was carried out with either 0.4 or 4.0 mA in the sulfuric acid solution containing oxidant. The detailed condition and procedure for chemical oxidation were exactly the same as those described in the previous chapter, except that

temperature in the cell was controlled at 25 ^{o}C.

Characterization of the H_2SO_4-GICs formed was carried out with X-ray powder diffractometry by preventing the decomposition in a polyethylene bag.

5.3 Results

5.3.1. Potential change during electrochemical reduction of H_2SO_4-GICs

The curves of potential versus electric quantity during galvanostatic reduction with 0.4 mA of H_2SO_4-GICs synthesized from the sample NG400 by galvanostatic oxidation and by chemical oxidation with potassium permanganate ($KMnO_4$/carbon = 3.3) are shown in Fig. 5-1. On these potential changes, characteristic potential plateaux are observed at around 0.75 and 0.45 V, which correspond to the transformation from the stage-1 to -2 structures and the decomposition of the stage-3 compound, respectively. The potential plateau corresponding to the transformation from the stage-2 to -3 structures is not clearly observed on the potential change. The electric quantity for de-intercalation of the H_2SO_4-GIC synthesized by galvanostatic oxidation (galvano-GIC, solid line in Fig. 5-1), i. e., the electric quantity needed for the potential decrease down to 0.2 V, which is rest potential of the original graphite electrode, is about 80 mAh/g-carbon, smaller than the theoretical quantity for the formation of the stage-1 H_2SO_4-GIC (93 mAh/g-carbon) [5-5].

In the GIC synthesized by potassium permanganate oxidation (manganate-GIC, dashed line in Fig. 5-1), on the other hand, the electric quantity for de-intercalation is 130 mAh/g-carbon, which is much larger than that measured in the galvano-GIC and also larger than the theoretical one.

The curve of potential versus electric quantity during

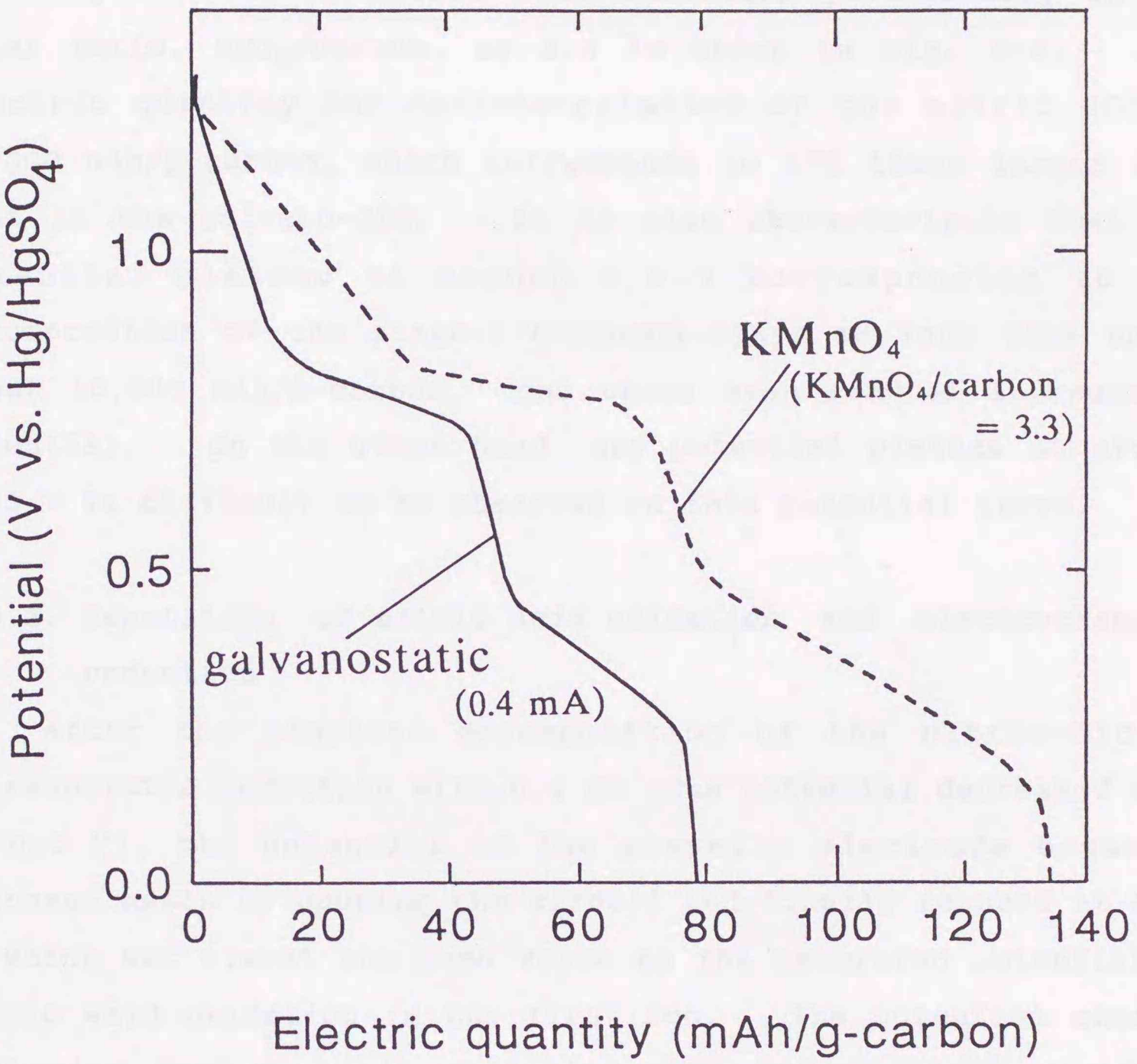


Fig. 5-1 Curves of potential versus electric quantity during galvanostatic reduction (with the current of 0.4 mA) of H_2SO_4-GICs prepared from NG400 by galvanostatic oxidation and by chemical oxidation with potassium permanganate ($KMnO_4$/carbon = 3.3). (1 mAh = 3.6 C)

galvanostatic reduction with 0.4 mA of H_2SO_4-GIC prepared from the sample NG400 by nitric acid oxidation (nitric-GIC) in the molar ratio, HNO_3/carbon, of 3.3 is shown in Fig. 5-2. The electric quantity for de-intercalation of the nitric-GIC is 14,000 mAh/g-carbon, which corresponds to 175 times larger than that in the galvano-GIC. It is also characteristic that the potential plateau at around 0.8 V corresponding to the decomposition of the stage-1 compound stays so long time up to about 10,000 mAh/g-carbon, and shows even gradual increase in potential. On the other hand, any potential plateau at around 0.45 V is difficult to be observed on this potential curve.

5.3.2. Repetition of nitric acid oxidation and electrochemical reduction

After the complete decomposition of the nitric-GIC by galvanostatic reduction with 0.4 mA (the potential decreased down to 0.0 V), the potential of the graphite electrode began to increase again by opening the circuit and finally reached at 1.05 V, which was almost the same value as the saturated potential by nitric acid oxidation in the first run. The potential changes with time during nitric oxidation and with electric quantity during galvanostatic reduction of the sample NG400 electrode are shown continuously in Fig. 5-3. When the potential reaches at 0.0 V by galvanostatic reduction, the the curves return to the time "0" on the figure of potential vs. time (left-hand side in Fig. 5-3), i. e., start point of nitric acid oxidation. The first reduction needs so large electric quantity that the potential curve only in the beginning is shown on the figure. The stage numbers determined with X-ray powder diffractometry in an additional experiment are also indicated in the same figure.

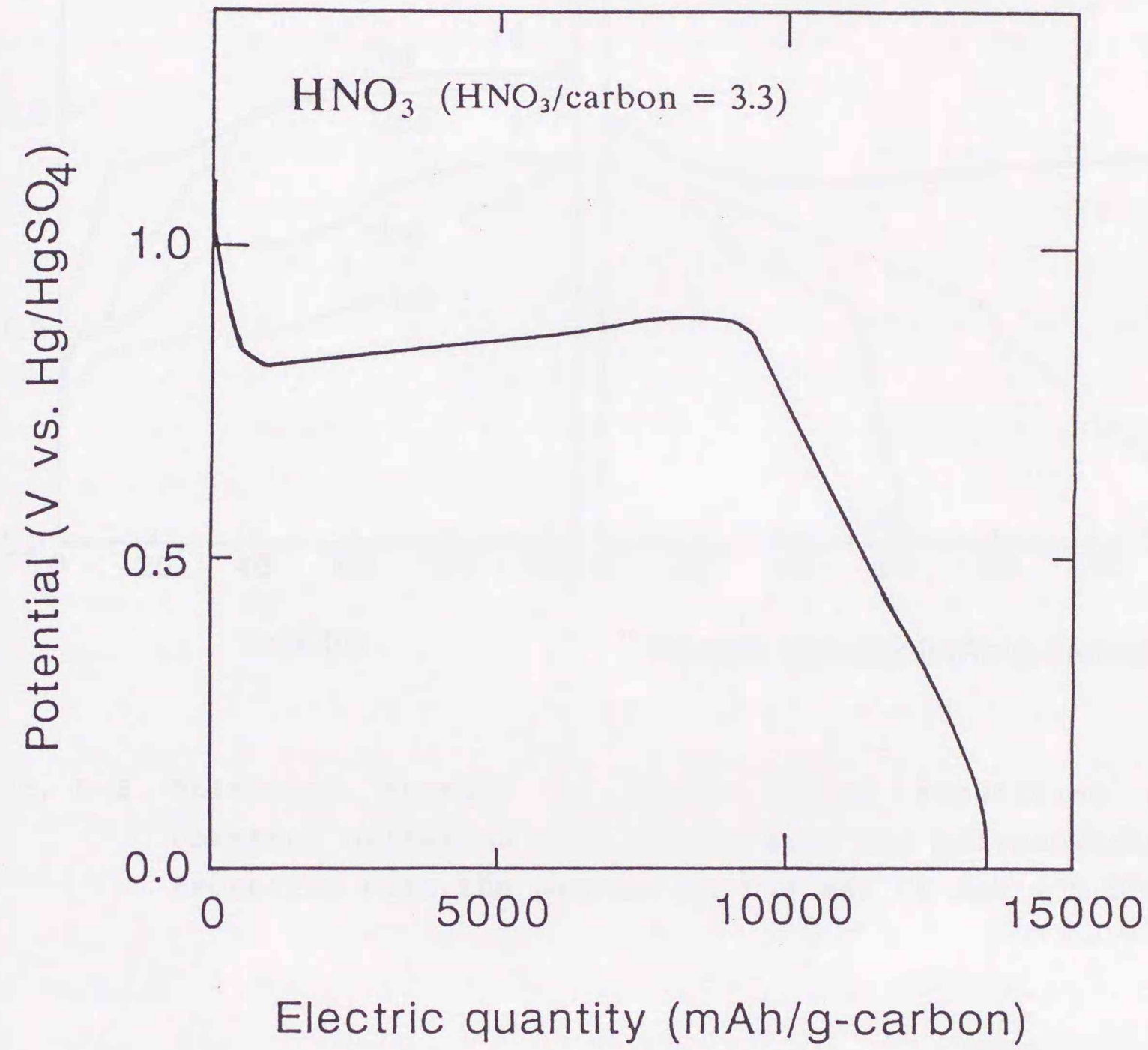


Fig. 5-2 Curve of potential versus electric quantity during galvanostatic reduction (with the current of 0.4 mA) of H_2SO_4-GICs synthesized from NG400 by chemical oxidation with nitric acid (HNO_3/carbon = 3.3).
(1 mAh = 3.6 C)

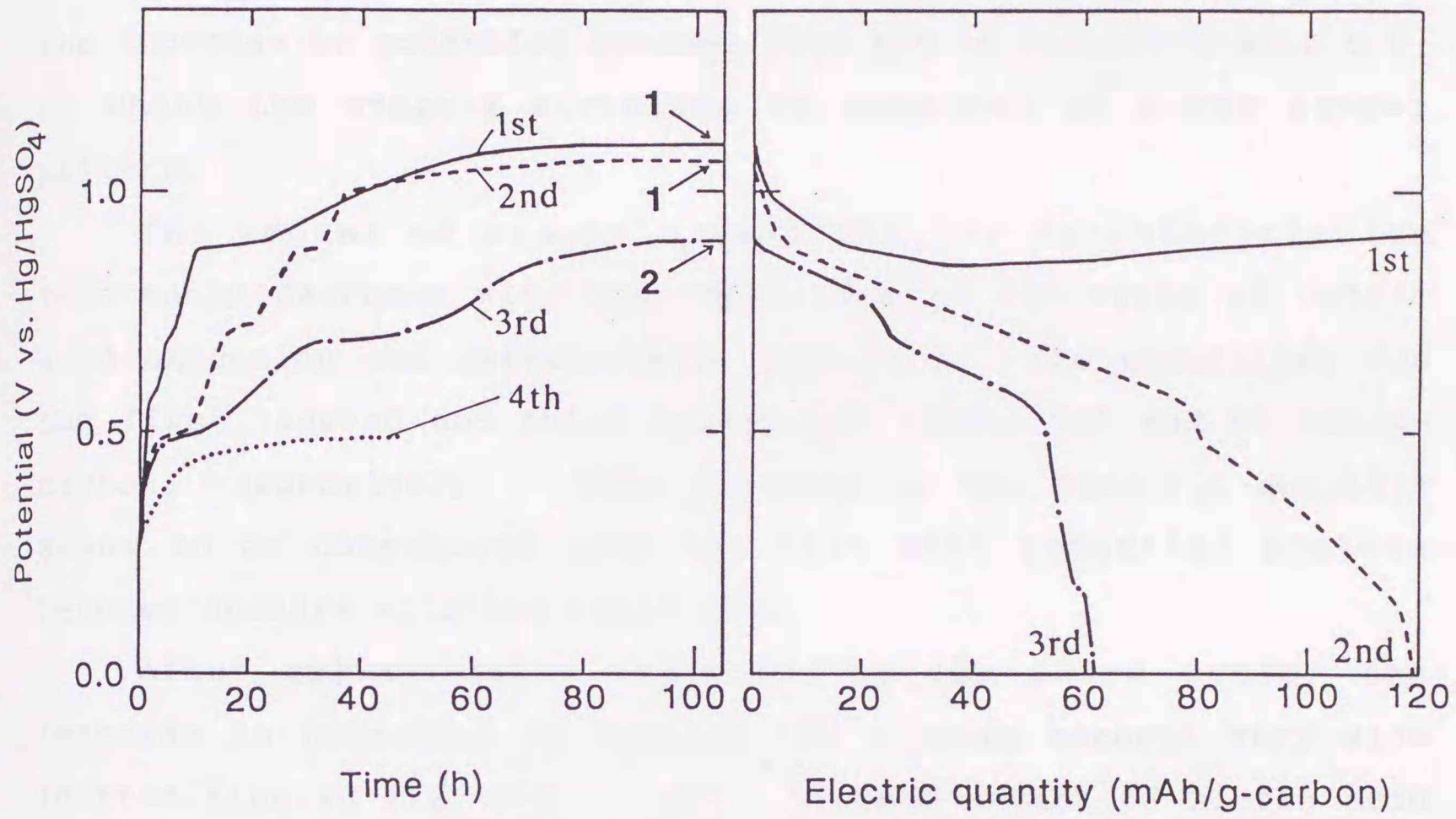


Fig. 5-3 Potential changes of NG400 during repetition of chemical oxidation with nitric acid and galvanostatic reduction with the current of 0.4 mA. (1 mAh = 3.6 C)

At the saturated potential of 1.05 V in the second cycle, the stage-1 compound is formed, being similar to the first cycle. This result suggests that the second potential increase is based on the intercalation of sulfuric acid by nitric acid oxidation. On the second increase in potential, three potential plateaux corresponding to the transformations to the stage-3, to the stage-2 and to the stage-1 structures from each higher stage ones are observed at 0.5, 0.7 and 0.85 V, respectively, which are a little lower than those on the first increase.

It is shown for the potential increase at third cycle that the increase in potential becomes slow and it saturates at 0.8 V, on which the stage-2 structure is observed on X-ray powder pattern.

The amount of electric quantity for de-intercalation remarkably decrease with the repetition of the cycle of nitric acid oxidation and galvanostatic reduction; the quantities for the first, second and third cycles are 14000, 120 and 65 mAh/g-carbon, respectively. This decrease in the electric quantity seems to be consequent upon the fact that potential plateau becomes obscure with the repetition.

After galvanostatic reduction in the third cycle, the increase in potential by opening the circuit becomes very slow (dotted line in Fig. 5-3). So, the same amount of nitric acid as the first cycle (HNO_3/carbon = 3.3) was added into the electrochemical system. The potential changes with time by the oxidation and with electric quantity by the galvanostatic reduction, after the addition of nitric acid again, are shown in Fig. 5-4, with the stage numbers determined by X-ray powder diffraction.

After the addition of nitric acid again, the potential of electrode rapidly increases up to 1.05 V and the stage-1 compound is formed. The amount of electric quantity for de-intercalation also increases up to 900 mAh/g-carbon. However, potential values showing the plateaux decrease down to about 0.7 and 0.3 V. By opening the circuit after the reduction, the potential also increases and then saturated at 0.85 V. The stage-2 compound is formed at the saturated potential.

The potential changes with time during nitric acid oxidation and with electric quantity during galvanostatic reduction, when electric current value is altered from 0.4 to 4 mA, are shown in

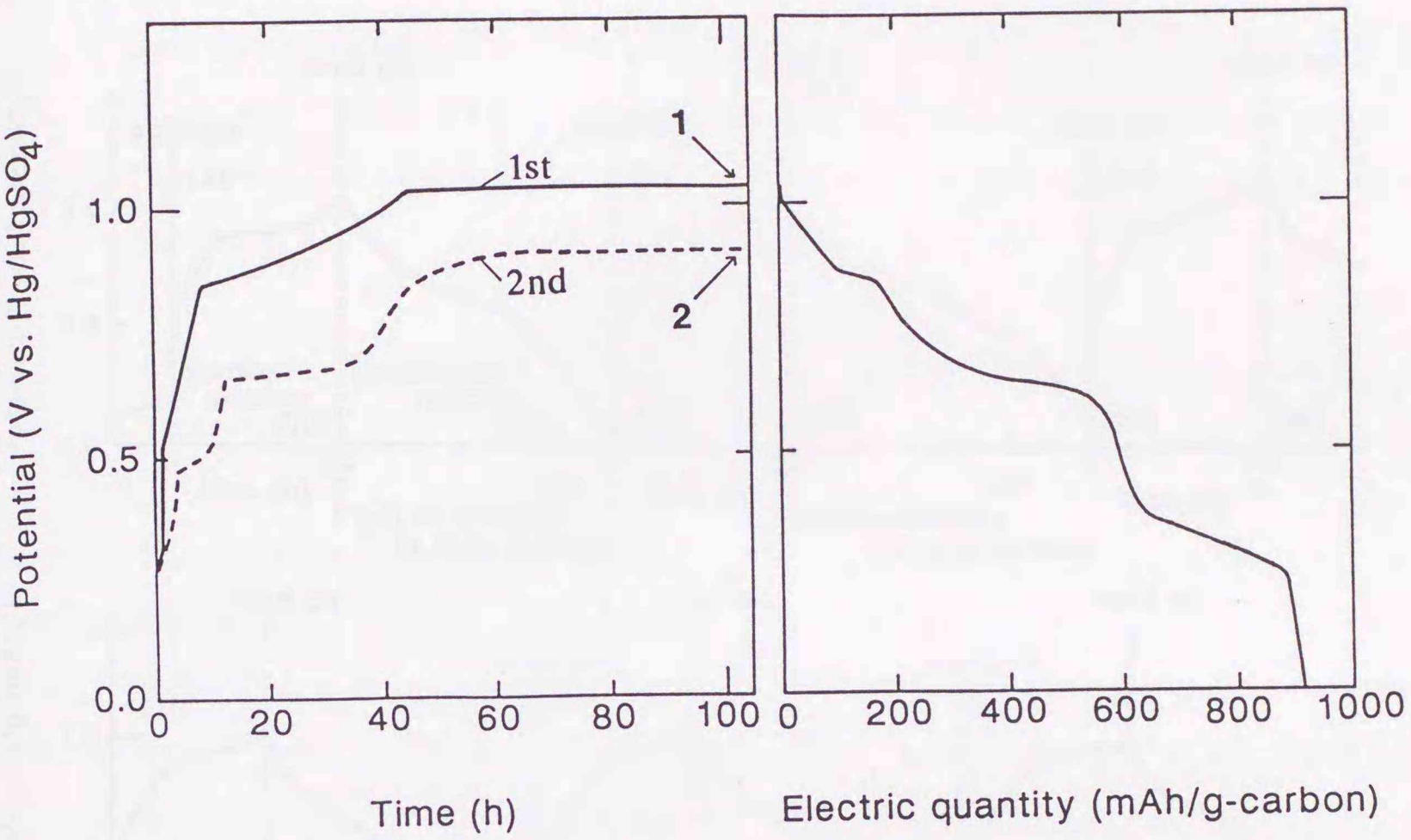


Fig. 5-4 Potential changes of NG400 during repetition of chemical oxidation with nitric acid and galvanostatic reduction with the current of 0.4 mA, after adding of nitric acid in the system used in Fig. 5-3 again (HNO_3/carbon = 3.3). (1 mAh = 3.6 C)

Fig. 5-5. The amount of electric quantity for the de-intercalation with a current of 4 mA is extremely small, down to about 100 mAh/g-carbon, but it dose not almost decrease with the repetition of chemical oxidation and electrochemical reduction. As shown in Fig. 5-5, more than 20 cycles of electrochemical discharging and chemical charging could be performed by using the current of 4 mA.

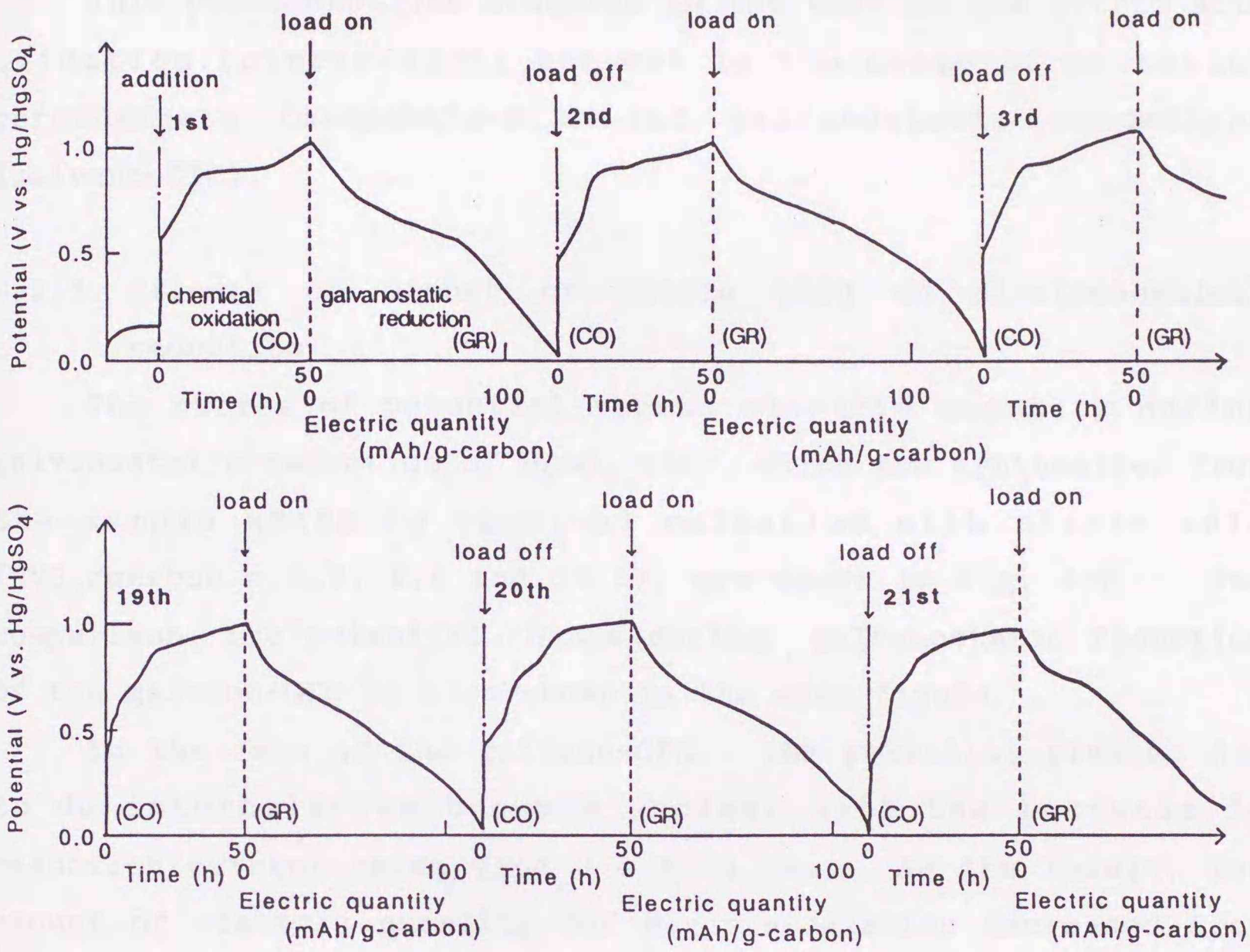


Fig. 5-5 Potential changes of NG400 during of chemical oxidation with nitric acid (HNO_3/carbon = 3.3) and galvanostatic reduction with the current of 4 mA. (1 mAh = 3.6 C)

Such phenomenon that after the electrochemical reduction of the nitric-GIC increased again the potential of host electrode was also observed by opening the circuit on the way during

galvanostatic reduction.

This phenomenon was observed in the case of the nitric acid oxidation (nitric-GIC), but not in the cases of potassium permanganate (manganate-GIC) and galvanostatic oxidations (galvano-GIC).

5.3.3. Effects of amount of nitric acid on electrochemical reduction

The curves of potential versus electric quantity during galvanostatic reduction of H_2SO_4-GICs, which are synthesized from the sample NG400 by chemical oxidation with nitric acid (HNO_3/carbon = 3.3, 6.6 and 16.6), are shown in Fig. 5-6. For comparison, the potential change during galvanostatic reduction of the galvano-GIC is also shown in the same figure.

In the case of the galvano-GIC, the potential plateau due to de-intercalation becomes unclear with the increase in reduction current value from 0.4 to 4 mA. As the result, the amount of electric quantity for de-intercalation decreased from 80 to 60 mAh/g-carbon, which is smaller than that of the nitric-GIC in the molar ratio HNO_3/carbon of 3.3 (100 mAh/g-carbon).

For the nitric-GICs, on the other hand, the potential plateau at around 0.8 V is apparently observed with increase in the amount of nitric acid added. The potential changes during the galvanostatic reduction of the nitric-GICs in the molar ratios HNO_3/carbon of 6.6 and 16.6 become almost constant at 0.25 and 0.45 V, respectively. The amount of electric quantity for de-intercalation seems to increase with the increase in the amount of nitric acid added, as shown in Fig. 5-6, although is is not determined in the present work because of so long reduction time more than 3 months.

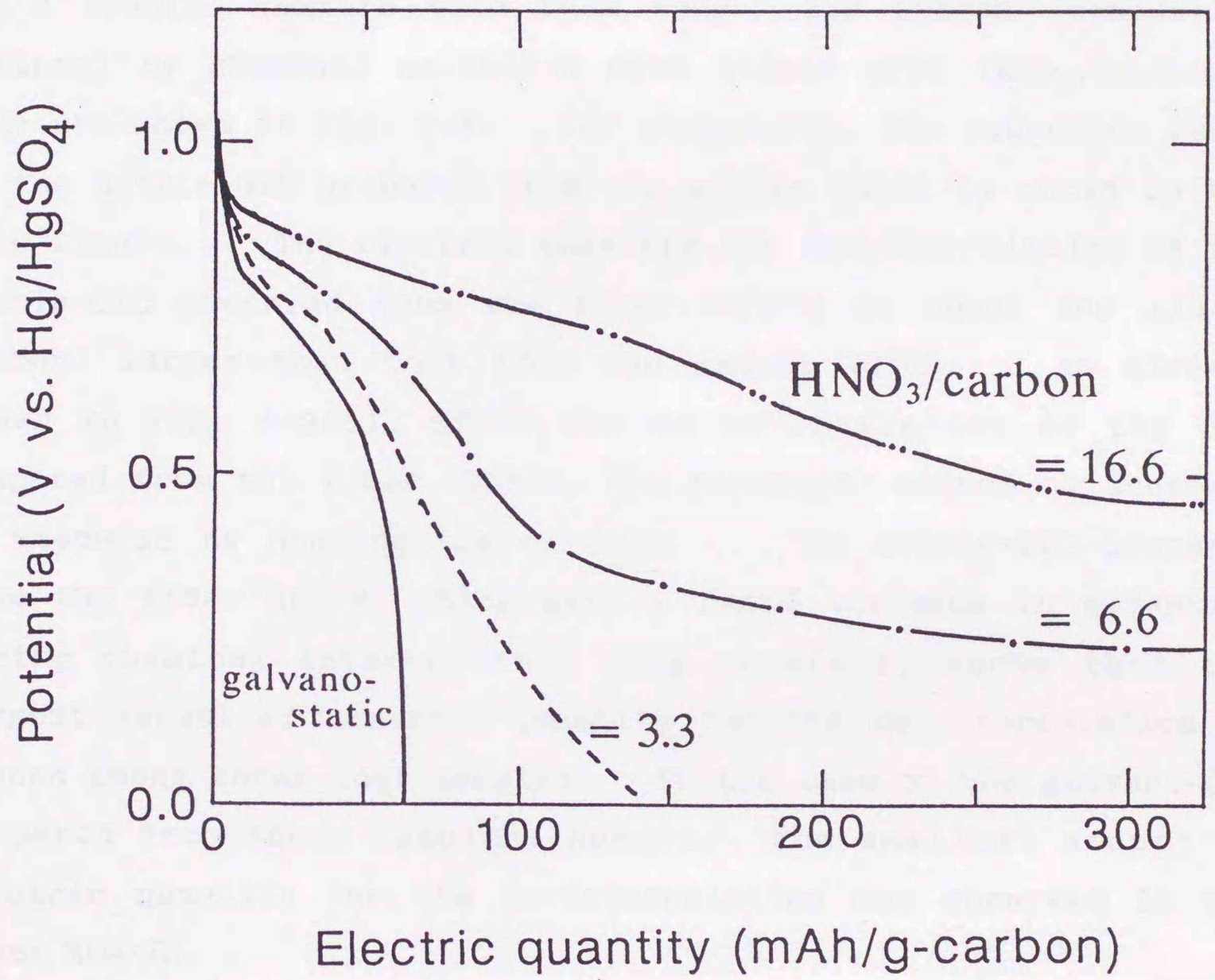


Fig. 5-6 Curves of potential versus electric quantity during galvanostatic reduction (with the current of 4 mA) of H_2SO_4-GICs prepared from NG400 by galvanostatic oxidation and chemical oxidation with different amounts of nitric acid (HNO_3/carbon = 3.3, 6.6 and 16.6). (1 mAh = 3.6 C)

5.3.4. Effect of host material on electrochemical reduction

The potential changes during galvanostatic de-intercalation (4 mA/50 mg-carbon) of H_2SO_4-GICs prepared from the fiber samples KOA-R (radial texture with open wedge) and OVCF30 (concentric texture) by chemical oxidation with nitric acid (HNO_3/carbon = 3.3) are shown in Fig. 5-7. For comparison, the reduction curve of the nitric-GIC prepared from the sample NG400 is shown in the same figure. The electric quantity for de-intercalation of the nitric-GIC prepared from the fiber OVCF30 is about 500 mAh/g-carbon, larger than that from the sample NG400. As already shown in Fig. 4-2(b), after the de-intercalation of the GIC prepared from the fiber OVCF30, the potential showed to increase in stepwise by opening the circuit. The nitric-GIC prepared from the fiber KOA-R, which gave a rapid increase in potential during chemical intercalation (Fig. 4-3(a)), shows that the largest amount of electric quantity for the de-intercalation is needed among three host samples. In the case of the galvano-GIC prepared from these samples, however, the smallest amount of electric quantity for the de-intercalation was observed in the fiber KOA-R.

The potential changes during galvanostatic de-intercalation (4 mA/50 mg-carbon) of H_2SO_4-GICs prepared from the samples in the SSG-series by electrochemical and chemical oxidation (HNO_3/carbon = 3.3) are shown in Fig. 5-8(a) and 8(b), respectively. In H_2SO_4-GICs prepared by electrochemical oxidation (Fig. 5-8(a)), the current value for the de-intercalation is too large to observe potential plateaux corresponding to the stage transformations. The electric quantity for the de-intercalation is the larger for the sample heat-treated at the higher temperature. However, it has to pointed out that the electric quantity for the sample SSG30 is

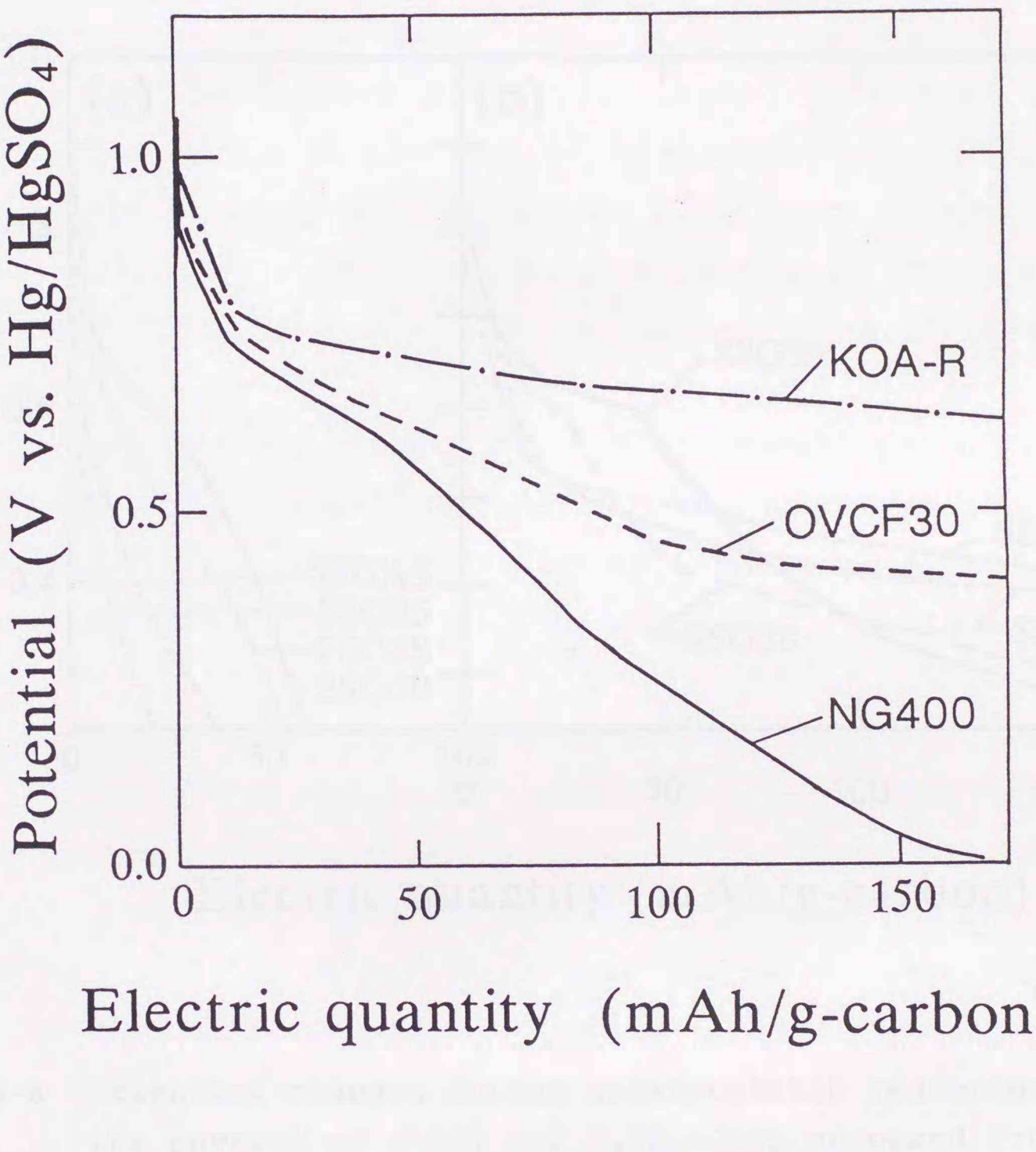


Fig. 5-7 Potential changes during galvanostatic reduction (with the current of 4 mA) of H_2SO_4-GICs prepared from the samples KOA-R, OVCF30 and NG400 by chemical oxidation with nitric acid (HNO_3/carbon = 3.3). (1 mAh = 3.6 C)

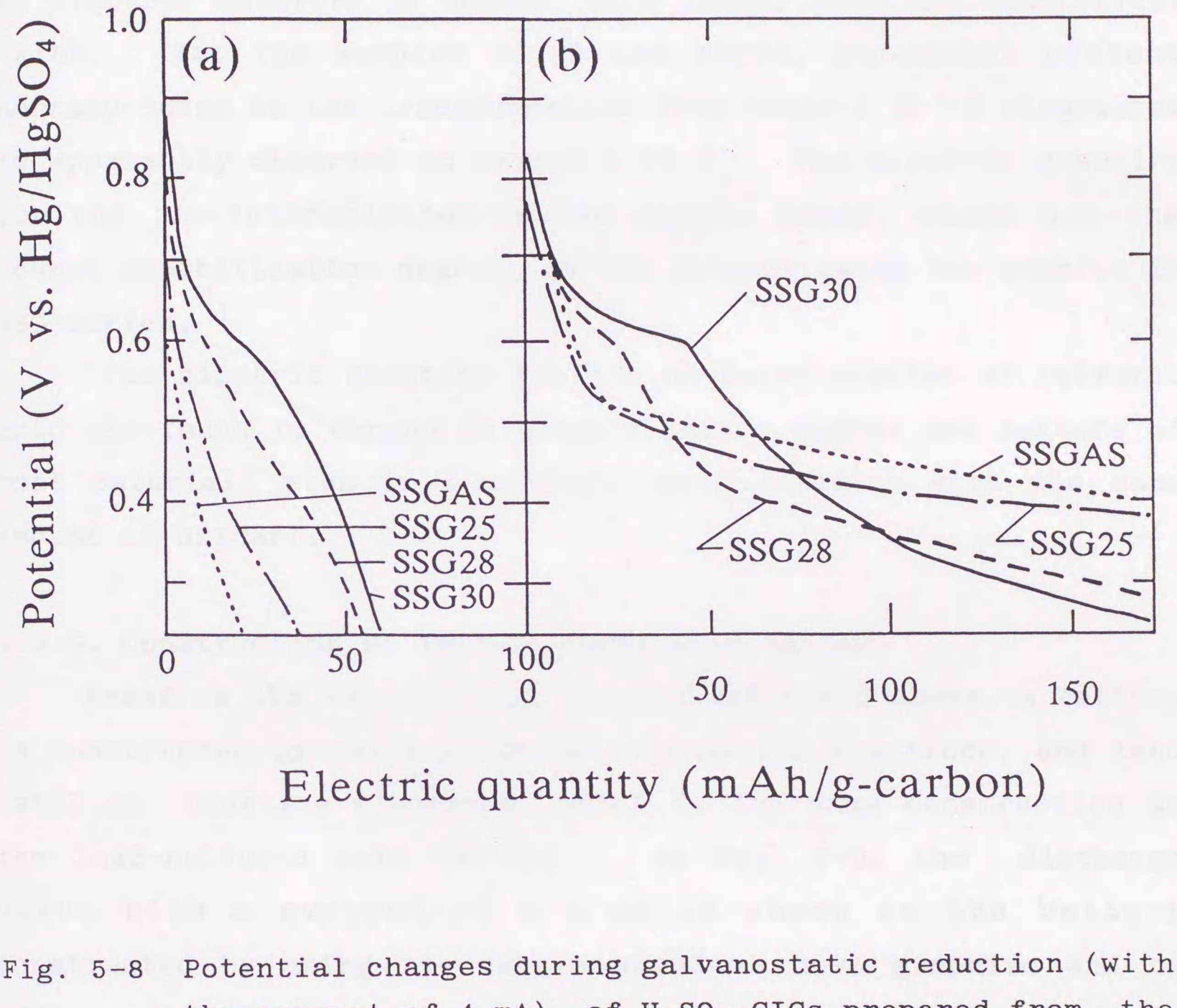


Fig. 5-8 Potential changes during galvanostatic reduction (with the current of 4 mA) of H_2SO_4-GICs prepared from the pyrolytic carbons in SSG-series by (a) galvanostatic and (b) chemical oxidation with nitric acid (HNO_3/carbon = 3.3). (1 mAh = 3.6 C)

much smaller than the theoretical value (93 mAh/g-carbon).

For the de-intercalation of the nitric-GICs, a large amount of electric quantity is needed, much larger than the theoretical value. For the samples SSG28 and SSG30, potential plateau corresponding to the transformation from stage-1 to -2 structures is apparently observed at around 0.65 V. The electric quantity for the de-intercalation in the sample SSGAS, which has the lowest graphitization degree, is the largest among the samples in SSG-series.

The electric quantity for the de-intercalation of sulfuric acid was found to depend on graphitization degree and texture of host material, even in a sulfuric acid solution with the same amount of oxidant.

5.3.5. Construction of lead-sulfuric acid battery

Based on the experimental results described above, a battery is constructed by using graphite as positive electrode, and lead metal as negative electrode, which is the same construction as the lead-sulfuric acid battery. In Fig. 5-9, the discharge curve with a current of 0.4 mA is shown on the battery constructed by using the sample NG400 as host graphite and by adding nitric acid into the battery system (HNO_3/carbon = 3.3). The open circuit voltage of the battery is about 1.4 V. During discharge, well-defined plateau is observed. Even beyond the theoretical electric quantity which needed for the formation of the stage-1 H_2SO_4-GIC (93 mAh/g-carbon), voltage of the battery keeps on 0.85 V. In the battery constructed, therefore, larger capacity than the theoretical one can be obtained.

By discharging above the electric quantity of 3 mAh (60 mAh/g-carbon), an oscillation is observed on the discharge curve. This oscillation behavior is not observed on the measurement of

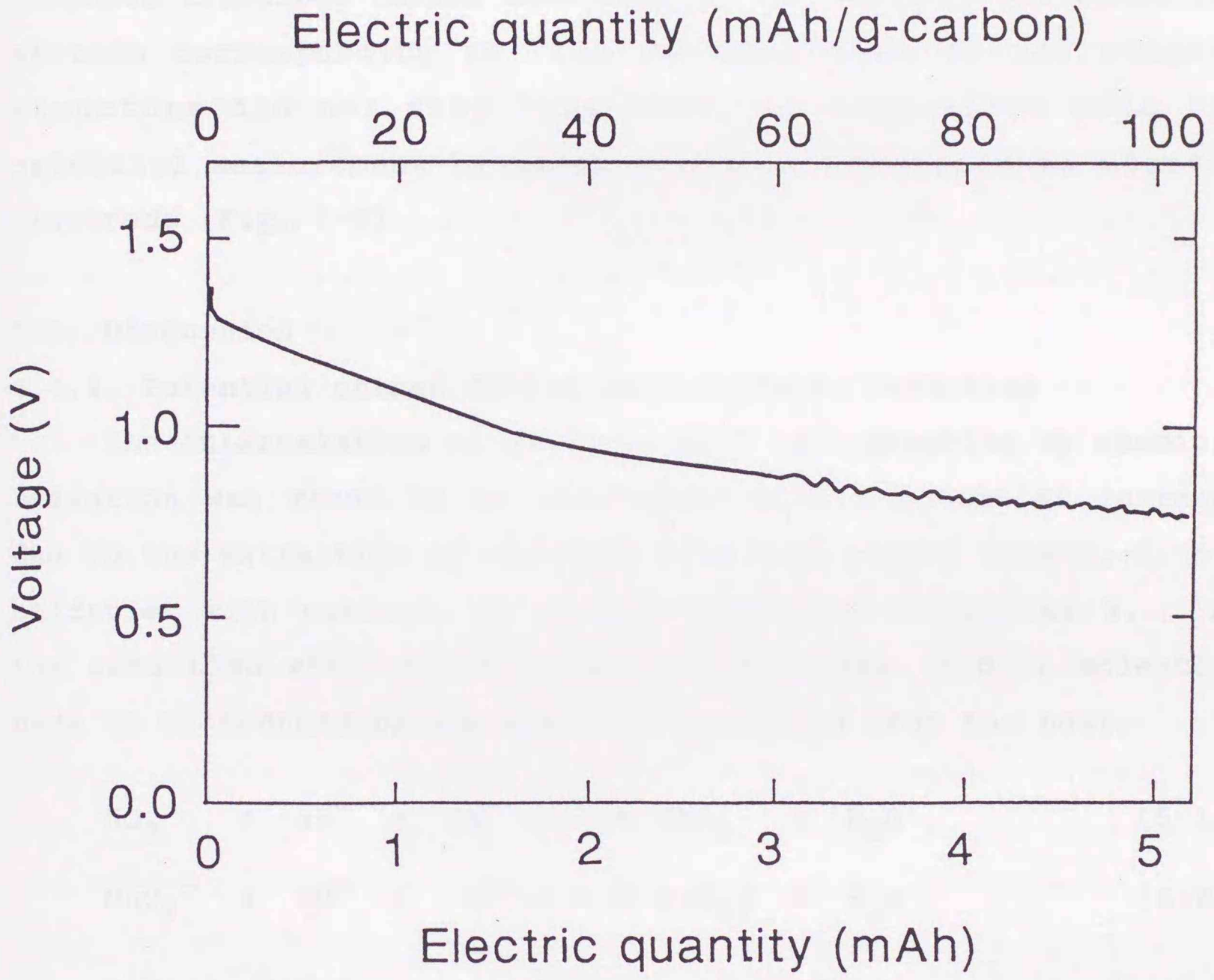


Fig. 5-9 Discharge curve with the current of 0.4 mA for a battery constructed by positive electrode of H_2SO_4-GIC, synthesized by chemical oxidation with nitric acid (HNO_3/carbon = 3.3), and lead negative electrode. (1 mAh = 3.6 C)

potential change of graphite electrode (Fig. 5-2).

The voltage of battery could be also recovered to 1.4 V by just opening the circuit. On the potential change of the graphite electrode during discharge of the battery, the potential plateau corresponding to the decomposition of the stage-1 structure did not stay long time, in comparison with the potential measurement by using platinum electrode as counter electrode (Fig. 5-2).

5.4. Discussion

5.4.1. Potential change during galvanostatic reduction

The intercalation of sulfuric acid into graphite by chemical oxidation was found to be associated with a potential increase due to the extraction of electron from host carbon layers, i. e., oxidation with oxidant, as already discussed in Chapter 3. At the same time with oxidation of the host, the oxidant molecules have to be reduced by the electron extracted from the host;

$$NO_3^- + 3H^+ + 2e^- \longrightarrow HNO_2 + H_2O \ , \qquad (5\text{-}1)$$

$$MnO_4^- + 2H^+ + e^- \longrightarrow MnO_3\downarrow + H_2O \ . \qquad (5\text{-}2)$$

For electrochemical reduction of H_2SO_4-GICs synthesized by chemical oxidation in sulfuric acid solution with an excess amount of oxidant, a large mount of electric quantity was needed, in comparison with the case of the GIC synthesized by electrochemical oxidation. The electric quantity for de-intercalation from the GICs synthesized by nitric acid oxidation (nitric-GICs) decreased with the increase in electric current value during the galvanostatic reduction from 0.4 to 4 mA, in other words, the increase in reaction rate of the de-intercalation (Fig. 5-5). With the increase in amount of nitric

acid added, however, the electric quantity for the de-intercalation increased (Fig. 5-6). As already discussed in Chapter 4, relative reaction rate of the intercalation of sulfuric acid increased with the increase in amount of oxidant. Therefore, the present result that a large amount of electric quantity was needed for electrochemical reduction of H_2SO_4-GICs synthesized by chemical oxidation seems to be explained by the competition between the chemical oxidation to H_2SO_4-GICs in sulfuric acid solution with the oxidant and the electrochemical reduction of H_2SO_4-GICs.

The fiber sample KOA-R having radial texture with open wedge showed rapid increase in potential during the intercalation by chemical oxidation (Fig. 4-3(a)), because of its radial texture, as discussed in Chapter 4. The increase in potential during the chemical intercalation into the sample KOA-R was more rapid than those into the samples OVCF30 and NG400. In other words, the sample KOA-R was easily oxidized. Consequently, electrochemical de-intercalation of H_2SO_4-GIC prepared from the fiber KOA-R by chemical oxidation needed larger amount of electric quantity than those from the samples OVCF30 and NG400 (Fig. 5-7), because a large part of de-intercalation was compensated by the intercalation even during electrochemical reduction.

On the potential change during galvanostatic reduction of the nitric-GICs prepared from the samples SSG28 and SSG30, the plateau at around 0.65 V, which corresponded to the transformation from the stage-1 to -2 structures, was clearly observed, though this plateau was not observed on the potential change in the galvano-GICs. The appearance of well-defined plateau is due to the fact that a relative rate of de-intercalation is lowered by chemical oxidation. A large amount

of electric quantity was needed for electrochemical de-intercalation of the nitric-GICs prepared from the samples SSG25 and SSGAS, because these sample showed rapid increase in potential during intercalation by chemical oxidation (Fig. 4-8), in other words, were oxidized easily.

These effects of host carbon materials on the electrochemical reduction of H_2SO_4-GIC synthesized by chemical oxidation, therefore, can support the fact that potential change during electrochemical de-intercalation for H_2SO_4-GICs prepared by chemical oxidation is explained by the competition of reaction rates between chemical oxidation in sulfuric acid with oxidant and electrochemical reduction of H_2SO_4-GICs.

5.4.2. Repetition process of nitric acid oxidation and electrochemical reduction

The difference in the electric quantity for the de-intercalation of sulfuric acid between the nitric- and manganate-GICs seems to be consequent upon ability of oxidation to host carbon in sulfuric acid of 18 mol/dm^3. Nitric acid could be quickly oxidized host even in the same amount of addition. For example, in the case of molar ratio of oxidant/carbon = 0.33, the oxidation by nitric acid resulted in the formation of the stage-2 compound (Fig. 3-2), but potassium permanganate oxidation in a high stage compound (Fig. 3-4).

Nitrous acid (HNO_2), which is product of reduction of nitric acid (Eqn. (5-1)), in sulfuric acid solution may be re-oxidized to nitric acid on platinum counter electrode, i. e., reverse reaction in Eqn. (5-1). On the other hand, the reduction reaction of permanganate ions (Eqn. (5-2)) has to be irreversible. Since it is reasonably supposed that nitric acid re-oxidized on platinum electrode contributes again to chemical

oxidation of graphite, potential plateau at 0.8 V corresponding to the transformation from the stage-1 to -2 structures during the galvanostatic reduction with 0.4 mA at first time is extended and a large amount of electric quantity for the de-intercalation is needed (Fig. 5-3).

In the case where a battery was constructed by using graphite and lead metal as positive and negative electrodes, respectively, on the other hand, potential difference between both electrodes was 1.4 V. It shows that the potential of lead electrode shows more negative than that of graphite. During discharge of the battery, the following reaction occurs on lead electrode;

$$Pb + SO_4^{2-} \longrightarrow PbSO_4 + 2e^- . \qquad (5-3)$$

Nitrous acid as the reduced product is not re-oxidized on the lead electrode. As the result, the potential plateau corresponding to the decomposition of the stage-1 compound did not stay long time in the discharging of the battery.

Since host graphite is oxidized by a small amount of nitric acid, even if the nitric-GIC is electrochemically reduced to graphite, the graphite is chemically oxidized when the circuit is opened and again sulfuric acid is able to be intercalated into the gallery of graphite, accompanying the increase in potential. In fact, charging by chemical oxidation and discharge by electrochemical reduction of the nitric-GIC can be repeated (Figs. 5-4 and -5).

The electric quantity for the de-intercalation by galvanostatic reduction with 0.4 mA decreases with the repetition of nitric acid oxidation and electrochemical reduction cycles. The lowering of electric quantity for the de-intercalation is probably due to evolution of nitric acid on platinum electrode to the outside of the system. Since electrolysis time in the case

of 4 mA is shorter than that in 0.4 mA, it is reasonably supposed that the evolution of nitric acid on platinum electrode is a small amount. Consequently, more than 20 cycle can be repeated. Even though nitric acid was evolved from the electrochemical system, by adding nitric acid into the system again, both the potential of graphite electrode and the electric quantity for the de-intercalation returned to be original values. This experimental result is again consistent with the fact that potential change during the electrochemical de-intercalation of H_2SO_4-GICs prepared by chemical oxidation was explained by the competition of reaction rates between chemical oxidation in sulfuric acid with oxidant and electrochemical reduction of H_2SO_4-GICs.

5.4.3. Application to lead-sulfuric acid battery

Based on the cycle of chemical oxidation of graphite and electrochemical reduction of H_2SO_4-GIC, a battery could be constructed. A well-defined plateau on the discharge curve was observed, and larger capacity than the theoretical value was obtained (Fig. 5-9). Above the electric quantity of 3 mAh (60 mAh/g-carbon), an oscillation was observed on the discharge curve. Since this oscillation behavior has never been observed on the measurement of potential changes of graphite electrode (for example, Fig. 5-2), it is reasonably supposed that this oscillation is due to the formation of lead sulfate on lead metal electrode (Eqn. (5-3)). In order to prevent this oscillation, sulfuric acid as electrolyte has to be diluted. However, the formation of H_2SO_4-GICs by chemical oxidation becomes difficult with dilution of sulfuric acid, as already discussed in Chapter 3. To improve the battery performance, therefore, there is two ways, either to get high surface area for lead negative electrode

or to find out an oxidant which can be formed the H_2SO_4-GIC in a diluted sulfuric acid.

A well-defined potential plateau during the electrochemical de-intercalation is not be necessarily obtained on H_2SO_4-GIC prepared from the host with high graphitization degree, as discussed in section 5.4.1.. In order to apply this cycle of chemical oxidation of graphite and electrochemical reduction of H_2SO_4-GIC to a battery, there must be a suitable host carbon material. Probably such host is susceptible to chemical oxidation and easily intercalated or de-intercalated with sulfuric acid.

It is worth while to note that, in the battery attempted, any electric power dose not need to the charging process at all, and that there is no self discharging. Therefore, the battery seems to be is useful as urgent electric source.

5.5. Summary

When graphite intercalation compounds with sulfuric acid synthesized by chemical oxidation were electrochemically decomposed in sulfuric acid solution in the presence of an excess amount of nitric acid, a large amount of electric quantity was needed, much larger electric quantity than that expected theoretically for the de-intercalation. This experimental result was explained by the competition in reaction rate between chemical oxidation of host graphite to H_2SO_4-GICs and electrochemical reduction of H_2SO_4-GICs in sulfuric acid solution with nitric acid. The electric quantity for de-intercalation depended strongly on the host carbon material, because structure and texture of the host give the influence on overall reaction rate of intercalation by chemical oxidation.

In the case of nitric acid oxidation, even though H_2SO_4-GICs

was electrochemically reduced to graphite, the graphite was chemically oxidized by opening the circuit and again sulfuric acid was intercalated into the gallery of graphite, accompanying the increase in potential. More than 20 cycles of chemical oxidation and electrochemical reduction were performed with 4 mA discharge current.

Based on this reaction cycle, i. e., chemical charging and electrochemical discharging, a battery constructed by using graphite and lead metal as positive and negative electrodes, respectively. During discharge of the battery, a well-defined plateau was observed and larger capacity than theoretical one was obtained.

References

5-1 P. Schaufauetl, J. Pracet. Chem., 21, 155 (1841).

5-2 J. Bertin, H. B. Kagan, J. L. Luche and R. Setton, J. Am. Chem. Soc., 99, 8113 (1974).

5-3 Ph. Touzan and R. Yazami, J. Power Source, 14, 99 (1985).

5-4 R. Fujii, Report of Gov. Ind. Res. Inst., Osaka, No. 353, pp. 57-60.

5-5 B. Bouayad, H. Fuzellier, M. Lelaurain, A. Metrot and F. Rousseaux, Synth. Met., 7, 325 (1983).

CHAPTER 6

Exchange reaction of metal chlorides for metal hydroxides in graphite gallery

6.1. Introduction

Flandrois, et al. [6-1, -2] used graphite intercalation compounds with nickel chloride ($NiCl_2$-GICs) as a starting material for the positive electrode (cathode) of an alkaline secondary battery and obtained a GIC with nickel hydroxide by repetition of the charge-discharge process in alkaline medium. The exchange reaction of nickel chloride for hydroxide was followed by measuring paramagnetic susceptibility of nickel during charge-discharge cycle. However, mechanism for the exchange reaction in graphite gallery is not clear yet.

In order to synthesize the $NiCl_2$-GIC, the addition of chlorine gas above 800 kPa and prolonged heating at a temperature between 490 and 700^{o}C were required [6-3]. A group of Inagaki [6-4, -5, -6] developed a new process to synthesize the ternary intercalation compounds of graphite with different metal chlorides (chloride-GICs) by using a mixture of different metal chlorides, for examples the mixtures of $NiCl_2$ with $FeCl_3$ and $CuCl_2$. In this process, chloride-GICs were obtained under mild conditions, i. e., at low temperatures in a short time without any intentional addition of chlorine gas. The compounds obtained were rather stable in air and even in boiling water.

On the other hand, nickel hydroxide synthesized by exchange reaction is electrochemically active material. Therefore, the amount of nickel hydroxide formed from chloride can be followed by electrochemical process, for instance measurement of potential.

In the present chapter, the GICs with metal hydroxides

(hydroxide-GICs) from the chloride-GICs are synthesized by electrochemical treatment with galvanostatic oxidation and repetition of charge-discharge cycle. For comparison, non-electrochemical treatment of chloride-GICs is also examined. The confirmation and mechanism for the exchange reaction of metal chlorides for hydroxides in graphite gallery are discussed with the measurement of potential, cyclic voltammetry, X-ray powder diffractometry and X-ray microprobe analysis.

6.2. Experimental

6.2.1. Synthesis of chloride-GICs

Flaky natural graphite powders with average flake size of 400, 46 and 5 μm (NG400, NG46 and NG5, respectively) were used as the host materials for GICs. The mixtures of graphite powder and metal chlorides (graphite/$NiCl_2$/$FeCl_3$ = 30/10/7 and = 30/5/5, and graphite/$NiCl_2$/$CuCl_2$ = 30/10/7 in mole) were heated up to 120^{o}C in a glass ampoule for 2 hours under vacuum in order to dry the mixture, and then the ampoule was sealed. The synthesis of the chloride-GICs was carried out at a temperature between 400 and 550^{o}C for 3 days. The sample code, host graphite used, molar ratio in the starting chloride mixtures and reaction temperature are summarized in Table 6-1. $NiCl_2$-$FeCl_3$ and $NiCl_2$-$CuCl_2$ systems are classified as the sample code Ni-Fe and Ni-Cu, respectively. The chloride-GICs synthesized were separated from unreacted metal chlorides by washing repeatedly with 1 mol/dm^3 hydrochloric acid.

6.2.2. Electrochemical treatment of chloride-GICs and characterization of treated samples

The electrode and cell assembly for the electrochemical treatment and for electrochemical characterization with cyclic

Table 6-1 Synthesis condition for GICs with metal chlorides.

Sample code	Host graphite	Molar ratio (graphite/$NiCl_2$/$FeCl_3$)	Reaction temperature
Ni-Fe-1	NG400	30/10/7	550 ^oC
Ni-Fe-2	NG46	30/10/7	550 ^oC
Ni-Fe-3	NG400	30/ 5/5	400 ^oC
		(graphite/$NiCl_2$/$CuCl_2$)	
Ni-Cu-1	NG400	30/10/7	550 ^oC
Ni-Cu-2	NG5	30/10/7	550 ^oC

voltammetry is schematically shown in Fig. 6-1. The chloride-GIC powders of 0.5 g were held in between two plastic plates (50 X 50 mm^2) with a supporting electrode of platinum wire. Many small holes (1.5 mm in diameter) were drilled to make the GIC contact with electrolyte. A thin filter papers was required in order to avoid GIC powders falling through these holes. The counter electrode was a platinum wire and a Hg/HgO electrode with Luggin capillary as the reference. Aqueous solutions of potassium hydroxide of 7 mol/dm^3 and of potassium sulfate of 0.5 mol/dm^3 were used as the electrolyte.

Galvanostatic oxidation of the chloride-GIC electrode was carried out with 2 mA. The charge-discharge process was repeated by constant currents of 0.2, 2 and 8 mA. The charging time was determined from electric quantity to be oxidized all nickel ions, which is active material for positive electrode of alkaline secondary battery, in the chloride-GICs. The terminal discharge potential was set at 0.2 V. The potential change during charge-discharge cycle and discharge capacity on the GIC electrode were

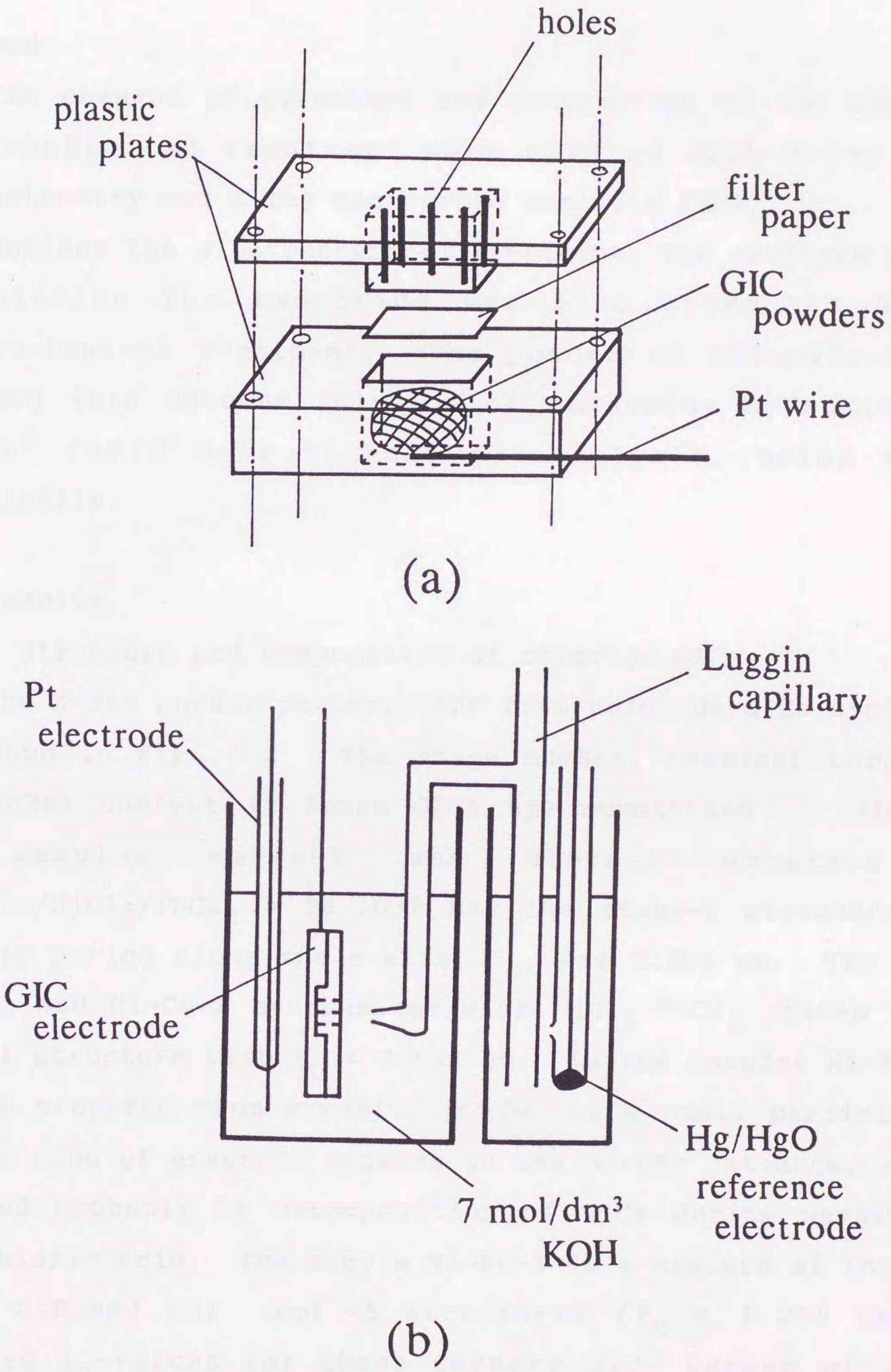


Fig. 6-1 Cell assembly.
(a) Scheme of the GICs electrode,
(b) Scheme of electrochemical cell.

measured.

The changes of structure and composition of the GICs after electrochemical treatment were studied with X-ray powder diffractometry and X-ray microprobe analysis (XMA).

Besides the electrochemical treatment, the exchange reaction of chloride for hydroxide was also attempted by non-electrochemical treatment. The powder of chloride-GIC was immersed into aqueous solution of potassium hydroxide of 7 mol/dm^3 for 3 days without electrolysis, being stirred magnetically.

6.3. Results

6.3.1. Structure and composition of chloride-GICs

The X-ray powder patterns for five chloride-GICs synthesized are shown in Fig. 6-2. The stage number, chemical composition and nickel content in these GICs are summarized in Table 6-2. The samples Ni-Fe-1 and Ni-Fe-2 obtained from graphite/$NiCl_2$/$FeCl_3$ = 30/10/7 has the stage-2 structure. The identity period along the c-axis, I_c, was 1.283 nm. The samples Ni-Cu-1 and Ni-Cu-2 synthesized with $NiCl_2$-$CuCl_2$ system has the stage-1 structure with I_c = 0.942 nm. In the samples Ni-Fe-2 and Ni-Cu-2 prepared from graphite powder with small particle size, the 002 line of graphite appears on the powder patterns, which is produced probably by decomposition of GICs during washing with hydrochloric acid. The sample Ni-Fe-3 is a mixture of the stage-1 (I_c = 0.943 nm) and -2 structures (I_c = 1.279 nm). The observed I_c-values for these ternary GICs agreed with those reported for binary GICs with each metal chlorides.

The SEM micrographs and the distribution of each elementals on a flake of samples Ni-Fe-1 and Ni-Cu-1 by XMA are shown in Fig. 6-3 (a) and (b), respectively. In the sample Ni-Fe-1,

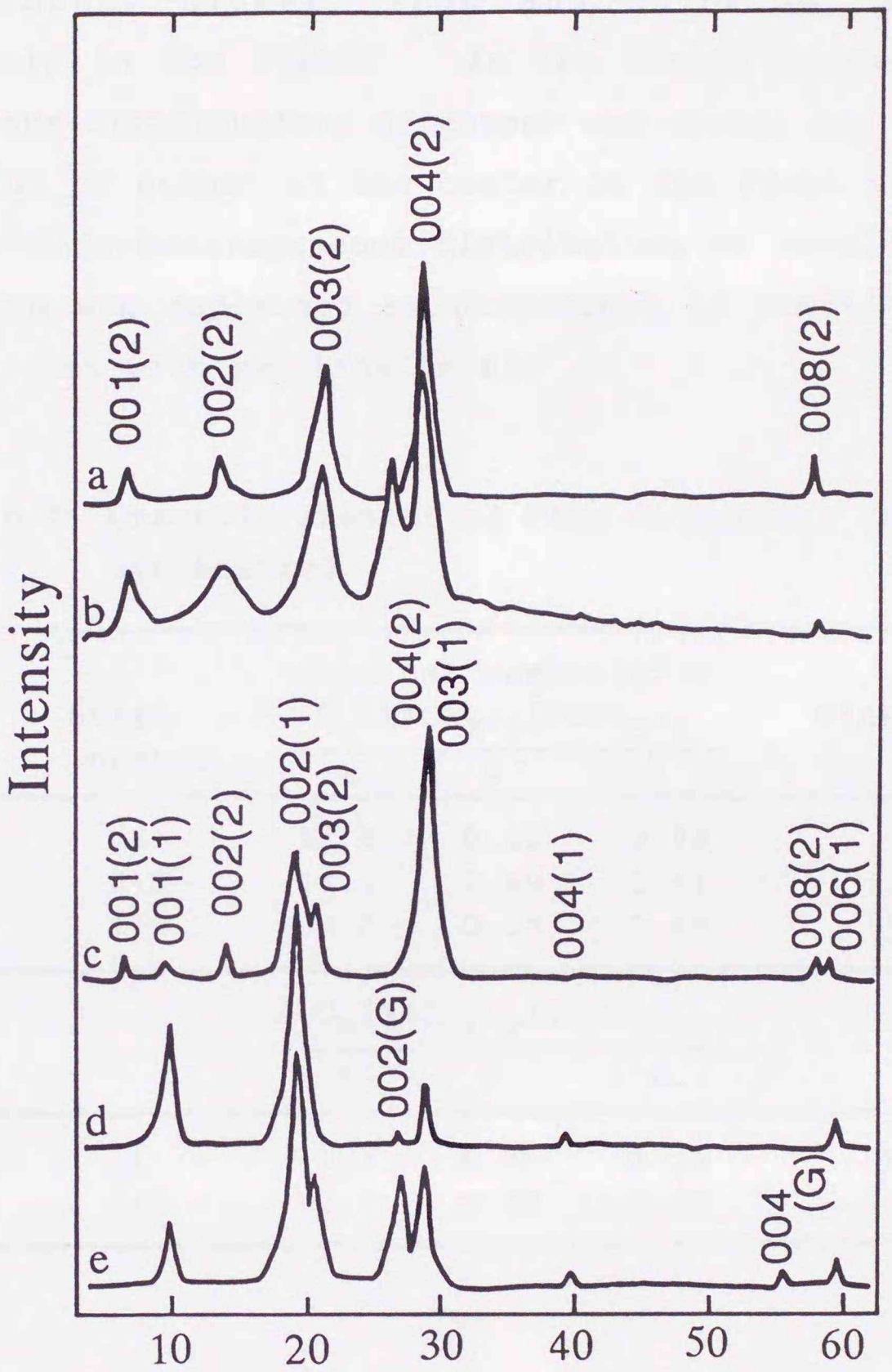


Fig. 6-2 X-ray powder patterns of GICs with metal chlorides, as original sample.
a: Ni-Fe-1, b: Ni-Fe-2, c: Ni-Fe-3,
d: Ni-Cu-1, e: Ni-Cu-2.

every element, nickel, iron and chlorine, distributes homogeneously in the flake. In the sample Ni-Cu-1, however, heterogeneous distributions of copper and nickel are observed; a large amount of copper at the center on the flake and nickel at the edge. This heterogeneous distribution of metals in $NiCl_2$-$CuCl_2$ system was explained by difference in reactivity of both metal chlorides with graphite [6-6].

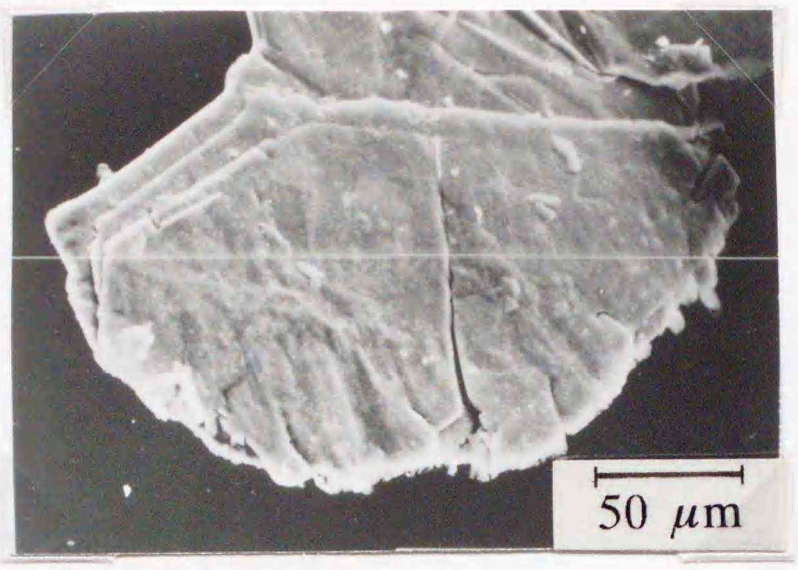
Table 6-2 Characterization of GICs with metal chlorides synthesized.

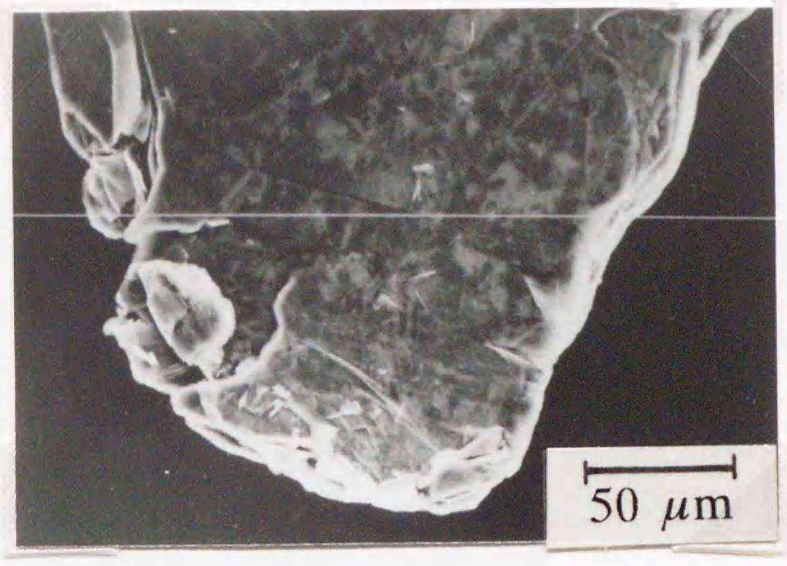
Sample code	Stage number	Chemical composition $C_x(NiCl_2)_y(FeCl_3)_z$ x	y	z	Nickel content
Ni-Fe-1	2	11.8	0.43	0.59	8.6 wt.%
Ni-Fe-2	2+G	14.5	0.49	0.51	8.4 wt.%
Ni-Fe-2	1+2	6.5	0.32	0.68	8.0 wt.%
		$C_x(NiCl_2)_y(CuCl_2)_z$ x	y	z	
Ni-Cu-1	1	5.4	0.61	0.39	17.3 wt.%
Ni-Cu-2	1+G	22.4	0.57	0.43	8.5 wt.%

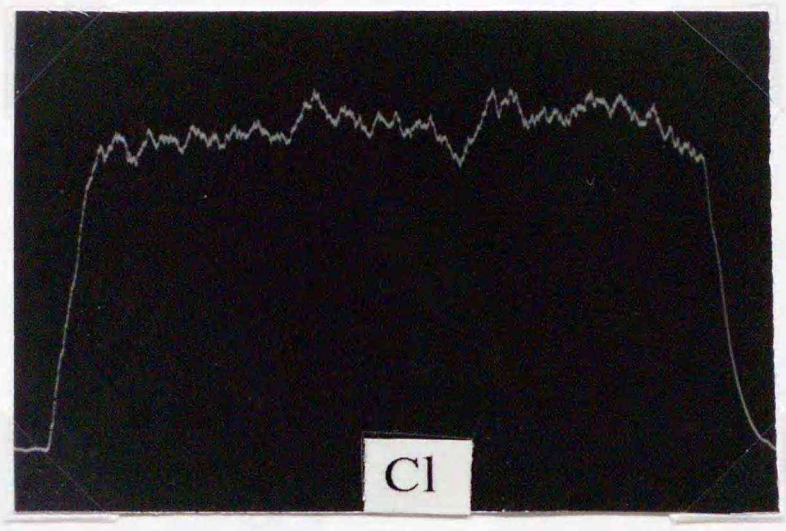
6.3.2. Electrochemical treatment of chloride-GICs

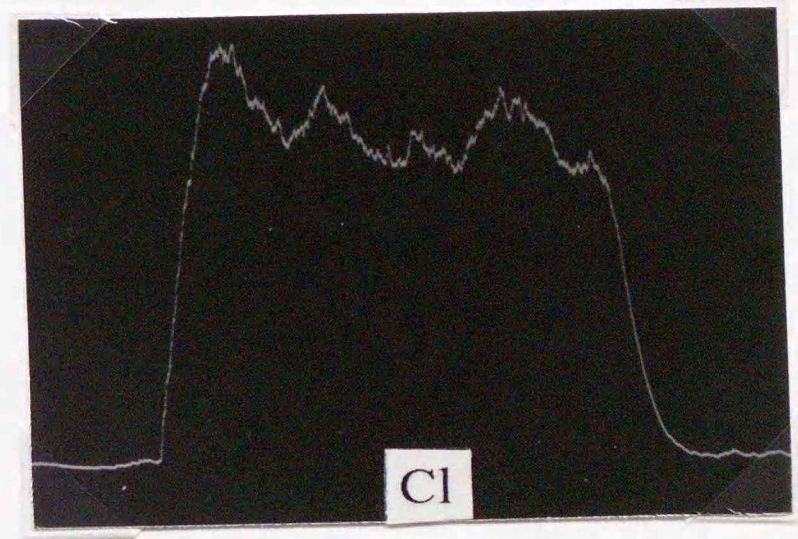
a) Galvanostatic oxidation

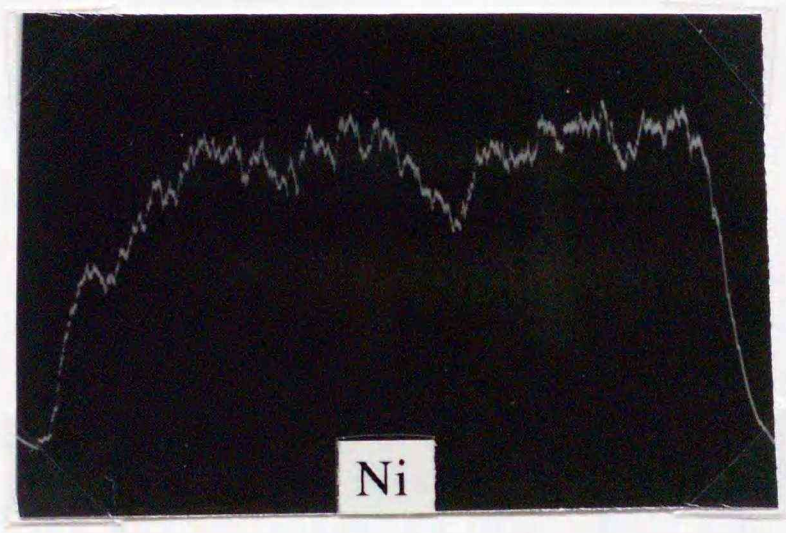
X-ray powder patterns for the samples Ni-Fe-1, Ni-Fe-3 and Ni-Cu-1 after galvanostatic oxidation with 2 mA for 80 hours in KOH solution of 7 mol/dm^3 are shown in Fig. 6-4. The patterns of the samples Ni-Fe-1 and Ni-Cu-1 after galvanostatic oxidation (Fig. 6-4a and c, respectively) are almost the same as those of

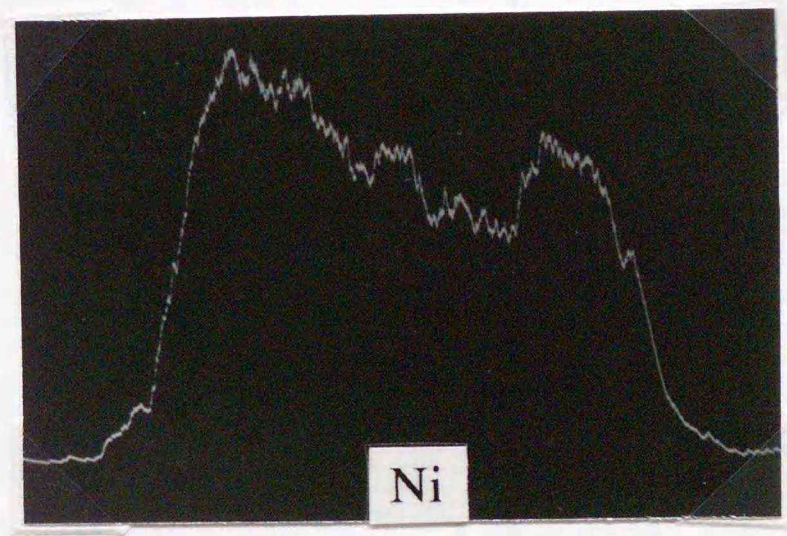


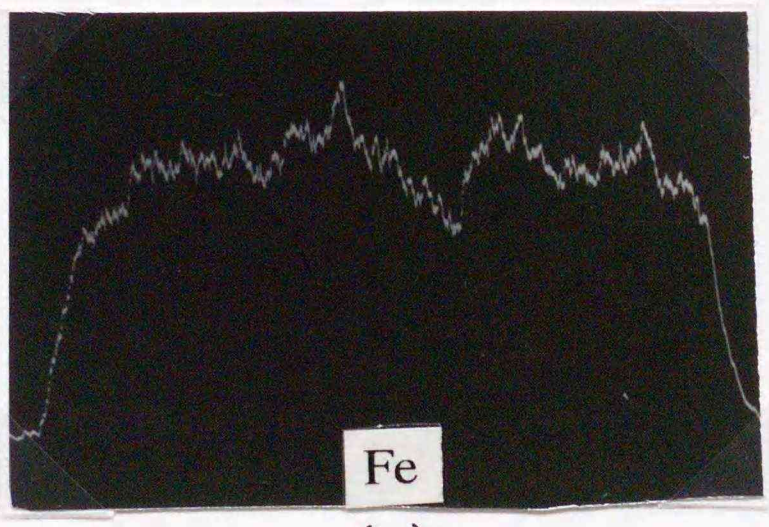




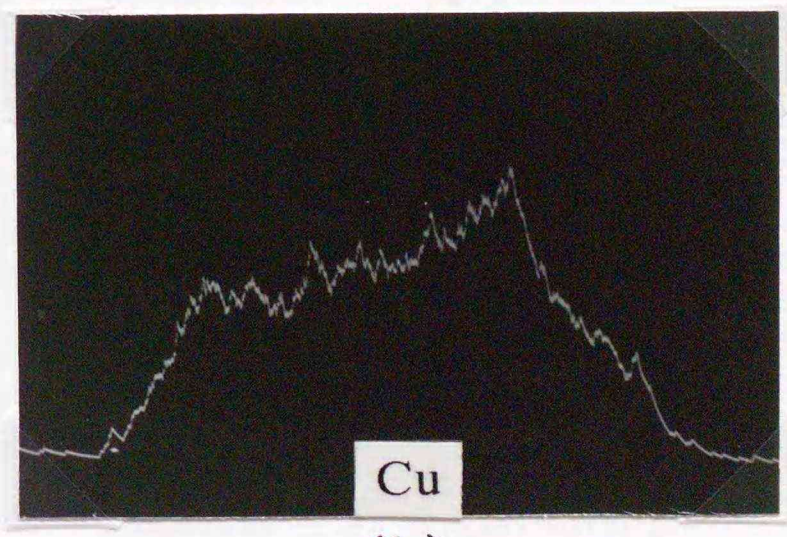








(a)



(b)

Fig. 6-3 SEM micrographs and distribution of elements in the flake of the original GICs.
(a) Ni-Fe-1, (b) Ni-Cu-1.

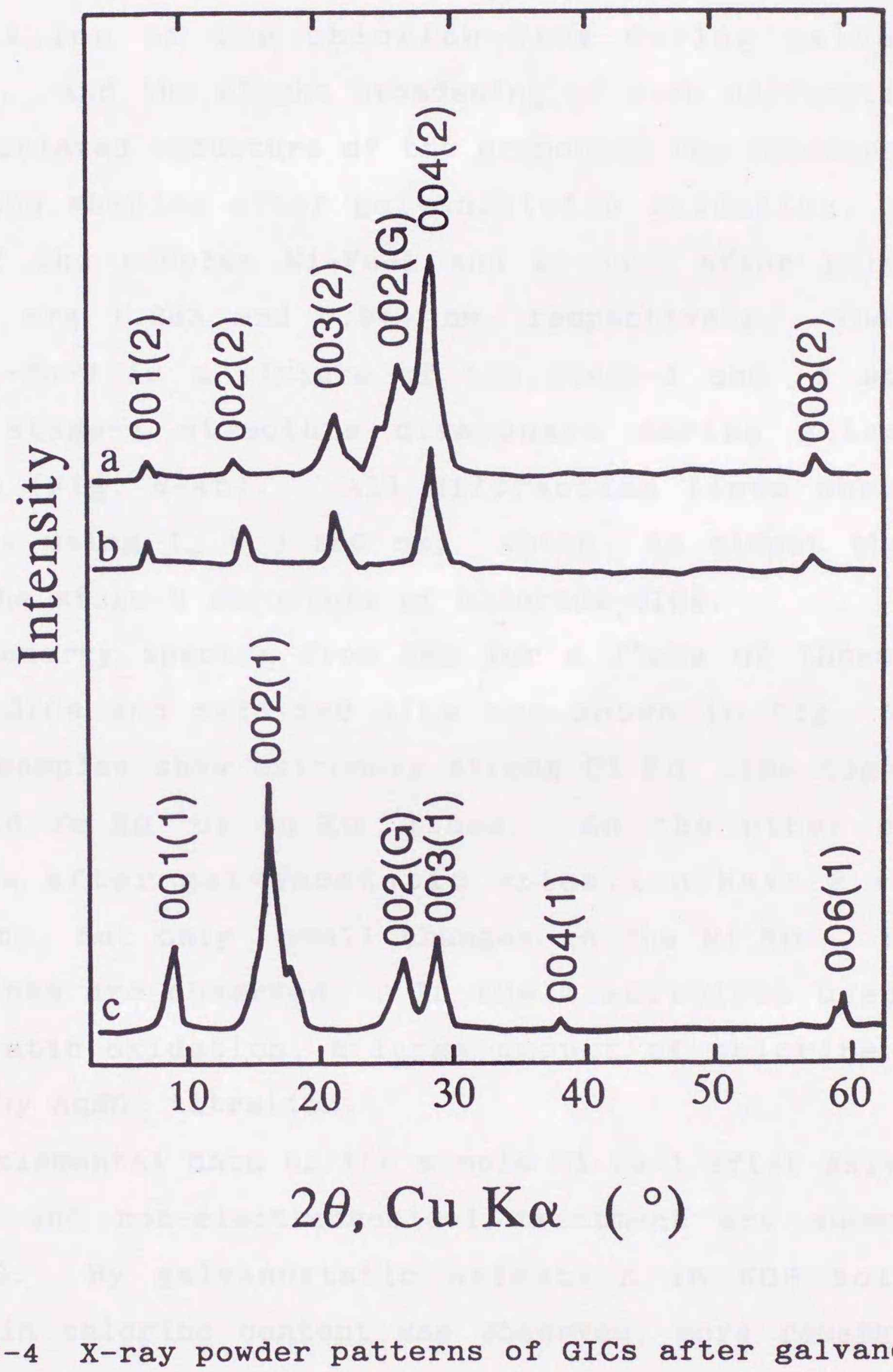


Fig. 6-4 X-ray powder patterns of GICs after galvanostatic oxidation in KOH solution of 7 mol/dm^3.
a: Ni-Fe-1, b: Ni-Fe-3, c: Ni-Cu-1.

the original chloride-GICs, except the appearance of the 002 line of graphite, which is produced probably by partial decomposition of the chloride-GICs during galvanostatic oxidation, and the slight broadening of each diffraction lines. The intercalated structure of the compounds was retained in major part of the samples after galvanostatic oxidation. The I_c-values of the samples Ni-Fe-1 and Ni-Cu-1 after galvanostatic oxidation are 1.283 and 0.944 nm, respectively. The original sample Ni-Fe-3 is a mixture of the stage-1 and -2 structures, but the stage-1 structure disappears during galvanostatic oxidation (Fig. 6-4b). All diffraction lines observed are indexed by using I_c = 1.280 nm, which is almost the same as that of the stage-2 structure of chloride-GICs.

The energy spectra from XMA for a flake of these original chloride-GICs and oxidized GICs are shown in Fig. 6-5. The original samples show extremely strong Cl Kα line together with Ni Kα and Fe Kα or Cu Kα lines. On the other hand, the compounds after galvanostatic oxidation have a very weak Cl Kα line, but only small changes in the Ni Kα , Fe Kα and Cu Kα lines are observed. In the electrolyte used for the galvanostatic oxidation, a large amount of chlorine ions was detected by $AgNO_3$ titration.

The elemental data on the sample Ni-Fe-1 after galvanostatic oxidation and non-electrochemical treatment are summarized in Table 6-3. By galvanostatic oxidation in KOH solution, a decrease in chlorine content was observed, more remarkable with the increase in treatment time, although the sample treated non-electrochemically had almost the same elemental composition as the original. The chlorine content in the GIC by galvanostatic oxidation in K_2SO_4 solution, which is neutral medium, decreases a little.

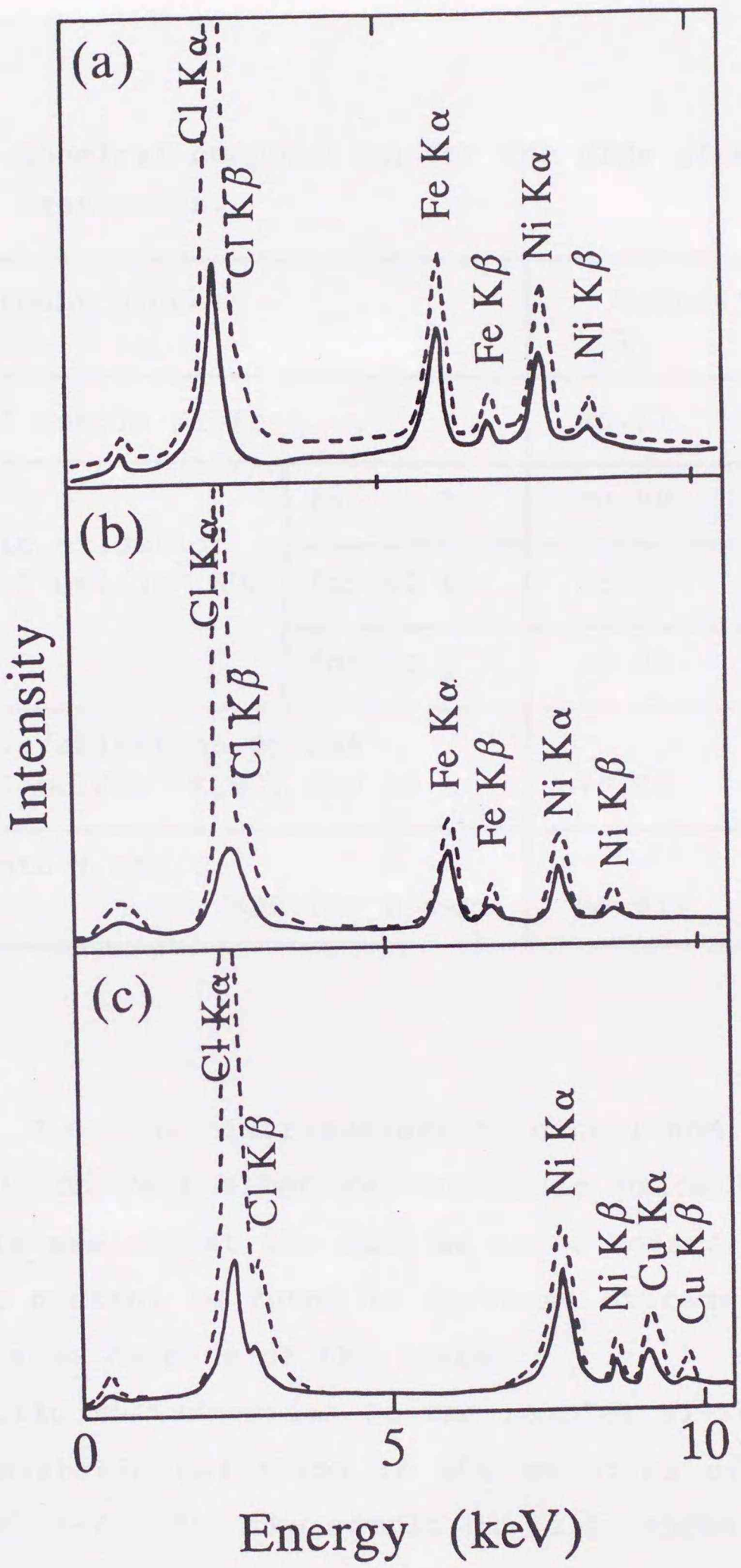


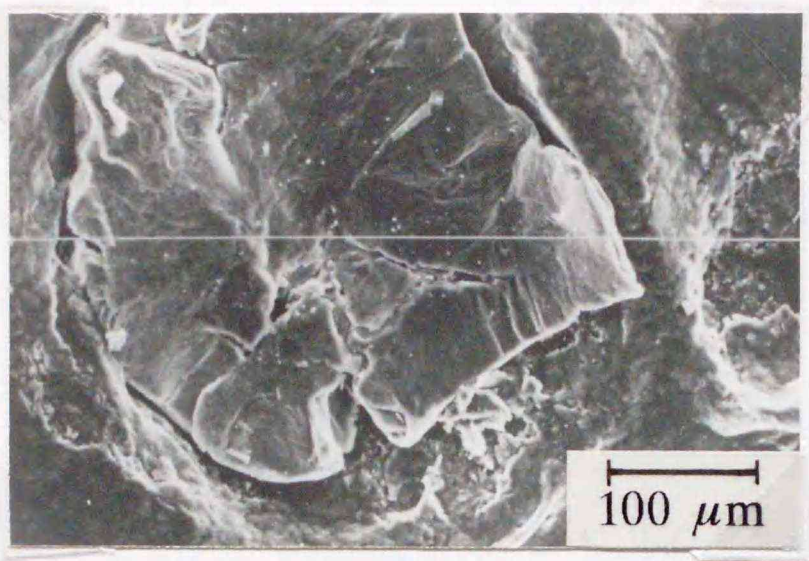
Fig. 6-5 Energy spectra by XMA of the samples (a) Ni-Fe-1, (b) Ni-Fe-3 and (c) Ni-Cu-1.
------- :original compound,
_____ :after galvanostatic oxidation.

Table 6-3 Chemical composition for the GICs after different treatments.

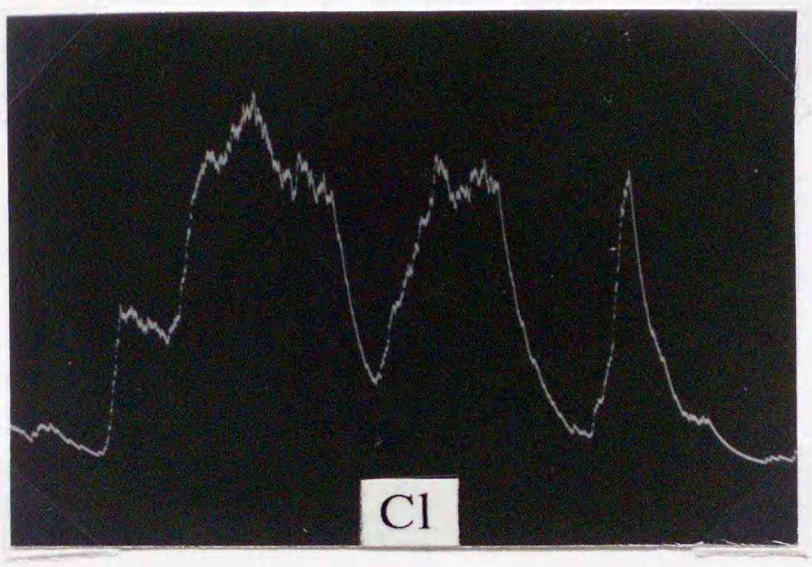
Treatment process		Composition [at.%] Cl	Fe	Ni
Original sample Ni-Fe-1		80.51	10.84	8.65
Galvanostatic oxidation by 2 mA in 7 mol/dm^3 KOH	for 10 h	60.88	22.11	17.01
	for 40 h	48.87	29.37	21.76
	for 80 h	26.89	42.65	30.46
Galvanostatic oxidation by 2mA in 0.5 mol/dm^3 K_2SO_4	for 80 h	76.55	13.18	10.27
Immersion into 7 mol/dm^3 KOH	for 3 days	80.51	11.08	7.81

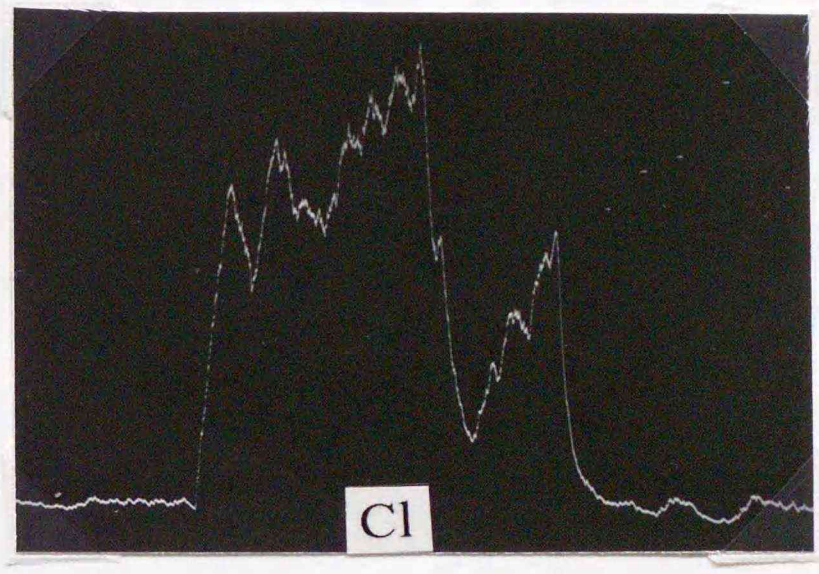
In Fig. 6-6, the distributions of nickel and iron in a flake of the sample Ni-Fe-1 after galvanostatic oxidation measured by line analysis are almost the same as those before (Fig. 6-3 (a)). The chlorine content is found to decrease extremely at edge part and also at some defects of the flake.

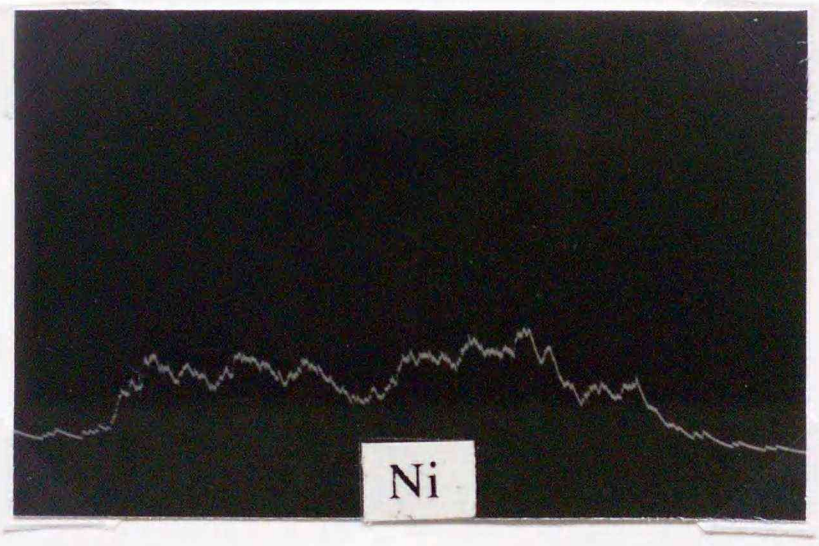
The cyclic voltammograms on the samples Ni-Fe-1 and Ni-Cu-1 after galvanostatic oxidation in KOH solution of 7 mol/dm^3 are shown in Fig. 6-7. For the sample Ni-Fe-1, three cathodic peaks at the potential values of 0.4, -0.05 and -0.9 V, except one due to hydrogen evolution above -1.0 V, appear on the voltammogram. Reversible anodic peaks, i. e., redox couple peaks are found at 0.4 and -0.9 V (Fig. 6-7a). Two redox couple peaks at 0.4 and -0.45 V are observed on cyclic voltammogram in the oxidized

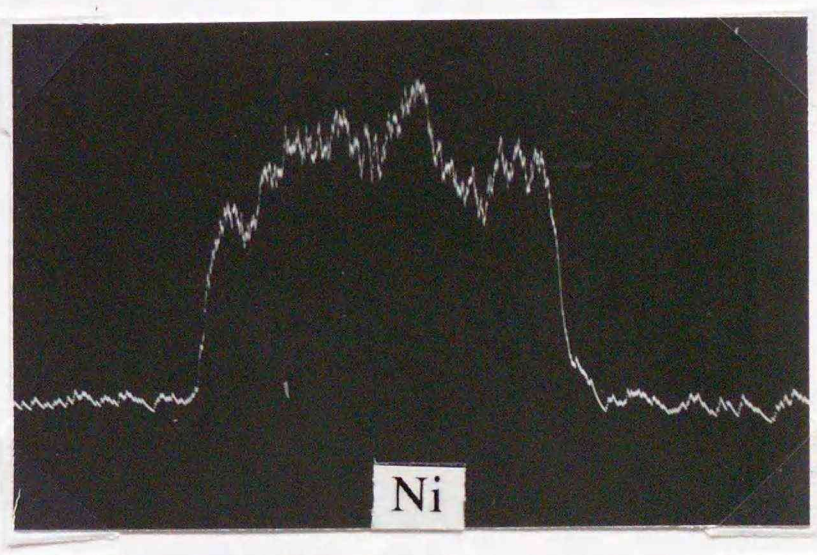


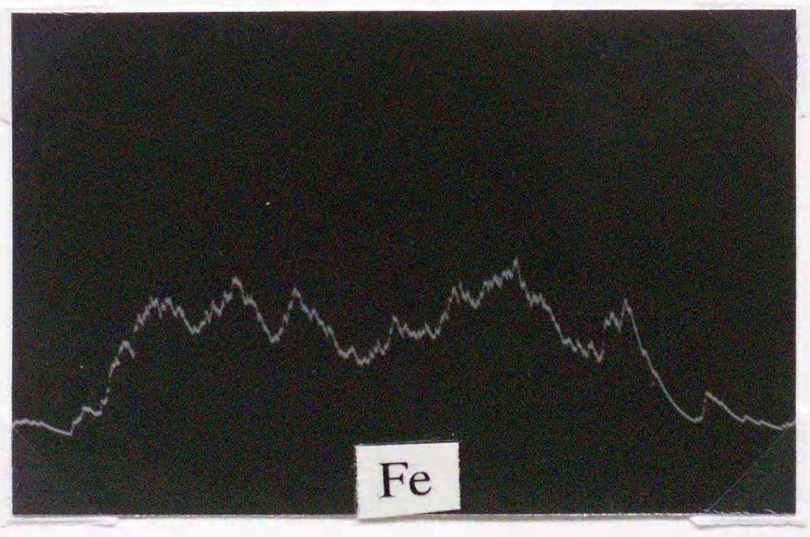












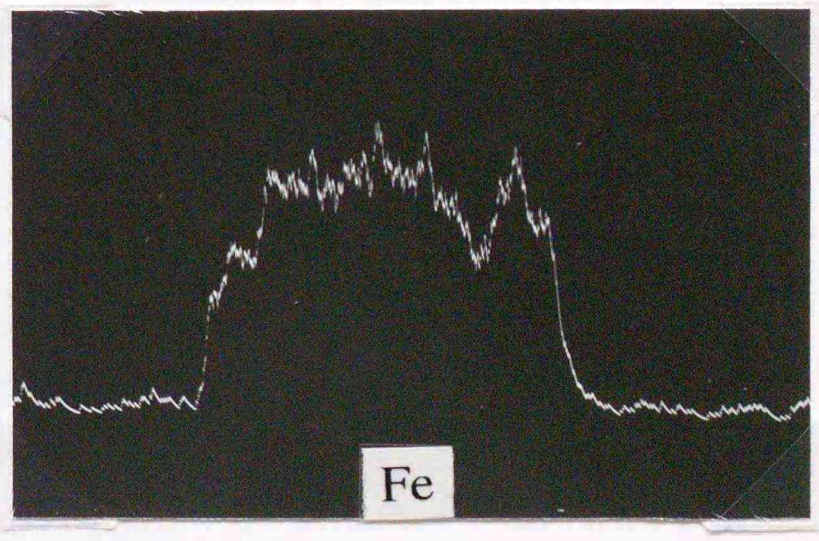


Fig. 6-6 SEM micrographs and distribution of elements in the flake of the sample Ni-Fe-1 after galvanostatic oxidation.

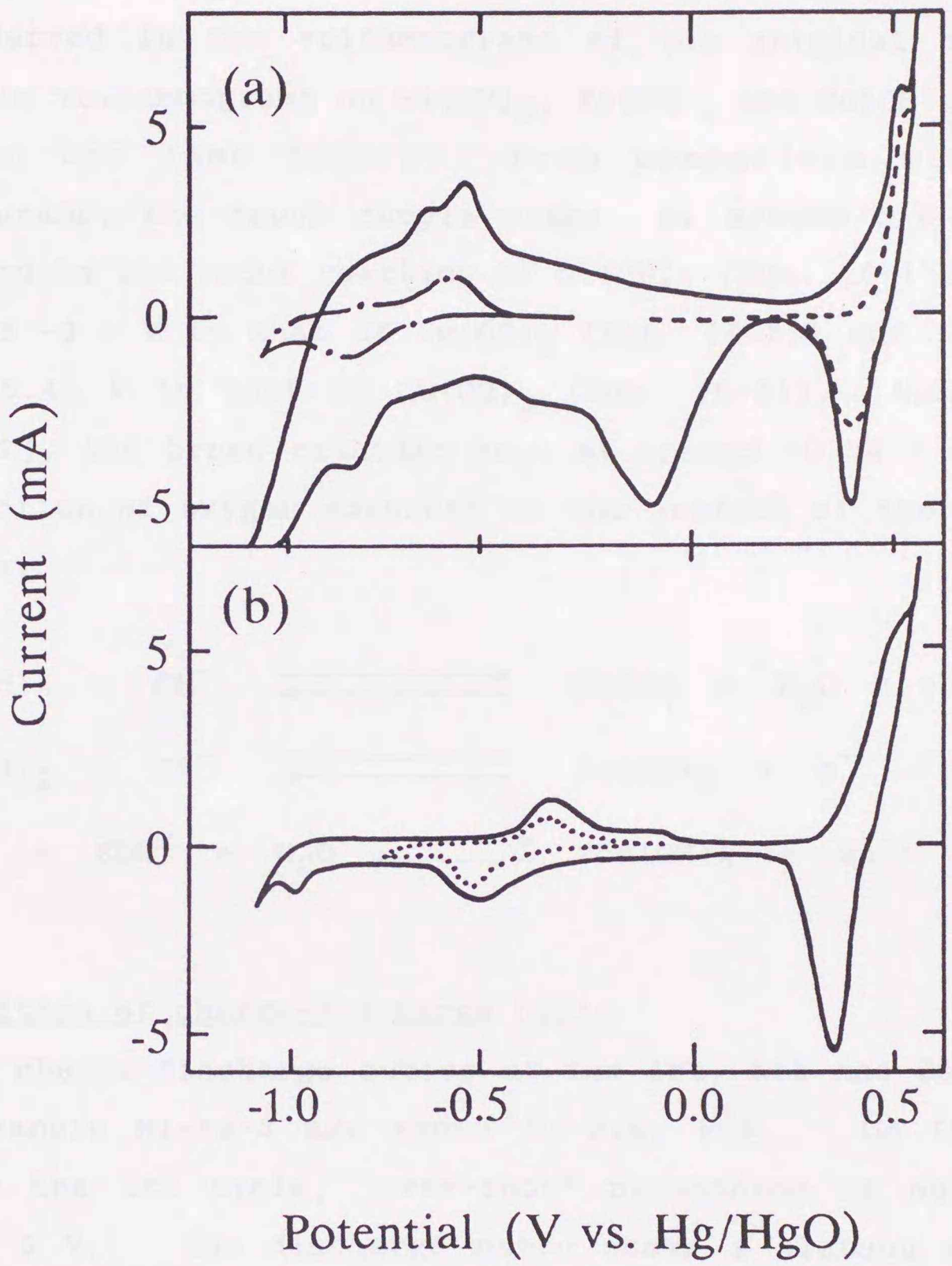


Fig. 6-7 Cyclic voltammograms of the electrodes of the GICs after galvanostatic oxidation.
For comparison, voltammograms of $Ni(OH)_2$, $Fe(OH)_3$ and $Cu(OH)_2$ are also shown.
———— : the GICs after galvanostatic oxidation,
(a) Ni-Fe-1, (b) Ni-Cu-1
- - - - : $Ni(OH)_2$, —·— : $Fe(OH)_3$,
····· : $Cu(OH)_2$.

sample Ni-Cu-1 (Fig. 6-7b). The redox couple peaks have never been observed in the voltammograms of the original compounds. The cyclic voltammograms on $Ni(OH)_2$, $Fe(OH)_3$ and $Cu(OH)_2$ are also shown in the same figure. From comparison with these voltammograms, the redox couple peaks at around 0.4 V can be attributed to the redox reaction of $Ni(OH)_2$ (Eqn. (6-1)), the one at around -0.9 V to that of $Fe(OH)_3$ (Eqn. (6-2)) and the one at around -0.45 V to that of $Cu(OH)_2$ (Eqn. (6-3)). According to Falk [6-7], the broad cathodic peak at around -0.05 V is due to the reduction of oxygen adsorbed on the surface of the electrode materials.

$$Ni(OH)_2 + OH^- \rightleftharpoons NiOOH + H_2O + e^- \quad (6\text{-}1)$$

$$Fe(OH)_2 + OH^- \rightleftharpoons Fe(OH)_3 + e^- \quad (6\text{-}2)$$

$$Cu_2O + 2OH^- + H_2O \rightleftharpoons 2Cu(OH)_2 + 2e^- \quad (6\text{-}3)$$

b) Repetition of charge-discharge cycle

The charge-discharge curves at the 1st, 5th and 20th cycles of the sample Ni-Fe-3 are shown in Fig. 6-8. On the charge curve in the 1st cycle, "over-shot" phenomenon is observed at around 0.5 V. The discharge curve shows a plateau at 0.4 V, which is exactly the same as the cathodic peak of $Ni(OH)_2$ on cyclic voltammograms (Fig. 6-7). From the comparison among the discharge curves for 1st, 5th and 20th cycles, the discharge capacity is supposed to increase with the increase in the number of charge-discharge cycle.

The change of capacity of the samples used are plotted as a function of the cycle number in Fig. 6-9. The capacity on each sample electrode increases linearly at the beginning of cycles, but around 20th cycle it starts to saturate at specific value.

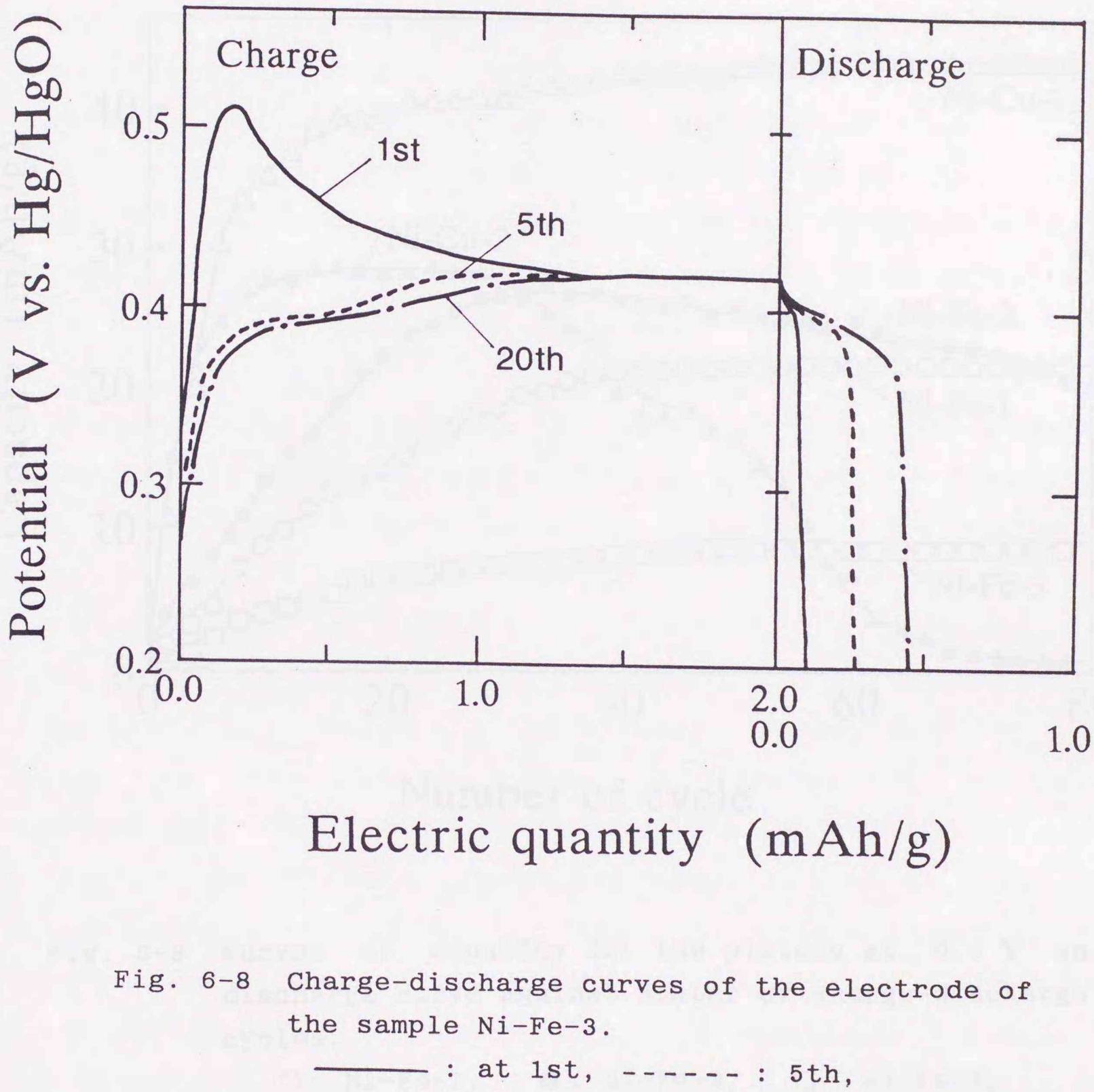


Fig. 6-8 Charge-discharge curves of the electrode of the sample Ni-Fe-3.

——— : at 1st, - - - - - - : 5th,

——·—— : 20th cycles.

(1 mAh = 3.6 C)

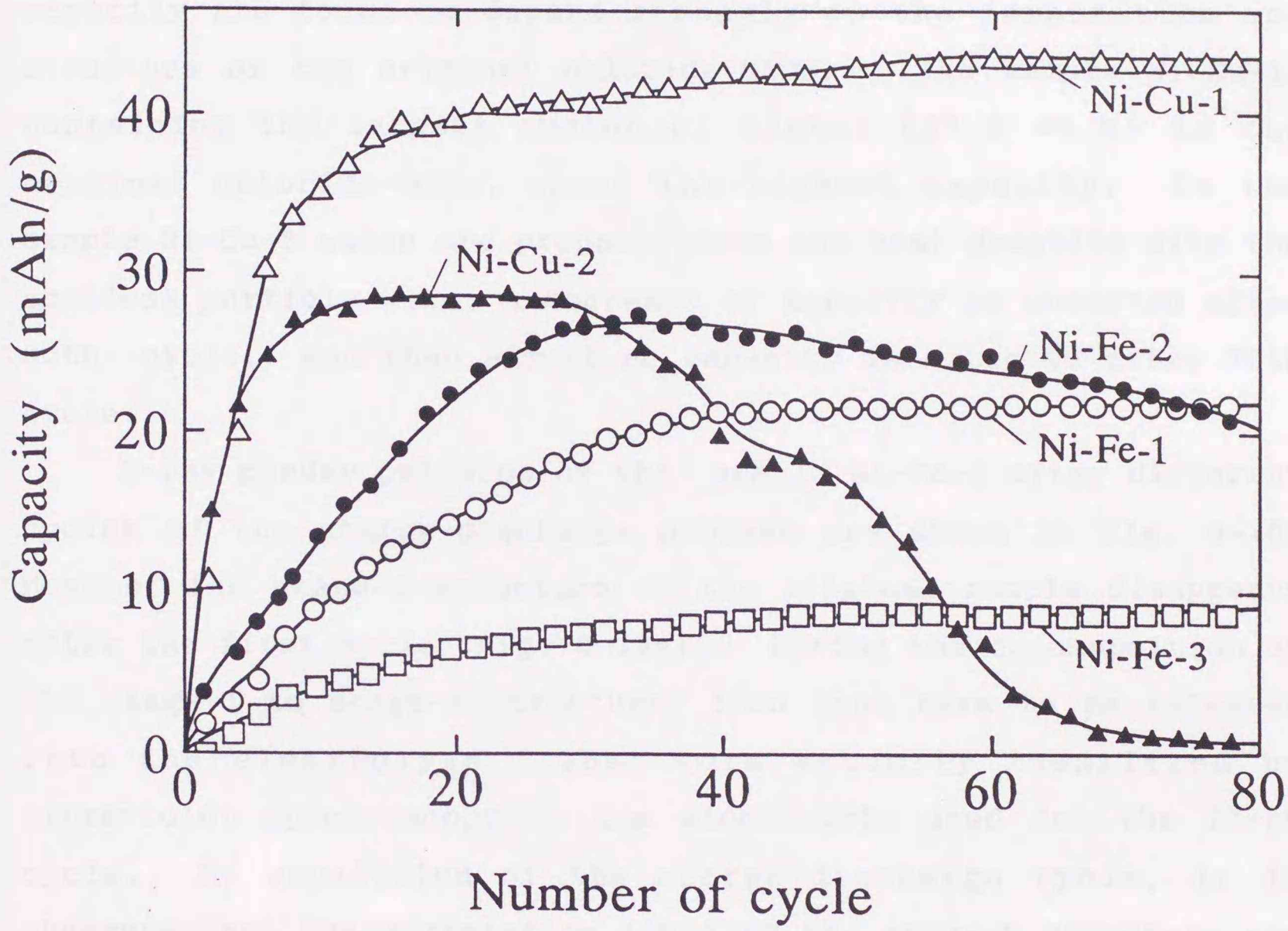


Fig. 6-9 Curves of capacity for the plateau at 0.4 V on discharge curve against number of charge-discharge cycles.

○: Ni-Fe-1, ●: Ni-Fe-2, □: Ni-Fe-3,

△: Ni-Cu-1, ▲: Ni-Cu-2.

(1 mAh = 3.6 C)

The saturated capacities of each samples Ni-Fe-1, Ni-Fe-2, Ni-Fe-3, Ni-Cu-1 and Ni-Cu-2 are 22.0, 27.0, 9.0, 45.0 and 29.0 mAh/g, respectively. The increasing behavior and the saturated value of capacity are found to depend strongly on the composition and structure of the original chloride-GICs. The sample Ni-Cu-1, containing the largest amount of nickel (17.3 wt.%) in the original chloride-GICs, shows the highest capacity. In the sample Ni-Cu-2 which are prepared from the host graphite with the smallest particle size, a decrease of capacity is observed after 30th cycle, and then almost no capacity is detected after 70th cycle.

X-ray powder patterns of the sample Ni-Fe-3 after different cycles of the charge-discharge process are shown in Fig. 6-10. Most of the stage-1 structure in the original sample disappears after the first cycle (Fig. 6-10a). During the decomposition of the stage-1 to stage-2 structure, iron ions have to be released into the electrolyte. They were actually identified by ultraviolet spectroscopy in the electrolyte used for the first cycle. By repetition of the charge-discharge cycle, it is observed that the diffraction lines of the stage-2 structure are broadened, particularly those with high indices as 008. The broadening of the diffraction lines is probably due to the introduction of some stacking disorder in the stage structure. After 50th cycle of charge-discharge, a remarkable decrease of the Cl Kα line was observed on the XMA energy spectrum and chlorine ions were detected in the electrolyte.

The possible number of charge-discharge repetitions of the sample Ni-Fe-3 electrode was more than 300 cycles. Above 200 cycles, however, a slight decrease in capacity was observed, which seemed to be due to partial decomposition of the GICs to graphite, as detected by the appearance of 002 line of graphite

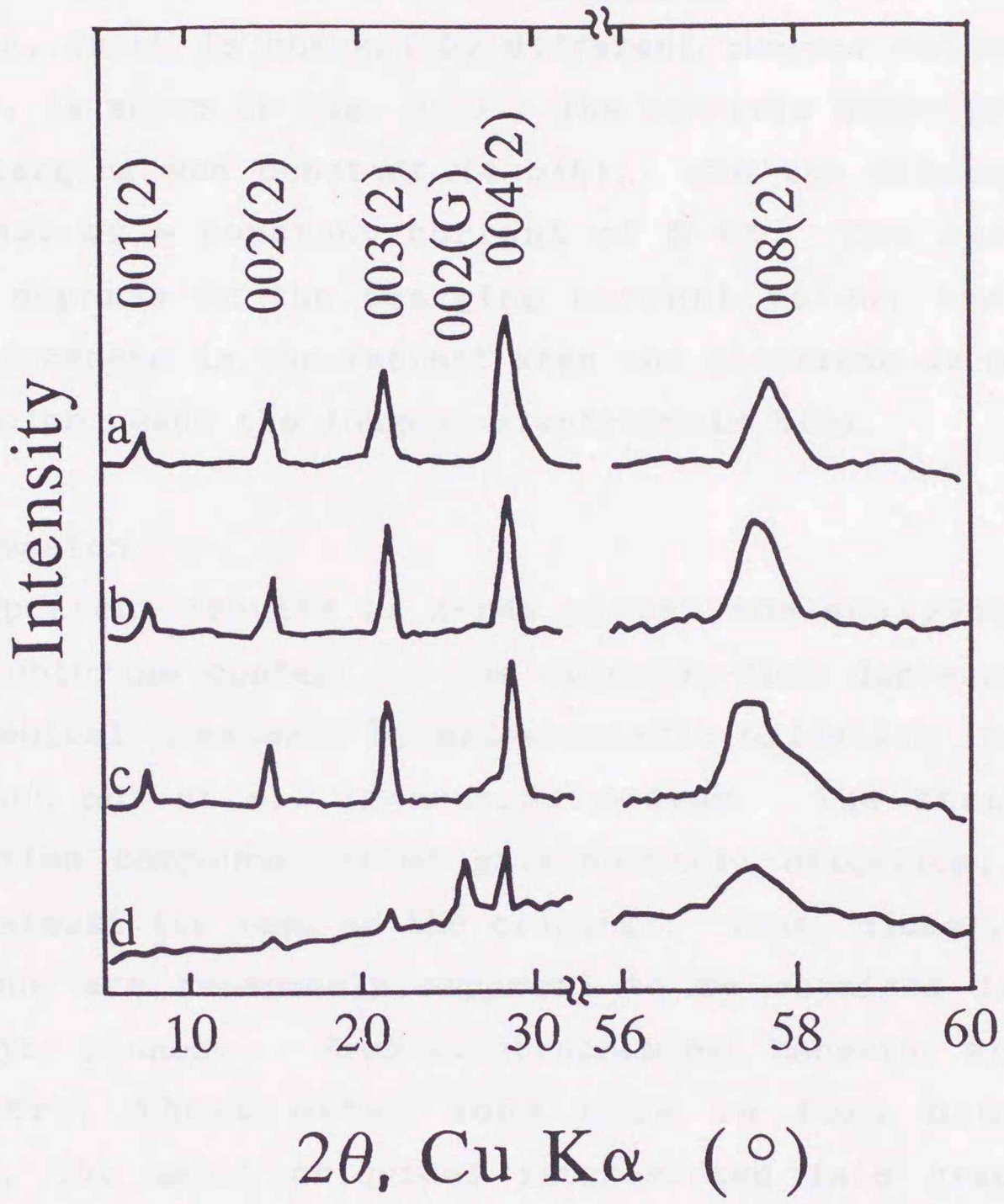


Fig. 6-10 X-ray powder patterns of the sample Ni-Fe-3 after different numbers of charge-discharge cycles.
a: after 1st cycle of charge-discharge,
b: after 15th cycle, c: after 50th cycle,
d: after 200th cycle.

in Fig. 6-10d.

The change of capacity of the sample Ni-Fe-1 with the repetition, which is charged by different current values (0.2, 2 and 8 mA), is shown in Fig. 6-11. The electric quantity consumed in the charging was constant (4 mAh), and the discharging was carried out by a constant current of 2 mA. The increase of capacity depends on the charging current value; the rate of capacity increase is the fastest when the electrode is charged by 0.2 mA, which needs the longest electrolysis time.

6.4. Discussion

The present results of X-ray microprobe analysis suggest that the chlorine content in the chloride-GICs decreases during electrochemical treatment by galvanostatic oxidation in alkaline medium, but not at all in neutral medium. The structure of intercalation compounds after galvanostatic oxidation, however, was kept almost the same as the original. Thus, nickel, iron and copper ions are reasonably supposed to be retained in between carbon layer planes. From electrochemical behavior with cyclic voltammetry, these metal ions seem to form hydroxides. Therefore, the metal chlorides intercalated into graphite are converted into hydroxides by galvanostatic oxidation in alkaline medium. In other words, metal chlorides are exchanged for the corresponding metal hydroxides in the gallery of graphite.

Montmorillonite intercalated with nickel hydroxide could be synthesized by titrating a sodium hydroxide solution into a suspension of montmorillonite particles intercalated with nickel ion [6-8]. Mechanism for the formation of montmorillonite intercalation compounds with nickel hydroxide during titration of the alkaline solution was investigated with potentiometry [6-9] and X-ray powder diffractometry [6-10]. However, the hydroxide-

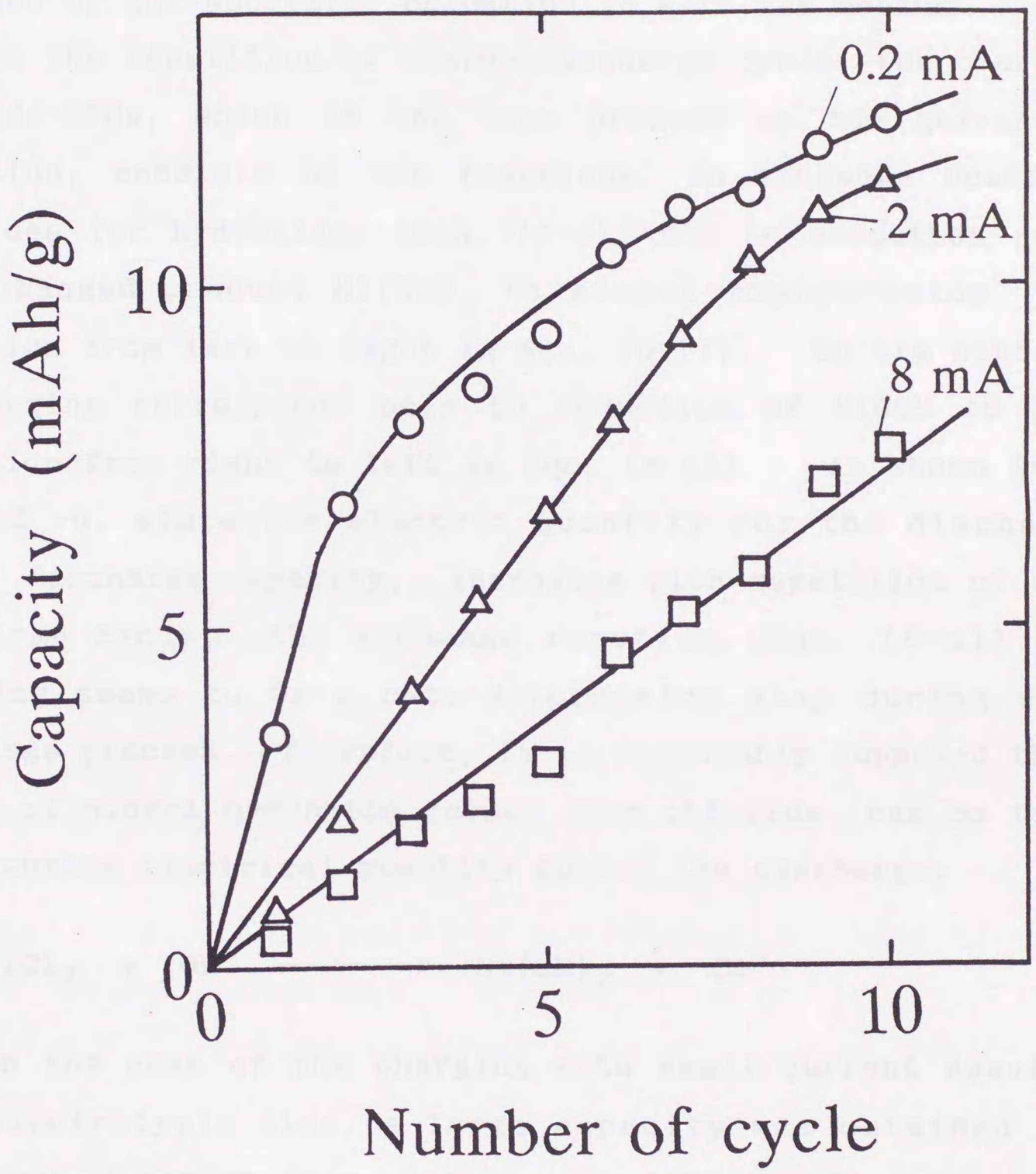


Fig. 6-11 Curves of capacity on the electrode of the sample Ni-Fe-1 against number of charge-discharge cycles by different charging current densities.
○ : by 0.2 mA, △ : by 2 mA,
□ : by 8 mA in charging. (1 mAh = 3.6 C)

GICs could not be synthesized by non-electrochemical treatment of the corresponding chloride-GICs, and was only possible to be obtained by galvanostatic oxidation in alkaline medium.

In the repetition of charge-discharge cycle, the charging of chloride-GICs, which is the same process as the galvanostatic oxidation, consists of two reactions; an exchange reaction of chlorides for hydroxides (Eqn. (6-4)) and an oxidation reaction of exchanged product $Ni(OH)_2$ to nickel oxyhydroxide, NiOOH, (reaction from left to light in Eqn. (6-1)). On the other hand, discharging corresponds only to reduction of NiOOH to $Ni(OH)_2$ (reaction from right to left in Eqn. (6-1)). As shown in Figs. 6-8 and -9, since the electric quantity for the discharging, i. e. discharge capacity, increases with repetition of charge-discharge cycle, the exchange reaction (Eqn. (6-4)) in the charging seems to be a rate-determining step during charge-discharge process. Therefore, it is reasonably supposed that the amount of nickel hydroxide formed from chloride can be followed by measuring electrical quantity during the discharge.

$$NiCl_2 + OH^- \longrightarrow Ni(OH)_2 + Cl^- \qquad (6\text{-}4)$$

In the case of the charging with small current density for long electrolysis time, a large capacity was obtained in the beginning of cycles (Fig. 6-11). In other words, the amount of nickel hydroxide formed from chloride depended on electrolysis time, even under a constant electric quantity. This fact dose not obey Faraday's law. Although electrochemical oxidation of chloride-GICs in alkaline solution is found to be essential for the synthesis of hydroxide-GICs, the exchange reaction (Eqn. (6-4)) itself is not an electrochemical one. During electrochemical oxidation, oxygen gas is evolved (Eqn. (6-5));

$$4OH^- \longrightarrow O_2 + H_2O + 4e^- . \qquad (6\text{-}5)$$

With oxygen evolution in alkaline solution, water (H_2O) is reasonably supposed to be produced on the surface of the GIC electrode. It was observed by XANES and EXAFS that the metal chloride in the chloride-GICs was formed MCl_6 octahedra in the graphite gallery [6-11]. For GIC with iron chloride in air, it was reported that water diffused into the graphite gallery and partial exchange of ligand in $FeCl_6$ octahedra took place according to following scheme [6-12];

$$[FeCl_6]^{3-} + 4H_2O \longrightarrow [FeCl_2(OH_2)_4]^+ + 4Cl^- . \qquad (6\text{-}6)$$

This $[FeCl_2(OH_2)_4]^+$ octahedron in the GIC was detected by Moessbauer spectrum [6-12]. In order to form iron hydroxide, further exchange of ligand and also elimination of hydrochloric acid from the octahedron seem to be needed.

During oxygen evolution in alkaline solution, water produced on the surface of chloride-GIC electrode seems to diffuse from the edge of the flakes into the graphite gallery and to exchange ligands of MCl_6 octahedra. The charging with small current density for long time is advantageous for the formation of $[MCl_2(OH_2)_4]^+$ octahedra, because an enough time is needed for water diffusion. If protons and chlorines were quickly eliminated from the octahedra as hydrochloric acid into alkaline solution, the metal hydroxide might be retained in the gallery of graphite.

The maximum of efficiency for exchange of $NiCl_2$ for $Ni(OH)_2$ (nickel efficiency) is calculated from the saturated capacity and nickel content in the original chloride-GICs and summarized on all samples in Table 6-4. The saturated capacity does not depend on the nickel content in the original chloride-GICs. The sample

Table 6-4 Nickel content, saturated capacity and nickel efficiency of the each sample.

Original sample code	Nickel content [wt.%]	Saturated capacity [mAh/g]	Nickel efficiency [%]
Ni-Fe-1	8.6	22.0	45
Ni-Fe-2	8.4	27.0	70
Ni-Fe-3	8.0	9.0	25
Ni-Cu-1	17.3	45.0	57
Ni-Cu-2	8.5	29.0	75

Ni-Cu-2, prepared from the host with the smallest particle size (sample NG5), shows the highest nickel efficiency (75 %) among the samples used. In the sample Ni-Fe-2 synthesized from NG46, nickel efficiency of 70 % is higher than that in the sample Ni-Fe-1 synthesized from the host with large flake size (sample NG400). From the distribution of chlorine on a flake of the samples after the galvanostatic oxidation (Fig. 6-6, for examples), the exchange reaction of chloride for hydroxide in the graphite gallery is found to proceed at the edge and also at some defects of the flake, where water produced by galvanostatic oxidation in alkaline solution seems to diffuse into the graphite gallery. Since the host with small particle size has a large edge surface area, it is reasonable that the samples Ni-Fe-2 and Ni-Cu-2, prepared from the samples NG46 and NG5, respectively, show higher rate of exchange reaction and also higher nickel efficiency than the samples prepared from the sample NG400. In the samples Ni-Fe-1, Ni-Fe-3 and Ni-Cu-1, showing low nickel efficiency, the exchange reaction for hydroxide does not

complete. In other words, the chloride-GIC is remained at the center of a flake even after galvanostatic oxidation for long time, due to probably the diffusion of water into graphite gallery is limited by size effect.

The nickel efficiency in the sample Ni-Cu-1 is higher than that in the sample Ni-Fe-1. This experimental result is explained by the fact that a lot of nickel in the sample Ni-Cu-1 already existed at the edge of the flakes in the original chloride-GIC, as shown in Fig. 6-3.

The thickness of intercalated metal hydroxide layers, Δd, calculated from I_c-values on the hydroxide-GICs is about 0.61 nm, being the same as the one for metal chlorides layers in the chloride-GICs. The crystal structure of metal hydroxides belongs to CdI_2-type, which consist of $M(OH)_6$ octahedron. Therefore, it is reasonably supposed that the chloride ions on MCl_6 octahedra are displaced by hydroxyl ions during galvanostatic oxidation in alkaline medium, and the monolayer of metal hydroxides was sandwiched between conductive carbon layer planes.

6.5. Summary

The GICs with metal hydroxides were synthesized through a galvanostatic oxidation in alkaline medium from GICs with corresponding chlorides. The amount of nickel hydroxide formed from nickel chloride in the graphite gallery could be followed by measuring electric quantity during discharge, i. e., by the discharge capacity. The capacity depended strongly on the composition of the original chloride-GICs and on the electrolysis time. The nickel efficiency of the original GIC prepared from the host with small flake size was higher than the compound from large size. Water produced by galvanostatic oxidation in

alkaline solution seemed to diffuse from the edge of the flake into the graphite gallery. Consequently, the formation of hydroxide-GICs is due to the exchange of ligand chlorides in MCl_6 octahedra for hydroxyl ions in the gallery of graphite.

In most commercial alkaline secondary batteries, graphite powders are mixed with nickel hydroxide which acts as a positive electrode material, in order to improve the electrical conductivity of electrode. In the present GIC electrode, nickel hydroxides, NiOOH and $Ni(OH)_2$, are held in between carbon layer planes to form graphite intercalation compounds, in which a single layer of hydroxide is sandwiched by conductive carbon layers. Although the capacity and nickel content of the GIC electrode is low, there might a possibility of improving the battery performance. The hydroxide-GICs will be used as a positive electrode of alkaline secondary battery and its charge and discharge performances will be discussed in the next chapter.

References

6-1 S. Flandrois, J. M. Masson and J. C. Rouillon, Synth. Met., 3, 195 (1981).

6-2 S. Flandrois, F. Baron, Mat. Res. Soc. Syp. Proc., 20, 237 (1983).

6-3 S. Flandrois, J. M. Masson, J. C. Rouillon, J. Gaultier and C. Hauw, Synth. Met., 3, 1 (1981).

6-4 M. Inagaki, Z. D. Wang, Y. Okamoto and M. Ohira, Synth. Met., 20, 9 (1987).

6-5 Z. D. Wang, Doctor Thesis, Toyohashi University of Technology (1990).

6-6 M. Inagaki and M. Ohira, J. Mater. Res., 5, 1703 (1990).

6-7 S. U. Falk, J. Electrochem. Soc., 107, 661 (1960).

6-8 S. Caillère and S. Hénin, Mineral Mag., 28, 612 (1949).

6-9 S. Yamanaka and G. W. Brindley, Clays and Clays minerals, 26, 21 (1978).

6-10 Fuda, T. Yuri, Y. Saito and T. Matsunaga,
Soseibusseigaku. Mag., 3, 84(1990).
6-11 Z. D. Wang, M. Ohira, N. Inagaki, N. Kosugi, K. Yamazaki
and H. Kuroda, Tanso, 1990[No. 141], 30 (1990).
6-12 R. Schlogel, W. Jones and H. Boehm, Synth. Met., 7,
133 (1973).

CHAPTER 7

Application of GICs with metal hydroxides to alkaline secondary battery and its performance

7.1. Introduction

In Chapter 6, it was mentioned that the metal hydroxides-GICs ($Ni(OH)_2$-$Fe(OH)_3$- and $Ni(OH)_2$-$Cu(OH)_2$-GICs) were easily prepared by electrochemical treatment of corresponding metal chlorides-GICs ($NiCl_2$-$FeCl_3$- and $NiCl_2$-$CuCl_2$-GICs) in alkaline medium.

In most commercial alkaline secondary batteries, graphite powders are mixed with nickel hydroxide, in order to improve the electrical conductivity of electrode. In the case of GICs with metal hydroxides (hydroxide-GICs), nickel hydroxides ($Ni(OH)_2$ and NiOOH) are held in between conductive carbon layer planes and and the compounds themselves are reasonably assumed to have better electrical conductivity than graphite. Therefore, a battery in which the hydroxides-GICs are used as electrode material is expected to give better performance of charge and discharge reactions than a conventional electrode of the mixture of nickel hydroxide and graphite, for instance, discharge under a large electrical current density.

In the present work, the charge and discharge reactions on the electrode of hydroxide-GICs are followed by measuring potential. The performance of charge and discharge reactions on the electrodes is studied by measuring activation energies for both reactions, which are assumed to be controlled by the diffusion of protons in the nickel hydroxide crystals. A possibility of discharge under a large current density is also discussed.

7.2. Theory of charge and discharge reactions on nickel hydroxide electrode

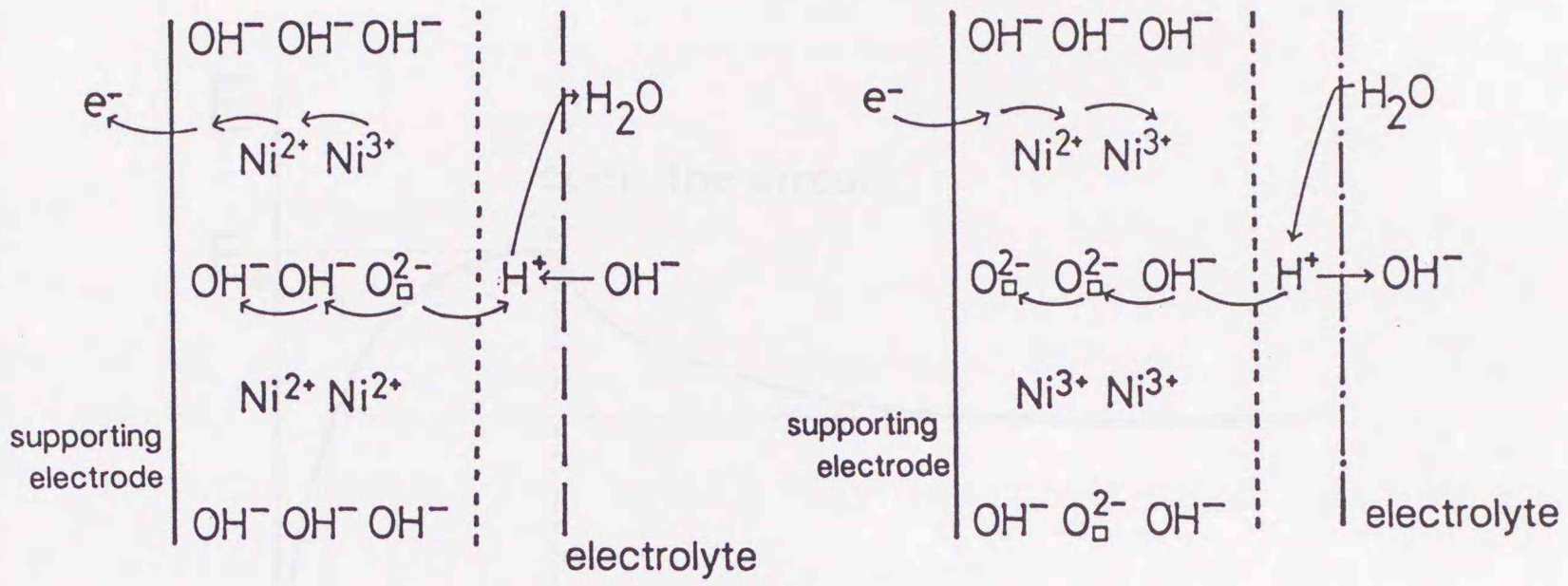
The charge and discharge reactions on nickel hydroxide electrode are expressed by the following equation;

$$Ni(OH)_2 + OH^- \underset{\text{discharging}}{\overset{\text{charging}}{\rightleftharpoons}} NiOOH + H_2O + e^- . \qquad (7-1)$$

Yoshizawa, et al. [7-1] pointed out that the rate-determining step of charge and discharge reactions was the diffusion of protons in nickel hydroxide crystals, which shown schematically in Fig. 7-1. During the charging, the gradient in the activity of NiOOH is generated in the bulk of $Ni(OH)_2$ electrode. In the case of discharge reaction, in contrast, the activity gradient of $Ni(OH)_2$ is produced in NiOOH electrode due to diffusion of protons into electrode material. Thus, the motion of protons in a nickel hydroxide electrode seems to affect on the overvoltage in the charge and discharge reactions of Eqn. (7-1). Yoshizawa, et al. developed the theoretical formulae for charge and discharge reactions in the nickel hydroxide electrode, in order to analyze the change of the potential with time after opening the circuit during charging or discharging processes [7-1].

Representative examples of potential changes during charging and discharging processes on nickel hydroxide electrode are shown in Fig. 7-2. In charging process, motion of protons in the nickel hydroxide crystal, in other word, change of activity gradient of NiOOH in the $Ni(OH)_2$ bulk with time is expressed by Fick's secondary law in a plane sheet;

$$\frac{\partial a_{NiOOH}}{\partial t} = D \cdot \frac{\partial^2 a_{NiOOH}}{\partial x^2} . \qquad (7-2)$$



(a) (b)

Fig. 7-1 A scheme of the charge and discharge reactions on a nickel hydroxide electrode.
(a) charge and (b) discharge reactions.

In the nickel hydroxide electrode, the boundary conditions of Eqn. (7-2) are

$$a_{NiOOH}(x, 0) = 0, \quad D\left(\frac{\partial a_{NiOOH}}{\partial x}\right)_{x=0} = -\phi ,$$

$$a_{NiOOH}(\infty, t) = 0, \quad D\left(\frac{\partial a_{NiOOH}}{\partial x}\right)_{x=0} = 0, \qquad (7\text{-}3)$$

$$a_{NiOOH}(x, \infty) = a_{NiOOH}(0, t_e) = \left(a_{NiOOH}\right)_e ,$$

where ϕ is an amount of product (NiOOH in charging process and $Ni(OH)_2$ in discharging process) per unit time and unit surface area of the electrode.

Nernst's equation for Eqn. (7-1) is expressed by Eqn. (7-4);

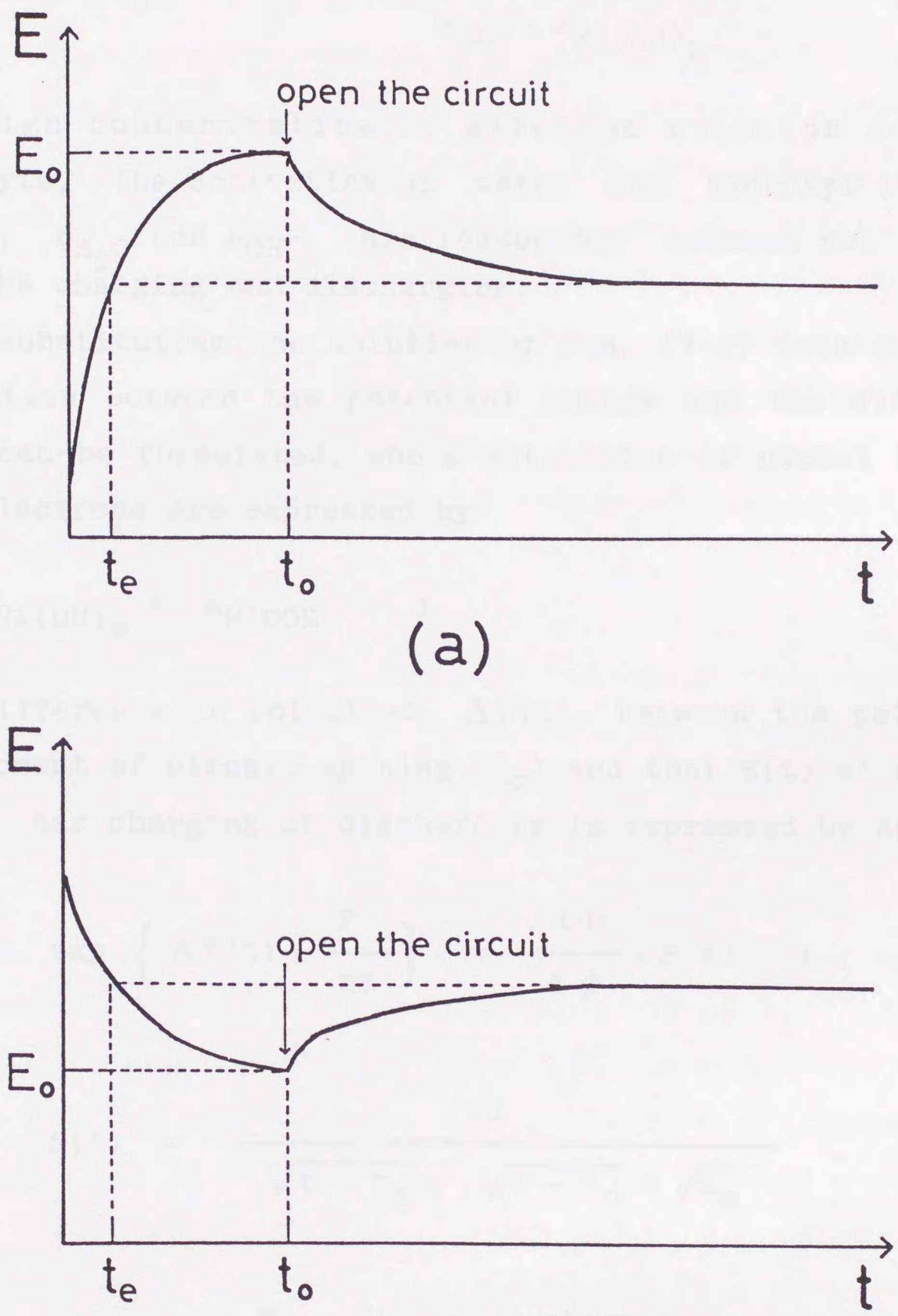


Fig. 7-2 Potential changes of a nickel hydroxide electrode during (a) charging and (b) discharging processes.

$$E = E_o + \frac{RT}{F} \cdot \ln \frac{a_{H_2O} \cdot a_{NiOOH}}{a_{OH^-} \cdot a_{Ni(OH)_2}} \quad . \qquad (7\text{-}4)$$

Since high concentration of alkaline solution is used as electrolyte, the activities of water and hydroxyl ions in the solution, a_{H_2O} and a_{OH^-}, are reasonably assumed not to change during the charging and discharging.

By substituting the solution of Eqn. (7-2) into Eqn. (7-4), the relation between the potential change and the diffusion of protons can be formulated, where activities of nickel hydroxides in the electrode are expressed by

$$a_{Ni(OH)_2} + a_{NiOOH} = 1. \qquad (7\text{-}5)$$

A difference in potential, $\Delta E(t)$, between the potential E_o at the moment of circuit opening (t_o) and that E(t) at any time t during either charging or discharging is expressed by Eqn. (7-6).

$$\exp\left\{\Delta E(t) \cdot \frac{F}{RT}\right\} = \frac{\sqrt{\pi \cdot D}}{2 \cdot \phi} \cdot S(t) - 1 \ , \qquad (7\text{-}6)$$

where

$$S(t) = \frac{1}{\sqrt{t - t_e} - \sqrt{t - t_o} + \sqrt{t_e}} \ ,$$

and

$$\Delta E(t) = \begin{cases} E_o - E(t) \ ; \text{ in charging,} \\ E(t) - E_o \ ; \text{ in discharging processes.} \end{cases}$$

From Eqn. (7-6), diffusion coefficient of protons in the nickel hydroxide electrode, D, can be determined, and then activation energy for the proton diffusion is estimated from the dependence of D on temperature [7-1].

7.3. Experimental

7.3.1. Preparation of hydroxide-GIC electrode

The GIC with $NiCl_2$-$FeCl_3$ and with $NiCl_2$-$CuCl_2$ (exactly the same as the samples Ni-Fe-1 and Ni-Cu-1 in Chapter 6, respectively) were used as the original compounds for the hydroxide-GIC electrodes. The chloride-GIC powders of 0.5 g were held in between two plastic plates (20 X 20 mm^2) with a supporting electrode of platinum wire, as already shown in Chapter 6 (Fig. 6-1(a)). For the synthesis of hydroxide-GIC, galvanostatic oxidation of chloride-GIC electrodes in an aqueous solution of potassium hydroxide of 7 mol/dm^3 was carried out with 2 mA for 80 hours.

7.3.2. Determination of activation energies for charge and discharge reactions on the hydroxide-GIC electrodes

The cell used for the measurement of activation energies of charge and discharge reactions on the hydroxide-GIC electrodes is shown schematically in Fig. 7-3. The hydroxide-GIC electrode was covered with paraffin except for the small holes in plastic plate, in order to make protons diffuse through the holes in a plane. An aqueous solution of potassium hydroxide of 7 mol/dm^3 was used as the electrolyte, and a Hg/HgO electrode as the reference. The temperature of the cell was controlled at a constant level (0, 10, 20, 30, 40 and 50^oC) in a water bath.

After the GIC electrode was polarized by a constant current of 5 mA for 10 minutes, as shown in Fig. 7-2, the circuit was opened and the potential of the GIC electrode was followed by being memorized into a computer through an analogue-digital converter.

A diffusion coefficient, D, is supposed to be proportional to the slope of the plot of $\exp\left\{\Delta E(t)\cdot F/RT\right\}$ against S(t)

(Eqn. (7-6)). Because the value of ϕ in Eqn. (7-6) was a cell constant and unfortunately not known, the absolute values of D would not be determined. However, ϕ seemed to be independent of temperature, so that the activation energies for the charge and discharge reactions on the electrode were able to be determined from Arrhenius plot of D/ϕ^2 values, obtained from the relation between $\exp\left\{\Delta E(t)\cdot F/RT\right\}$ and S(t), against the reciprocal temperature.

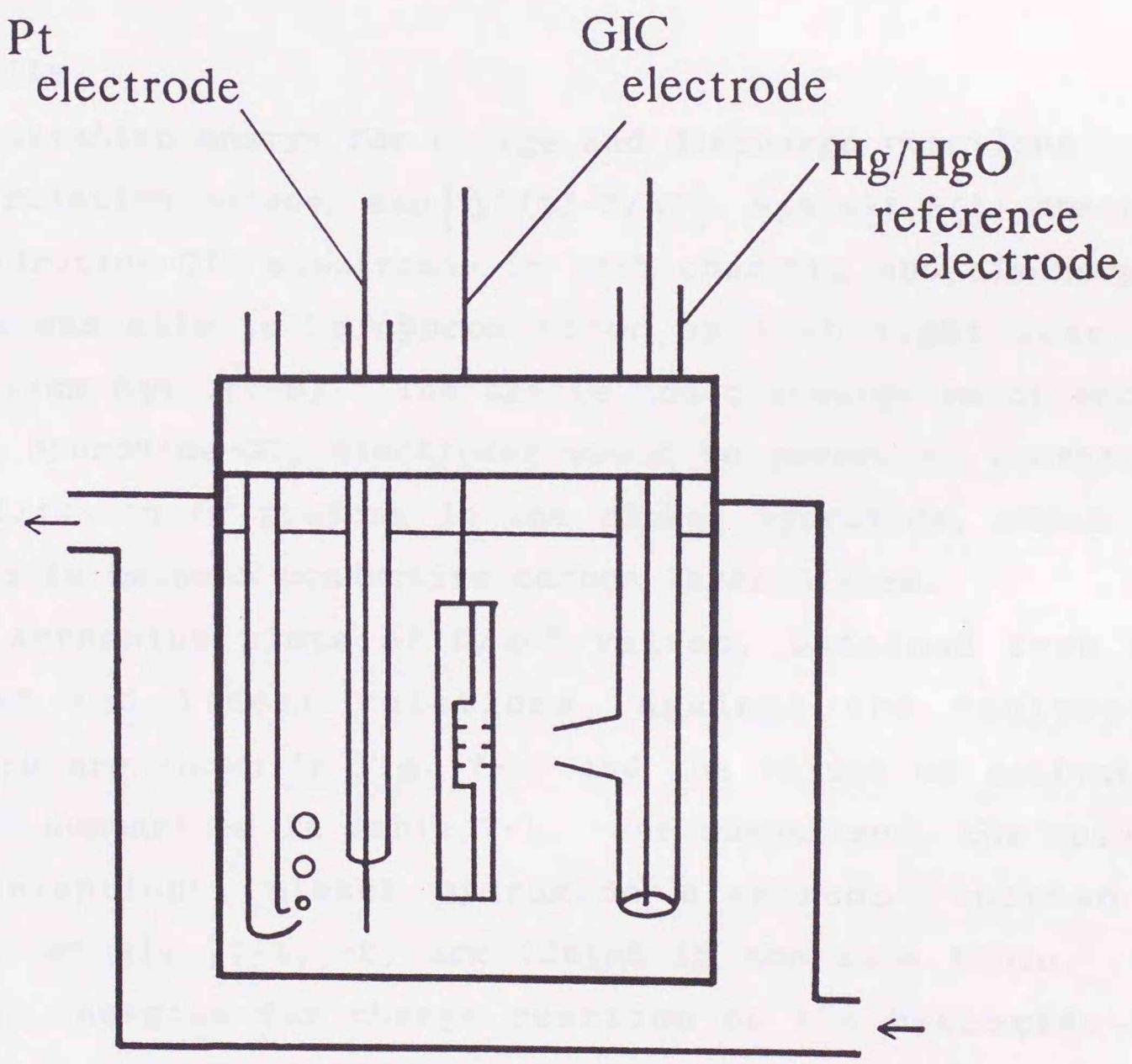


Fig. 7-3 Cell assembly.

7.3.3. Discharge performance under a large current density

In order to determine the possibility of discharging under a large current density, discharging tests by different current values (0.2, 2.0 and 20.0 mA) were also carried out at constant temperature of 20^{o}C. The potential was continuously recorded during the discharge. For comparison, a pocket-type electrode containing the mixture of nickel hydroxide with graphite powder was prepared in the laboratory. The charging of the electrode was performed under a constant current of 2.0 mA for 1 hour (2.0 mAh).

7.4. Results

7.4.1. Activation energy for charge and discharge reactions

The relation between $\exp\{\Delta E(t)\cdot F/RT\}$ against S(t) observed on two hydroxide-GIC electrodes in both charging and discharging processes was able to be approximated by a straight line, as expected from Eqn. (7-6). The charge and discharge reactions on these two hydroxide-GIC electrodes would be governed, therefore, by the diffusion of protons in the nickel hydroxide, which was sandwiched in between conductive carbon layer planes.

The Arrhenius plots of D/ϕ^2 values, obtained from the slopes of the linear relations, against the reciprocal temperature are shown in Fig. 7-4, and the values of activation energy are summarized in Table 7-1. For comparison, the results for a conventional nickel hydroxide electrode reported by Yoshizawa, et al. [7-1, -2] are listed in the same table. The activation energies for charge reaction on the hydroxide-GIC electrodes are about 42 kJ/mol and almost twice as large as the one reported on the conventional electrode. On the other hand, those for discharge reaction on the GIC electrodes, 6.7 and 9.2 kJ/mol, are about a half of that for the conventional electrode.

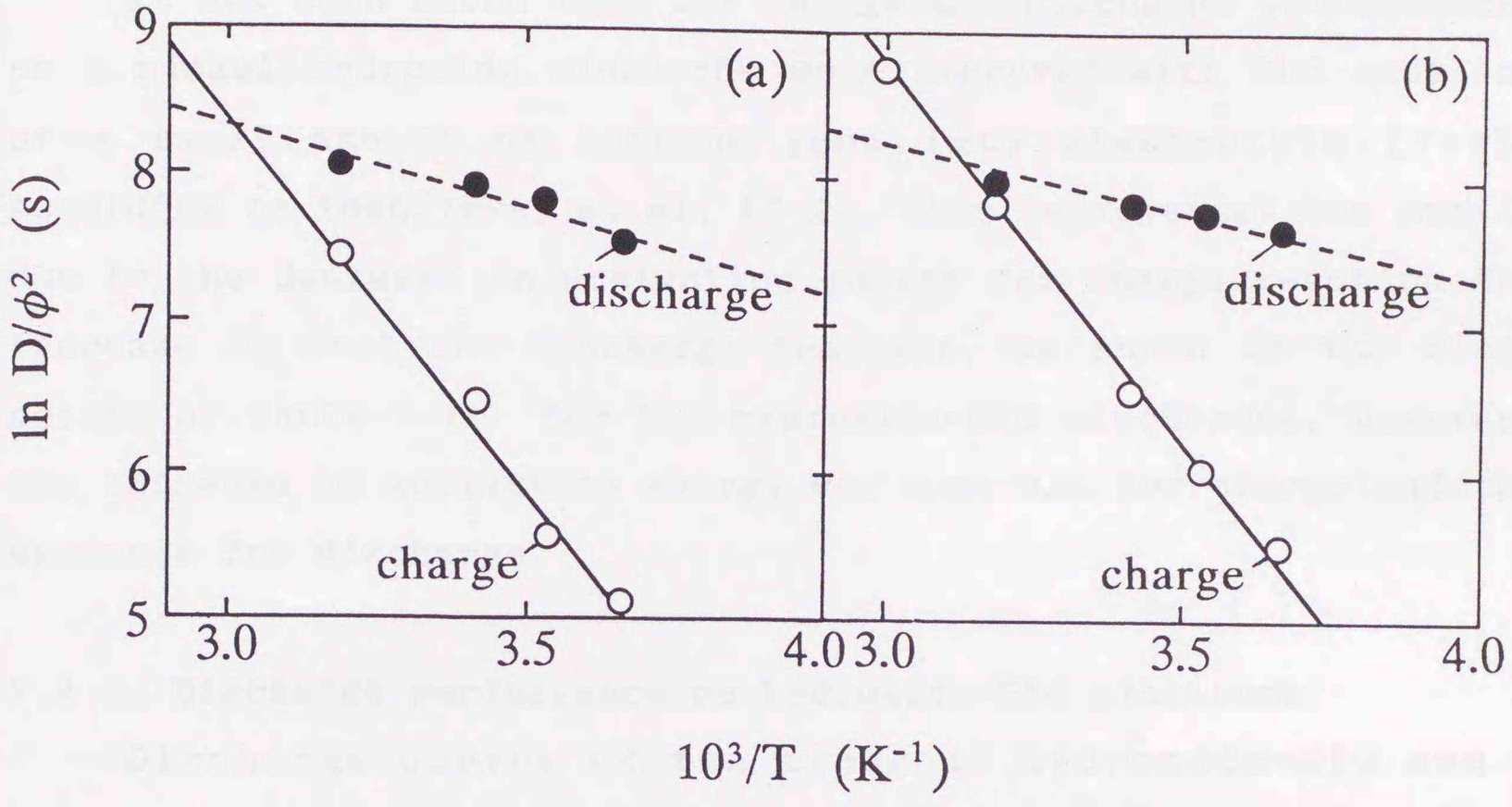


Fig. 7-4 Arrhenius plots of D/ϕ^2 values.
(a) $Ni(OH)_2$-$Fe(OH)_3$-GIC electrode,
(b) $Ni(OH)_2$-$Cu(OH)_2$-GIC electrode.

Table 7-1 Activation energies for charge and discharge reactions on various nickel hydroxide electrodes.

Electrode	Activation energy [kJ/mol] Charge	Discharge
$Ni(OH)_2$-$Fe(OH)_3$-GIC	41.8	6.7
$Ni(OH)_2$-$Cu(OH)_2$-GIC	42.3	9.2
$Ni(OH)_2$	20.9*1	13.4*1
$Ni(OH)_2 + Li^+$	16.3*2	15.1*2

*1: From Ref. [7-1].
*2: From Ref. [7-2].

It has been known that the charge and discharge performances on a nickel hydroxide electrode were improved with the addition of a small amount of lithium ions into electrolyte [7-3]. According to Yoshizawa, et al. [7-2], this improvement was mostly due to the decrease in activation energy for charge reaction and increase in that for discharge reaction, as shown in the final column of Table 7-1. For the hydroxide-GIC electrodes, however, the increase in activation energy was observed for charge and the decrease for discharge.

7.4.2. Discharge performance on hydroxide-GIC electrode

Discharge curves of two kinds of hydroxide-GIC and a conventional pocket-type electrodes are shown in Fig. 7-5.

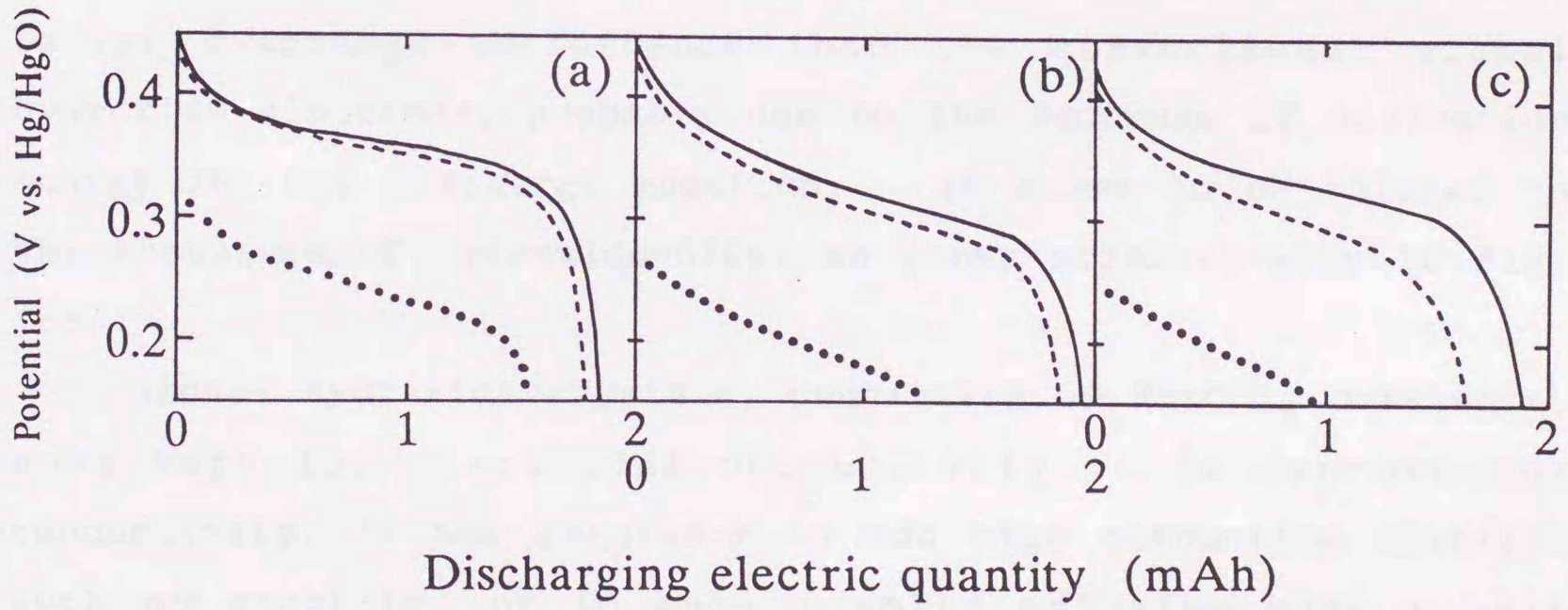


Fig. 7-5 Discharge curves of (a) $Ni(OH)_2$-$Fe(OH)_3$-GIC, (b) $Ni(OH)_2$-$Cu(OH)_2$-GIC and (c) a conventional nickel hydroxide electrodes.
———— : 0.2 mA, - - - - - : 2.0 mA,
.....: 20.0 mA. (1 mAh = 3.6 C)

In the case of the hydroxide-GIC electrodes, particularly the $Ni(OH)_2$-$Fe(OH)_3$ system (Fig. 7-5(a)), each discharge curve shows a well-defined plateau, even better than the pocket-type electrode.

It is known that discharge potential in batteries decreases with increasing current density, mostly due to increase in overvoltage which is related to internal resistance for discharge reaction on the electrode. In the case of electrode with small internal resistance, the decrease of potential with increasing current density is expected to be small extent.

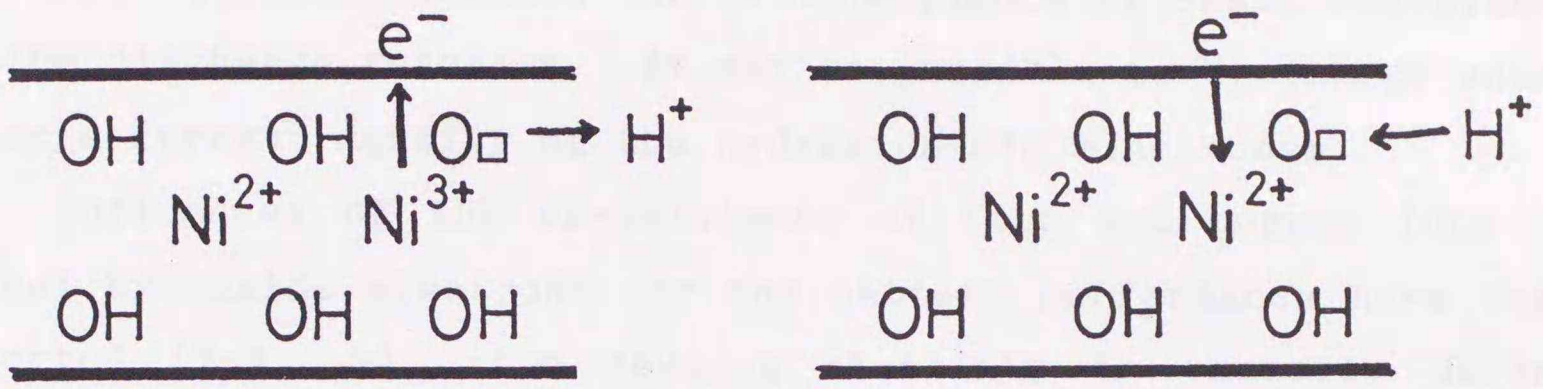
An overvoltage is assumed to be small in the hydroxide-GIC electrodes even under a large current density, in comparison with the conventional pocket-type one.

7.5. Discussion

In the present results, the hydroxide-GIC electrode showed better discharge performance than the conventional nickel hydroxide electrode, probably due to the decrease of activation energy for the discharge reaction. It seems to be related to the structure of hydroxide-GICs, as shown schematically in Fig. 7-6.

Nickel hydroxide crystals, consisting of $Ni(OH)_6$ octahedra, have very low electrical conductivity. To improve the conductivity, it was necessary to add high conductive material such as graphite, or to make a solid solution with cobalt hydroxide [7-4]. In the case of hydroxide-GICs, however, no admixture was required because the layer of nickel hydroxide was sandwiched between conductive carbon layer planes and their high electrical conductivity.

In most graphite intercalation compounds, except graphite fluoride with covalent bonding, charge transfer occurs between



(a) (b)

Fig. 7-6 Scheme of charge and discharge reactions on the nickel hydroxide intercalated between graphite layers.
(a) charge and (b) discharge reactions.

intercalated species (guests) and host graphite. They are classified into donor-type (electrons are given from guest to host) and acceptor-type compounds (electrons from host to guest). The hydroxide-GICs belong to the latter. In Fig. 7-6, the movement of electrons and protons during the charge and discharge reactions in the hydroxide-GIC electrode are schematically shown. The direction of the electron transfer for discharge reaction is the same as the one of the charge transfer in acceptor-type compounds. Therefore, the electron transfer from nickel hydroxides to carbon layers seems to be easier than the opposite one from graphite to nickel hydroxides. Indeed, the activation energies of hydroxide-GIC electrodes were larger for charge reaction and smaller for discharge one than those for both reactions on a conventional nickel hydroxide electrode. That is, the resistance for discharge reaction on the hydroxide-GIC

electrode becomes smaller. As a consequence of small resistance of the discharge reaction, it may be possible to discharge under a large current density on the hydroxide-GIC electrodes.

Influences of the co-existence of iron and copper ions in nickel hydroxide electrode for the battery performance have been reported [7-3, -5], iron causing stability in capacity during repetition of charge-discharge cycle on the electrode, but copper making discharge performance worse. In the present results, however, the discharge performance of the hydroxide-GIC electrode was improved even in $Ni(OH)_2$-$Cu(OH)_2$ system. The existence of co-intercalated species, $Cu(OH)_2$ and $Fe(OH)_3$, in the hydroxide-GIC electrodes seems to have no appreciable effect on the performance of electrode.

7.6. Summery

The present results lead to the conclusion that the metal hydroxide-GIC electrode has a surpassing discharge performance, compared with the conventional electrode of nickel hydroxide mixed with graphite, having low activation energy for discharge reaction. This high performance was reasonably supposed to be due to the structure of hydroxide-GIC, in which a layer of nickel hydroxide was sandwiched between conductive carbon layers and electrons seemed to be easily transferred from intercalated species to host graphite. The existence of co-intercalated species in the hydroxide-GICs, iron and copper hydroxides, which have been used to make the synthesis of the original metal chloride-GICs easier, has no appreciable effect on the discharge reaction.

References

7-1 S. Yoshizawa, Z. Takehara, M. Kato and K. Kumazaki, Denki Kagaku, 34, 661 (1966).

7-2 S. Yoshizawa, Z. Takehara and M. Kato, Denki Kagaku, 35, 559 (1967).
7-3 E. J. Casey, A. R. Dubois, P. E. Lake and W. J. Moroz, J. Electrochem. Soc., 112, 371 (1965).
7-4 D. Yamashita, Denki Kagaku, 34, 228 (1963).
7-5 R. L. Tichenor, Ind. Eng. Chem., 44, 973 (1952).

CHAPTER 8
Conclusion

8.1. Conclusion for the present work

The present thesis leads to the following conclusions.

1) It was shown to be important to relax some strain on hexagonal carbon layer planes in order to proceed graphitization. Whether the strain in carbon layers can be removed during heat-treatment at high temperatures is strongly influenced not only by its starting material, but also its texture.

2) The graphitization degree P_1 was a volume fraction of the graphitic structure in a carbon material, but the average interlayer spacing $\bar{d}_{002}$ was affected by a well-graphitized region. Between P_1 and $\bar{d}_{002}$, therefore, an exponential relation was observed and found to depend strongly on the texture of each materials.

3) The intercalation behavior of sulfuric acid into host graphite by chemical oxidation could be followed by in-situ measurement of potential. From the potential change, the intercalation process of sulfuric acid into graphite by chemical oxidation was found to be fundamentally the same as that by electrochemical one. The intercalation reaction is divided into two processes; charging of host carbon layers corresponding to potential increase and transformation of stage structure in the gallery of carbon layers showing the plateau on the potential change.

4) The potential increase of carbon material in sulfuric acid by chemical oxidation is limited by equilibrium potential, which is given by Nernst's equation of oxidant used and also depends strongly on the activities of each chemical species in the solution. The relation between upper limit of saturated

potential of the oxidant used and onset potential for each stage structure governs the stage structure of graphite intercalation compounds with sulfuric acid (H_2SO_4-GICs) which finally reaches.

5) The intercalation behavior of sulfuric acid by chemical oxidation depended strongly on structure, texture and particle size of host carbon materials. The effect of host on potential change during intercalation by chemical oxidation could be explained on the basis of competition of reaction rates between the charging of host carbon layers and the transformation of stage structure in the gallery of graphite.

6) The host must have certain degree of graphitization in order to form H_2SO_4-GICs. A structural criterion on the host for the intercalation was found to have the crystallite thickness along the c-axis, $L_c(002)$, of more than 20 nm. A electronic criterion on the host seemed to have a positive value of magnetoresistance $(\Delta\rho/\rho)_{max}$ at room temperature, in other words, the host has the electrons which be transferred to sulfuric acid.

7) For the electrochemical decomposition of H_2SO_4-GICs synthesized by chemical oxidation in sulfuric acid solution with an excess amount of oxidant, a large amount of electric quantity was needed, much larger than that expected theoretically. This result was explained by the fact that the chemical oxidation to H_2SO_4-GICs in sulfuric acid solution with the oxidant species, which were remained in the solution, occurred together with the electrochemical reduction of H_2SO_4-GICs.

8) The overall rate of intercalation of sulfuric acid by chemical oxidation depended not only on the amount of oxidant added, but also on the structure and texture of host carbon materials. As a result, the electric quantity for the de-intercalation from H_2SO_4-GICs synthesized by chemical oxidation depended strongly on the texture of host carbon materials.

9) Even during electrochemical reduction of H_2SO_4-GICs, the graphite formed by reduction was chemically oxidized by opening the circuit and again sulfuric acid was able to be intercalated into the gallery of graphite, accompanying the increase in potential. Based on this reaction cycle, i. e., chemical charging and electrochemical discharging, a battery was constructed by using graphite and lead metal as positive and negative electrodes, respectively. In the discharging of the battery constructed, well-defined plateau and larger capacity than theoretical one were obtained.

10) The graphite intercalation compounds with metal hydroxides (hydroxide-GICs) were synthesized through a galvanostatic oxidation in alkaline medium from GICs with corresponding chlorides (chloride-GICs). The amount of nickel hydroxide formed in the graphite gallery could be followed by measuring electric quantity during discharge, i. e., discharge capacity. The capacity depended strongly on the composition of the original chloride-GICs and on the electrolysis time. The nickel efficiency of the original GIC prepared from the host with small flake size was higher than the compound from large size.

11) The hydroxide-GIC electrode had a surpassing discharge performance, compared with the conventional electrode of nickel hydroxide mixed with graphite, having low activation energy for discharge reaction. This high performance is due to structure of hydroxide-GIC, in which a layer of nickel hydroxide is sandwiched in between conductive carbon layers, and electrons are easily transferred from intercalated species to host carbon layers.

8.2. Prospect

8.2.1. Potential measurement

In the present work, the formation process of graphite intercalation compounds with sulfuric acid by chemical oxidation was followed by measuring potential of host carbon material in situ. Thus, the in-situ potential measurement can be applied not only to electrochemical intercalation but also to chemical one. Other intercalation process and the effect of host carbon material on its intercalation behavior may be discussed on the basis of potential change obtained. Particularly, the relation between saturated potential by chemical intercalation and onset potential for each stage structure of GICs is thermodynamically discussed on intercalation reaction.

If the potential measurement is applied to the formation of donor-type GICs, such as intercalation of potassium ions and tetrahydrofurane (THF) by potassium-naphthalene complex [8-1], the potential measurement becomes more powerful procedure in order to study intercalation chemistry.

8.2.2. Effect of host carbon material on intercalation

The effect of host carbon material on intercalation of sulfuric acid was kinetically discussed from the potential change, i. e., on the basis of competition of reaction rates between the charging of host carbon layers and the transformation of stage structure in the gallery of graphite. The appearance of plateaux on the potential change depended strongly on the host used. Therefore, the potential measurement during intercalation of sulfuric acid seems to be used for the characterization of carbon materials.

With lowering the graphitization degree of hosts, the intercalation of sulfuric acid became difficult, and the hosts having below a certain graphitization degree could not be intercalated with sulfuric acid. The value of threshold

potential for the intercalation of sulfuric acid increased with the decrease in graphitization degree of the hosts, as shown in Fig. 4-15. This seems to be consequent upon a thermodynamic effect of the hosts on the intercalation of sulfuric acid. In the future, thermodynamic effect of host material on intercalation reaction have to be studied.

Potassium has been known to intercalate into even the carbons with turbostratic structure. A criterion for the intercalation of alkali metal is not explained by simple structural parameters of host carbon material. However, a criterion for intercalation by electronic structure, as proposed in Chapter 4, seems to be applied to donor-type GIC as well as acceptor-type GIC. Because turbostratic carbons, which show one-carrier conduction of hole (Fig. 4-17), can be transferred its hole to alkali metal, in other words, can accept electrons from the intercalates. Therefore, the characterization of host carbon materials based on electronic properties, such as magnetoresistance, is sure to help understanding the intercalation phenomena.

8.2.3. Graphite intercalation compounds with metal hydroxide

GICs with nickel and iron hydroxides ($Ni(OH)_2$-$Fe(OH)_3$-GIC) and with nickel and copper hydroxides ($Ni(OH)_2$-$Cu(OH)_2$-GIC) could be synthesized by electrochemical oxidation of GICs with corresponding metal chlorides in alkaline medium. Many kinds of metal chlorides have been intercalated into graphite and so different kinds of GICs with metal hydroxides may be able to be synthesized through the same procedure as in the present work. This may create a new field in the science and applications of GICs.

8.2.4. Application to battery

a) Lead-sulfuric acid battery

The lead-sulfuric acid battery constructed by using graphite as positive and lead as negative electrode, as shown in Chapter 5, had well-defined discharge plateau and a large capacity, which was larger than the amount expected theoretically. The potential change during electrochemical discharge of H_2SO_4-GIC synthesized by chemical oxidation depended strongly on host carbon material. For the application of the electrochemical discharge to a lead-sulfuric acid battery, a suitable host is necessary to be obtained, which is susceptible to chemical oxidation and is easily intercalated or de-intercalated with sulfuric acid.

In the battery constructed, any electric power dose not need for charging, and there is no self discharging. Therefore, the battery is available to an urgent electric source.

b) Alkaline secondary battery

The maximum capacity on the GICs with metal hydroxides (hydroxide-GICs) used in Chapter 7 was 45 mAh/g. The GIC with nickel hydroxide ($Ni(OH)_2$-GIC) synthesized by Flandrois, et al. was 66 mAh/g [8-2]. Theoretically, nickel hydroxide electrode has capacity of 290 mAh/g, but a commercialized electrode is about 200 mAh/g. Although the capacity in the present hydroxide-GIC electrode is rather low, there is a possibility for the discharge under a large current density. The hydroxide-GIC may replace the graphite powders which had been mixed with positive electrode material as conductive material in most commercial alkaline secondary battery, because it is not only more conductive than graphite, but also contains active material for the battery.

References

8-1 M. Nomine and L. Bonnetain, J. Chim. Phys., 66, 1731 (1969).

8-2 S. Flandrois, J. M. Masson and J. C. Rouillon, Synth. Met., 3, 195 (1981).

List of publications

1. N. Iwashita and M. Inagaki,
Synthesis of nickel- and iron-hydroxides graphite intercalation compounds and their application to alkaline secondary battery.
NATO ASI "Chemical Physics of Intercalation", Ed. by A. P. Legrand and S. Flandrois, Plenum, New York, 1988, pp. 383-385.

2. M. Inagaki, N. Iwashita, Z. D. Wang and M. Maeda,
Electrochemical synthesis of graphite intercalation compounds with nickel- and iron-hydroxides.
Synthetic Metals, **26**, 41-47 (1988).

3. N. Iwashita and M. Inagaki,
Potential survey of intercalation of sulfuric acid into graphite by chemical oxidation.
Synthetic Metals, **34**, 139-144 (1989).

4. M. Inagaki, N. Iwashita and E. Kouno,
Potential change with intercalation of sulfuric acid into graphite by chemical oxidation.
Carbon, **28**, 49-55 (1990).

5. N. Iwashita and M. Inagaki,
Electrochemical reduction of graphite intercalation compound with sulfuric acid synthesized by chemical oxidation.
Tanso, 1990[No. 145], 288-237 (1990).

6. N. Iwashita and M. Inagaki,
Discharge performance on the electrode of ternary intercalation compounds of graphite with metal hydroxides.
Electrochimca Acta, **36** 591-595 (1991).

7. M. Inagaki, N. Iwashita, Y. Hishiyama, Y. Kaburagi,
A. Yoshida, A. Oberlin, K. Lafdi and Y. Yamada,
Studies on "mesophase"-pitch-based carbon fibers, Part I.
Structure and texture.
Tanso, 1991[No. 147], 57-65 (1991).

8. N. Iwashita and M. Inagaki,
Studies on "mesophase"-pitch-based carbon fibers, Part Ⅲ.
Intercalation of sulfuric acid.
Tanso, 1991[No. 149], 204-210 (1991).

9. N. Iwashita and M. Inagaki,
Effect of graphitization degree on potential changes during intercalation and de-intercalation of sulfuric acid for pyrolytic carbons.
Materials Science Forum, (in press).

Acknowledgment

The study represented in the present thesis has been carried out under the guidance of Professor Michio Inagaki for the period 1986-1990 in Toyohashi University of Technology and -1992 in Hokkaido University.

The author is greatly indebted to Professor Inagaki for his kind guidance and valuable discussions for study.

The author thanks sincerely Profs. Y. Sanada, S. Seo and K. Kodaira for their valuable comments and advice.

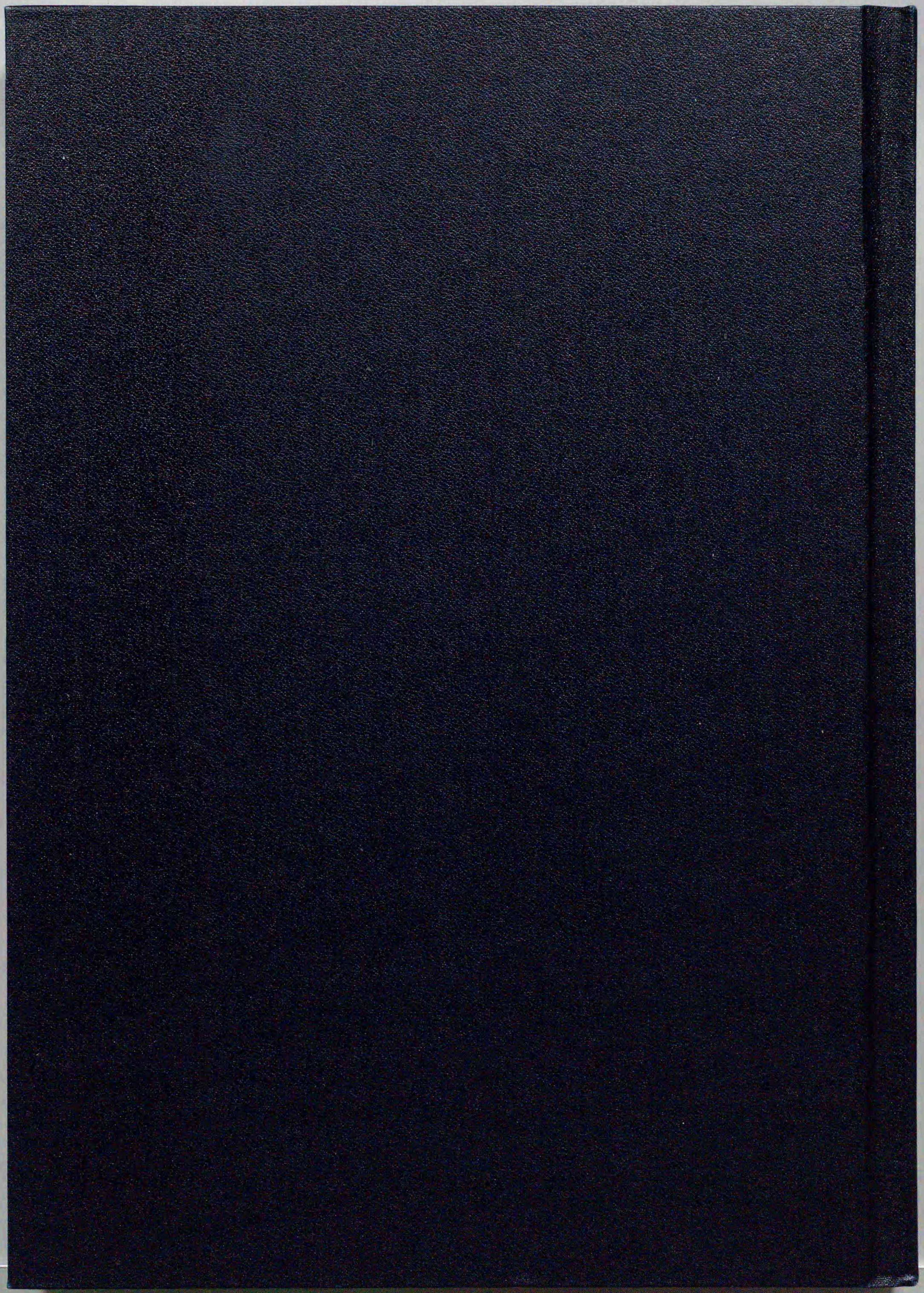
The author thanks sincerely Prof. Y. Hishiyama, Prof. M. Sakai and Mr. Yoshida for kind supply of samples and SEM micrographs on the present work and for their valuable comments and advice.

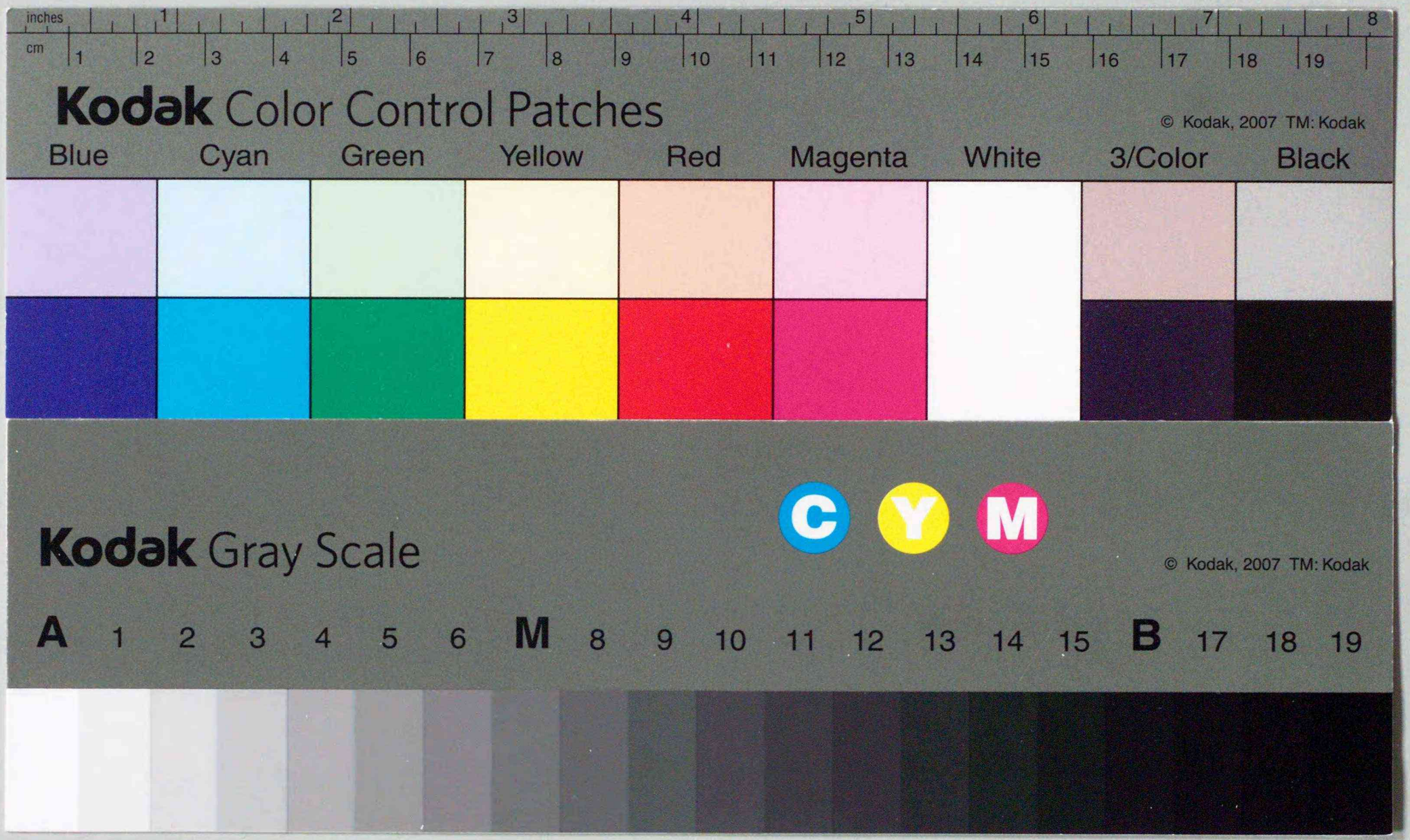
The author would like to express sincere thanks to Prof. Shimada and to all the members of the laboratories to which he has been belong for their encouragements and kind cares during his stay in Toyohashi and Sapporo.

Grateful acknowledgment is made to Koa Oil Co., Nippon Kokuen Co., NKK corporation, Showa Denko K. K., Tokai Carbon Co. and Toyo Tanso Co. for their kind supply of carbon samples on the present work.

Finally the author wished to express his greatest gratitude to his parents and sister for their continuous encouragements, without which the present study would be impossible to be finished.

Norio IWASHITA




inches
cm
Kodak Color Control Patches
© Kodak, 2007 TM: Kodak
Blue
Cyan
Green
Yellow
Red
Magenta
White
3/Color
Black
Kodak Gray Scale
C
Y
M
© Kodak, 2007 TM: Kodak
A 1 2 3 4 5 6 M 8 9 10 11 12 13 14 15 B 17 18 19